University of Southampton

Faculty of Medicine

School of Cancer Sciences

Understanding the role of CD96 in human T-cell activation and its potential as a target for cancer immunotherapy

Volume 1 of 1

by

Michael John Spurway

ORCID ID: 0000-0002-3259-4064

Thesis for the degree of Doctor of Philosophy

May 2025

University of Southampton

Abstract

Faculty of Medicine

School of Cancer Sciences

Thesis for the degree of Doctor of Philosophy

Understanding the role of CD96 in human T-cell activation

and its potential as a target for cancer immunotherapy

by

Michael John Spurway

CD96 (TACTILE) is a type I transmembrane receptor and a member of the immunoglobulin superfamily (IgSF). It is commonly expressed on hematopoietic cells, including $CD4^+$ and $CD8^+$ T-cells, as well as Natural Killer (NK) cells. CD96 interacts with CD155 on tumour and antigen-presenting cells (APCs), competing with the TIGIT and CD226 receptors. Since its isolation in 1992, CD96 has been implicated in cell-cell adhesion, immune regulation, and cytotoxicity mediation. While blockade of CD96 in murine tumour models suggests it inhibits NK cytotoxicity, contrasting findings in human T-cells indicate that antibody targeting of CD96 in fact enhances T-cell activation and pro-inflammatory cytokine release and therefore may represent a suitable target of clinical immunostimulatory antibodies.

Antibody targeting of immunoreceptors such as 4-1BB and OX40 has shown promising results in enhancing anti-tumour immune responses. However, patient-specific factors often limit therapeutic efficacy, leading to treatment resistance or relapse. Expanding the current repertoire of immunotherapeutics is therefore essential.

To address the limited availability of CD96-targeting antibodies, we employed a phage-display panning strategy to generate novel antibodies against human and mouse CD96, as well as clones with cross-species specificity. We identified 77 antibody clones, including several that do not interfere with CD155 binding. Notably, pan-species clones were found to enhance T-cell activation in the presence of anti-CD3 antibodies, highlighting CD96's potential role in T-cell activation and its viability as an immunotherapeutic target.

CD96 contains key intracellular signalling domains, including a proline-rich domain (PRD), an ITIM, and a YxxM motif in human CD96 - common features of co-stimulatory receptors such as CD28 and ICOS. Using a chimeric antigen receptor (CAR) model incorporating the ICD of CD96 and subsequent site-directed mutagenesis, we demonstrated that CD96 facilitates T-cell activation through its PRD. Kinase profiling further revealed that the CD96 PRD mediates activation of key protein-tyrosine and serine/threonine kinases, including ITK, PDK1, and the MEK/ERK pathway.

Finally, by employing a T-cell activation model using bacterial superantigens as MHC-II presented peptides, we have shown that CD96 augments T-cell activation via physiological interactions with CD155. However, this activity is significantly influenced by the co-expression of TIGIT and CD226.

These findings establish CD96 as a critical modulator of T-cell activation and a promising target for immunotherapy.

Table of Contents

Table of Figures ..... **ix**

Table of Tables ..... **xiii**

Research Thesis: Declaration of Authorship ..... **xiv**

Acknowledgements ..... **xv**

Definitions and Abbreviations ..... **xvi**

Chapter 1 Introduction **1**

1.1 The Immune System **1**

1.1.1 The innate immune system 1

1.1.1.1 The complement system 1

1.1.1.2 Dendritic cells 2

1.1.1.3 Macrophages 3

1.1.1.4 Neutrophils 3

1.1.1.5 Natural Killer Cells 4

1.1.1.6 γδ T-cells 5

1.1.2 The adaptive immune system 6

1.1.2.1 B-cells 6

1.1.2.2 T-cells 6

1.1.3 T-Cell Development 7

1.1.4 T-cell Receptor Activation 9

1.1.5 CD4+ T-cell Activation 10

1.1.6 CD8+ T-cell Activation 11

1.1.7 T-cell Co-Stimulation 12

1.1.8 T-cell Inhibition 14

1.2 Cancer **16**

1.2.1 Recognition of cancer 17

1.3 Cancer Immunotherapy **19**

1.3.1 Antibodies 19

1.3.2 Current antibody therapeutics 21
1.3.2.1 Direct targeting antibodies 21
1.3.2.2 Immunomodulatory antibodies 22
1.3.2.3 Bispecific antibodies 23
1.3.3 T-cell Engineering 24
1.4 CD96 25
1.4.1 CD96 structure and signalling 26
1.4.2 CD96 in Natural Killer Cells 28
1.4.3 CD96 in T-cells 29
1.5 Hypothesis and aims 32
Chapter 2 Methodology 2
2.1 Cell culture 2
2.2 Flow Cytometry Antibodies 3
2.3 Flow cytometry 4
2.4 CD96 and CD226 γ-Retrovirus plasmid production 4
2.5 γ-Retroviral transduction of Rat Basophilic Leukaemia cells 5
2.6 Assessing anti-CD96 scFv binding of CD96 6
2.7 Truncated CD96 ELISA 6
2.8 Assessing scFv inhibition of CD155 binding to CD96 7
2.9 PBMC T cell isolation 7
2.10 PBMC antibody proliferation 7
2.11 CAR retroviral plasmid generation 8
2.12 HEK293FT lentivirus transfection 9
2.13 Lentiviral transduction of Jurkat cells 9
2.14 Jurkat CAR-T cell activation assay 10
2.15 Lentiviral transduction of primary T-cells 10
2.16 CAR-T Expansion 11
2.17 CAR-T Killing 11

2.18 Enzyme-Linked Immunosorbent Assay (ELISA) 11

2.19 PamGene Co-Culture 12

2.20 PamGene Kinase Analysis Run 12

2.21 SEE Loading 12

2.22 SEE induced CD155 ligand upregulation 13

2.23 SEE induced T-cell proliferation 13

2.24 Software 13

2.25 Statistical Analysis 13

Chapter 3 Developing novel CD96 targeting antibodies 2

3.1 Phage display screening for CD96 binding scFv clones 2

3.2 Generating CD96 expressing RBL cells 3

3.2.1 Cloning of genes of interest into the retrovirus vector pMP71 4

3.2.2 Retroviral transduction of rat basophilic leukaemia cells 8

3.3 Characterisation of phage-display panned scFv clones 9

3.3.1 Characterisation of scFv panned against human CD96v2 9

3.3.2 Characterisation of scFv panned against mouse CD96 12

3.3.3 Characterisation of scFv panned against both human and mouse CD96 15

3.4 Mapping phage-display panned scFv to CD96 domains 21

3.4.1 Human panned scFv binding of truncated CD96 22

3.4.2 Mouse Panned IgG Binding of Truncated mCD96 24

3.4.3 Dual-panned anti-CD96 scFv binding of truncated CD96 26

3.5 Phage-display isolated anti-CD96 antibody T-cell Proliferation 27

3.5.1 Soluble anti-CD96 antibody induced human T-cell activation 27

3.5.2 Plate-captured anti-CD96 antibody induced human T-cell activation 32

3.6 Chapter Discussion 38

Chapter 4 CARs as a model system for investigating huCD96 signalling 42

4.1 Generating CAR T-cells containing a CD96 intracellular domain 42

4.1.1 Chimeric Antigen Receptor design 43

4.1.2 Generating CAR lentivirus for transduction of Jurkat T-cells 45
4.1.3 Generated CAR expressing Jurkat cells 45
4.2 Investigating the sub-optimal activation of J-CAR cells 47
4.2.1 Activation of J-CAR with recombinant human CD19.....47
4.2.2 Activation of J-CAR with huCD19 expressing target cells.....50
4.3 Dissecting the source of CD96 stimulatory signalling 53
4.3.1 The CD96 ICD enables effective cell activation in the context of CARs 53
4.3.2 Point mutations of the CD96 ICD 56
4.3.3 Mutations of the CD96 ICD PRD impair J-CAR activation.....57
4.3.4 Targeted mutations of four core prolines ablates stimulatory capacity of CD9658
4.4 Downstream kinase activity of the CD96 intracellular domain..... 60
4.4.1 Upstream kinase analysis scoring system 62
4.4.2 CD96 PRD mutations limit tyrosine kinase targeted substrate phosphorylation64
4.4.3 Upstream Kinase Analysis of CD96 induced tyrosine kinase targeted peptide phosphorylation 66
4.4.4 CD96 PRD mutations ablate serine/threonine kinase substrate phosphorylation 68
4.4.5 The CD96 PRD drives activation and inhibition of key serine/threonine kinases70
4.4.6 PRD mutations limits key tyrosine kinase activation by CD96 72
4.4.7 Mutations of the CD96 PRD alters CD96-mediated serine/threonine kinases activity 74
4.4.8 Proline mutations of CD96 ablate Akt phosphorylation 76
4.5 Inclusion of the CD96 ICD in primary CAR-T 77
4.5.1 Transduction of primary CAR-T 77
4.5.2 Impact of the CD96 ICD upon primary CAR-T cell expansion.....80
4.5.3 Cytokine secretion by primary CAR-96ζ is reduced with respect to CAR-BBζ..82
4.5.4 Killing capacity of CD96 ICD primary CAR-T 83
4.6 Chapter 4 Discussion..... 86
Chapter 5 The role of CD96 in primary human T-cell activation..... 94

5.1 T-cell activation utilising bacterial superantigens 94

5.1.1 Confirmation of HLA-DR expression on Raji B-cells 94

5.1.2 Raji presented SEE induces strong primary T-cell proliferation.....95

5.2 Expression of CD155 receptors across T-cell donors..... 98

5.3 CD155 augments sAg-mediated T-cell proliferation 100

5.3.1 CD155 receptor upregulation in response to sAg stimulation in $TIGIT^{LO}CD226^{LO}$ T-cells.....100

5.3.2 CD4+ $TIGIT^{LO}CD226^{LO}$ proliferation is unaffected by CD96 blockade 103

5.3.3 CD8+ $TIGIT^{LO}CD226^{LO}$ proliferation is limited by CD96 blockade.....105

5.4 CD96 augments the activation of $TIGIT^{INT}CD226^{HI}$ T-cells 107

5.4.1 $TIGIT^{INT}CD226^{HI}$ T-cells upregulate CD155 receptors upon activation.....107

5.4.2 Raji expression of CD155 promotes sAg mediated $TIGIT^{INT}CD226^{HI}$ T-cell activation through CD96 109

5.5 $TIGIT^{INT}CD226^{LOW}$ T-cells exhibit reduced activation potential 112

5.5.1 $TIGIT^{INT}CD226^{LOW}$ T-cells exhibit reduced sAg-mediated CD155 receptor upregulation 112

5.5.2 $TIGIT^{INT}CD226^{LO}$ T-cells proliferation is inhibited by B-cell presentation of CD155 114

5.6 CD96 blockade has limited impact on $TIGIT^{HI}CD226^{HI}$ T-cells 117

5.6.1 CD155-mediated $TIGIT^{HI}CD226^{HI}$ T-cell proliferation is partially reliant on CD96 118

5.7 Discussion..... 122

Chapter 6 Discussion 129

6.1 Developing a panel of novel anti-CD96 antibodies..... 129

6.2 Understanding the signalling network utilised by CD96 133

6.3 The role of CD96 within the TIGIT, CD96, and CD226 network 137

6.4 Future work and concluding remarks..... 139

Bibliography..... 144

Appendix A γ-retrovirus maps 161

A.1 pMP71-huCD96v2 plasmid map 161
A.2 pMP71-mCD96 plasmid map 162
A.3 pMP71-huCD226 plasmid map 163
A.4 pMP71-mCD226 plasmid map 164
A.5 pCL-Eco plasmid map 165
Appendix B Lentivirus plasmid maps 167
B.1 pM13328 Plasmid Map 167
B.2 pMDG.1 Plasmid Map 168
B.1 pMDLgp.RRE Plasmid Map 169
B.1 pRSV.Rev Plasmid Map 170
Appendix C CD96 CAR Sequences 172
Appendix D T-cell co-culture with unloaded Raji 176
D.1 $TIGIT^{LO}CD226^{HI}$ T-cell proliferation induced by unloaded Raji 176
D.2 $TIGIT^{INT}CD226^{LO}$ T-cell proliferation induced by unloaded Raji cell 177
D.3 $TIGIT^{HI}CD226^{HI}$ T-cell proliferation induced by unloaded Raji cell 178

Table of Figures

Figure 1.1 T-cell Development Within The Thymus 8

Figure 1.2 Association of CD3, CD4 and CD8 molecules with the TCR 10

Figure 1.3 TCR, CD28 and 4-1BB activation results in a synergetic effect to promote cell activation and survival 13

Figure 1.4 Overview of CTLA-4 and PD-1 mediated T-cell inhibition 15

Figure 1.5 Schematic overview of antibody structure 20

Figure 1.6 Schematic overview of T-cell chimeric antigen receptors 24

Figure 1.7 The structure of human and mouse CD96 27

Figure 3.1 Graphical overview of the phage-display panning strategy utilised to identify novel anti-CD96 scFv clones 3

Figure 3.2 Cloning of human and mouse CD96 and CD226 into the pMP71 vector 5

Figure 3.3 Diagnostic digests of pMP71-huCD226 and pMP71-mCD226 7

Figure 3.4 Expression of human or murine CD96 or CD226 on FACs sorted RBL Cells 8

Figure 3.5 Human panned scFv binding of RBL-huCD96 10

Figure 3.6 Human panned scFv blocking of huCD155 binding to RBL-huCD96 11

Figure 3.7 Correlation between the IC50 and EC50 values of human CD96 reactive scFv 12

Figure 3.8 Mouse panned scFv binding of RBL-mCD96 13

Figure 3.9 Mouse CD96 panned scFv blocking of mCD155 against RBL-mCD96 14

Figure 3.10 Correlation between the IC50 and EC50 values of mCD96 reactive scFv 15

Figure 3.11 Dual-panned scFv binding of RBL-huCD96 16

Figure 3.12 Dual-panned scFv blocking of huCD155 binding huCD96 17

Figure 3.13 Correlation between binding and blocking capacity of dual-panned scFv against RBL expressed huCD96v2 18

Figure 3.14 Dual-panned scFv binding of RBL-mCD96 19

Table of Figures

Figure 3.15 Dual-panned scFv blocking of RBL expressed mCD96 20

Figure 3.16 Correlation between binding and blocking capacity of dual-panned scFv against RBL expressed mCD96 21

Figure 3.17 Schematic overview of truncated CD96 to determine scFv binding 22

Figure 3.18 Binding of truncated huCD96 by human-panned scFv clones 24

Figure 3.19 Binding of truncated mCD96 by mouse-panned scFv clones 25

Figure 3.20 Mapping binding of dual-panned scFv to domains of huCD96v2 27

Figure 3.21 Soluble dual-panned anti-CD96 antibody induced T-cell proliferation 29

Figure 3.22 Soluble dual-panned anti-CD96 antibody induction of CD25 expression 31

Figure 3.23 Plate-bound dual-panned anti-CD96 antibody induced T-cell proliferation 33

Figure 3.24 Plate-bound dual-panned anti-CD96 antibody induced CD25 expression 35

Figure 3.25 Relationship between scFv clone affinity and antibody induced T-cell proliferation 37

Figure 4.1 Schematic representation of utilised CAR constructs 44

Figure 4.2 Transduction efficiency of Jurkat T cells utilising CAR construct containing lentivirus 46

Figure 4.3 Recombinant Human CD19 binding of BBζ expressing J-CAR cells 47

Figure 4.4 Recombinant huCD19 effectively binds J-CAR but fails to induce cell activation 49

Figure 4.5 CD20 expression on Ramos target cells distinguishes target cell from Jurkat 50

Figure 4.6 J-CAR upregulation of CD69 upon co-culture with CD19+ Ramos B cells. 51

Figure 4.7 J-CAR IL-2 production increases in response to increased target co-culture 52

Figure 4.8 Background expression of CD69 across J-CAR cell lines 54

Figure 4.9 Inclusion of the CD96 ICD imparts strong J-CAR activation over CD3ζ signalling alone. 55

Figure 4.10 Mutation of CD96 PRDI limits CD69 upregulation but not IL-2 production 58

Figure 4.11 Mutation of CD96 PRDI and PRDII limits both CD69 upregulation and IL-2 production 59

Figure 4.12 Experimental workflow for kinase analysis utilising PamChips 61

Table of Figures

Figure 4.13 Upstream Kinase Analysis scoring systems utilised to class significance and specificity of kinase activity 63

Figure 4.14 Tyrosine kinase substrate phosphorylation is inhibited by a PRD mutation of CD9665

Figure 4.15 Upstream kinase analysis of 96ζ highlights progressive loss of PTK activity through PRD mutations 67

Figure 4.16 96ζ induced STK substrate phosphorylation is largely ablated by PRD mutations .. 69

Figure 4.17 CD96 PRD mutations ablates the activity of serine/threonine kinases 71

Figure 4.18 CD96 PRD mutation induced loss of tyrosine kinase activity and implicates key Src family members 73

Figure 4.19 PRD mutation induced loss of serine/threonine kinase activity implicates both MAPK and PI3K/Akt pathways 75

Figure 4.20 Western Blot of J-CAR lysate indicates Akt activation is mediated by CD96 PRDs .. 77

Figure 4.21 CAR transduction of donor primary T-cells 79

Figure 4.22 Expansion of CD4+CAR+ primary T-cells co-cultured with Raji target cells 81

Figure 4.23 Expansion of CD8+ CAR+ primary T-cells co-cultured with Raji target cells 82

Figure 4.24 Cytokine production by primary CAR-T 83

Figure 4.25 Target cell lysis by primary CAR-T cells 85

Figure 4.26 Alignment of TSAD, CD28 and CD96 indicates an Itk consensus sequence 88

Figure 4.27 Proposed signalling pathway of CD96 in the context of CAR-T utilising UKA data .. 89

Figure 5.1 Raji and Raji-CD155 expression of MHC-II HLA-DR and CD155 95

Figure 5.2 sAg-loaded Raji induce strong primary T-cell activation 97

Figure 5.3 Expression of CD96, TIGIT and CD226 on isolated T-cells is varied between donors 99

Figure 5.4 CD155 receptor expression changes upon sAg stimulation of $TIGIT^{LO}CD226^{LO}$ T-cells102

Figure 5.5 CD155 enhancement of CD4+ $TIGIT^{LO}CD226^{LO}$ proliferation is not impacted by CD96 blockade. 104

Figure 5.6 CD96 augments CD155 mediated proliferation of $TIGIT^{LO}CD226^{LO}$ CD8+ T-cell proliferation 106

Figure 5.7 TIGIT^{INT}CD226^{HI} T-cells upregulate each CD155 receptor in response to CD155 108

Figure 5.8 TIGIT^{INT}CD226^{HI} T-cell proliferation is enhanced by CD96 expression 110

Figure 5.9 IL-2 but not IFN-γ secretion by TIGIT^{INT}CD226^{HI} T-cells is promoted by CD96 111

Figure 5.10 TIGIT^{INT}CD226^{LO} T-cells (Donor 2) upregulate CD155 receptors in response to CD155113

Figure 5.11 TIGIT^{INT}CD226^{LO} T-cell proliferation is inhibited by APC presentation of CD155 ... 115

Figure 5.12 TIGIT^{INT}CD226^{LO} IL-2 and IFN-γ secretion is limited by CD155 provision and CD96 blockade 116

Figure 5.13 TIGIT^{HI}CD226^{HI} T-cells increase CD96 upregulation in response to target expression of CD155 118

Figure 5.14 TIGIT^{HI}CD226^{HI} T-cell proliferation is not affected by CD96 blockade..... 120

Figure 5.15 TIGIT^{HI}CD226^{HI} IL-2 release is promoted by CD96-CD155 interactions 121

Figure 6.1 Schematic overview of CD96 dimerisation..... 131

Table of Tables

Table 2.1 Antibodies used for flow cytometry 3

Table 2.3 PCR primers for CD96 CAR point-mutations..... 9

Table 2.4 ELISA Antibodies 12

Table 3.1 Dual-panned scFv clone binding and blocking of human or mouse CD96 38

Table 4.1 CAR constructs utilised and their corresponding ICD..... 43

Table 4.2 Site-directed mutations of the CD96 ICD utilised for CAR-96ζ..... 56

Table 5.1 Donor T-cell pre-activation phenotyping of TIGIT and CD226 expression 123

Research Thesis: Declaration of Authorship

Print name: Michael Spurway

Title of thesis: Understanding the role of CD96 in human T-cell activation and its potential as a target for cancer immunotherapy

I declare that this thesis and the work presented in it are my own and has been generated by me as the result of my own original research.

I confirm that:

1. This work was done wholly or mainly while in candidature for a research degree at this University;
2. Where any part of this thesis has previously been submitted for a degree or any other qualification at this University or any other institution, this has been clearly stated;
3. Where I have consulted the published work of others, this is always clearly attributed;
4. Where I have quoted from the work of others, the source is always given. With the exception of such quotations, this thesis is entirely my own work;
5. I have acknowledged all main sources of help;
6. Where the thesis is based on work done by myself jointly with others, I have made clear exactly what was done by others and what I have contributed myself;
7. None of this work has been published before submission

Signature: ..... Date: 13.05.2025 .....

Acknowledgements

I would like to thank my supervisors, Professor Aymen Al-Shamkhani and Dr. Anne Rogel for their support and guidance throughout the course of the project.

I'd also like to thank Dr. Claude Chan for his patient support in generating seemingly endless CAR variants. I'm incredibly grateful to Dr. Jinny Kim and Chris Penfold for their support generating antibodies. Also, to Dr. Savi Rangarajan at PamGene for helping make sense of my data, and the team at BioInvent for their support throughout the project.

A special mention must go to Amatta, Dylan, Marcus, Rosa, and Vici, for their support, suggestions and good food. Also, to my Dad, Mum, Shauna, Raj, Harry, Joseph and McKenna for their support and love during what has seemed to them an endless time at University. Finally, I'd like to thank Charlotte, without whom I would not have finished this thesis.

Definitions and Abbreviations

ADCC..... Antibody dependent cellular cytotoxicity

ADCD ..... Antibody dependent complement deposition

ADCP..... Antibody dependent cellular phagocytosis

AIRE ..... Autoimmune regulator

Akt ..... Protein kinase B

AP-1 ..... Activator Protein-1

ATP..... Adenosine triphosphate

B-ALL..... B-cell acute lymphoblastic leukaemia

BCMA..... B-cell maturation antigen

BCR ..... B-cell receptor

B_{Max} ..... Maximal binding

bp..... Basepairs

bsAb..... Bispecific antibody

CAR ..... Chimeric antigen receptor

CAR-T ..... Chimeric antigen receptor T-cell

cDC..... Conventional dendritic cell

CDR ..... Complimentary-determining region

CFSE ..... Carboxyfluorescein diacetate succinimidyl ester

CLEC..... C-type lectin receptor

CMP ..... Common myeloid progenitor

CRC ..... Colorectal cancer

CRS..... Cytokine release syndrome

CSF-1..... Colony-stimulating factor-1

cSMAC ..... Central supramolecular activation cluster

cTEC ..... Cortical thymic epithelial cells

CTLA-4..... Cytotoxic T-lymphocyte antigen-4

DC ..... Dendritic cells

DN ..... Double negative

DNA ..... Deoxyribonucleic acid

DP ..... Double positive

dSMAC ..... Distal supramolecular activation cluster

E. coli ..... *Escherichia coli*

E:T ..... Effector : Target

EC_{50} ..... Half-maximal effective concentration

EF1α ..... Elongation factor 1-alpha

ELISA ..... Enzyme-linked immunosorbent assay

ERK ..... Extracellular signal-regulated kinase

FACs ..... Fluorescence-activated cell sorting

FcR ..... Fc receptor

FcγR ..... Fc gamma receptor

FcγRI ..... Fc gamma receptor 1

FcγRIIA ..... Fc gamma receptor 2a

FcγRIIB ..... Fc gamma receptor 2b

FcγRIIIA ..... Fc gamma receptor 3a

FcγRIIIB ..... Fc gamma receptor 3b

FcεR ..... Fc epsilon receptor

FOXP3 ..... Forkhead box protein 3

GATA3 ..... GATA binding protein 3

GFP ..... Green fluorescent protein

Grb2 ..... Growth factor receptor-bound protein 2

GRZB ..... Granzyme B

GSK ..... GlaxoSmithKline

HER2 ..... Human-epidermal growth factor receptor 2

HLA ..... Human leukocyte antigen

HSC ..... Haematopoietic stem cell

huCD226 ..... Human CD226

huCD96 ..... Human CD96

huTIGIT ..... Human TIGIT

IC ..... Isotype control

IC_{50} ..... Half-maximal inhibitory concentration

ICAM-1 ..... Intercellular adhesion molecule-1

ICB ..... Immune checkpoint blockade

ICD ..... Intracellular domain

IFNGR ..... Interferon-γ receptor

IFN-α ..... Interferon-alpha

IFN-β ..... Interferon-beta

IFN-γ ..... Interferon-gamma

IgA ..... Immunoglobulin A

IgE ..... Immunoglobulin E

IgG ..... Immunoglobulin G

IgM ..... Immunoglobulin M

IgM ..... Immunoglobulin M

IgSF ..... Immunoglobulin superfamily

IL-1 ..... Interleukin-1

IL-10 ..... Interleukin-10

IL-10 ..... Interleukin-10

IL-12 ..... Interleukin-12

IL-12 ..... Interleukin-12

IL-1β ..... Interleukin-1 beta

IL-2 ..... Interleukin-2

IL-21 ..... Interleukin-21

IL-4 ..... Interleukin-4

IL-4 ..... Interleukin-4

IL-4R ..... Interleukin-4 receptor

IL-7 ..... Interleukin-7

Irdf8 ..... Interferon regulatory factor 8

ITAM ..... Intracellular tyrosine-based activation motif

ITIM ..... Intracellular tyrosine-based inhibitory motif

iT_{reg} ..... Induced regulatory T-cell

ITSM ..... Immunoreceptor tyrosine-based switch motif

ITT ..... Immunoreceptor tyrosine tail-like motif

IκBα ..... NFκB inhibitor alpha

J-CAR ..... Jurkat CAR-T

K_d ..... Dissociation constant

KLRG1 ..... Killer-cell lectin-like receptor G1

KO ..... Knockout

LAG-3 ..... Lymphocyte-activation gene 3

LDL-R ..... Low-density lipoprotein receptor

LFA-1 ..... Lymphocyte function-associated antigen 1

LogFC ..... Log fold change

LPS ..... Lipopolysaccharide

mAb ..... Monoclonal antibody

MAC ..... Membrane Attack Complex

MAPK ..... Mitogen-activated protein kinase

MBL ..... Mannan-binding lectin

mCD226 ..... Mouse CD226

mCD96 ..... Mouse CD96

MCMV ..... Mouse cytomegalovirus

mCRC ..... Metastatic colorectal cancer

MDM ..... Monocyte derived macrophage

MEK ..... Mitogen-activated protein kinase

MEK ..... Mitogen-activated protein kinase

mg..... Miligram

MHC-I..... Major histocompatibility complex class I

MHC-II..... Major histocompatibility complex class II

MIC ..... MHC class I chain-related protein

mL..... Millilitre

MPEC ..... Memory precursor effector cells

mRNA..... Messenger ribonucleic acid

mTEC..... Medullary thymic epithelial cells

mTIGIT ..... Mouse TIGIT

NET ..... Neutrophil extracellular trap

NFAT ..... Nuclear Factor of Activated T-cells

NFκB ..... Nuclear factor kappa-light-chain enhancer of activated B-cells

NK-cell ..... Natural Killer cell

NKG2A ..... Natural Killer Group 2 Member A

NKG2D ..... Natural Killer Group 2 Member D

nM ..... Nanomolar

^{o}C ..... Degree Celsius

PBMC ..... Peripheral blood mononuclear cells

PD-1 ..... Programmed cell-death protein 1

pDC ..... Plasmacytoid dendritic cell

PD-L1 ..... Programmed-death ligand 1

PD-L2 ..... Programmed-death ligand 2

Phoenix-Eco ..... Phoenix Ecotrophic cells

PI3K..... Phosphatidylinositol 3-kinase

PIP_2 ..... Phosphatidylinositol (4,5)-biphosphate

PIP_3 ..... Phosphatidylinositol (3,4,5)-triphosphate

PKC..... Protein kinase C

pMHC..... Peptide MHC complex

PRD ..... Proline-rich domain

PRR ..... Pathogen recognition receptor

pSMAC ..... Peripheral supramolecular activation cluster

PTK..... Protein tyrosine kinase

PVR ..... Polio-virus receptor

RBL..... Rat basophilic leukaemia cells

rhuCD19..... Recombinant human CD19

RNA..... Ribonucleic acid

ROS ..... Reactive oxygen species

RRE..... Reverse Response Element

rSEE..... Recombinant *Staphylococcal* Enterotoxin E

sAg ..... Superantigen

scFv ..... Single chain fragment variable

SEC-MALS ..... Size exclusion chromatography with multi-angle light scattering

SEE ..... *Staphylococcal* Enterotoxin E

SH2 ..... Src-homology 2

SH3 ..... Src-homology 3

SHP-2 ..... Src-homology region 2 domain-containing phosphatase-2

SLEC ..... Shorter-lived effector cells

SMAC ..... Supramolecular activation cluster

STAT6..... Signal transducer and activator of transcription 6

STK..... Serine/threonine kinase

TAA ..... Tumour associated antigen

TAB1/2..... TAK1-binding proteins

TACTILE..... T cell activation, increased late expression

TAK1 ..... Transforming growth factor-β activated kinase 1

TAM ..... Tumour associated macrophages

TAP1 ..... Transporter associated with antigen processing 1

T_{CM} ..... Central memory T-cell

TCR..... T-cell receptor

tDC ..... Thymic dendritic cell

T_{EM} ..... Effector memory T-cell

T_{EMRA}..... Effector memory CD45RA-expressing T-cell

T_{FH} ..... Follicular helper T-cell

TGF-β ..... Transforming growth factor beta

T_H1 ..... T Helper 1

T_H2 ..... T Helper 2

TIGIT ..... T-cell immunoreceptor with Ig and ITIM domains

TIL ..... Tumour infiltrating lymphocytes

TLR ..... Toll-like receptor

TLT-1 ..... TREM-like transcript 1

TM ..... Transmembrane

TME..... Tumour microenvironment

TNFR ..... Tumour necrosis factor receptor family

TNF-α ..... Tumour necrosis factor alpha

TRAF1/2 ..... TNF receptor associated factor ½

T_{reg}..... Regulatory T-cells

TRM ..... Tissue resident macrophage

TSAD ..... T-cell specific adapter protein

TSS ..... Toxic shock syndrome

tT_{reg} ..... Thymus-derive regulatory T-cell

UKA..... Upstream Kinase Analysis

ULBP ..... UL16 binding protein

UTR ..... Untransduced

VEGF ..... Vascular endothelial growth factor

VLA-4 ..... Very late antigen-4

VLA-5 ..... Very late antigen-5

VSVG ..... Vesicular stomatitis virus G glycoprotein

WT ..... Wild-type

ZAP70..... Zeta-chain-associated protein kinase 70

µg..... Microgram

µL..... Microlitre

Chapter 1 Introduction

1.1 The Immune System

The immune system is a complex network of mechanisms and cells which acts to protect the body against both internal and external threats. It is capable of identifying and eliminating a diverse range of dangers, including pathogens such as bacteria, viruses and parasites, as well as abnormal cells which have acquired a mutational burden and are at risk of becoming cancerous.

The immune system is divided into two main components according to their specificity for a target: the innate immune system, and the adaptive immune system. The innate immune system can respond to non-specific threats, identifying common features which are shared by various pathogens. Conversely, the adaptive immune system recognises more specific features which may not be common or shared amongst pathogens, allowing for a more targeted response.

1.1.1 The innate immune system

The largest aspect of the innate immune system is the physical barrier provided by the epithelial surface. The internal epithelial surface is often covered with a mucus layer, containing key glycoproteins which can act to physically limit the ability of pathogens to access the epithelium. Contained within this mucus layer is a number of antimicrobial factors, known as defensins. These short peptides exhibit a range of antimicrobial activities and can inhibit the growth of bacteria, fungi and parasites [1]. Beyond this initial layer of defence are further specialised networks of non-specific proteins and cells, each of which contributes to the innate immune system.

1.1.1.1 The complement system

A second form of innate defence is a family of 20 soluble proteins which interact with one another to form the complement system [2]. This system is commonly triggered by the activation of the C1-complex. Activation of the C1-complex results in a downstream cascade of proteolytic cleavage involving multiple complement proteins, amplifying with each subsequent step. The end result of this is the formation of the membrane attack complex (MAC), which acts to puncture the membrane of pathogens, inducing target lysis and cell death [3]. This system of defence can be carried out using a number of similar pathways, differing in their trigger [3, 4]. The classical pathway is activated by binding of the C1-complex to either immunoglobulin G (IgG) IgG or IgM antibodies which are bound to the surface of a target pathogen. The alternative pathway utilises the low-level constitutive activation of the complement protein C3. Host cells are capable of inactivating this C3 activity, whilst pathogens are not. This allows for complement targeting of microbes without being triggered by bound IgG

molecules whilst protecting from complement targeting of host. A third pathway is triggered by the mannan-binding lectin protein (MBL) which specifically targets mannose sugars present in the cell wall of bacteria to trigger a microbe targeting complement cascade.

Whilst the innate immune response utilises mechanisms which can act independently of cells, host cells themselves are capable of recognising certain characteristics common to groups of pathogens to initiate a non-specific immune response themselves [5]. Toll-like receptors (TLRs) are a family of host expressed pattern recognition receptors (PRRs), acting to recognise conserved and common pathogenic features. This family of PRRs consists of 10 receptors in humans (TLRs 1-10). Each has specificity for certain conserved targets, such as TLR4 recognition of bacterial lipopolysaccharide (LPS) or TLR5 to bacterial flagella [6]. TLR activation results in the downstream activation of key transcription factors pivotal for the production of pro-inflammatory cytokines such as interleukin-1 (IL-1), IL-12 and type-I interferons (IFNs) [7].

1.1.1.2 Dendritic cells

Complimentary to these innate mechanisms of pathogen recognition are specific immune cells with specialised roles. Forming a part of the innate immune system and acting as a bridge to the adaptive response, dendritic cells (DCs) are involved in the recognition of both extrinsic and intrinsic threats, allowing for the priming of effector cell responses.

DCs originate from progenitor haematopoietic stem cell (HSC) precursors within the bone marrow and are present in both human and mouse [8]. Classical or conventional DCs (cDC) are divided into two further subsets, cDC1 ($CD11c^{LO}$CD141+) and cDC2 ($CD11c^{HI}$CD1c+). Expression of the Zbtb46 transcription factor has been found to distinguish cDCs from other immune lineages with a shared progenitor, including monocytes and macrophages [9]. Plasmacytoid DCs (pDC; CD123+, CD303+) represent a further subset of DC which also originate from a common DC precursor and is characterised by high expression of the interferon regulatory factor 8 (Irf8) [10].

The core role of DCs is as antigen presentation cells (APCs), mediating the uptake, processing, and presentation of antigen to members of the adaptive immune system. DCs act as sentinel cells, patrolling tissue whilst taking up proteins. DCs take-up exogenous protein through endocytosis prior to peptide loading of either class I or class II major histocompatibility complex (MHC-I/II) molecules. Processed peptides may then be presented to effector cells utilising either MHC-I or MHC-II.

The function of each DC subset is varied, with each having specialisation for distinct roles. The cDC1 class of DC is specialised for the presentation of intracellular pathogen peptides by MHC-I, as well as mediating the presentation of exogenous peptides in a process known as cross-presentation. MHC-I is typically utilised for the presentation of intracellular antigens, however cross-presentation by cDC1 cells allows for the priming of cytotoxic CD8+ T-cells using endocytosed protein. This method of

peptide presentation enables the priming of CD8+ T-cells against tumour associated antigens (TAA) taken up by cDC1 cells [11]. The second class of cDC, cDC2 cells have proven critical for the differentiation and functionality of helper T-cells (T_H). This subclass of DC act to polarise T_H T-cells into their further subclasses (T_H1, T_H2) [12]. A third class of DCs, pDCs, are crucial to both anti-viral and anti-tumour responses [13]. Increased expression of the IRF7 transcription factor enables pDCs to be specialised in the production of type I interferons [14].

1.1.1.3 Macrophages

Macrophages represent a key phagocytic subset of innate immune cells, intrinsically involved in the internalisation and removal of both host and pathogen-derived cellular debris resulting from apoptotic and necrotic cells [15]. Two key subsets of macrophages arise during either embryogenesis, or from HSC. Tissue-resident macrophages (TRM) are seeded in tissue during embryogenesis and are endowed with longevity, allowing for self-renewal. Further to this are a subset of monocyte-derived macrophages (MDM), developing from HSC precursors. Monocyte development into MDMs is predominantly driven by local secretion of the colony-stimulating factor-1 cytokine (CSF-1) by stromal cells during monocyte recruitment [16].

Classically, macrophages were grouped into two subsets, with the 'M1' subset typically associated with a pro-inflammatory response and the production of pro-inflammatory cytokines such as tumour necrosis factor alpha (TNFα), IL-1β as well as release of reactive oxygen species (ROS). The alternative M2 subset subtype is associated with greater capacity for phagocytosis and release of immunosuppressive cytokines such as IL-10 and transforming growth factor β (TGBβ). However, plasticity exists between the two subtypes, with an M1/M2 approach viewed as an oversimplification of macrophage functions [17].

Macrophages induced by localised inflammation within tumours can become tolerant, with prolonged exposure to inflammation resulting in an immunosuppressive phenotype. Tumour associated macrophages (TAMs) exposed to a chronic inflammation may in fact act to promote tumour progression, inducing a state of immunosuppression by release of IL-10 and enabling tumour metastasis [18].

1.1.1.4 Neutrophils

Neutrophils, whilst similar in their capacity for phagocytosis, fulfil a different role to that of macrophages. Developing within the bone marrow from the same common myeloid progenitors (CMP) which give rise to monocytes, neutrophils undergo a series of maturation stages before developing into mature $CD16^{HI}CXCR2^{HI}CD62L^{HI}$ circulating neutrophils. Upon activation, cells upregulate CD11b as well as the granulocyte marker, CD66b, upon degranulation.

Not present within healthy tissue, neutrophils are recruited from circulating blood to sites of infection and inflammation by chemotactic cytokines (chemokines) released by both macrophages and surrounding tissue [19]. This process of neutrophil recruitment also acts to prime neutrophils prior to their activation [20]. Primed neutrophils may subsequently be activated by a number of PRRs such as TLRs and C-type lectin receptors (CLECs) [21]. Further to their capacity to phagocytose, neutrophils can also undergo NETosis. Neutrophil extracellular traps (NETs) are released by neutrophils, acting as a net-like system to bring pathogens into close proximity with neutrophil and macrophage-derived antimicrobial peptides [22].

Anti-tumour activity driven by neutrophils has been shown to induce IL-12 release by TAMs, aiding polarisation of T_H T-cells and driving interferon-gamma (IFN-γ) release [23]. Greater evidence exists however for the pro-tumour activity of neutrophils within the tumour microenvironment (TME). Release of ROS is reported to increase the mutational burden in certain cancer models, increasing DNA damage and promoting tumour development [24].

1.1.1.5 Natural Killer Cells

Natural Killer (NK-) cells represent a further class of immune lymphocyte, forming an intrinsic part of innate immunity. NK-cells recognise targets through a multitude of inherent non-specific inhibitory and activating receptors, acting in balance with one another to facilitate NK-cell mediated immunity [25]. Key to the inhibition of NK activity are receptors which recognise human leukocyte antigen type 1 (HLA-1) molecules, repressing NK activity against host cells which intrinsically express MHC-I [26]. Expression of the Killer Ig-like Receptors (KIRs) family allow for recognition of HLA-A, -B and -C molecules, whilst NK expression of Natural Killer Group 2 Member A (NKG2A) allows for recognition of HLA-E [27]. Both these families of receptors contain inhibitory signalling domains, acting to limit NK activation.

NK-cells express the high-affinity Fc receptors CD16 and CD32, allowing for the mediation of antibody-dependent cellular cytotoxicity (ADCC) following interaction with target-bound IgG antibodies [28]. Also expressed are activating receptors such as Natural Killer Group 2 Member D (NKG2D), which helps identify virally infected and malignant cells. NKG2D binds ligands that are not normally expressed on cells but can be upregulated in cases of cellular stress, including the MHC class I polypeptide-related (MIC) and ULBP families of proteins [29]. Each of these receptors allows for a series of checks and balances to facilitate NK cell activation or inhibition, controlling the immune response mediated by NK-cells.

1.1.1.6 γδ T-cells

CD3+ T-cells may exist in the body as one of two subsets, dependent on their expression of either an αβ T-cell receptor (TCR), or the less common γδ TCR. As with αβ TCR expressing T-cells, γδ T-cells begin their development within the thymus. Development of γδ T-cells has been most extensively studied in mouse models and has shown that γδ development occurs prior to that of αβ T-cells. Signal strength of either αβ or γδ TCR during murine T-cell development drives specific T-cell lineage development, with sufficient γδ TCR signalling in the absence of Notch signalling ensuring commitment to γδ T-cell development [30, 31]. In mice, T-cells heterogenous for a Notch1 mutation were found to favour development of γδ T-cells, indicating an intrinsic role for Notch signalling in T-cell lineage development [31]. Evidence in humans however suggests that Notch signalling is required for development of γδ T-cells [32].

Unconventional γδ T-cells differ from their αβ TCR counterparts in that they can be activated in an MHC-independent manner, allowing recognition of peptides, stress molecules and self-antigens without specific presentation by APCs such as DCs. This ability to recognise targets in the absence of MHC is reflected in their lack of the adapter proteins CD4 and CD8. A large proportion of γδ T-cells express the Vγ9Vδ2 TCR, known to recognise phosphoantigens [33]. Interestingly, these Vγ9Vδ2 T-cells are capable of cross-presentation, acting as APCs to conventional αβ T-cells [34]. This process requires the 'licencing' of γδ T-cells by the recognition of antibody bound to tumour cells, mediating the uptake of TAAs [35].

Activation of γδ T-cells drives the release of pro-inflammatory cytokines such as IFN-γ and TNF, as well as the release of cytolytic molecules such as granzyme A and B [36]. High expression of CD16 enables γδ T-cells to utilise ADCC against opsonised target cells [37]. Release of IFN-γ encourages tumour upregulation of MHC-I, enhancing their recognition by conventional CD8+ αβ T-cells [38].

1.1.2 The adaptive immune system

The adaptive immune system is a specialized component of the immune system capable of identifying and establishing an immune response against specific pathogen targets or malignancies. Its specificity and ability to develop immune memory enables a more precise response which can be recalled upon re-exposure. The adaptive immune system is comprised of two major cells: B-cells and T-cells.

1.1.2.1 B-cells

Developing from HSCs within the bone marrow, B-cells represent a proportion of humoral immunity and are responsible for the production of unique and antigen-specific antibodies. Receptor gene rearrangement is critical to the adaptive immune response, with antibodies generated by B-cell immunoglobulin gene rearrangement subsequently expressed on the surface of B-cells as the B-cell receptor (BCR) or secreted as a soluble immunoglobulin. Whilst B-cells express common innate receptors such as TLRs, the activation of an adaptive B-cell response involves the recognition of a cognate antigen by the BCR. Antigen is endocytosed and presented to specialised T-cells subsets (Follicular helper T-cells, T_{FH}) by MHC-II. This enables T_{FH} to enter an active state, upregulating CD40L and releasing cytokines such as IL-4 and IL-21 [39, 40]. These stimulatory ligands and cytokines provided to B-cells enable them to enter an active state, promoting B-cell proliferation and immunoglobulin class switching for a more effective humoral response.

1.1.2.2 T-cells

The second major component of the adaptive immune system are T-cells. T-cells develop from bone marrow derived progenitor cells called thymocytes within the thymus, and following a series of developmental stages and checks, mature into two distinct subclasses: CD4+ or CD8+ T-cells [41]. These two subclasses have further specialised roles within the adaptive immune response, with further subclasses of CD4+ T-cells such as T_H1, T_H2 and regulatory T-cells (T_{reg}) enabling a more specific response for distinct pathogenic threats such as bacterial and parasitic infections or immune regulation, whilst CD8+ T-cells play a crucial role in the elimination of intracellular pathogens and viruses, as well as control of malignant host cells. T-cell development within the thymus involves the selection of lymphocytes which have undergone a series of receptor recombination steps, analogous to that of BCR rearrangement. As the focus of this thesis, the development of T-cells within the thymus and control of their activation and immune regulation is further reviewed within this chapter.

1.1.3 T-Cell Development

The immune response against malignant cells within the body is mediated though a number of key immune cells. T-cells represent a cell population which allows for a maintained response, enacting targeted anti-tumour activity which seeks to limit tumour development and survival through TCR recognition of antigens. T-cells begin their differentiation within the thymus following the migration of progenitor thymocytes from the bone marrow (Figure 1.1). T-cells express antigen specific receptors, formed through TCR rearrangement to give rise to either $CD4^+$ or $CD8^+$ T cells. Within the thymus, early T-cell development takes place in the peripheral cortex region where thymocytes lacking the CD4 and CD8 receptors migrate towards the central medulla region. As these double-negative (DN) thymocytes begin to migrate, differentiation into the two main subsets of T-cells begins. The most common T-cell subset, αβ T-cells, begin their expression of TCRs following somatic TCR rearrangement. Variable (V), diversity (D), junction (J) rearrangement (VDJ) of αβ TCR DNA is carried out, allowing a diversity of TCRs against both self- and foreign-peptides to form. At this stage, thymocytes enter a double positive stage of development (DP), expressing both the CD4 and CD8 co-receptors alongside a VDJ rearranged αβ TCR. DP thymocytes engage self-peptides in a process known as 'positive selection' to identify DP thymocytes capable of interacting with peptide presented by thymic epithelial cells within the cortex region. To identify thymocytes expressing TCRs capable of interacting with peptides, self-peptides are presented by both MHC-I and MHC-II proteins on the surface of cortical thymic epithelial cells (cTECs). cTECs form a 3D mesh within the cortex through which DP thymocytes migrate, enhancing interactions to allow more effective presentation [42]. The majority of pre-cursor thymocytes undergo 'death by neglect' during positive selection due to a lack of TCR engagement with cTEC expressed MHC. Thymocytes which successfully interact with MHC-I or MHC-II further migrate into the medullar region of the thymus following loss of expression of the inappropriate co-receptor. DP thymocytes which interact with MHC-Ilose their expression of CD4, while thymocytes which interact with MHC-II lose expression of CD8, becoming single positive thymocytes (SP). As SP thymocytes migrate into the thymic medullary region, the process of 'negative selection' takes place. Negative selection allows for the deletion of SP thymocytes which recognise self-peptides, controlling for immune responses against self. Within the medulla, medullary thymic epithelial cells (mTECs) express the autoimmune regulator (AIRE) protein. Expression of AIRE allows for mTECs to present otherwise tissue-restricted antigens to developing SP thymocytes, identifying those which are reactive against self-peptide for deletion [43]. Similar to AIRE-driven presentation of tissue-restricted peptides by mTECs, thymic dendritic cells (tDCs) can mediate the presentation of self-peptides for the deletion of self-reactive SP thymocytes [44]. tDCs can acquire self-antigens from mTECs, presenting peptides with co-stimulatory molecules to drive development of a regulatory subset of T-cells (T_{reg}). Strong binding of self-antigens to CD4+ SP thymocytes, alongside binding of the co-stimulatory receptor CD28 and concurrent interleukin-2 (IL-2) signalling promotes

upregulation of the T_{reg} transcription factor, forkhead box protein 3 (FOXP3). T_{reg} differentiation during this stage of negative selection allows for the development of a T-cell subset which recognise peripheral self-peptide but promote an immunosuppressive response.

SP thymocytes which successfully navigate both negative and positive selection undergo a final maturation stage, priming them for their role as functional T-cells. This late-stage maturation is dependent upon Nuclear factor kappa-light-chain-enhancer of activated B-cells (NFκB) signalling and results in thymocytes changing from an apoptotic response to strong TCR signalling, to an activated proliferative response [45]. These changes allow mature T-cells to egress from the thymus and enter circulation and secondary lymphoid organs such as the spleen and more localised lymph nodes through CD62L upregulation.

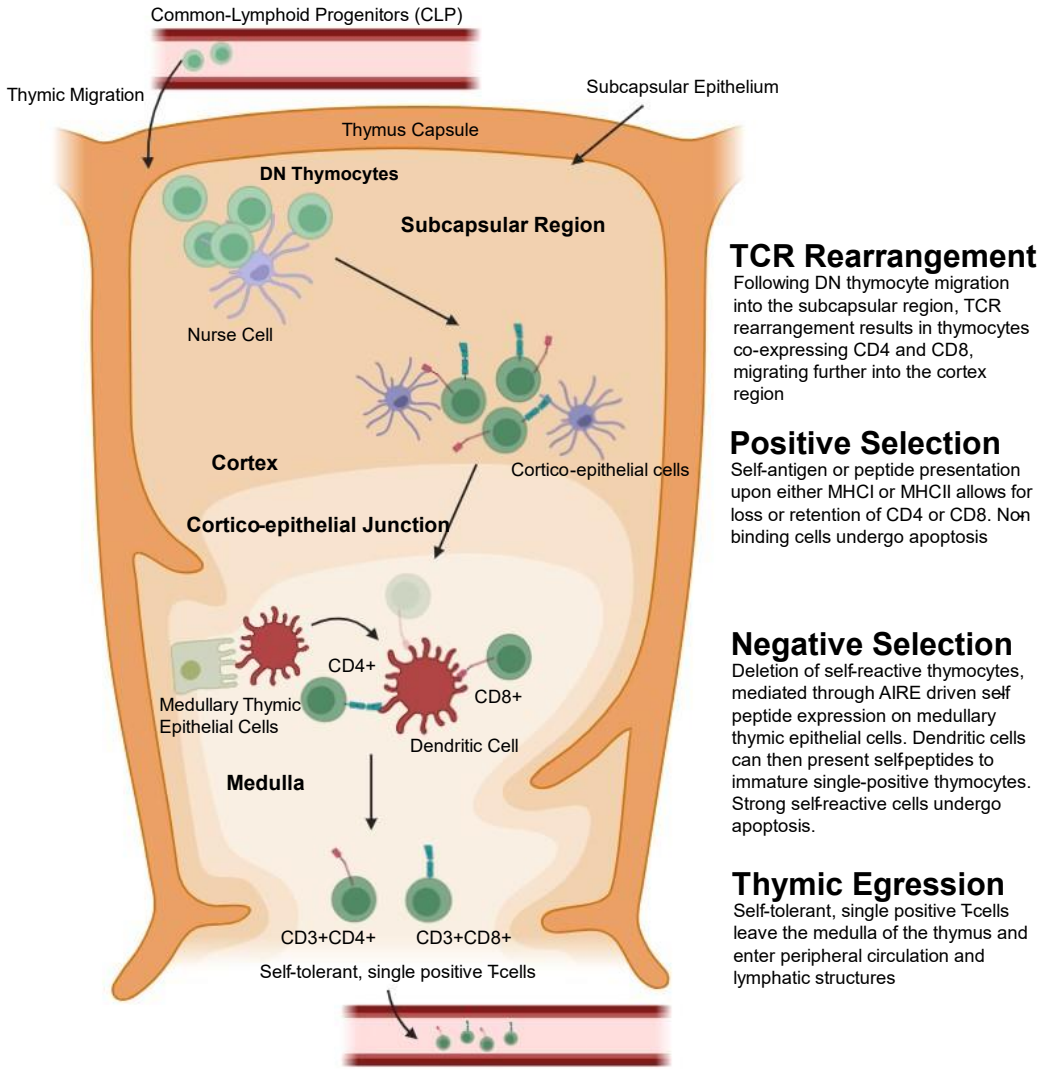

Figure 1.1 T-cell Development Within The Thymus

A) Schematic overview of the development of T cells within the thymus. Briefly, CD4-CD8- thymocytes (DN) migrate from the bone marrow to the thymus where they move towards the central medullar region. Following TCR rearrangement, they are exposed to MHC I and MHC II on the surface of cortical epithelial cells to ensure a capable interaction. Cells failing to recognise MHC I or MHC II fail to proceed (Positive Selection) and undergo apoptosis mediated cell death. Viable cells progress

and are exposed to self-peptides through medullary thymic epithelial cells, under the guidance of the AIRE transcription factor, and antigen presenting cells (APCs) (Negative Selection). T cells which exhibit limiting binding of self-peptides exit this selection process as single positive CD3+CD4+ or CD3+CD8+ T cells, egressing from the thymus to the periphery. (Figure adapted from Janeways Immunobiology, 5th Edition, 2005).

1.1.4 T-cell Receptor Activation

The maturation and egress of T-cells from the thymus results in the circulation of mature CD4 and CD8 T-cells with functional TCRs. CD4+ and CD8+ T-cells represent distinct subclasses of effector T-cells, with phenotypical differences allowing each to be better suited for certain roles. Common to both however is their use of unique TCRs to actively survey for their cognate ligand. The majority of mature T-cells which leave the thymus express a TCR complex comprised of an α and β chain (αβ T-cells). Whilst this TCR is capable of recognising peptides when presented in the context of an MHC-I or MHC-II molecule, it inherently lacks the capacity to induce T-cell activation alone. Therefore, TCRs form a complex with the CD3 chains δ, γ, ε, and ζ (Figure 1.2). Intracellular tyrosine-based activation motifs (ITAMs) present within the intracellular domains of CD3 provide phosphorylation sites, mediating signal transduction through the TCR:CD3 complex [46]. Lck, a member of the serine family kinases (Src) associated with the CD4 and CD8 co-receptors, acts to phosphorylate these CD3 ITAM sites. Phosphorylation of the CD3 ITAM allows for recruitment of the ZAP70 kinase, which upon further LCK-mediated phosphorylation can trigger the downstream cascade of TCR signalling resulting in the activation of key transcription factors such as Nuclear factor of activated T-cells (NFAT), NFκB and the mitogen-activated protein kinase (MAPK) family [47]. This complex of molecules at the site of the T-cell interaction with an APC forms a synaptic region known as the immune synapse, or the supramolecular activation cluster (SMAC), with a common bullseye-like structure and organisation of key molecules. CD3, CD4 and CD8 accumulate within the central SMAC region (cSMAC) with the TCR, whilst LFA-1, a key adhesion molecule, clusters within the peripheral SMAC region (pSMAC). Outside of these more central regions, the phosphatase molecule CD45 predominantly accumulates in a region known as the distal SMAC (dSMAC).

Whilst this TCR signalling constitutes one aspect of T-cell activation, T-cells in fact require a multitude of signals to induce effective activation termed Signals 1, 2 and 3. The recognition of a peptide by TCR constitutes ‘Signal 1’, whilst Signal 2 consists of interactions between specific co-stimulatory receptors with their ligand on antigen-presenting cells, such as CD28 interactions with CD80/86. The third signal, Signal 3, is reliant on specific signalling received by a naïve T-cell by extracellular cytokines.

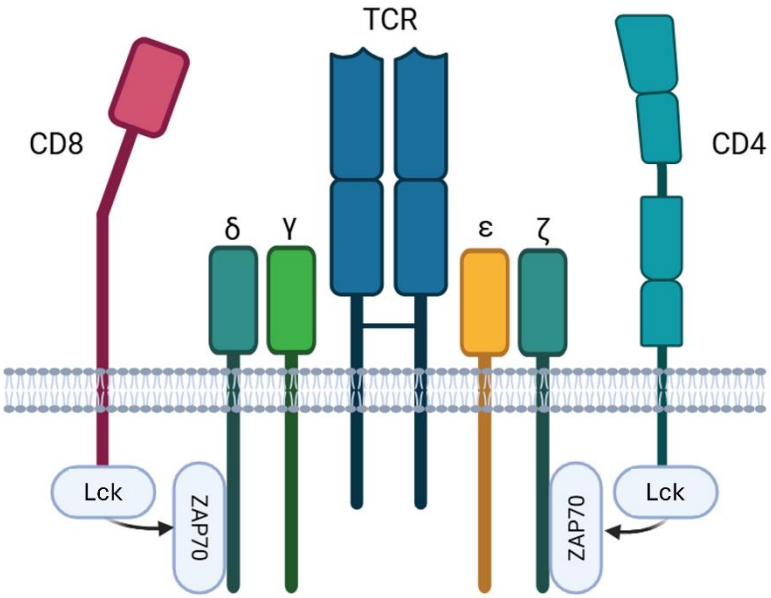

Figure 1.2 Association of CD3, CD4 and CD8 molecules with the TCR

A) Schematic highlighting the association of the TCR with the CD3 molecules δ, γ, ε, and ζ. Shown also are the adapter molecules CD4 and CD8 which are associated with the Lck kinase, mediating CD3 ITAM phosphorylation and recruitment of ZAP70. Diagram generated using BioRender.

1.1.5 CD4+ T-cell Activation

CD4 T-cells recognise peptides when presented by MHC-II molecules on the surface of APCs such as DCs and B-cells. Naïve CD4 T-cells are capable of further differentiation, with the most common of these being T_H1, T_H2, and the previously mentioned T_{reg} subset.

Differentiation of naïve CD4+ T-cells into specialised subsets is dependent on initial activation by Signals 1 and 2 in conjunction with specific cytokines (Signal 3). The provision of IL-12 and IFN-γ during naïve CD4+ T-cell activation results in the transcription factor T-bet mediating T-cell differentiation into a T_H1 phenotype [48, 49]. T-bet, a T_H1 specific transcription factor, induces the downstream expression of key T_H1 cytokines such as IFN-γ, as well as upregulating the expression of the IFN-γ receptor (IFNGR). Upregulation of both IFN-γ and its receptor enables for a positive feedback loop, promoting self-activation of T_H1 CD4+ T-cells [50]. This phenotype allows T_H1 T-cells to be well suited for counteracting intracellular pathogens.

As with TH_1 CD4+ T-cells, differentiation of naïve CD4+ T-cells into the T_H2 subset is reliant on the provision of extracellular cytokines. Differentiation into the T_H2 subset is reliant on exposure to IL-4 and IL-2 during naïve CD4+ T-cell activation. IL-4 binding and subsequent signalling through the IL-4 receptor (IL-4R) results in signal transducer and activator of transcription 6 (STAT6) activation, upregulating the T_H2 transcription factor GATA3 [51]. Expression of GATA3 enables T-cell expression of IL-4, allowing for a positive feedback loop to enhance T_H2 differentiation. Differentiated T_H2 cells are notable for their role in extracellular defensive mechanisms, acting as the predominant T-cell subset

against extracellular pathogens such as helminths. Through secretion of IL-4, T_H2 cells enable antibody class switching in B cells to promote secretion of IgE antibodies, an Ig subclass better suited for promoting clearance of extracellular pathogens by mast cells.

Whilst the majority of T_{reg} cells develop within the thymus during T-cell development (tT_{reg}), a subset of T_{reg} may also develop as induced T_{reg} (iT_{reg}) in the periphery. These CD4+FOXP3+ iT_{reg} develop from CD4+FOXP3- T-cells which express the IL-2 receptor alpha chain (CD25) following exposure to transforming growth factor β (TGF-β) and IL-2 during T-cell activation and account for approximately 10% of peripheral CD4T-cells [52].

1.1.6 CD8+ T-cell Activation

Activation of naïve CD8+ T-cells by both Signals 1 and 2 results in their expansion into distinct subsets, each with specific effector functions. These subsets include the memory precursor effector cells (MPEC) as well as the shorter-lived effector cells (SLEC) [53]. These two subsets can be differentially defined by surface expression of either the IL-7 receptor (IL-7R) by MPECs, or by expression of the killer-cell lectin-like receptor G1 (KLRG1) by SLECs [54]. Whilst both these subsets may be differentiated by their expression of either IL-7R or KLRG1, both can be characterised by high expression of the effector molecules granzyme B (GRZB) and IFN-γ [55]. The differentiation of naïve CD8+ T-cells into MPEC or SLEC subsets has been suggested to be reliant on the strength of IL-12 signalling, and subsequent downstream T-bet activity. Strong IL-12 signalling and subsequent T-bet activity promotes SLEC differentiation, whilst weaker IL-12 signalling results in MPEC development [54]. This provision of IL-12 to naïve CD8+ T-cells is commonly from APCs such as DCs during their presentation of antigen to T-cells [56]. Differences between these two subgroups also arises when assessing their longevity. While MPECs have the potential to remain as a pool of long-lived memory CD8+ T-cells, SLECs are found to die during the contraction phase of an infection by apoptosis. SLEC death is induced by the increased extracellular presence of TGF-β, acting to inhibit the anti-apoptotic molecule Bcl-2 [57].

Signal 1 activation of CD8+ T-cells utilises the intracellular peptide loading of MHC-I by target cells. However, DCs are capable of presenting exogenously sourced peptides on MHC-I to CD8+ T-cells by cross-presentation [58]. This non-classical method of peptide loading by DCs allows for the priming of naïve CD8+ T-cells with extracellular peptides and is an important method of priming these cytotoxic T-cells against TAA. When CD8+ T-cells are activated by cross-presentation without the addition of Signal 3 (IL-12) from a DC, an impaired clonal expansion phase takes place whereby cells proliferate but become tolerant to any further stimulation and so fail to develop the appropriate cytotoxic functions normally associated with effector CD8+ T-cells [59]. Notably however is that when T-cells are consistently exposed to their cognate antigen, such as in the case of chronic infections or within a

tumour microenvironment (TME), T-cells may enter a state of exhaustion. These exhausted T-cells lose their effector functionality and begin to constitutively express inhibitory receptors such as programmed cell-death protein 1 (PD-1) and cytotoxic T-lymphocyte antigen 4 (CTLA-4). Whilst this mechanism of T-cell inhibition can serve to limit an overactive T-cell response in the case of autoimmune disease, it can also act to limit an appropriate response in the case of cancers [60].

1.1.7 T-cell Co-Stimulation

Whilst initial recognition of target peptides and the subsequent activation of T-cells is mediated through TCR interactions with peptide:MHC complexes, the requirement of additional co-stimulation is equally critical for effective T-cell activation. Co-stimulatory molecules function to regulate the activation of T-cells and serve a critical role in T-cell differentiation, downstream effector functionality, and overall survival of T-cells.

Mediators of T-cell co-stimulation commonly fall into either the Immunoglobulin superfamily (IgSF) or the Tumour Necrosis Factor Receptor (TNFR) superfamily of proteins. Whilst members of these families cannot mediate T-cell activation alone, they can act in unison with both the TCR and one another to provide necessary signals to support TCR-mediated T-cell activation.

Forming a crucial part of the T-cell activation Signal 2 is CD28, a member of the IgSF which acts to augment the primary TCR signal. Present within the cSMAC region, CD28 acts to bind its cognate ligands CD80/86 on APCs and is expressed on both naïve and activated CD4+ and CD8+ T-cells [61]. The necessity of CD28 in the activation of T cells becomes clear in models of CD28 knockout (KO) mice, whereby T-cell responses to antigen and subsequent differentiation is limited [62].

CD28 contains three distinct motifs within its ICD: a YMNM sequence, a class I proline rich domain (PRD) and a YAPP sequence. The most characterised of these is YMNM, a YxxM motif which when tyrosine phosphorylated, can act to bind to the SH2 domain of phosphatidylinositol 3-kinase (PI3K) or growth factor receptor-bound protein 2 (Grb2) [63, 64]. The kinase activity of PI3K in turn results in the phosphorylation and conversion of phosphatidylinositol (4,5)-biphosphate (PIP_2) to phosphatidylinositol (3,4,5)-triphosphate (PIP_3), activating the downstream kinase Protein Kinase B (Akt) [61] (Figure 1.3). Akt activation through CD28 subsequently results in upregulation of the pro-survival and activation cytokine, IL-2, as well as promoting expression of the anti-apoptotic protein Bcl-X_L [65, 66]. Similarly, activation of the LCK kinase has been linked to the proline rich region of CD28 through the adapter protein, Grb2 [67]. Containing an SH3 binding site within this poly-proline domain, CD28 can bind Grb2, mitigating the need for tyrosine phosphorylation as with Src-homology 2 (SH2) binding of the CD28 YMNM domain [68]. These downstream effects of CD28 ligation synergise with TCR signalling to promote T-cell activation and survival (Figure 1.2).

A second crucial molecule responsible for T-cell activation is 4-1BB, a member of the TNFR superfamily. 4-1BB mediates its signalling through a group of scaffold proteins which facilitate the recruitment and binding of kinases key to 4-1BB signalling. Following the binding of 4-1BB with its cognate ligand, 4-1BBL, the 4-1BB ICD associates with TNF receptor associated factor 1/2 (TRAF-1/2). By bringing together multiple TRAF-1/2 proteins, each containing intrinsic E3 ubiquitination domains, continuous ubiquitination of neighbouring TRAF-1/2 proteins is thought to result in a chain of ubiquitin molecules to which a central signalosome consisting of both Transforming growth factor-β (TGF-β)-activated kinase 1 (TAK1) and TAK1-binding proteins (TAB1/2) can bind [69, 70] (Figure 1.3). The formation of this signalling complex is thought to result in the canonical activation of the NFκB pathway, mediating T-cell activation. TRAF-1 expression is itself found to be induced through the NFκB pathway and so involvement in 4-1BB signalling is thought to take place following initial T-cell activation [71].

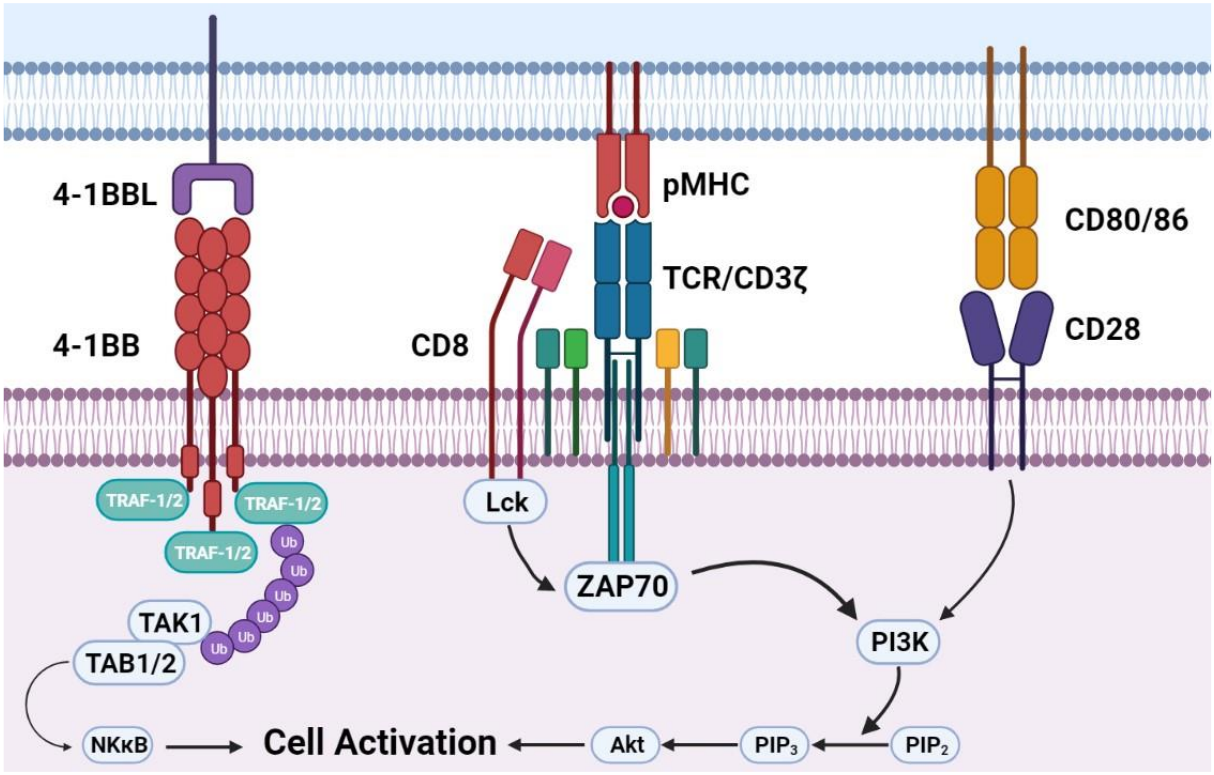

Figure 1.3 TCR, CD28 and 4-1BB activation results in a synergetic effect to promote cell activation and survival

Following TCR ligation of an peptide:MHC complex, the kinase LCK associates with the CD4 or CD8 coreceptor to phosphorylate the ITAM present in CD3ζ. Subsequent recruitment of ZAP70 is further phosphorylated by localised LCK to activate PI3K. CD28:CD80/86 ligation results in CD28 ICD phosphorylation by kinases LCK and FYN, allowing for the binding of PI3K through its resident SH2 domain, activating PI3K mediated PIP_2 phosphorylation to form PIP_3. PIP_3 can then in turn activate Akt to result in sustained cell survival. 4-1BB binding of 4-1BBL results in 4-1BB clustering and association with TRAF-1/2. Ubiquitination of TRAF-1/2 forms a scaffold to allow TAK1 and TAB1/2 complexes to form, which in turn promotes activation of the canonical NFκB pathway. While not shown for simplicity, also involved downstream of these activating signals is the NFAT, NF-κB, AP-1 and MAPK pathways.

CD226, also known as DNAM-1, is a member of the IgSF group of co-stimulatory proteins and expressed on CD8+ T-cells and NK cells [72]. CD226 binds to the polio-virus receptor (PVR, CD155) and, albeit weakly, CD112 [73]. This interaction is mediated through the two most membrane-distal domains, competing for binding of CD155 with both 'T-cell immunoreceptor with Ig and ITIM domains' (TIGIT) and CD96 [74]. Upon binding of CD226 to its cognate ligands, CD226 provides an activating signal. This signalling is initiated by the phosphorylation of a serine residue within the CD226 ICD by Protein Kinase C (PKC) and results in physical association with the adhesion molecule, lymphocyte function-associated antigen 1 (LFA-1) [75]. Subsequent binding of LFA-1 to intercellular adhesion molecule-1 (ICAM-1) on an interacting cell results in the recruitment of the kinase FYN to phosphorylate the CD226 Y319 residue within the CD226 ICD. However, more recent data has suggested that both FYN and LFA-1 are in fact dispensable for CD226-mediated T-cell activation [76]. Mutational analysis of the Y319 residue has shown that its phosphorylation is critical for initiating CD226 mediated signalling, allowing the binding of the adapter protein Grb2 through its SH2 domain and facilitating the downstream activation of PI3K and Akt [76].

1.1.8 T-cell Inhibition

To counteract the activation of T-cells by both TCR and co-stimulatory proteins, and to limit excessive T-cell activation, a range of inhibitory receptors are expressed on the surface of T-cells. Chronic activation of T-cells can result in a state of cell exhaustion, whereby T-cells consistently exposed to high levels of cognate antigen become non-functional. While this can be beneficial in the context of an auto-immune disorder, whereby T-cells recognise self-antigens as foreign and are inappropriately activated, in the context of tumour recognition it can result in a population of cells which ultimately fail to respond to a legitimate target. Two of the most researched inhibitory receptors expressed on T-cells are PD-1 and CTLA-4.

The PD-1 protein has two ligands: programmed-death ligand 1 and 2 (PD-L1 and PD-L2). PD-L1 is most commonly expressed on macrophages, however it is also expressed by tumour cells as a method of circumventing immune recognition to limit the capacity of tumour infiltrating lymphocytes (TILs) to mount effective responses. Malignancies such as gastric or ovarian cancer can promote an immunosuppressive TME by upregulating PD-L1, often resulting in a poorer prognosis for patients [77]. The expression of PD-1 is rapidly induced within 24 hours of T-cell activation as a method of T-cell tolerance when T-cells are activated in the absence of IL-2 [78]. Following the engagement of a pMHC by TCR, the transcription factor NFAT is dephosphorylated and enters the cell nucleus to associate with the CD28-induced Activator Protein-1 (AP-1) transcription factor to enable PD-1 upregulation [79] (Figure 1.4). Whilst PD-1 expression is lost following antigen clearance, in models of

chronic infection with sustained antigen presence, PD-1 expression is preserved and T-cells may enter a state of anergy [78, 80]. The upregulation of PD-L1 by malignant cells can allow the attenuation of TILs, circumventing an effective immune response. As an IgSF member, PD-1 contains two distinct tyrosine-based signalling motifs: an immunoreceptor tyrosine inhibitory motif (ITIM) and an immunoreceptor tyrosine-based switch motif (ITSM). Activation of PD-1 by either PD-L1 or PD-L2 results in the recruitment of Src homology region 2-containing protein tyrosine phosphatase 2 (SHP-2). Close proximity of SHP-2 to the TCR allows for SHP-2 mediated dephosphorylation of ZAP70, attenuating TCR activation [81]. More recent studies however have suggested that PD-1 recruitment of SHP-1 may in fact preferentially target the CD28 signalling domain for dephosphorylation, acting to attenuate T-cell co-stimulation [82].

A second mediator of T-cell inhibition is CTLA-4, which acts to inhibit T-cell activation by outcompeting CD28 for the binding of CD80/86 [83] (Figure 1.4). Primarily stored within intracellular compartments in naïve and unstimulated T-cells, CTLA-4 is trafficked to the cell surface upon T-cell activation as a result of increased intracellular calcium levels. Surface expression of CTLA-4 following trafficking is primarily focussed to the point of TCR activation [84]. As a CD28 homolog, CTLA-4 exhibits a much greater affinity for CD80/86 than CD28 (K_d CTLA-4:CD80/86; 0.42µM, K_d CD28:CD80/86; 4µM) resulting in CTLA-4 acting as an effective inhibitor of CD28:CD80/86 binding [85]. CTLA-4 also contains two tyrosine-based motifs, YVKM and YFIP. In addition to outcompeting CD28 for binding of CD80/86, the presence of the YVKM motif can contribute to the suppression of TCR activation, although this role has been shown to be dispensable for mediating T-cell inhibition by CTLA-A [86].

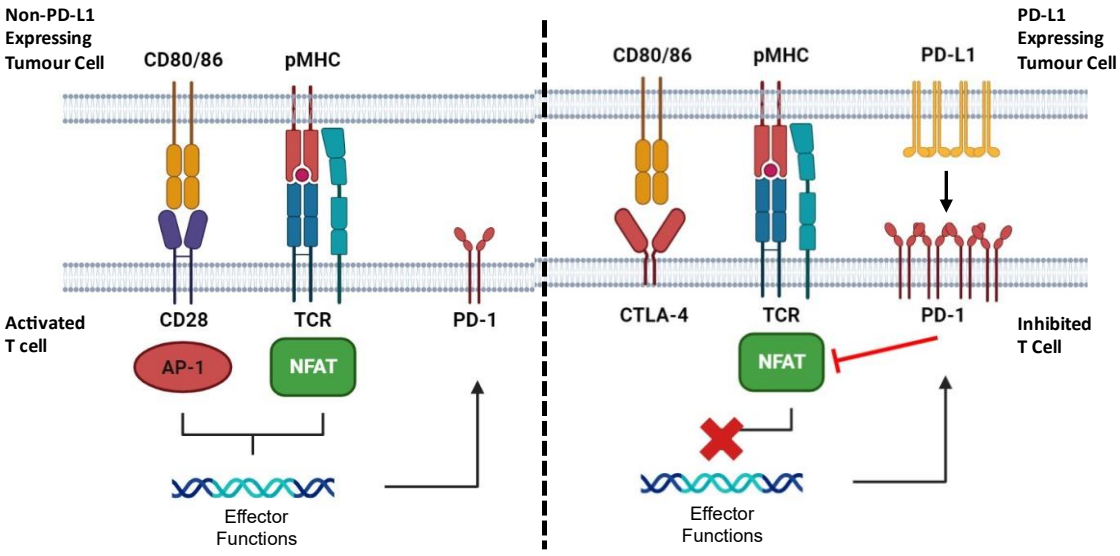

Figure 1.4 Overview of CTLA-4 and PD-1 mediated T-cell inhibition

Translocation of NFAT and AP-1 to the cell nucleus following TCR and CD28 activation results in a synergistic effect to promote both cell effector functions and PD-1 upregulation. Expression of PD-L1 on tumour cells and subsequent binding of PD-1 on T-cells results in PD-1 mediated inhibition of TCR signalling through ZAP70 dephosphorylation. CTLA-4 trafficking to the cell surface following CD28

downregulation and endocytosis results in competitive binding of CD80/86 to further limit CD28 binding. (Adapted from Simon et al., 2017.)

TIGIT (T-cell immunoglobulin and ITIM domain), a member of the IgSF, has also been shown to mediate an inhibitory signal in T cells. Expressed predominantly on T and NK cells, TIGIT contains both an ITIM and immunoreceptor tyrosine tail-like (ITT-like) motif within its ICD. While TIGIT can bind both CD112 and CD113, its primary ligand is CD155, competing with both CD226 and CD96 to form a competitive network analogous to that of CD28/CTLA-4/CD80/86 [73, 87]. TIGIT mediates T-cell inhibition via multiple mechanisms of action. Firstly, the binding of T-cell expressed TIGIT to DC expressed CD155 has been found to induce DC upregulation of the immunosuppressive cytokine, IL-10 [88]. This interaction induces phosphorylation of CD155 and the downstream kinase extracellular signal-regulated kinase (ERK). A further method of T-cell inhibition utilises intrinsic inhibitory domains within the TIGIT ICD. TIGIT is recruited to the immune synapse following T-cell interaction with a CD155-expressing target and can directly limit cytokine secretion utilising its ITT-like domain [89]. The overexpression of CD155 on melanoma cells has been shown to suppress the activity of cytotoxic CD8+ T-cells and found to be intrinsically linked to TIGIT signalling, with T-cell inhibition sustained even when TIGIT bound a truncated form of CD155 lacking an intracellular region [90]. The requirement of TIGIT to control T-cell activation is notable in murine models, whereby the loss of TIGIT expression is seen to result in hyperresponsive T-cell activation [91].

The role of TIGIT has been assessed in NK cells, with differences between the roles of inhibitory domains noted between human (huTIGIT) and mouse TIGIT (mTIGIT). As with huTIGIT, mTIGIT contains both an ITIM and an ITT-like domain. Loss of the huTIGIT ITIM domain, either through truncation or point mutation, results in enhanced targeted killing by NK cells against CD155 expressing cells [92]. Following the binding of CD155, TIGIT is phosphorylated by Src-family kinases FYN and LCK and acts to recruit either the Grb2 adapter protein or β-arrestin-2 through their SH2 binding sites [93, 94]. These adapter proteins can then mediate the binding of SH-2 containing inositol 5' polyphosphatase 1 (SHIP1), converting PIP_3 to PIP_2 and inhibiting PI3K activation and downstream MAPK signalling cascade. In addition to the inhibitory signalling mediated by ligand interactions, TIGITs affinity for CD155 binding is much greater than that of CD226 (TIGIT:CD155 K_D = 1-3nM, CD226:CD155 K_D = 119nM) [88]. This increased affinity is thought to outcompete CD226, limiting CD226-mediated T-cell activation.

1.2 Cancer

Cancer represents one of the most wide-spread diseases worldwide, with 1 in 2 people predicted to be diagnosed during their lifetime [95]. Cancer may arise from a multitude of intrinsic and extrinsic

factors, however these all result in a cell which is capable of unchecked ability to infiltrate, expand, and cause disease. Mutations gained and inherited by cells can override checks in place which act to control cell division, allowing cells to proliferate freely and unconstrained. This continuous proliferation of cells can lead to the further accumulation of mutations in a greater number of cells, resulting in a population of cancerous cells containing numerous mutations. While normally these cells may be identified by the immune system as cancerous, malignant cells can circumvent an immune response utilising a multitude of methods to evade recognition. Promoting and enhancing the immune recognition of cancerous cells whilst limiting the ability of cancerous cells to inhibit immune responses can allow for more effective immune recognition and subsequent targeting of cancer cells. Therefore, a clearer understanding of the immune system and the mechanisms utilised to control and eliminate cancerous cells is pivotal in the development of clinical therapeutics.

1.2.1 Recognition of cancer

While the role of the immune system and how it acts as a sentinel to patrol, recognise and eliminate malignant cells was first proposed over 50 years ago, more extensive research has revealed how immunoediting can shape the progression of cancer [96, 97] . This theory of cancer development is known as the three E's: 'Elimination, Equilibrium and Escape'. This theory describes the gradual loss of control over malignant cells.

Within the elimination phase of this theory, immune cells are successful at the recognition and deletion of malignant cells. Following a cells loss of intrinsic ability to correct acquired DNA mutations, changes to the cell begin to activate innate immune responses. This can be a result of localised changes to tissue during tumour development, including the invasiveness of tumour tissues and local angiogenesis, two key stages of early cancer development. These two characteristics of tumour progression can induce production of pro-inflammatory cytokines such as IFN-γ, alerting immune cells to local tissue changes. Alerted by the secretion of pro-inflammatory cytokines, an innate immune response is activated, mediated by NK cells and γδ T-cells. These respond by recognising non-specific ligands commonly expressed on the surface of malignant cells, acting to limit further expansion and tissue invasion [98, 99]. Malignant cell downregulation of MHC-I to limit CD8+ T-cell responses allows for recruited NK cells to differentiate cancerous cells from host utilising KIRs. Similarly, the upregulation of NKG2D ligands by cells during periods of cellular stress mediates NK activation and can override KIR inhibitory signals should MHC-I be retained by tumours [100]. γδ T-cells represent a unique subset of innate immune cells, essential for containing early tumour development. The γδ T-cell subset expresses receptors with restricted specificity as opposed to the large variability found in conventional αβ T-cells, and are activated by specific non-peptide phosphorylated antigens such as heat-shock proteins or butyrophilins [101, 102] . Butyrophilins, a family of proteins which belong to the IgSF and expressed by certain cancers are known to modulate the

activation of γδ T cells [103]. These proteins can be upregulated during periods of cellular stress as a result of oncogenic changes, and expression of butyrophilin 3A1 (BTN3A1) is found to positively correlate with immune cell infiltration within TMEs [104].

Complimentary to the innate immune systems control of tumour growth is that of the adaptive immune system. Release of TAAs following innate elimination of malignant cells can result in the priming and activation of antigen-specific T-cells, as well as their subsequent migration. This recruitment of antigen-specific CD8+ T-cells is a result of the ability of cDC to take up TAA and cross-present to naïve CD8+ T-cells via MHC-I [105]. This cross-presentation method requires both IFN- γ and STING, enhancing the cytotoxic activity of $CD8^+$ T cells through the release of IL-12 [106]. The exposure of tumour cells to IFN-γ from both innate and adaptive responses enables the assembly of the inflammasome, a multi-protein complex which can act to upregulate MHC-I. This increased expression of MHC-I enhances immunogenicity, enabling greater immune recognition by $CD8^+$ T cells [107].

Upon recognition of target cells, cytotoxic CD8+ T-cells respond by releasing perforin, present within granules in cytotoxic cells, which acts to polymerise and puncture the cell surface to allow access of the granzyme family of proteins [108]. Granzymes, a family of serine proteases found within granules of both cytotoxic T-cells and NK cells, act as pro-apoptotic molecules and have been identified as triggering distinct pathways of induced cell death. The release of these cytotoxic granules is highly organised and directional, with cytotoxic T-cells and NK cells releasing granules at the site of the immune synapse. In humans, there are 5 active granzymes – Granzymes A, K, B, H and M. Within primed CD8+ T-cells, granzymes are found to be co-expressed in granules with perforin, with most cells expressing only one type of active granzyme [109]. The two most common, A and B, initiate cell death through distinct mechanisms from one another. Granzyme A acts independently of caspases, acting to target nuclear proteins for degradation such as key DNA repair proteins (Ku70) and histones [110]. Granzyme B, the most well characterised of the granzymes, acts to mimic the action of caspases to activate the initiator caspases 8 and 10, thereby triggering cell apoptosis [111].

The equilibrium phase of cancer development describes a phase whereby the most immunogenic of cells have been eliminated by immune responses, while tumour cells not immunogenic enough to stimulate a response remain in a senescent-like state. A study by Koebel et al. highlighted that while mice did develop small but stable tumour masses upon carcinogen exposure, tumour control was rapidly lost following the inhibition of certain immune components, suggesting that in certain cases, cancers may exist in a state of dormancy before expanding when the immune landscape is advantageous [112].

The final phase of cancer development within the 'Three E's' paradigm is the escape phase. Here, malignant cells which have gained mutations advantageous to circumventing immune detection

expand with limited resistance. This phase is linked to the development of tumour cells with the ability to undermine immune responses, orchestrated by the release of immunosuppressive cytokines such as TGF-β and IL-10 by recruited T_{reg}. Further methods of immune escape can result from a high mutational burden and loss of specific antigen expression, resulting in limited recognition by CD8+ T cells. The prolonged exposure of tumour cells to IFN-γ can place selective pressure on cells, resulting in desensitisation. IFN-γ induces the expression of MHC-I on target cells, promoting the immunogenicity of target cells [113]. Desensitisation of cells to IFN-γ can therefore result in decreased MHC-I presentation of peptides, limiting malignant cell recognition by effector immune cells [114]. Loss of tumour expressed MHC-I plays a crucial role in tumour escape, and has been shown to be mediated by multiple components of peptide processing including deficiency of antigen processing 1 protein (TAP1) and loss of HLA class 1 proteins [115].

1.3 Cancer Immunotherapy

Cancer immunotherapeutics encompass a broad range of therapies which utilise components of the immune system to target, enhance, and regulate the bodies anti-tumour immune response. These therapies include the use of synthetic antibodies designed to target molecules on both immune cells and cancer cells. Additionally, some treatments involve engineering patient immune cells, such as chimeric antigen receptor T-cells (CAR-T), to specifically enhance cytotoxic activity against tumours and boost the immune system's ability to recognize and attack cancer.

1.3.1 Antibodies

Antibodies constitute a large proportion of recent advances in anti-cancer therapeutics, allowing the direct targeting of tumour cells while mediating cell-based anti-tumour responses. Belonging to the IgSF of proteins, antibodies secreted by B-cells as soluble forms of the BCR allow for highly specific responses. Opsonisation of tumour cells by antibodies enables activation of a multitude of immune responses, including the complement system, ADCC, ADCP, and bystander immune cell activation [116]. The potential for utilising antibodies to promote both the effective targeting of cancer and advancing anti-tumour immune activity has been demonstrated extensively, however current antibody therapies have limitations, with low therapeutic response and loss of target expression often resulting in inadequate responses in a number of patients. Therefore, further work is essential to enable identification and targeting of other potential targets.

Antibodies are generated as 1 of 5 distinct classes, IgG, IgM, IgA, IgD and IgE, with B-cell class switching enabling the generation of antibodies best suited for certain immune responses. These antibodies consist of two distinct regions, a Fab region containing the antigen recognising variable domains, and an Fc region, capable of interacting with Fc Receptors (FcR) on effector cells, as well as

mediating activation of the classical complement system. Each antibody is composed of two heavy (H) and two light (L) chains, with each light chain being either Lκ or Lλ. Each heavy and light chain consists of one variable domain (V_H and V_L), containing the site of antigen recognition (Figure 1.5).

IgG antibodies represent the most predominant antibody class, with 75% of circulating antibody being one of four IgG subclasses. Of these, IgG1 is the most prevalent (67% of total IgG). IgG2 are the second most prevalent (22%), whilst IgG3 and IgG4 make up 7 and 4%, respectively. Each subclass exhibits different capacity for Fc-gamma receptor (FcγR) binding, as well as various properties pertaining to their capacity to induce complement activation or target opsonisation. While IgG1 is capable of inducing completement activation, IgG4 can not [117]. Whilst it was previously held that the IgG4 subclass could not opsonise target cells to enable their deletion, more recent work has opposed this view. Treatment of patients with refractory rheumatoid arthritis using the anti-CD52 antibody Alemtuzumab found that IgG4 antibodies could deplete peripheral blood lymphocytes [118].

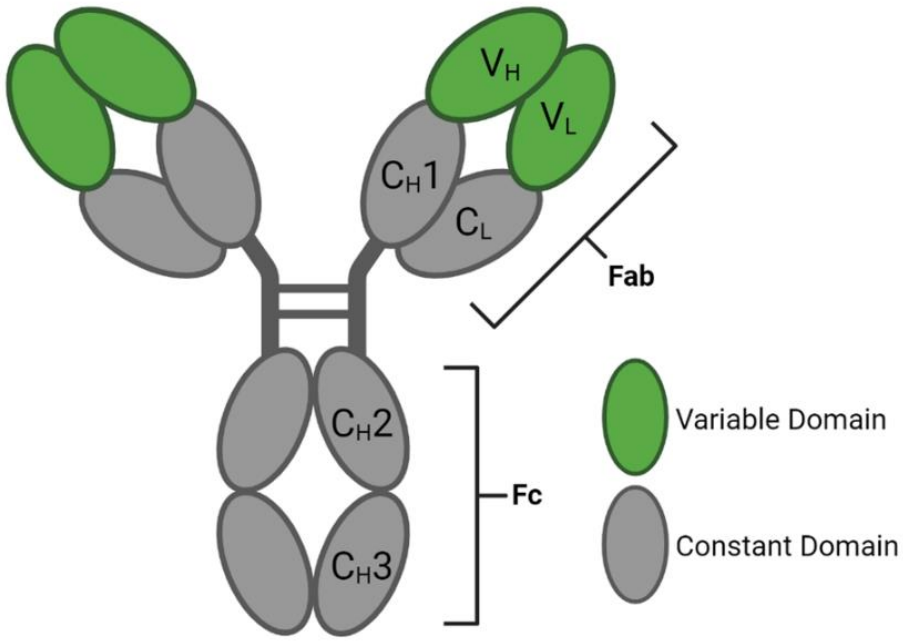

Figure 1.5 Schematic overview of antibody structure

A) Simplified diagram indicating the specific regions common to antibodies. Highlighted in green is the variable region of both the heavy and light chains. Labelled are the Fab regions and Fc regions.

These IgG subclass characteristics are important to consider when designing novel antibody therapeutics, with their capacity to bind activating and inhibitory FcγRs an important attribute when considering antibody design [119]. The vast majority of approved antibody therapeutics for cancer utilise the IgG1 isotype due to their high potency and capacity to activate bystander immune cells, however a small number of therapies utilise either the IgG2 (Panitumumab) or the IgG4 (Nivolumab, Pembrolizumab) subclass [120]. The use of these non-IgG1 isotypes is predominantly employed when the involvement of FcR expressing cells is either not beneficial or not required for therapy.

Additional advances have also been made in the field of Fc-engineering. IgG antibodies are commonly altered with the addition of a fucose sugar by fucosylation. The removal of this core fucose from IgG1 antibodies is found to enhance the binding of FcγRIIIA, improving ADCC [121]. Likewise, mutations of S239D and I332E are found to enhance FcγRIIIA binding and ADCC, whilst not limiting complement activation [122]. Engineering of antibodies targeting receptors such as 4-1BB has proven successful, with the increased binding of an anti-4-1BB IgG4 antibody to FcγRIIB enabling strong antibody cross-linking and has proven promising in early-stage clinical trials [123, 124].

1.3.2 Current antibody therapeutics

Current antibody therapies for the treatment of cancer tend to fall under two categories, dependent on their mechanism of action. Direct targeting antibodies act to directly target tumour or immune cells, inducing receptor signalling or enabling the activation of innate mechanisms to mediate anti-tumour activity. Immunomodulatory antibodies however interact with immune receptors, to either propagate or inhibit immune cell signalling. These can be agonistic in action, or by inhibiting receptor-ligand interactions. By acting to modulate the activity of immune cells, this class of antibody can promote and augment the activation of effector immune cells and anti-tumour mechanisms, allowing for a more effective anti-tumour response.

1.3.2.1 Direct targeting antibodies

The direct targeting of antigens utilising antibody therapy can prove to be beneficial, as in the case of the CD20 targeting antibody, Rituximab. Used in cases of B cell lymphomas, Rituximab targets the CD20 protein expressed on the surface of both normal and malignant B cells [125]. As an IgG1 antibody, Rituximab can act to mediate CD20 expressing cell deletion by ADCC as well as complement-mediated cytotoxicity. The Fc domain of Rituximab is capable of binding FcγRs expressed on innate immune cells such as NK cells to mediate NK cell degranulation [126]. Macrophages are also expressors of FcγRs, and so can be directed to phagocytose target cells through antibody dependent cellular phagocytosis (ADCP) [127]. A more direct method of Rituximab-mediated target cell death has also been suggested. Rituximab is capable of inhibiting survival signals within B-cells through CD20 binding, inhibiting both the PI3K/Akt and NFκB signalling pathways [128, 129].

A second direct targeting antibody is Bevacizumab. This antibody acts to bind and neutralise circulating vascular endothelial growth factor (VEGF), inhibiting the survival and expansion of epithelial cells [130]. Approved for the treatment of metastatic colorectal cancer (mCRC), Bevacizumab inhibits angiogenesis, acting to starve developing tumours of the essential nutrients and oxygen required for their progression. When combined with chemotherapeutics, Bevacizumab treatment is shown to enhance progression-free survival of patients with respect to those treated with only chemotherapy [131].

1.3.2.2 Immunomodulatory antibodies

A second class of immunotherapeutics are immunomodulatory antibodies. These antibodies are designed to enhance or inhibit the function of immunoreceptors, acting as direct agonists to induce activation, or as antagonists to block ligand binding. These antibodies can therefore be used to mediate and promote the activity of immune cells, augmenting intrinsic anti-tumour responses and augmenting an effective immune response.

1.3.2.2.1 Immune checkpoint inhibitors

One of the first-in-class immunomodulatory antibodies utilised was ipilimumab, a human IgG1 mAb which binds and blocks the T-cell receptor, CTLA-4. Competing with CD28 for the binding of CD80/86, CTLA-4 acts as a T-cell checkpoint to inhibit the co-stimulatory signalling required for effective T-cell activation and increase the availability of CD80/86 to bind CD28 (Figure 1.3) [83, 132]. This method of immunotherapy is known as immune checkpoint blockade (ICB) and is approved for the treatment of melanoma, as well as in combination with nivolumab, an anti-PD-1 mAb, for treatment of metastatic colorectal cancer (mCRC) [133].

Nivolumab, a human IgG4 antibody first approved in 2014, acts to disrupt the binding of PD-L1, limiting inhibitory signalling mediated through PD-1. Approved for a number of cancers including non-small-cell lung cancer, melanoma and squamous lung cancer, both as a monotherapy and as combination therapy with Ipilimumab, Nivolumab has shown greater overall survival than chemotherapy treatment [134]. In a study assessing the long-term survival of advanced melanoma patients treated with either Ipilimumab, Nivolumab or in combination, 5-year survival was lowest in those treated with Ipilimumab alone (26%) whilst treatment with Nivolumab increased this to 44%. However, combinational therapy further increased 5-year survival to 52% [135].

1.3.2.2.2 Immunostimulatory antibodies

A further class of immunomodulatory antibodies are those that target immunoreceptors mediating stimulatory signalling, known as immunostimulatory antibodies. 4-1BB, through binding of its ligand 4-1BBL, has been shown to enhance T-cell activity through the activation of the NFκB pathway (Figure 1.3). Urelumab, a human IgG4 antibody, acts to target 4-1BB and augment T-cell activation and specific cytotoxicity. As a monotherapy, Urelumab has been shown to perform poorly in cancers with weak immune infiltration and low tumour immunogenicity, therefore current studies are working to assess its potential in combinational therapy [136]. Data from two clinical studies combining Urelumab with either Rituximab for the treatment of B-cell lymphomas, or with cetuximab or nivolumab for the treatment of mCRC, found that the addition of Urelumab offered no clinical benefit [137, 138].

The TNFR OX40 has also been the subject of antibody therapeutic targeting. As with 4-1BB, interaction of OX40 with its ligand OX40L on APCs is found to enable the recruitment of both TRAF1 and TRAF2 to activate the NFκB pathway. In mice, antibody targeting of OX40 enhanced anti-tumour responses, reliant on antibody isotypes and interactions with FcγRs, with mIgG1 found to act directly as an agonistic antibody, whilst mIgG2a was suggested to act indirectly by mediating OX40-expressing T_{reg} depletion [139, 140]. Data from antibodies targeting the OX40 receptor highlights that not only is the target an important factor when designing novel agonistic antibodies, but also the antibody isotype.

While progress in developing truly agonistic antibodies has been mixed, certain developments have highlighted the field's difficulties. Theralizumab (TGN1412), a novel superagonist antibody against CD28, was assessed in a phase 1 clinical trial and resulted in a widespread inflammatory response and cytokine release syndrome (CRS) [141]. Whilst preclinical work found no limiting safety concerns, retrospective work found that CD28 was not expressed on CD4+ effector memory T-cells in the non-human primates utilised for pre-clinical studies [142]. This failure highlights the fine line immunotherapy treads between providing a clear and effective benefit to patients, versus initiating wide-spread non-specific immune responses.

1.3.2.3 Bispecific antibodies

Bispecific antibodies (bsAbs) represent a relatively new approach to antibody therapy, enabling the targeting of both a TAA and effector cell receptor. The most common form of bsAb utilises two distinct F(ab) domains, one binding a TAA and the other binding a co-stimulatory domain. This specificity against TAAs allows for antibody localisation to the tumour site, limiting circulating therapeutic antibodies and enabling greater concentration of antibody within the tumour site. Targeting of receptors such as 4-1BB using mAbs has resulted in limited benefit, due in part to the requirement of local FcγR expressing cells to mediate antibody cross-linking. The use of bsAbs targeting activating receptors allows for effective cross-linking between TAA-expressing tumour cells and co-stimulatory receptors, circumventing the necessity for FcγRs.

A bsAb targeting both the tumour antigen B7-H3 and effector T-cell expressed 4-1BB (B7-H3x4-1BB) was found to augment CD8+ T-cell activation within tumours, increasing proliferation and cytokine release. Within the tumour, 4-1BB was found to be expressed on terminally differentiated PD-1+TIM-3+ CD8+ T-cells, with B7-H3x4-1BB treatment inhibiting tumour growth when combined with PD-1 blockade [143]. These bsAbs represent a novel approach to enhancing the anti-tumour potential of effector T-cells whilst increasing their association with target tumour cells and reducing off-target toxicity.

1.3.3 T-cell Engineering

A novel and more recent development in cancer immunotherapy is the development of chimeric antigen receptor T-cells (CAR-T). Patient-derived T-cells are retrovirally engineered to express novel receptors against tumour targets, utilising the ICD of co-stimulatory receptors to trigger targeted cytotoxicity against malignant cells. These receptors exploit the scFv of antibodies and therefore can recognise a target independent of MHC.

CAR-T cells can utilise multiple co-stimulatory domains in conjunction with the ICD of CD3ζ, allowing both Signal 1 and Signal 2 activation from a single ligand interaction. Whilst early CAR-T research utilised only the CD3ζ ICD, later iterations began to incorporate co-stimulatory domains such as 4-1BB or CD28 (Figure 1.6). The inclusion of these secondary signalling domains was found to be imperative to mounting an effective CAR-T response, enhancing targeted killing and improving the formation of memory T-cells for a long-lasting response [144]. CAR-T has most commonly been used for the treatment of B-cell malignancies which can show limited and refractory responses to both traditional chemotherapeutic agents and immunomodulatory antibodies such as Rituximab.

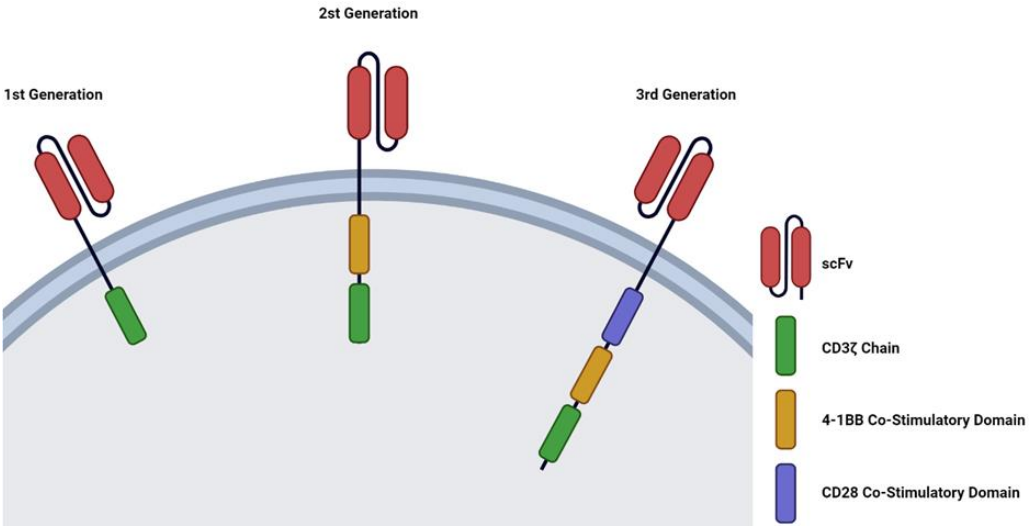

Figure 1.6 Schematic overview of T-cell chimeric antigen receptors

Schematic overview of each generation of CAR design. 1st Generation CAR constructs utilised only the CD3ζ as a signalling domain for the CAR, while the 2nd Generation CAR incorporated the 4-1BB co-stimulatory domain also. 3rd Generation CAR constructs use both the 4-1BB and CD28 co-stimulatory domains.

There are currently six approved therapies utilising CAR-T, all targeting either the B-cell marker CD19, or the B-cell maturation antigen (BCMA). Current limitations in effective CAR-T therapy are often a result of poor immune infiltration in solid tumours as a result of immune exclusion. The physical barrier presented by solid tumours, as well as their immunosuppressive nature, makes haematological cancers a more viable target for current CAR-T approaches [145]. Medulloblastomas are a form of brain tumour common to children, with 40% found to over express the human-epidermal

growth factor receptor-2 (HER2) [146]. In a study investigating the local direct infusion of a HER2 targeting 4-1BB-based CAR-T therapy for medulloblastoma patients, a much lower dose of CAR-T was required with more effective tumour clearance when compared to traditional intravenous application, indicating that more localised application of CAR T cells may be beneficial [147]. The design of these engineered receptors can have a profound impact on the success of CAR-T therapy. Affinity of the antigen-recognising scFv domain for tumour targets can impact the therapeutic response, with the use of higher affinity scFv enabling effective T-cell activation with lower target antigen expression [148].

Two CD19-targeting CAR-T therapies approved for clinical application are Kymriah (Tisagenlecleucel) and Yescarta (Axicabtagene ciloleucel). While both Kymriah and Yescarta target the same B-cell marker (CD19), each utilise a different receptor design. Both therapies incorporate the same anti-CD19 scFv (FMC63), however each utilises distinct co-stimulatory domains. Within the ICD of Kymriah, the 4-1BB signalling domain is placed in conjunction with the CD3ζ domain [149]. Yescarta differs by using the CD28 ICD in place of 4-1BB [150]. Similarly, each uses a distinct method of introducing CARs into patient T-cells. While Kymriah uses a lentivirus vector for inserting the CAR gene, Yescarta employs a γ-retrovirus [151]. Whilst both of these are retroviruses which utilise reverse transcriptase to insert CAR-encoding DNA into a host T-cell, lentivirus is capable of infecting non-dividing cells whilst γ-retrovirus can only infect cells undergoing division. While there have been links to severe side-effects in some patients treated with CAR-T, such as the activation of bystander immune cells resulting in CRS and certain neurological toxicities, the response in some patients has been positive - In clinical trials treating acute lymphoblastic leukaemia patients with Kymriah, 68% of patients showed a complete response to treatment [149].

1.4 CD96

CD96 was first isolated in 1992 as a type I transmembrane glycoprotein and initially named “T-cell activation, increased late expression” (TACTILE) [152, 153]. As a member of the IgSF of proteins which includes both TIGIT and CD226, CD96 is predominantly expressed on cells of hematopoietic origin – notably on CD4+ and CD8+ T-cells, as well as NK cells. As with TIGIT and CD226, CD96 is suggested to compete for binding of CD155, analogous to CD28 and CTLA-4 competition for CD80/CD86 [154]. Structurally, both human (huCD96) and mouse CD96 (mCD96) comprise of three extracellular immunoglobulin-like (Ig-like) domains, a highly *O*-glycosylated rod-like structure, and a short ICD containing common signalling domains. Within the CD96 ICD is a proline-rich domain (PRD), an ITIM consensus sequence, and in human CD96, a YxxM motif commonly associated with co-stimulatory proteins such as CD28 and Inducible T-cell Costimulator (ICOS) [155].

1.4.1 CD96 structure and signalling

Human CD96 is expressed as two similar but distinct isoforms, differing only in their second Ig-like domain. These two isoforms are produced by alternative splicing, with huCD96v2 being the most predominant [156]. Domain 1, the most membrane distal domain forms the same V-like IgSF structure in huCD96v1, huCD96v2, and mCD96. Domain 2 of huCD96v1 also forms a V-like structure, whilst in huCD96v2 and mCD96 it is predicted to form either an I-like or C-like IgSF domain. Both huCD96 isoforms and mCD96 share the same C-like IgSF domain in their most membrane-proximal domain, as detailed in Figure 1.7A [152]. The rod-like stalk structure which acts to connect the three extracellular domains to the transmembrane domain consists of a long and highly *O*-glycosylated region, allowing for protrusion of CD96 from the cell surface for ligand interaction.

The cytoplasmic domain of CD96 is relatively short but contains a number of key motifs which may contribute to signalling (Figure 1.7B). IgSF receptors such as CD96 commonly contain conserved motifs within their ICD, allowing for the binding of adapter molecules and kinases which can mediate and propagate downstream signalling. Src homology 3 domains (SH3) are one of the largest groups of binding sites found within signalling associated proteins, notable for their capacity to bind proline-rich domains. SH3 domains present within kinases may bind proline-rich peptide sequences within the ICD of signalling receptors. A large number of SH3 domains recognise two subsets of PRDs, deemed Class I (RxxPxxP) or Class II (PxxPxIR/K), with each focussed around a core PxxP region [157, 158]. Interestingly, both of these PRD classes are present within the PRD of both human and mouse CD96 as RPPPFKP (Class I) and PPPPIK (Class II), with PRDII overlapping with the ITIM consensus sequence (Figure 1.7B). Common binding partners of these PRD are the tyrosine protein kinases, a group of enzymes responsible for the phosphorylation of tyrosine residues. These include the Src-family kinases SRC, LYN and FYN, each noted for their ability to bind both Class I and Class II PRDs [158]. Notably, a third class of PRD is found in both human and mouse CD96. This non-canonical Class III PRD (RxxxxxP) may allow for the binding of the Tec class of kinases [157]. This class of kinases is common in cells of hematopoietic origin and have been shown to be activated through SH3 domain interactions following TCR activation, enhancing IL-2 production [159].

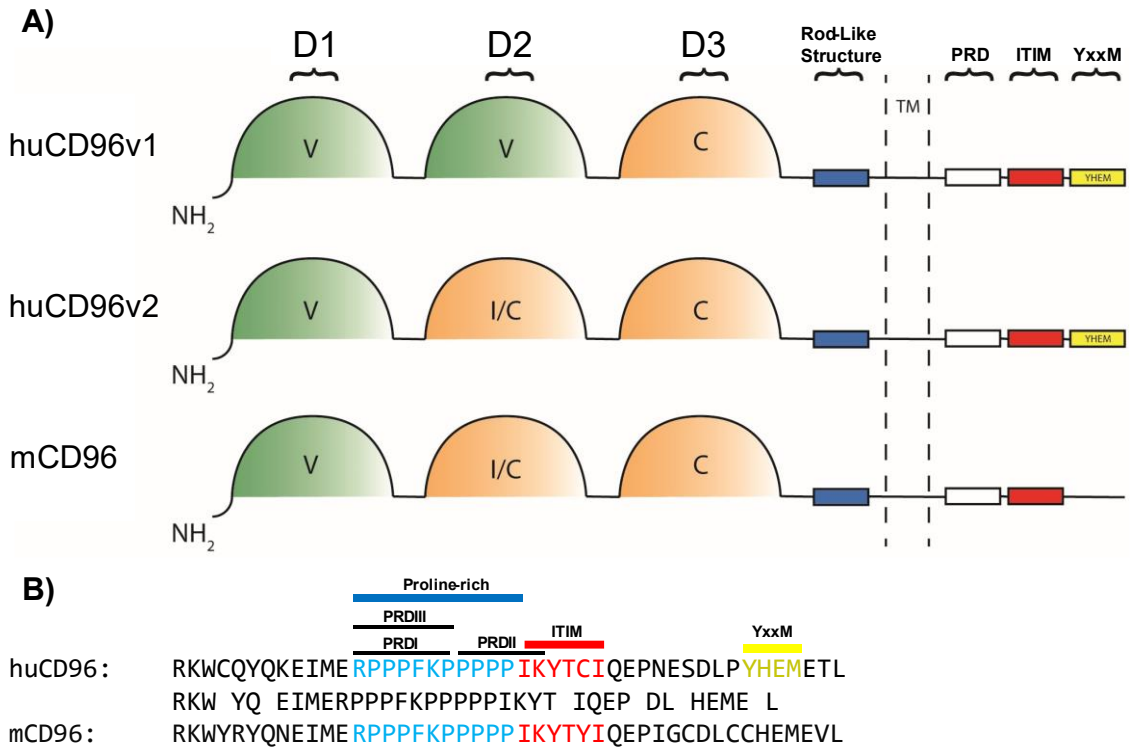

Figure 1.7 The structure of human and mouse CD96

A) Schematic overviews of both isoforms of human CD96 (huCD96v1, huCD96v2) and the single isoform of mouse CD96 (mCD96). Both huCD96 isoforms share the same V- and C-like domain as domain 1 and domain 3 respectively, while huCD96v2 differs in its domain 2 with a predicted I- or C-like domain where huCD96v1 contains a second V-like domain. mCD96 shares similarity with huCD96v2 by containing a V-like, a I/C-like and a C-like domain as its 1st, 2nd and 3rd domain respectively. Human and murine CD96 share a *O-glycosylated* rod-like structure rich in proline/serine/threonine, along with a short intracellular domain containing a proline-rich domain (PRD) and ITIM consensus sequence. Only huCD96 contains a YxxM motiff. **B)** Sequence homology between the intracellular domains of mCD96 and huCD96 showing a shared PRD, similar ITIM consensus sequence and a lack of the YxxM motif in mCD96. Adapted from Georgiev et al., 2018.

Present downstream of the PRD in both human and murine CD96 is an ITIM. While the sequence of the ITIM present in mCD96 differs slightly due to the presence of a second tyrosine, the ITIM consensus sequence is present in both structures (S/I/V/LxYxxI/V/L). In both species, this ITIM sequence overlaps with the Class II PRD previously described (Figure 1.7B). ITIM activation is characterised by the phosphorylation of a tyrosine residue and subsequent binding of SH2 domain-containing phosphatases which act to remove phosphate groups from neighbouring activated receptors. TIGIT, a member of the same IgSF as CD96 and also commonly expressed in cells of haematopoietic origin, also binds CD155 [92]. Conversely, TIGIT contains two inhibitory motifs, an ITIM domain and an Ig tail-tyrosine (ITT)-like motif [89]. In human NK cells, these inhibitory domains act to suppress NK cytotoxicity of CD155-expressing tumour cells [92, 160]. In work by Li et al, TIGIT-CD155 interactions were shown to suppress the activation of the transcription factor NF-κB through the recruitment of β-Arrestin 2 to the phosphorylated tyrosine of the TIGIT ITT. Further to this, Grb1 and

SHIP-1 were found to be recruited by β-Arrestin 2, acting to limit both PI3K and MAPK downstream signalling, suggesting that it is in fact the ITT domain of TIGIT that plays a greater role in the biophysical suppression of NK activation over its neighbouring ITIM [94]. Supporting this idea was the observation that the introduction of the mutation $Y^{231}A$ within the TIGIT ITIM was shown to disrupt the suppressive nature of TIGIT, but that this was to a lesser degree than a similar mutation within the ITT motif [93]. In a piece of work looking at the impact of TIGIT ligation in $CD8^+$ T cells, a similar result was observed. In this study, antibody blockade of TIGIT in CD155 stimulated $CD8^+$ T cells resulted in an increased presence of p-ERK and p-IκBα, both indicators of cell activation [161]. Whether the ITIM consensus sequence present within CD96 acts in a similar fashion to that of TIGIT remains to be be seen.

Present at the most membrane-distal region of huCD96s intracellular tail is a YxxM motif (where X being any amino acid). This motif is commonly found in co-stimulatory proteins, notably in both CD28 and ICOS. Interestingly however is the fact that while this YxxM motif is conserved across both human and mouse CD28 and ICOS, it is lacking in mCD96.

1.4.2 CD96 in Natural Killer Cells

Although CD96 was initially identified as a potential tumour marker due to high expression in cases of acute leukaemia, later work seeking to categorise which surface proteins expressed on NK cells may recognise CD155 identified CD96 as a binding partner [162]. This early work in human NK cells hypothesised that this CD96-CD155 interaction could both mediate the cell-cell adhesion between CD96 expressing NK cells and CD155 expressing target cells, as well as inducing cytotoxicity of NK cells. Noted by this group however was that while targeting of CD96 on NK cells was capable of inducing targeted cell lysis, cytotoxicity was reduced with respect to CD226 stimulation.

A notable difference in the function of murine CD96 in NK cells was identified by Chan et. al, who recorded that following lipopolysaccharide (LPS) administration, activation of NK cells was greater in mice lacking CD96. Their data highlighted that in murine NK cells, as opposed to the previously noted observation in human NK cells, CD96 ligation acts to inhibit the activation of NK cells resulting in reduced IFN-γ release [154]. NK cells serve a crucial role in controlling and limiting the metastasis of tumours and are intrinsically linked to the immunoediting stage of tumour control [163]. To assess whether CD96 may play a role in NK control of tumour metastasis, Chan et. al evaluated the metastasis of the B16F10 lung tumour model in mice either lacking CD96, or immunodeficient mice reconstituted with either $CD96^{-/-}$ or wild-type NK cells. The metastatic burden of both mice lacking CD96, and immunodeficient mice reconstituted with $CD96^{-/-}$ NK cells was greatly reduced, indicating that in the context of murine NK cells, CD96 acts to inhibit cell activation and can limit the effective anti-tumour responses of NK cells. Interestingly, the increased tumour control following loss of CD96

was diminished when CD226 was also removed, providing evidence that CD226 opposes the role of CD96 and functions as an activator of NK cell activity.

In the context of NK cells, it has been previously shown that antibody blockade of the CD96:CD155 interaction is in fact not essential to limit tumour metastasis. Utilising three antibodies, two blocking (3.3 and 6A6) and one non-blocking (8B10), it was shown that all three antibodies could limit tumour metastasis in numerous metastatic models, however both 3.3 and 6A6 were found to be more effective than 8B10. Notably however was that in the absence of CD155, only the non-blocking 8B10 antibody retained capacity for metastatic control [164]. Interestingly, application of all antibodies regardless of their blocking or non-blocking characteristic had no impact on metastasis control in CD226 KO mice, suggesting that for NK cell control of tumour metastasis, CD226 involvement is critical. While these data show that blocking the CD96:CD155 interaction is not necessary for anti-metastatic activity of NK cells, the understanding of why is less clear. The 3.3 anti-CD96 antibody has previously been defined by Blake et al. as being reliant on both NK cells and IFN-γ [165]. A similar observation was found with the antibodies 6A6 and 8B10, with a complete loss of anti-CD96 metastatic control following either NK cell depletion or IFN-γ neutralisation [164].

Interestingly, despite the evidence for CD96 as an inhibitory receptor in mouse NK-mediated tumour immunity, a role for CD96 as an activating receptor in mouse NK cells has also been reported. In experimental models of mouse cytomegalovirus (MCMV) infection, CD96 was found to augment the activity of the MCMV-specific receptor Ly49H$^+$ by maintaining ZAP70 phosphorylation [166].

1.4.3 CD96 in T-cells

Whilst evidence for the role of CD96 as a negative regulator of murine NK cells has been presented, work with CD96 in T-cells has in fact suggested that its role may be not so simple. Investigating the impact of anti-CD96 antibodies upon murine T-cells, Chiang et al. have found that CD96 cross-linking using anti-CD3/CD96 conjugated beads can induce both CD4+ and CD8+ mouse T-cell proliferation, with CD8+ T-cell proliferation comparable to that of activation through CD3 and CD28 [167]. To assess the signalling pathways mediated by CD96, Chiang et al. found that upon CD3/CD96 activation of mouse CD8+ T-cells, ERK was transiently phosphorylated. The ERK pathway is crucial for regulating T-cell activation, with a similar pattern of ERK phosphorylation observed when T-cells were activated through CD3/CD28 [168]. This activity was ablated in cells lacking CD96, suggesting that in the context of murine CD8$^+$ T-cells, CD96 can augment CD3 to activate cells. Interestingly, in CD96 KO T-cells, phosphorylation of ERK was sustained longer following CD3/CD226 stimulation, whereas it was diminished in CD96 expressing cells. This finding could suggest that while CD96 is capable of activating murine CD8+ T-cells and mediating ERK activation, its expression may also limit the prolonged activation of CD226 resulting in the transient phosphorylation of ERK observed in CD96+

cells. This finding however was not investigated further by the group. A similar experiment carried out by the group utilising the CD96$^+$ human CD8$^+$ T-cell line, HD-MAR-2, found a similar pattern of ERK phosphorylation. Furthermore, huCD96 activation of human CD8+ T-cells resulted in strong activation of mitogen-activated protein kinase (MEK), a kinase which acts upstream of ERK, mediating its phosphorylation. Considering that this pattern of ERK activation is found in both human and murine CD96 activated T-cells, it is plausible that CD96 mediated T-cell activation through its PRD, common to both species [152]. In the context of the CD96 role within TILs, deficiency or antibody blockade of CD96 was not found to inhibit initial T-cell infiltration of tumours in murine CT26 colorectal carcinoma models, however it did limit subsequent activation of CD8+ T-cells with a significant reduction in the expression of the CD8$^+$ T-cell transcription factors T-bet and Eomes, in conjunction with reduced IFN-γ and TNF-α production [167].

Considering the apparent stimulatory role of CD96 in human T-cells, work has been carried out previously to better understand how huCD96 may be better targeted utilising immunotherapeutic antibodies. Work carried out within our group by Rogel et al. utilising three novel anti-human CD96 antibodies highlighted that in a human peripheral blood mononuclear cell (PBMC) proliferation assay, huIgG1 antibody mediated T-cell activation was in fact reliant on FcγRI-mediated antibody cross-linking. When PBMCs were activated with soluble anti-CD3/CD96 antibodies, CD4+ and CD8+ T-cell proliferation was limited when anti-CD96 was applied as a Fc-silent antibody. This observation was mirrored when T-cells were isolated and cultured with antibody on plates coated with recombinant FcγRI, whereby antibody Fc-domain engagement of plate-bound FcγRI was essential to induce T-cell proliferation [169]. Whilst huIgG1 antibodies have the capacity to bind all huFcγRs, it is their binding of the activating FcγRI that is strongest [170, 171]. This result suggests that cross-linking of anti-CD96 antibodies and the induction of receptor clustering is a requirement for effective activation of T-cells through CD96. Currently, there is one clinical trial involving antibodies against CD96. GlaxoSmithKline (GSK) are currently investigating the impact of utilising a blocking anti-human CD96 antibody in solid tumours as both a monotherapy, and in conjunction with the anti-PD-1 antibody, Dostarlimab, however this study is currently still at Phase I [172].

While previous work has shown that the provision of CD96 signalling can induce greater CD8+ T-cell activation, the specific signalling pathways and mediators involved has yet to be understood. While the presence of a YxxM motif common to other co-stimulatory proteins is found in huCD96 may initially suggest involvement, the fact that mCD96 lacks this motif whilst still being capable of activating mouse T-cells suggests it may at least be partially dispensable for T-cell activation. Considering the PRD of CD96 is found to be identical across both species, it may in fact be this region that acts as the trigger for downstream activation signals. In a study by Liu et al., CD96 expression in gliomas was found to strongly correlate with expression of the Src family kinase, LCK [173]. Interestingly, whilst LCK can bind both Class I and II PRDs through its SH3 domain, LCK has been

shown to bind CD28 through a class II PRD similar to that of CD96 (Class II Consensus: PxxPxR/K, CD28: PYAPPR, CD96: PPPPIK) [67, 157, 158]. Considering the key role of LCK in the activation of T-cells by its ability to phosphorylate the TCR and CD3-associated ZAP70, CD96 activation could be speculated to be a result of LCK recruitment to the PRD of CD96. While evidence has been presented for some of the signalling mediators involved following CD96 activation, a clearer understanding of the CD96 signalling pathway and its impact on cell activation is lacking.

1.5 Hypothesis and aims

This project seeks to expand on current knowledge of the role of human T-cell expressed CD96, whilst expanding upon the current CD96 specific therapeutics available to utilise in models of cancer. We hypothesise that the interaction of CD96 with CD155 mediates a stimulatory signal and is reliant upon one of the intrinsic signalling domains present within the CD96 ICD.

Aim 1: Utilise phage-display panning of scFv libraries to identify panels of human, mouse and cross-species targeting CD96 antibodies:

- Generate the required cell lines and reagents to allow panning of scFv phage libraries for novel CD96 targeting antibodies.
- Characterise CD96-reactive scFv clones for both their binding of CD96 and blocking of CD155.
- Determine the capacity of newly generated CD96 targeting antibodies to augment T-cell activation.

Aim 2: Determine the intracellular domains within huCD96 responsible for the co-stimulatory action of CD96 in human T-cells:

- Develop and confirm the suitability of using a CD96-incorporating CAR-T model system to assess the co-stimulatory action of CD96.
- Introduce point-mutations within defined CD96 domains to determine the contribution of specific domains to CD96-mediated T-cell activation.
- Utilise a kinase profiling platform to understand the specific kinase activity mediated by CD96 signalling.

Aim 3: Assess whether CD96 interactions with APC-expressed CD155 mediates T-cell activation:

- Develop and confirm the suitable application of a novel method of primary T-cell activation utilising bacterial superantigens.
- Assess whether the provision of APC CD155 expression augments primary T-cell activation.
- Investigate the role of CD96 on primary T-cells activated with bacterial superantigens in the presence of CD155.

Chapter 2 Methodology

2.1 Cell culture

Phoenix-Ecotropic cells (Phoenix-Eco, ATCC) were grown in Dulbeccos Modified Eagle Media (DMEM, Gibco), supplemented with 10% v/v of Fetal Calf Serum (FCS, Sigma), 2mM L-Glutamine (Gibco), 1mM Sodium Pyruvate (Gibco), 100U/mL Penicillin (Sigma), 100µg/mL Streptomycin (Sigma) and were split 1:5 Monday and Wednesdays, and 1:12 on Fridays. Rat Basophilic Leukaemia cells (RBL, ATCC) were grown in Roswell Park Memorial Institute media (RPMI, Gibco), supplemented with 10% v/v of Fetal Calf Serum (FCS, Sigma), 2mM L-Glutamine (Gibco), 1mM Sodium Pyruvate (Gibco), 100U/mL Penicillin (Sigma), 100µg/mL Streptomycin (Sigma) and split at $0.3x10^6$/mL three times a week. HEK293FT cells (ATCC) were grown in cDMEM and were split 1:5 Monday and Wednesdays, and 1:12 on Fridays. Both wild-type and CAR expressing Jurkat cells (ATCC) were cultured in cRPMI and split at $0.5x10^6$/mL three times a week. Both Ramos and Raji cells (ATCC) were cultured in cRPMI and split at $0.5x10^6$/mL three times a week. For the culture of PBMC to be utilised for antibody experiments, cells were cultured in cRPMI. For PBMCs and isolated T cells for CAR-T experiments, cells were cultured in TexMACS media (Miltenyi Biotech) supplemented with 100U/mL Penicillin (Sigma), 100µg/mL Streptomycin (Sigma).

Cells were cultured at 37°C and 5% CO_2, with periodic testing for Mycoplasma infection.

2.2 Flow Cytometry Antibodies

Table 2.1 Antibodies used for flow cytometry

Target	Target Species	Clone	Isotype	Fluorochrome	Supplier	ID
RQR8		Rituximab	huIgG1	Unlabelled	UHS Pharmacy	
FMC63		Y45	mIgG1	PE	Acro Biosystems	FM3-HPY53
FMC63			mIgG1	Unlabelled	UCL/In-House	
6-His Tag		J095G46	mIgG2a	APC	BioLegend	362605
Biotin				APC	eBioscience	17-4317-82
Fcγ	Human	Polyclonal	Goat IgG	APC	Jackson IR	109-135-098
Fcγ	Human	Polyclonal	Goat IgG	PE	Jackson IR	109-115-190
Fcγ	Mouse	Polyclonal	Goat IgG	APC	Jackson IR	115-135-164
Fcγ	Mouse	Polyclonal	Goat IgG	PE	Jackson IR	115-115-164
Fcγ	Mouse	Polyclonal	Goat IgG	HRP	In-House	
CD3	Human	UCHT1	mIgG1	eF450	Invitrogen	48-0038-82
CD4	Human	RPA-T4	mIgG1	eF450	Invitrogen	48-0049-42
CD4	Human	RPA-T4	mIgG1	eF506	Invitrogen	69-0049-42
CD8	Human	RPA-T8	mIgG1	APC-eF780	Invitrogen	47-0088-42
CD20	Human	2H7	mIgG2b	PE	BioLegend	980214
CD25	Human	BC96	mIgG1	PE-Cy7	BioLegend	302612
CD69	Human	FN50	mIgG1	APC	BioLegend	985206
CD96	Human	NK92.39	mIgG1	APC	BioLegend	338410
TIGIT	Human	1G9	mIgG2a	BV421	BioLegend	142111
CD226	Human	DX11	mIgG1	PE	Miltenyi Biotec	130-124-232
HLA-DR	Human	LN3	mIgG2b	PE	Invitrogen	12-9956-42
Isotype	ChiLob7/4 idiotype	AT-171-2	huIgG1	Unlabelled	In-House	

Isotype	ChiLob7/4 idiotype	AT-171-2	mIgG1	Unlabelled	In-House	
Isotype	Unknown	MOPC-21	mIgG1	APC	BioLegend	400122
Isotype	Unknown	MOPC-21	mIgG1	PE-Cy7	BioLegend	400126
Isotype	Unknown	MOPC-173	mIgG2a	APC	BioLegend	400220
Isotype	Unknown	MPC-11	mIgG2b	PE	BioLegend	400312
Isotype	Unknown	MOPC-173	mIgG2a	BV421	BioLegend	400158
Isotype	Unknown	eBMG2b	mIgG2b	PE	Invitrogen	12-4732-81

2.3 Flow cytometry

Staining of cells for flow cytometry analysis was performed with $1x10^5$ cells per tube. Cells were washed twice with PBS (+ 0.1% w/v Bovine Serum Albumin (BSA), Europa Bioproducts), centrifuging at 450 *g* for 5 minutes between each wash. Cells were resuspended in 100 µL of PBS/0.1% BSA with 10 µg/mL of the appropriate staining antibody (Table 2.1) for 30 minutes at 4°C. In the case of secondary antibody staining, cells were washed twice of excess primary antibody before being resuspended in 100 µL of PBS/0.1% BSA with the appropriate secondary antibody diluted 1/200 for 20 minutes at 4°C. Cells were washed with PBS/1%BSA and centrifuged three times to remove excess antibody before being assessed through flow cytometry using either a FACS Canto II or FACS Canto Plate Reader (BD Bioscience). Cells were gated for viable cells using SSC-A vs. FSC-A, and single cells using FSC-W vs. FSC-A, with 10,000 single cell events recorded. Acquisition of cell staining analysis was carried out using BD FACSDiva (BD Bioscience) before final analysis of data which was carried out using FlowJo (FlowJo, Version 10.10).

2.4 CD96 and CD226 γ-Retrovirus plasmid production

Shuttle vectors containing human CD96v2 (NP_005807) or CD226 (NP_006557) and mouse CD96 (NP_115854) or CD226 (NP_848802) (R&D VersaClone) were digested with 5U/µg of both NotI and SalI (Promega, R6431/6051) at 37°C for 2 hours in 2 µL of Promega Buffer D (Promega, R004A) in a total volume of 20 µL with Milli-Q water). The retroviral vector pMP71-Inv was digested identically to remove a 1067 bp stuffer sequence. Using a 0.7% agarose gel (+ GelRed, 5 µL per 100 mL, Biotium), electrophoresis was used to separate 0.5 µg of each digested plasmid alongside 5 µL of Generuler 1 kbp DNA ladder (ThermoScientific, SMO313) at 100 V for 1.5 hours. The separated DNA fragments were identified by their molecular weight and excised under brief UV light before being extracted from agarose gel using a Monarch DNA extraction kit according to the manufacturers protocol (New England BioLabs, T1020L). Extracted *CD96* or *CD226* fragments were then ligated with digested

pMP71 vector at 4°C for 72 hours at a 3:1 insert:vector molar ratio using 3 µL of 10x T4 ligation buffer and 2 µL of T4 DNA ligase (Promega, M1801) in a volume made up to 30 µL with Milli-Q water.

15 µL of JM109 competent *E. coli* cells (Promega, L2005) were resuspended in 185 µL of 0.1M $CaCl_2$ with 50 ng of ligated product, incubated on ice for 30 minutes before being heat-shocked for 45 seconds at 42°C and rested for 2 minutes on ice. 0.5 mL of Super Optimal broth with Catabolite repression (S.O.C) culture medium (Invitrogen, 15544034) was added before transformed cells were incubated under agitation at 37°C for 2 hours (225RPM). 100 µL of transformed cells were then plated on LB agar plates (+ Ampicillin 100 µg/mL) and incubated overnight at 37°C. Individual colonies were picked and further grown in 7 mL of liquid LB broth (+ Ampicillin 100 µg/mL) overnight at 37°C under agitation before plasmid DNA was isolated using a Qiagen Mini-Prep kit (Qiagen 56304). Isolated plasmid was checked for concentration and purity using a NanoDrop ND-1000 (A_{260}/A_{280} value of 1.9) before being re-digested with either NotI and SalI (pMP71-hu/mCD96), EcoRI (pMP71-huCD226) or NotI, SalI and EcoRI (pMP71-mCD226) at 37°C for 1 hour. Digested plasmid was separated using a 0.7% agarose gel (100 V, 1.5 hours) and imaged using a BioRad UV imager to confirm the presence of the pMP71 vector and inserted *CD96* or *CD226*. One colony confirmed to express each correct plasmid was then expanded in 100 mL of liquid LB broth (+ Ampicillin 100 µg/mL) overnight at 37°C under agitation before plasmid DNA was isolated using a Qiagen Maxi-Prep kit (Qiagen 12643) and confirmed for purity and concentration.

2.5 γ-Retroviral transduction of Rat Basophilic Leukaemia cells

Phoenix-Eco cells were seeded at $1.5x10^5$ cells in DMEM (Gibco, + 10% v/v Foetal Calf Serum (FCS, Sigma) per well in a P6 plate and expanded to 70% confluency before cell media was refreshed. 15 µL of FuGene transfection reagent (Promega, E2311) was added to 135 µL of media containing 4 µg of either pMP71-CD96 or pMP71-CD226 plasmid and 4 µg of pCL-Eco plasmid (NovusBio, NBP2-29540) and incubated for 10 minutes at room temperature. The plasmid solution was added to plated Phoenix-Eco cells and incubated for 23 hours at 37°C. At 23 hours, cell media was replaced with cRPMI (Gibco, 10% v/v FCS, 2 µM L-Glutamine (Gibco), 1 mM Sodium Pyruvate (Gibco), 100 U/ml Penicillin (Sigma), 100 µg/ml Streptomycin (Sigma)) before being incubated for a further 24 hours. Non-treated tissue culture P6 plates were coated with 2.5 mL of RetroNectin (TakaraBio, 25 µg/mL) overnight at 4°C. RetroNectin was removed and blocked with PBS/2%BSA for 30 minutes at room temperature. Retrovirus containing media was removed from Phoenix-Eco containing wells and used to resuspend rat basophilic leukaemia cells (RBL) at $1.2x10^6$/mL. 2.5 mL of RBL/γ-retrovirus supernatant was added to each RetroNectin coated P6 well before being spun at 1000g for 90 minutes at 32°C. RBL cells were then incubated for 24 hours at 37°C before being stained with anti-

CD96 or anti-CD226 antibodies for expression of either human or mouse CD96 or CD226 and assessed through flow cytometry.

Transduced RBL cells were FACs sorted based on their expression of the GFP marker protein present within the pMP71 vector. Cell sorting was carried out by Dr. Anne Rogel using a BD FACSMelody. Cells were gated as either GFP^{HIGH} or GFP^{LOW} and sorted accordingly.

2.6 Assessing anti-CD96 scFv binding of CD96

Each scFv was prepared in serial dilution, ranging from 10 µg/mL to 0.05 µg/mL, in PBS /1% BSA. $1x10^5$ RBL-CD96 cells per scFv dilution were washed with PBS and resuspended in 100µL of scFv dilution before being incubated for 45 minutes at 4°C. Cells were washed once with PBS before being resuspended in 100 µL of anti-His-Tag-APC antibody (0.7µL per tube) for 30 minutes at 4°C. A mIgG2a APC isotype control was used to determine background fluorescence and non-specific binding. Cells were further washed three times with cold PBS/1% BSA, resuspended in PBS-1%BSA and assessed for scFv binding through flow cytometry. This assay was carried out identically for both RBL-huCD96v2 and RBL-mCD96 cells.

2.7 Truncated CD96 ELISA

Nunc Maxisorb ELISA plates (Thermo Scientific) were coated with 50 µL of anti-human Fc capture antibody (1 µg/mL. Jackson ImmunoResearch) diluted in coating buffer (15 mM Na_2CO_3, 35 mM $NaHCO_3$, pH 9.6) for 4 hours at 37°C before being left overnight at 4°C. Plates were then blocked with PBS (+1% BSA) for 1 hour at RT and washed four times with cold PBS (+0.05% Tween20). 100 µL of recombinant truncated CD96 was added to each corresponding well at 1 µg/mL for 1 hour at RT before wells were washed four times with cold PBS (+0.05% Tween20). Each scFv to be assessed was prepared at 5 µg/mL in PBS (+0.2% BSA) before 100 µL was added to the corresponding well for 1 hour at RT. After 1 hour, scFv dilutions were removed and wells washed four times with cold PBS (+0.05% Tween20). Biotinylated anti-c-Myc antibody (9E20, BioLegend) was diluted to 1 µg/mL in PBS (+ 0.2% BSA) before 100 µL was added to each well for 1 hour at RT. Antibody was removed before plates were washed a further 4 times in cold PBS (+0.05% Tween20). A streptavidin-HRP conjugate was diluted 1/1000 in PBS (+0.2% BSA) according to manufacturer's recommendations (21130, Pierce) before 100 µL was added to each well for 30 minutes at RT. For detection, 100 µL of OPD substrate was added (1 Sigma OPD tablet, 10 mM $C_6H_8O_7$, 5 mM Na_2HPO_4, 50 ml dH_2O, 20 µl H_2O_2) for 5 minutes before 50 µL of 2.5 M H_2SO_4 was added to stop colour change. Absorbance was read at 490 nm with an Epoch Microplate Reader.

Analysis of anti-mCD96 IgG using truncated mCD96 followed the same protocol, except mIgG was assessed at 5 µg/mL. Goat anti-mouse Fcγ-HRP was used in place of anti-c-Myc antibody (1/5000, In-house).

2.8 Assessing scFv inhibition of CD155 binding to CD96

Each scFv was prepared in serial dilution, ranging from 10 µg/mL to 0.05 µg/mL, in PBS (+ 1%BSA). $1x10^5$ RBL-CD96 cells per scFv dilution were washed and resuspended in 100 µL of scFv dilution before being incubated for 45 minutes at 4°C. 100 µL of recombinant CD155 (final concentration 0.5 µg/mL, SinoBiological) in PBS (+1% BSA) was further added and incubated for 1 hour at 4°C. To produce a non-blocking control, RBL-CD96 cells were incubated in rCD155 with no scFv incubation. Cells were washed once with cold PBS before being resuspended in 100 µL of Streptavidin-APC (1 µg/mL, eBioscience) for 30 minutes at 4°C. Cells were further washed three times with cold PBS (+ 1% BSA), resuspend in PBS and assessed for the binding of rCD155 through flow cytometry (BD Canto Plate Reader). This assay was carried out identically for both RBL-huCD96v2 or RBL-mCD96 cells.

2.9 PBMC T cell isolation

To isolate T-cells from peripheral blood mononuclear cells (PBMC), each leucocyte cone was allowed to drip into 2 mL of PBS-EDTA (2 mM) and further topped up to 40 mL with PBS-EDTA (2 mM). 20 mL was layered on top of 15 mL of lymphoprep density gradient medium (StemCell, 07851) and centrifuged at 800 g for 20 minutes. The PBMC interface layer was removed, added to 40 mL PBS-EDTA (2 mM) and centrifuged at 400 g for 10 minutes. This wash was repeated once. Cells were counted and utilised for downstream assays. Where required, T-cells were isolated utilising a StemCell T-cell negative isolation kit (StemCell, 17951) following manufacturers protocol. Briefly, 100 µL enrichment antibody cocktail was added per mL of PBMCs ($50x10^6$/mL) for 10 minutes at room temperature. Magnetic particles were added at 50 µL/mL for 5 minutes at room temperature. The PBMC mixture was topped up to 2.5 mL with PBS-EDTA (1mM + 2%FCS) before negatively selected T-cell were poured off to be used.

2.10 PBMC antibody proliferation

PBMCs were isolated as described in 2.9. PBMCs were resuspended at $2x10^7$/mL in PBS before an equal volume of CFSE (Invitrogen, C34554) at 3 µM in PBS was added. PBMCs were covered and incubated at 37°C for 10 minutes before the staining quenched and cells washed three times. Cells were resuspended at $1x10^6$/mL for plating.

For plate-bound anti-CD96 antibodies, each huIgG1 antibody was prepared at 2.5 µg/mL in sterile filtered coating buffer (15 mM Na_2CO_3, 35 mM $NaHCO_3$, pH 9.6) and 100 µL added to each well of a U-bottom 96-well plate and incubated overnight at 4^{o}C. Wells were washed twice with cold sterile PBS prior to addition of anti-human CD3 (OKT3, In-house) antibody and cells. 50 µL of OKT3 antibody at either 1.2 or 0.4 ng/mL was added to achieve 0.3 or 0.1 ng/mL, before 100 µL of CFSE stained PBMCs and 50 µL of cRPMI added.

For soluble antibodies, each huIgG1 antibody was prepared at 4 µg/mL in cRPMI. OKT3 antibody was prepared at 1.2 or 0.4 ng/mL and 50 µL added to achieve 0.3 or 0.1 ng/mL, before 100 µL of CFSE stained PBMCs and 50 µL of dual-panned CD96 antibody added to achieve 1 µg/mL.

Cells were incubated for 4 days before being stained for CD4 and CD8 T-cell proliferation and CD25 upregulation using flow-cytometry.

2.11 CAR retroviral plasmid generation

CAR constructs utilised the MP13328 plasmid as a backbone vector, a kind gift of Paul Maciocia (UCL, London). The original CAR-T expression cassette consists of a RQR8 sort/suicide gene, anti-CD19 FMC63 ScFv, CD8 transmembrane domain and Hu4-1BB + CD3ζ fragment. Generation of huCD96 CAR constructs was carried out by Dr. Claude Chan. 4-1BB + CD3ζ cDNA fragment was removed from the MP13328 plasmid using the BamH1 and Mlu1 restriction sites and the intracellular domains of WT huCD96 and CD3ζ (synthesized by GeneArt) was subcloned in place. CD96 point-mutational changes to alanine were introduced by overlapping PCR using complementary primers detailed in Table 2.2. PCR amplified 96ζ mutant fragments were cloned into the MP13328 backbone using CloneExpress II one step cloning kit (Vazyme global). All mutations were sequence verified. CAR sequences are shown in Appendix C.

Table 2.2 PCR primers for CD96 CAR point-mutations

FMC63-CD8-BamHI	F	CAGCGTGACCGTGAGCTCGGATCCCACCACCACCCCAGC
96-YAMAζ	R	CCGGAGGGTCTCGGCCTCATGGGCAGGCAGATCACTTTC
	F	TGATCTGCCTGCCCATGAGGCCGAGACCCTCCGGGTGAAG
96-Y566Aζ	R	CTCTTGAATGCAAGTGGCCTTGATGGGAGGTGGTGGTGG
	F	CCACCTCCCATCAAGGCCACTTGCATTCAAGAGCCCAAC
96-P3Aζ	R	TGGTGGTGGCTTGAAGGCGGCGGCTCTTTCCATTATTTC
	F	ATAATGGAAAGAGCCGCCGCCTTCAAGCCACCACCACCT
96-P4Aζ	R	AGGTGGTGCTGCCTTGAAAGCTGGAGGTCTTTCCATTATT
	F	AGCTTTCAAGGCAGCACCACCTGCCATCAAGTACACTTGC
HuZeta-pMP-MluI	R	CCGGGATCTCTCGAGACGCGTTCACCGGGGTGG

2.12 HEK293FT lentivirus transfection

HEK293FT cells were plated at $2x10^6$ cells per T75 flask and grown to 60% confluency in 15 mL of cDMEM. 587.5 µL of supplement-free DMEM was mixed with 37.5 µL of GeneJuice transfection reagent (Novagen, 70967-3), mixed gently and left for 5 minutes at room temperature. For each CAR construct, 3.91 µg of CAR plasmid was added to the DMEM and GeneJuice solution, along with 5.08 µg of pMDLg/pRRE, 3.91 µg of RSV-rev and 2.74 µg of pMD.G2. This solution was gently mixed and left for 15 minutes at room temperature. Plasmid/GeneJuice solution was added to 20 mL of fresh, pre-warmed cDMEM before being used to replace 293FT cell media. Lentivirus containing media was collected after 48-72 hours and either used immediately for target cell transduction or stored at -80^{o}C for future use.

2.13 Lentiviral transduction of Jurkat cells

Jurkat E6 cells were transduced in virus containing supernatant in Nunc non-treated P6 wells. Each P6 well was coated overnight in 400 µL of RetroNectin in sterile PBS (TakaraBio, 8 µg/mL) at 4^{o}C. RetroNectin was removed and each well was washed with sterile PBS before 3 mL of each lentivirus containing supernatant was added to each RetroNectin coated plate and incubated at 4^{o}C for 30 minutes. Jurkat cell media was refreshed with cRPMI the morning of the transduction to ensure optimal condition before being resuspended at $1.5x10^6$/mL prior to application. 1 mL of Jurkat cells was added to each lentivirus containing well (Final concentration of $0.38x10^6$/mL) before being centrifuged for 40 minutes at 1000 g at 32^{o}C. Jurkat CAR+ (J-CAR) cells were cultured for one week before both RQR8 and CAR expression were assessed using Rituximab-APC (2 µg/mL) and anti-FMC63 antibodies (In-house, 0.5 µg/mL). To purify J-CAR T cells, RQR8-tag expressing cells were isolated utilising biotinylated rituximab and a StemCell Biotin Selection Kit (StemCell, 17683) following manufacturers protocol. Briefly, $50x10^6$ J-CAR cells were resuspended at $100x10^6$/mL and incubated

with biotinylated rituximab (In-house, 0.5 µg/mL) for 15 minutes at room temperature. Biotin selection cocktail was added (100 µL/mL) and incubated for 15 minutes at room temperature before magnetic RapidSpheres (50 µL/mL) were added for 10 minutes. This mixture was topped up to 2.5 mL and placed in an EasySep magnet for 5 minutes before non-bound cells were discarded. This was repeated twice more before the retained J-CAR cells were collected and cultured.

2.14 Jurkat CAR-T cell activation assay

J-CAR T-cell were resuspended in cRPMI at $0.5x10^6$/mL before 100µL was added to each well of a U-bottom 96-well plate. Depending on the appropriate J-CAR:Target ratio, target Ramos cells were resuspended in cRPMI at varying concentrations before adding 100 µL to each well. Cells were incubated for the appropriate time points at 37°C + 5% CO_2. At each time point, cells were collected and spun at 450 g for 5 minutes. Cell supernatant was collected for analysis of cytokine production before cells were further washed and stained for flow cytometry analysis.

2.15 Lentiviral transduction of primary T-cells

Producing lentivirus for primary cell transduction followed the same method as for J-CAR generation, scaled down for 6-well plates.

Isolated PBMCs were resuspended at $1x10^6$/mL in TexMACS media (Miltenyi Biotech) supplemented with 100 U/mL Penicillin (Sigma), 100µg/mL Streptomycin (Sigma). Anti-CD3/CD28 TransAct (1/100, Miltenyi Biotech, 130-128-758) was added for 72 hours prior to transduction. 24 hours prior to lentivirus transduction, cells were supplemented with 100 IU/mL IL-2 (Peprotech, 200-02). On the day of lentivirus transduction, cells were washed with supplemented TexMACs to remove TransAct.

Activated primary cells were transduced with neat lentivirus containing supernatant in Nunc non-treated 24-well plates. Each well was pre-coated overnight with 400 µL of RetroNectin in sterile PBS (TakaraBio, 8 µg/mL) at 4°C. RetroNectin was removed and each well washed with sterile PBS before 3 mL of lentivirus containing media was added and incubated at 4°C for 30 minutes. 1 mL of activated cells was added at $1x10^6$/mL (+ 50 IU/mL IL-2) to each well before being centrifuged at 1000 *g* for 40 minutes at 32°C. Centrifuged cells were cultured for 48-72 hours before cells were collected, washed with sterile PBS and resuspended at $1x10^6$/mL in TexMACS (+50 IU/mL IL-2). Transduced cells were maintained at $1x10^6$/mL before transduction efficiency was assessed 6-7 days post-transduction using and an anti-FMC63 antibody (In-house, 0.5 µg/mL) and an anti-mFc PE antibody (1/1000, Jackson Immunoresearch).

2.16 CAR-T Expansion

Primary CAR-T cells were generated as described above. Percentage positive CAR-T cells were normalised using UTR cells. Cells were resuspended in supplemented TexMacs media at $0.5x10^6$ CAR+ T-cells per mL, and 100 µL added to each well. Raji cells were resuspended in supplemented TexMacs media at $0.5x10^6$/mL and 100 µL added to each well. Co-cultures were incubated for the indicated timepoints before being removed for staining. Cells were washed twice with PBS (+1% BSA) and resuspended in 50 µL PBS (+ 10% Heat inactivated human serum) for 10 minutes at 4°C. Cells were stained against CD4, CD8 and CAR (0.5 µg/mL) for 30 minutes at 4°C. Cells were washed and further stained using Biotin-APC (1/100) to stain anti-CAR antibody. CAR+ cells per µL was calculated using Biolegend FACs counting beads.

2.17 CAR-T Killing

Primary CAR-T cells were generated as described above. Percentage positive CAR-T cells were normalised using UTR cells. Cells were resuspended in supplemented TexMacs media at $0.5x10^6$ CAR+ T-cells per mL, and 100 µL added to each well. Raji-GFP cells were resuspended in supplemented TexMacs media at $0.5x10^6$/mL and 100 µL added to each well. Co-cultures were incubated for 6 or 24 hours. At each indicated timepoint, cells were washed once with PBS. Cells were resuspended in a 1/50 dilution of propidium iodide (PI) before GFP+ cell viability assessed.

2.18 Enzyme-Linked Immunosorbent Assay (ELISA)

96-well Nunc Maxisorb plates were coated with 100 µL of capture antibodies (Concentrations detailed in Table 2.3) diluted in coating buffer (Na2CO3 1.59g/L, NaHCO3 2.93g/L) overnight at 4oC. Coated antibodies were removed, and each well was blocked with 200 µL of PBS (+1% BSA) for 1 hour at room temperature. Each plate was washed 4 times with 200 µL of PBS (+1% BSA) before 100 µL of cell supernatant was added for 2 hours at room temperature. For J-CAR activation assays, neat supernatant was utilised, while for primary CAR-T assays supernatant was diluted between 1/50 and 1/200. Each plate was washed 4 times with 200 µL of PBS (+1% BSA) before 100 µL of biotinylated detection antibody (Detailed in Table 2.3) was added for 1 hour at room temperature. Plates were further washed 4 times with 200 µL of PBS (+1% BSA) and 100 µL of streptavidin-HRP (Pierce, 21130) added for 30 minutes at room temperature. Plates were washed 4 times with 200 µL of PBS (+1% BSA) and 100 µL of detection solution added for 5 minutes. Detection solution consisted of 1x Sigma OPD tablet (P9187) dissolved in 25 mL citrate buffer (19.2 g citric acid/L), 25 mL phosphate buffer (28.4 g Na2HPO4/L) and 50 mL dH2O. 50 µL of 2.5 M H2SO4 was added to stop the reaction before the colorimetric change was analysed at 490 nm using an Epoch Microplate Reader.

Table 2.3 ELISA Antibodies

	Target	Clone	Manufacturer	ID	Concentration
Capture	huIL-2	MQ1-17H12	BioLegend	500302	4 µg/mL
Capture	huIFN-γ	MD01	BioLegend	507502	2 µg/mL
Detection	huIL-2	Poly5176	BioLegend	517605	1 µg/mL
Detection	huIFN-γ	4S.B3	BioLegend	502504	4 µg/mL

2.19 PamGene Co-Culture

J-CAR T-cells and Ramos B-cells were washed and resuspended at $1x10^6$/mL and $0.1x10^6$/mL in non-supplemented RPMI before resting for 1 hour at 37°C. J-CAR T-cells were incubated with target Ramos at a cell ratio of 10:1 for 10 minutes at 37°C before being centrifuged at 500 *g* for 8 minutes at 4°C. Supernatant was removed and replaced with 1 mL ice-cold PBS. Cells were further centrifuged at 1000 *g* for 5 minutes at 4°C. Supernatant was removed and cells resuspended in 100 µL per $1x10^6$ cells of M-PER lysis buffer (+ 1:100 Halt Phosphatase Inhibitor, 1:100 Protease Inhibitor). Cells were lysed for 15 minutes on ice, resuspending every 5 minutes. Cell lysate was centrifuged for 15 minutes at 4°C using a table-top centrifuge at 16,000 RPM. Supernatant was collected and protein concentration quantified before being stored at -80°C prior to use.

2.20 PamGene Kinase Analysis Run

Use of the PamStation to assess phosphotyrosine and serine/threonine kinase activity in cell lysate was carried out according to manufacturer instructions. PamChips were first blocked with 30 µL 2% BSA solution for 30 minutes. Cell lysate samples were prepared using manufacturer reagents according to instructions. 10 µL of each cell lysate preparation was loaded onto PamChips and were run using manufacturers defined protocol. Further details on PamStation protocol are available at: https://pamgene.com/ps12/

2.21 SEE Loading

Raji or Raji-CD155 cells to be loaded with Staphylococcus enterotoxin type E (SEE) were washed twice in non-supplemented RPMI. Cells were resuspended in non-supplemented RPMI + 60 ng/mL SEE (Cusabio, CSB-MP320170FKZ) at $1x10^6$/mL and incubated at 37°C + 5% CO2 for 30 minutes. SEE loaded cells were further washed twice with cRPMI before counted and resuspended at the required concentration.

2.22 SEE induced CD155 ligand upregulation

PBMCs were processed and T-cells were isolated as described above. Isolated T-cells were resuspended at $0.5x10^6$/mL and 100 µL plated in triplicate in a U-bottomed 96-well plate. SEE loaded or unloaded Raji and Raji-CD155 cells were prepared at $0.05x10^6$/mL in cRPMI before 100 µL was added to T-cells for a 10:1 E:T ratio. CD4+ and CD8+ T-cell expression of CD96, TIGIT and CD226 was assessed daily by flow cytometry over 5 days.

2.23 SEE induced T-cell proliferation

PBMCs were processed and T-cells were isolated as described above. Isolated T-cells were resuspended in PBS at $20x10^6$/mL. An equal volume of PBS + 3 µM CFSE was added for a final concentration of 1.5 µM CFSE. Cells were mixed thoroughly, covered and incubated at 37°C for 10 minutes. CFSE was quenched by adding twice the initial volume of cRPMI and centrifuged at 450 *g* for 10 minutes. This wash was repeated before CFSE-labelled T-cells were counted and resuspended at $1x10^6$/mL in cRPMI.

Fc-silent anti-human CD96 (19-134 N297S, BliNK Therapeutics) or equivalent matched isotype were prepared at 100 µg/mL in cRPMI before 50 µL of antibody (Final 25 µg/mL) was added to 50 µL of CFSE labelled T-cells and incubated for 15 minutes at 37°C prior to target Raji cells being added. SEE loaded or unloaded Raji and Raji-CD155 cells were prepared at $0.05x10^6$/mL in cRPMI before 100 µL were added to T-cells/antibodies. Cells were incubated for 3, 4 and 5 days before CD4+ and CD8+ T-cell proliferation was assessed through CFSE dilution.

2.24 Software

FlowJo (v10.10) was used for analysis of flow cytometry data. GraphPad Prism 10 was used for the preparation of graphs and statistical analysis. ImageJ was used for analysis of western blots.

2.25 Statistical Analysis

Statistical analysis was carried out using GraphPad Prism 10. Statistical tests and corresponding *p* values utilised for each experiment are indicated in each figure. Mixed model analysis was utilised for PBMC antibody proliferation and CD25 upregulation. Two-way ANOVA with Tukey test was used for J-CAR assays. Mixed model analysis was used for primary CAR-T assays. Two-way ANOVA with Tukey test was used for SEE model PBMC proliferation. A *p* value of <0.05 was deemed significant.

Chapter 3 Developing novel CD96 targeting antibodies

3.1 Phage display screening for CD96 binding scFv clones

To identify novel anti-CD96 antibodies, phage-display antibody panning was utilised. Phage-display panning employs the use of bacterial-phage libraries, with bacteriophages expressing a collection of potential single chain variable fragments (scFvs) on their surface. These bacteriophage libraries are first panned against plate-captured non-target proteins (protein depletion), followed by plate-captured target proteins (protein selection). Following this, phages are first panned against transduced cells expressing a non-target protein (cell depletion), before panning against cells expressing a target protein (cell selection) (Figure 3.1A). Cell lines expressing both target (CD96) and non-target (CD226) were first generated before panning was carried out by Dr. Jinny Kim in conjunction with the company BioInvent. The specific phage display selection strategy employed by Dr. Jinny Kim first panned a BioInvent phage library against plate-bound recombinant human CD226 (23.6% homology with huCD96) or mouse CD226 (18.7% homology with mCD96), the chosen non-target. As a stimulatory receptor which also binds CD155, ensuring that isolated scFv clones did not bind CD226 was imperative, therefore CD226 was chosen as a non-target. Following this, scFv expressing bacteriophage libraries were panned against plate-bound recombinant human or mouse CD96 to select for binders of CD96. This initial panned stage enabled depletion of scFv clones which would bind CD226, whilst selecting for scFv which would recognise CD96.

Depleted libraries then underwent a second depletion stage against cell expressed human or mouse CD226. Following this, scFv expressing phage were further selected for their binding of cell expressed huCD96v2 or mCD96. This panning against cell expressed non-target and target was repeated a second time for a final third round of phage panning. This panning strategy resulted in two groups of scFv, one panned for huCD96v2 binding, the other for mCD96. To identify scFv capable of binding both human and mouse CD96, a third panning strategy was used. Rather than repeating the panning of phage against cell expressed non-target or target (round 3), phage initially panned against huCD96v2 was instead panned against cell expressed mCD226 and mCD96, whilst phage initially panned against mCD96 were further panned against cell expressed huCD226 and huCD96v2.

This panning strategy resulted in the identification of three groups of scFv, distinct from one another according to the panning strategy utilised. A total of 39 unique anti-human CD96 scFv were identified according to their binding of both plate-bound and cell-expressed huCD96v2, whilst 20 unique anti-mouse CD96 scFv were identified based on their similar binding of both plate-bound and cell-expressed mCD96. Finally, a third group of 23 scFv were identified according to their binding of both human CD96v2 and mouse CD96.

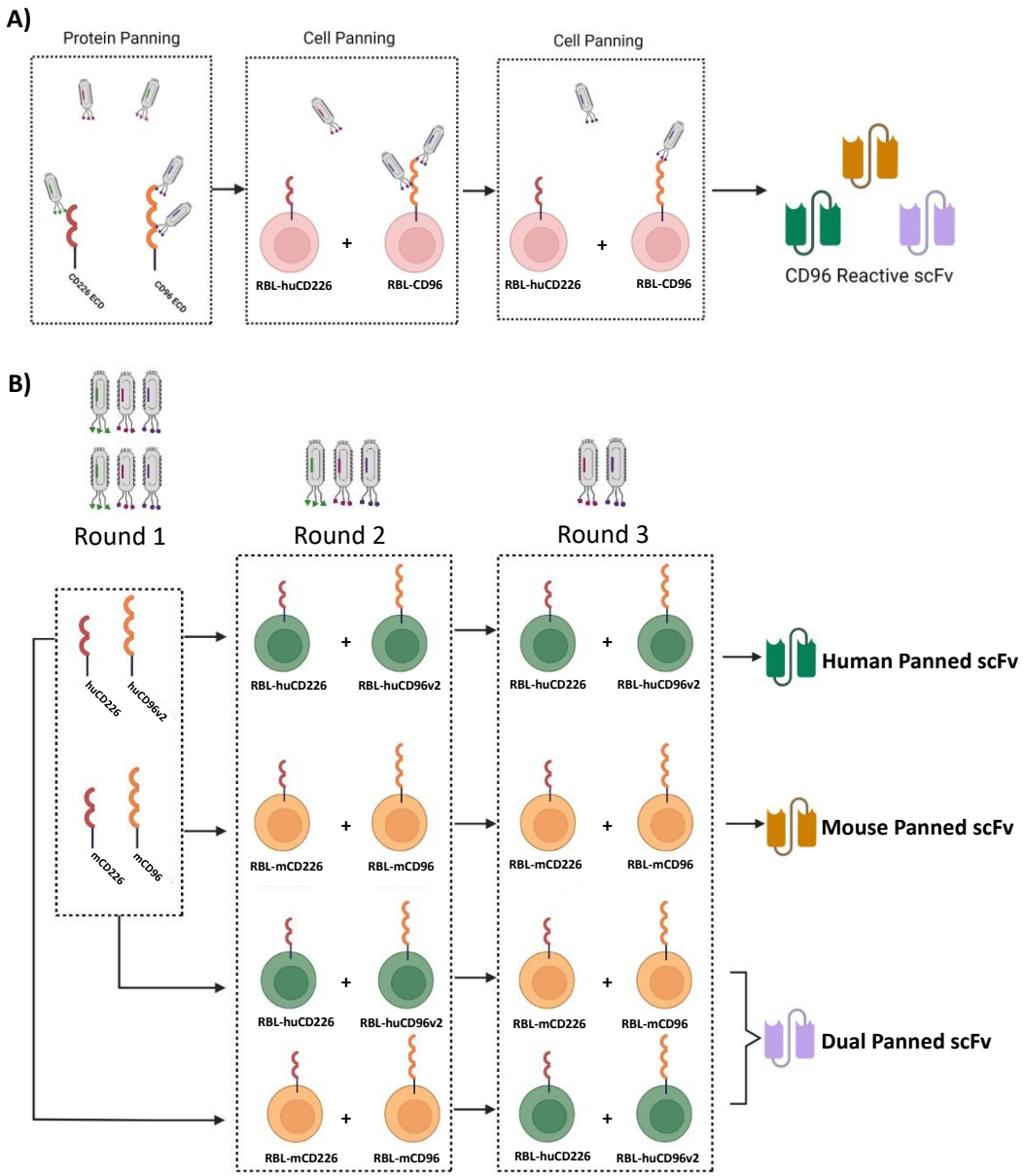

Figure 3.1 Graphical overview of the phage-display panning strategy utilised to identify novel anti-CD96 scFv clones

A) Graphical representation of phage-display panning indicating the three rounds of panning potential scFv expressing phages undergo to identify binding clones **B)** During the first round of panning, our phage library was passed over the plate-captured extracellular domain of either human or mouse CD226 followed by CD96. To isolate single species reactive clones, phage were further passed over RBL cells expressing either human or mouse CD226 before being passed over RBL cells expressing CD96. This panning was repeated twice to generate human or mouse CD96 reactive scFv. To generate cross-reactive scFv, phage panned against human CD96 were then panned against mouse CD96, while phage panned against mouse CD96 were panned against human CD96.

3.2 Generating CD96 expressing RBL cells

Panning for novel anti-CD96 antibodies required the generation of cells expressing either huCD96v2 or mCD96. Considering that CD226 is also known to bind CD155 and acts to transduce activating

signals in T-cells, ensuring panned scFv or downstream antibodies did not in fact bind CD226 was imperative. Therefore, both human and mouse CD226 were utilised as a negative control to pan potential scFv clones against, ensuring that identified antibodies were not in fact interacting with CD226. Rat basophilic leukaemia (RBL) cells were chosen as a target cell for bacteriophage panning for their ease of transduction and their inherent non-expression of both human or mouse CD96 and CD226. To generate RBL cells which express each required target and non-target, the insertion of each gene of interest was required such that it would be consistently expressed. Therefore, the retroviral vector pMP71 was identified as a suitable vector for the generation of γ-retroviruses for the transduction of target RBL cells.

3.2.1 Cloning of genes of interest into the retrovirus vector pMP71

To generate a γ-retrovirus suitable for the transduction of target RBL cells, each gene of interest was commercially sourced, isolated and cloned into the retroviral vector, pMP71-Inv (Figure 3.2A). Each commercially sourced gene was initially digested and removed from a shuttle vector using the restriction enzymes Not1 and Sal1 before being isolated and purified. pMP71-Inv was identically digested to remove a 1067 base pair (bp) stuffer sequence, into which each gene of interest was inserted. To confirm that the digestion and isolation of each gene of interest was successful, 20 and 40 ng of each were assessed by gel electrophoresis (Figure 3.2C-D). These gels indicated the presence of digested and isolated product at each of the appropriate molecular weights; 6797 bp (pMP71-inv), 1845 bp (huCD96v2), 1945 bp (mCD96), 1044 bp (huCD226), 1035 bp (mCD226). Subsequently, extracted DNA was ligated into the digested retroviral plasmid to produce pMP71-huCD96v2, pMP71-mCD96, pMP71-huCD226 and pMP71-mCD226 (Appendix A). Ligated product was then transformed into competent *E. coli* (JM109) cells before being maxiprepped.

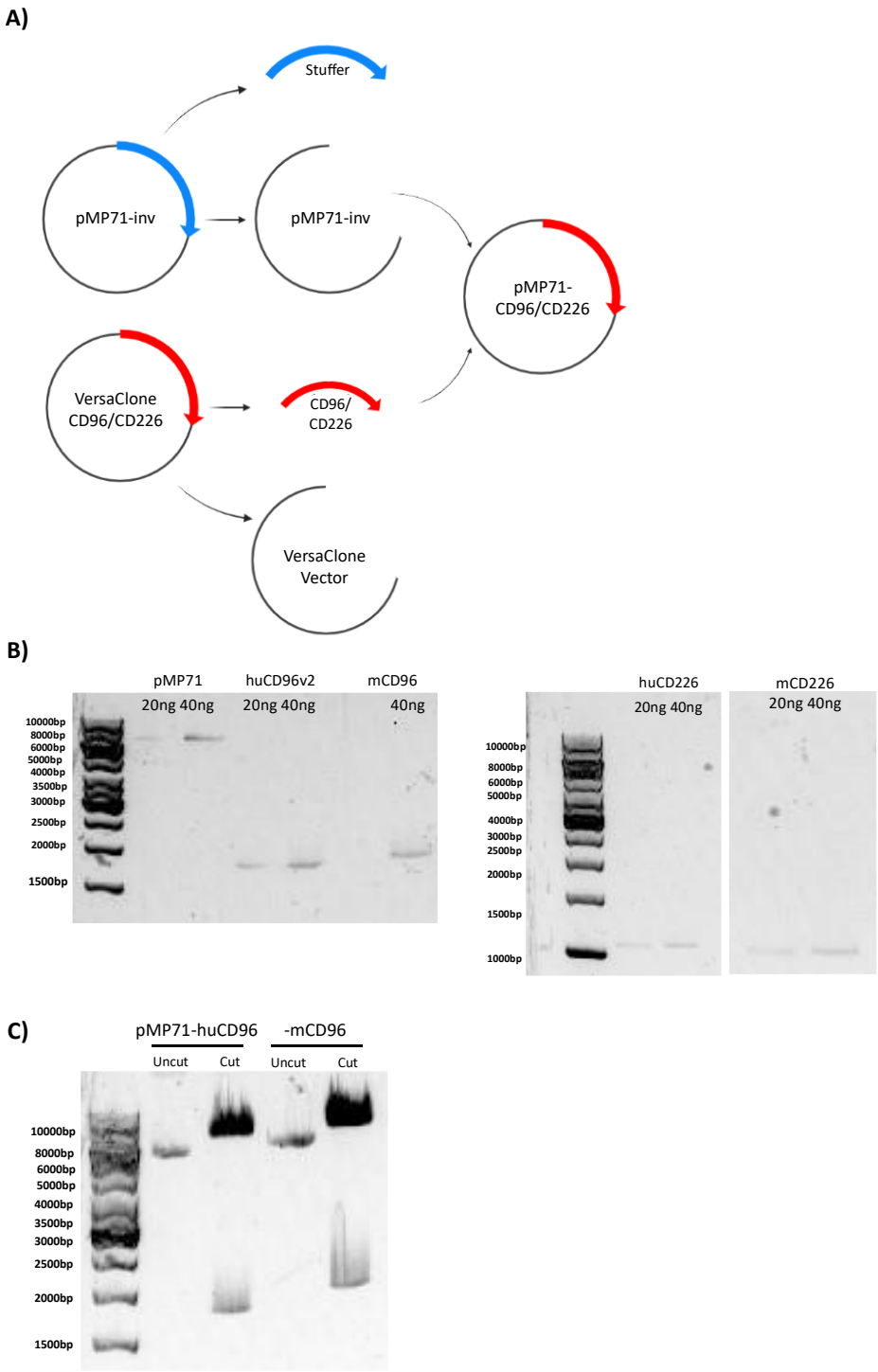

Figure 3.2 Cloning of human and mouse CD96 and CD226 into the pMP71 vector

A) Schematic diagram indicating the overall cloning method of removing the stuffer from pMP71-inv, or our gene of interest from its carrier vector, and the subsequent clonal insertion of each gene into the digested pMP71-inv vector. **B)** Digested and isolated pMP71-inv, huCD96, mCD96, huCD226 and mCD226 was gel electrophoresed with a 10% agarose gel **C)** Digested pMP71-huCD96 or pMP71-mCD96 was ran through an agarose gel to confirm the insertion of our gene of interest, indicated by the DNA band visible at the correct molecular weight.

To confirm the successful insertion of huCD96v2 or mCD96 into the pMP71 vector, purified plasmid was digested and distinguished by molecular weight (MW) using gel electrophoresis. Using the Not1 and Sal1 restriction enzymes, pMP71-huCD96v2 and pMP71-mCD96 were digested resulting in bands at the expected MW of 1845 bp and 1945 bp respectively, with a band representing pMP71 at the expected weight of 6797 bp (Figure 3.2C).

Due to the similar size of both human and mouse CD226 DNA to that of the stuffer sequence removed from pMP71, a different digestion method was required to confirm the insertion of huCD226 or mCD226 (Figure 3.3A). As such, if the transformation of JM109 cells had resulted in cells being transformed with undigested pMP71 vector which lacked either species CD226 insert, it would be indistinguishable in a diagnostic digest. To overcome this, specific restriction sites were identified which would digest the initial pMP71 vector and pMP71-CD226 in distinctly different ways, resulting in unique patterns of plasmid fragmentation. While pMP71-huCD226 was digested with EcoR1 alone, pMP71-mCD226 was digested with Not1, Sal1 and EcoR1. As highlighted in Figure 3.3B, this approach resulted in distinct differences in the digestion of CD226-containing plasmids. These resulting molecular weights correspond to the fragments predicted when interrogating our relevant plasmid maps and predicted cut sizes (Figure 3.3A). Figure 3.3B highlights the similarity in fragment molecular weight resulting from pMP71-inv and pMP71-CD226 plasmids being digested with Not1 and Sal1. When pMP71-huCD226 was digested with EcoRI alone, fragments corresponding to 4829bp, 2106bp and 906bp were generated whilst when the pMP71-inv vector is identically digested, fragments with the weights of 5626bp, 1332bp and 906bp are generated. Similarly, when pMP71-mCD226 was digested with EcoRI, NotI and SalI, fragments are generated with molecular weights of 4573bp, 1318bp, 906bp and 861bp whilst digestion of the pMP71-inv vector resulted in fragments of 4573bp, 1318bp, 1053bp and 906bp (Figure 3.3B). These observed digestion results align with the predicted fragments in Figure 3.3A.

The generation of retroviral transfer plasmids containing each gene of interest was integral to generate cell lines which express each protein of interest. This data shows that each of the required genes had been successfully cloned into the pMP71 transfer plasmid and was suitable to utilise for RBL cell transduction.

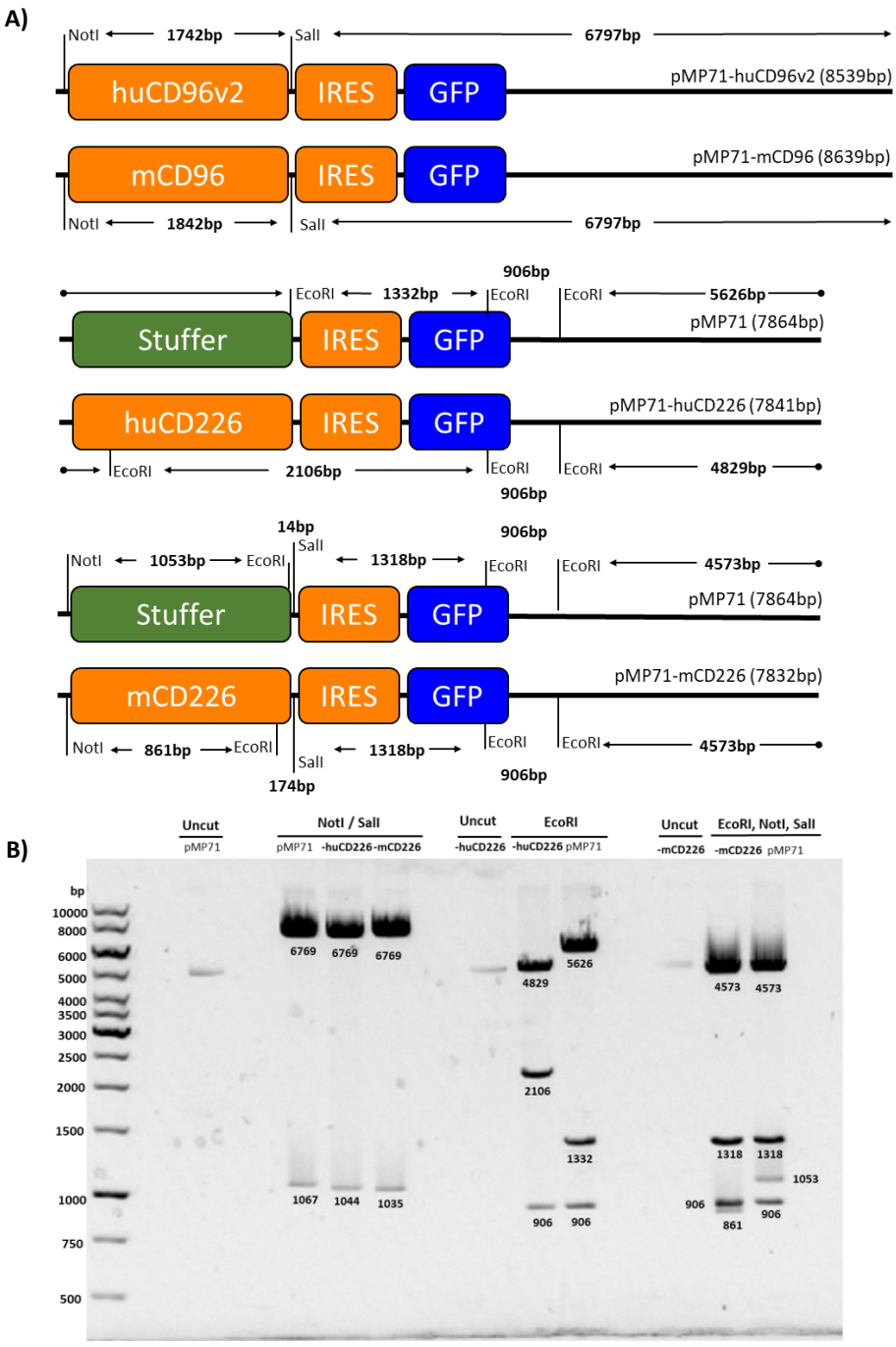

Figure 3.3 Diagnostic digests of pMP71-huCD226 and pMP71-mCD226

A) Schematic diagram of the constructed pMP71-inv plasmids, including the unique restriction sites utilised to confirm the presence of our gene of interest alongside the corresponding fragment sizes. **B)** Multi-digest of pMP71-huCD226 and pMP71-mCD226 with the indicated restriction enzymes to confirm the presence of our gene of interest within the pMP71-inv vector rather than the original stuffer. Not shown are the 14bp and 174bp fragments from pMP71 and pMP71-mCD226 digestion which are lost due to their small size.

3.2.2 Retroviral transduction of rat basophilic leukaemia cells

To facilitate the generation of γ-retroviruses for target cell transduction, the second-generation γ-retroviral production cell line Phoenix-Ecotrophic was utilised. Phoenix-Eco cells were developed at Stanford University to express the Gag-Pol and ecotropic Env components required for effective γ-retrovirus assembly. Phoenix-Eco cells were first transfected with each newly generated pMP71 transfer plasmid, before γ-retrovirus containing supernatant was collected and used to transduce target RBL cells. To ensure each cell population expressed a consistent level of target protein, cells were sorted utilising fluorescence-activated cell sorting (FACS) according to expression of green fluorescent protein (GFP), a marker protein present within the pMP71 vector. FACs of transduced RBL cells was carried out by Dr. Anne Rogel. Cells were routinely screened for CD96 or CD226 expression, as shown in Figure 3.4.

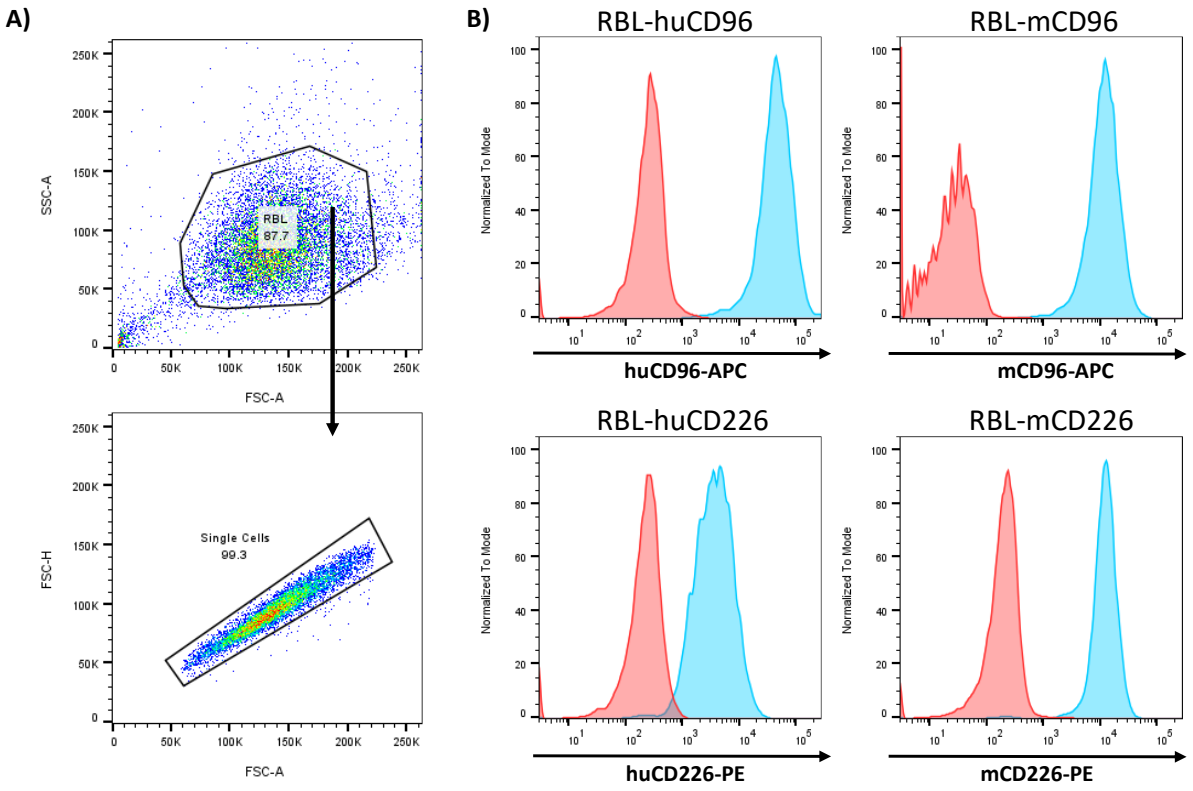

Figure 3.4 Expression of human or murine CD96 or CD226 on FACs sorted RBL Cells

A) Representative gating of RBL cells, gated for viable cells utilising SSC-A vs. FSC-A and for single cells utilising FSC-H vs. FSC-A. **B)** Staining of FACs sorted RBL cells against human or mouse CD96 and human or mouse CD226. Expression of each protein of interest is coloured blue, whilst a matched isotype control is shown in red.

3.3 Characterisation of phage-display panned scFv clones

To characterise scFv clones identified through the phage-display method described in Figure 3.1, RBL cell lines expressing huCD96v2 or mCD96 were utilised to assess both the capacity of scFv clones to bind CD96, as well as their ability to block the interaction between CD96 and CD155. CD96 expressing RBL cells were suspending in serial dilutions of each scFv clone (10 to 0.05 µg/mL) before scFv binding was quantified by detection of a histamine (His) tag on each scFv via fluorescently labelled anti-His antibody. In a similar fashion, the blocking capacity of each scFv was assessed by their ability to block the binding of recombinant human or mouse CD155 (CD155-Fc) to RBL expressed CD96. RBL cells were incubated with titrations of each scFv clone prior to being incubated with CD155-Fc containing an avidin tag. Binding of CD155-Fc was detected utilising fluorescently labelled streptavidin. To assess how each scFv clone may block binding of CD155-Fc, each clone was assessed compared to binding of CD155-Fc to RBL-CD96 in the absence of an scFv clone.

3.3.1 Characterisation of scFv panned against human CD96v2

To assess the capacity of scFv clones panned against huCD96v2 to bind RBL-huCD96v2, a titration of each clone were prepared and incubated with RBL cells. To quantify binding of each scFv, the EC_{50} of each clone was calculated to determine the concentration of scFv required to achieve 50% of maximum binding, as well as the B_{Max} value to indicate the maximum binding as determined by the maximal geometric mean. These values are shown in Figure 3.5A and Figure 3.5B.

The panel of scFv clones panned against huCD96v2 had a wide range of binding to RBL-huCD96v2. Of the 39 individual scFv clones identified by phage-display to bind huCD96v2, characterisation of their specific binding to cell expressed huCD96v2 indicated that 2 clones did not bind and so were false positives (clones H16 and H42). Of the remaining 37 scFv clones, 7 clones (H05, H11, H17, H25, H29, H36 and H46) were found to exhibit decreased binding of huCD96v2 with respect to other more capable clones, with EC_{50} values greater than 1.9 µg/mL. This increased EC_{50} value however did not preclude some clones from exhibiting strong binding of huCD96v2 at high concentrations, with clone H29 recording a B_{Max} value exceeding 5500 whilst having a comparatively high EC_{50} value of 2.16 µg/mL. Overall, scFv clones identified through phage-display panning against human CD96v2 resulted in a group of scFv clones exhibiting a range of binding capacity. These clones were then further analysed for their capacity to block binding of huCD155-Fc.

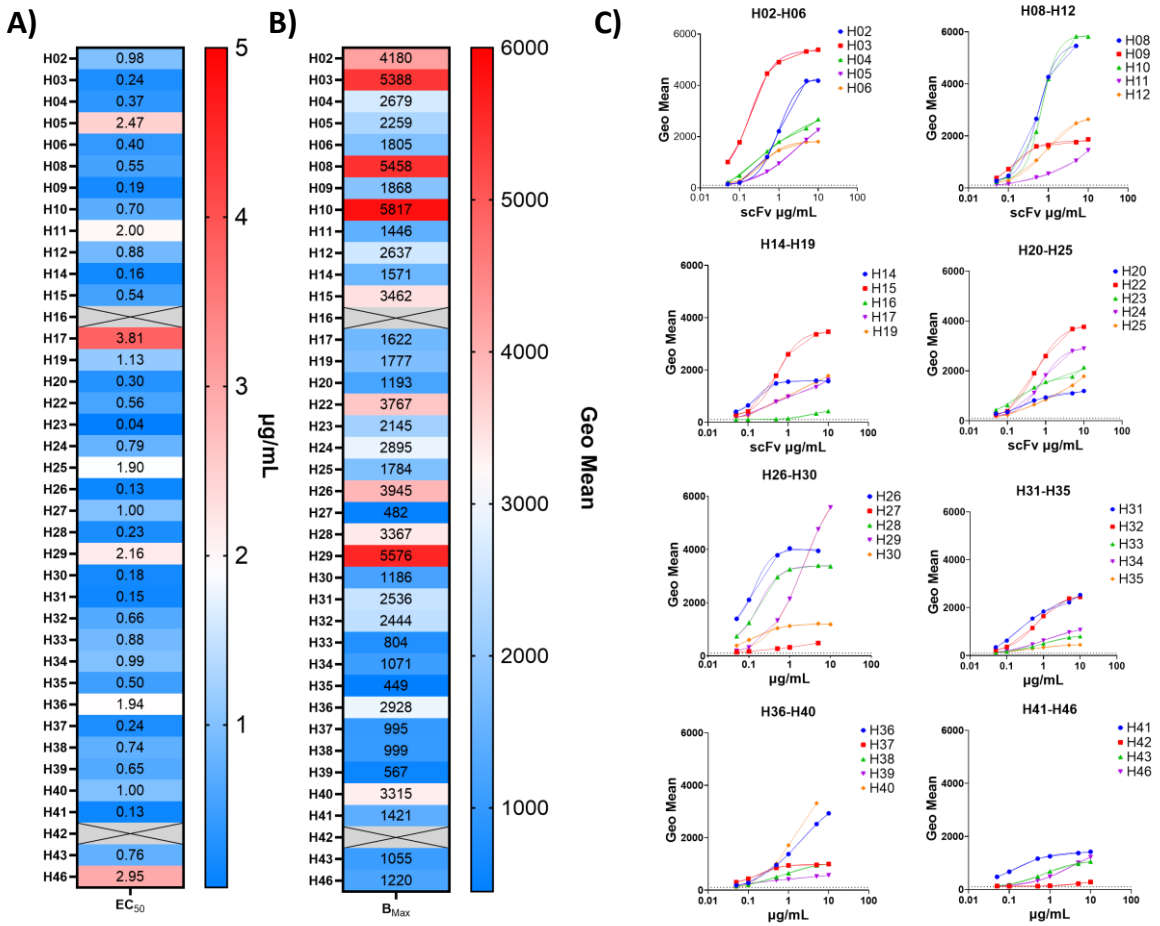

Figure 3.5 Human panned scFv binding of RBL-huCD96

A) EC_{50} values indicating binding of each huCD96v2 panned scFv clone to RBL expressed huCD96v2. EC_{50} values calculated using binding curve of each scFv titration. **B)** B_{Max} values for each huCD96v2 scFv clone, highlighting the maximum geometric mean of each scFv to RBL expressed huCD96v2. **C)** Titration of each dual-panned scFv, highlighting binding to RBL-huCD96v2. Binding of scFv was detected through anti-His antibody and is represented by the geometric mean of each scFv concentration. Heatmaps are coloured according to change in values. Red indicates an increased EC_{50} or IC_{50} value, whilst blue indicates a decreased value. Each scFv was assessed for binding of huCD96v2 once.

As with the binding of scFv clones panned against huCD96v2, their ability to block the binding of huCD155-Fc to huCD96v2 was varied (Figure 3.6A). Of the two clones which failed to bind huCD96v2 (H02 and H42), both also failed to inhibit huCD155-Fc binding, indicative of an inability to bind huCD96v2 (Figure 3.6B). Of the remaining 37 clones, 8 exhibited IC_{50} values greater than 2 μg/mL (H05, H27, H31, H33, H38, H39, H40 and H46). A greater number of huCD96v2 reactive scFv clones were capable of impeding the binding of huCD155-Fc, however two clones shown to bind huCD96v2 exhibited no inhibition of huCD155-Fc binding (H02 and H08). This result will be beneficial for future assessment of whether antibody blockade of huCD155 impedes intrinsic CD96 activity.

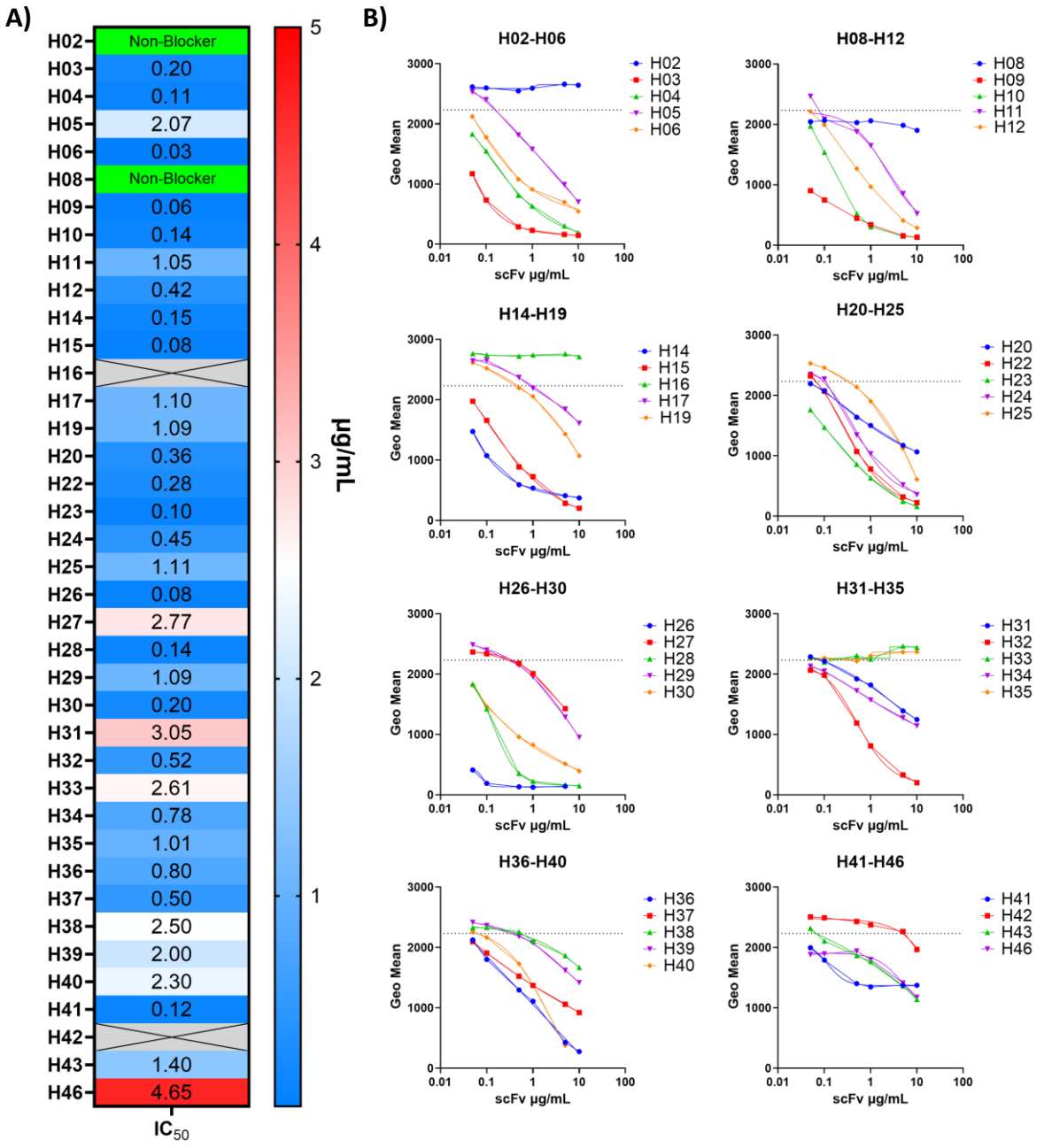

Figure 3.6 Human panned scFv blocking of huCD155 binding to RBL-huCD96

A) IC_{50} values for each scFv clone represented as a heatmap for each clone identified through phage-display panning against huCD96v2. IC_{50} values are coloured according to increasing inhibition - Blue represents low IC_{50} values, red indicates high IC_{50} values. **B)** Inhibition of huCD155 binding to RBL-huCD96v2 by titrated huCD96v2 specific scFv clones. Geometric mean shown highlights huCD155 binding, detected utilising fluorescently labelled Streptavidin against huCD155 avidin tag.

To better understand whether the ability of scFv to bind huCD96v2 may corelate with inhibition of huCD155-Fc binding, calculated IC_{50} values for each clone were plotted against EC_{50} values to calculate an r^2 value, indicating any correlation between the binding of huCD96v2 and blocking of huCD155-Fc (Figure 3.7). Correlating the EC_{50} and IC_{50} values of scFv clones reactive against huCD96v2 resulted in an r^2 value of 0.17. This r^2 value is low and so suggests no correlation between the two factors.

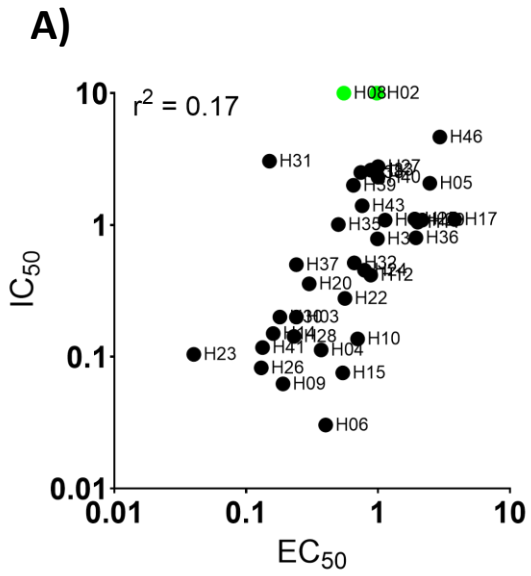

Figure 3.7 Correlation between the IC50 and EC50 values of human CD96 reactive scFv

A) The recorded IC_{50} and EC_{50} values for human CD96v2 panned scFv clones are plotted against each other to determine the correlation between the two values, represented by the calculated r^2 value. Green datapoints represent scFv clones which do not block the huCD96v2 interaction with huCD155.

3.3.2 Characterisation of scFv panned against mouse CD96

Following analysis of scFv clones panned against huCD96v2, the group of 20 scFv panned against mCD96 were characterised. These scFv were again assessed for both their binding of RBL expressed mCD96, as well as their ability to impede the binding of mCD155 to mCD96.

Of the 20 scFv identified by phage-display to bind mCD96, 18 exhibited effective binding of RBL expressed mCD96. Clones M14 and M17 failed to significantly bind mCD96 at any concentration (Figure 3.8A/B), and were therefore deemed to be false-positive non-binders. Of the 18 scFv which bound mCD96, a range of binding characteristics was recorded. As with scFv panned against huCD9v2, a low EC_{50} value was not indicative of greater overall target binding. Whilst the scFv clone M03 exhibited a low EC_{50} value of 0.69 µg/mL, overall total binding of mCD96 was low with a B_{Max} value of 705. Conversely, clone M06 bound mCD96 effectively at high concentrations with a B_{Max} value of 3243, however had a low affinity for mCD96 resulting in an EC_{50} value of 1.93 µg/mL.

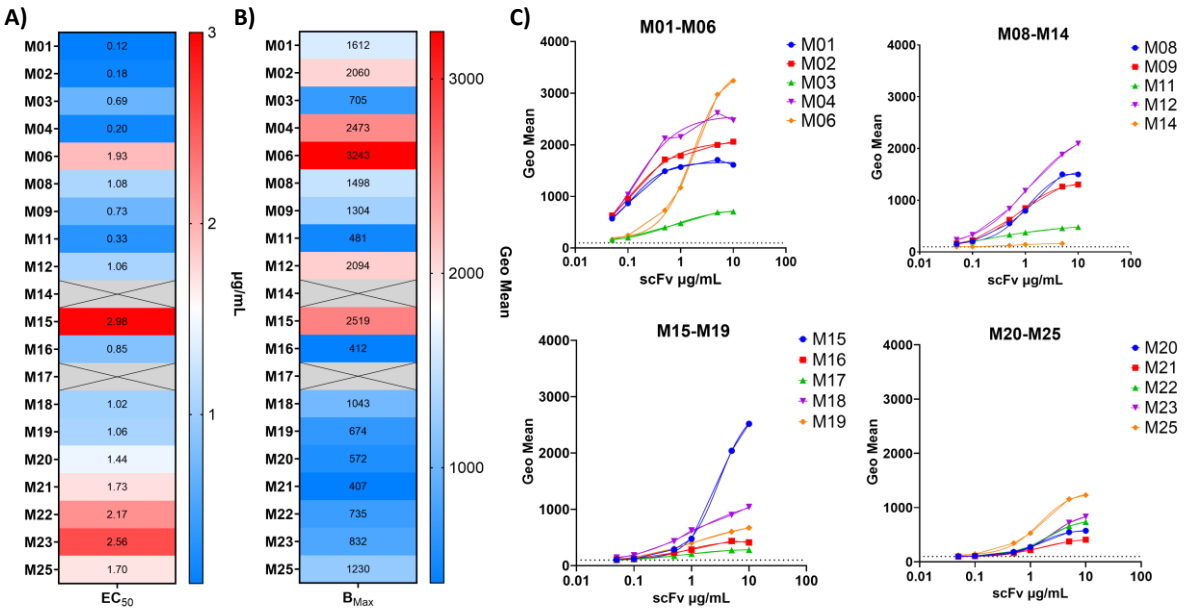

Figure 3.8 Mouse panned scFv binding of RBL-mCD96

A) EC_{50} values indicating binding of each mCD96 panned scFv clone to RBL expressed mCD96. EC_{50} values calculated using binding curve of each scFv titration. **B)** B_{Max} values for each CD96 scFv clone, highlighting the maximum geometric mean of each scFv to RBL expressed mCD96. **C)** Titration of each mCD96 panned scFv, highlighting binding to RBL-mCD96. Binding of scFv was detected with an anti-His antibody and is represented by the geometric mean of each scFv concentration. Heatmaps are coloured according to change in values. Red indicates an increased EC_{50} or IC_{50} value, whilst blue indicates a decreased value. Each scFv was assessed for binding of huCD96v2 once.

To determine how each mCD96-reactive scFv may act to limit the binding of recombinant mCD155-Fc to RBL-mCD96, each clone was titrated and incubated with RBL-mCD96 cells. Binding of mCD155-Fc was then assessed to determine the IC_{50} value for each scFv clone.

Of the 18 scFv clones which exhibited binding to RBL-mCD96 (Figure 3.8), 2 clones were subsequently identified to be non-blocking. Incubation of RBL-mCD96 with either M04 or M09 failed to inhibit the binding of mCD155-Fc to RBL expressed mCD96 (Figure 3.9A/B). When quantifying the ability of scFv panned against mCD96 to inhibit mCD155-Fc binding, a number of other clones also appeared to lack the capacity to block mCD155-Fc binding. However, comparison of this blocking data with the binding data presented in Figure 3.8 indicates that these clones are in fact poor binders of mCD96, suggesting that this is in fact due to a lack of ability to bind mCD96 rather than these clones being non-blockers. This group includes clones M16, M19, M20, M21 and M22 and are indicated by asterisks in Figure 3.9B. Interestingly, clone M25 was found to be a weak binder of mCD96 comparative to other clones yet was an effective blocker of mCD155-Fc. This suggests that weak scFv interaction with mCD96 does not preclude an scFv from being an effective blocker of mCD155.

Overall, this data suggests that of the 18 scFv clones panned against mCD96, only a fraction are capable of binding strongly to mCD96. Of these clones, 2 scFv are capable of binding effectively to mCD96 whilst not limiting its interaction with mCD155.

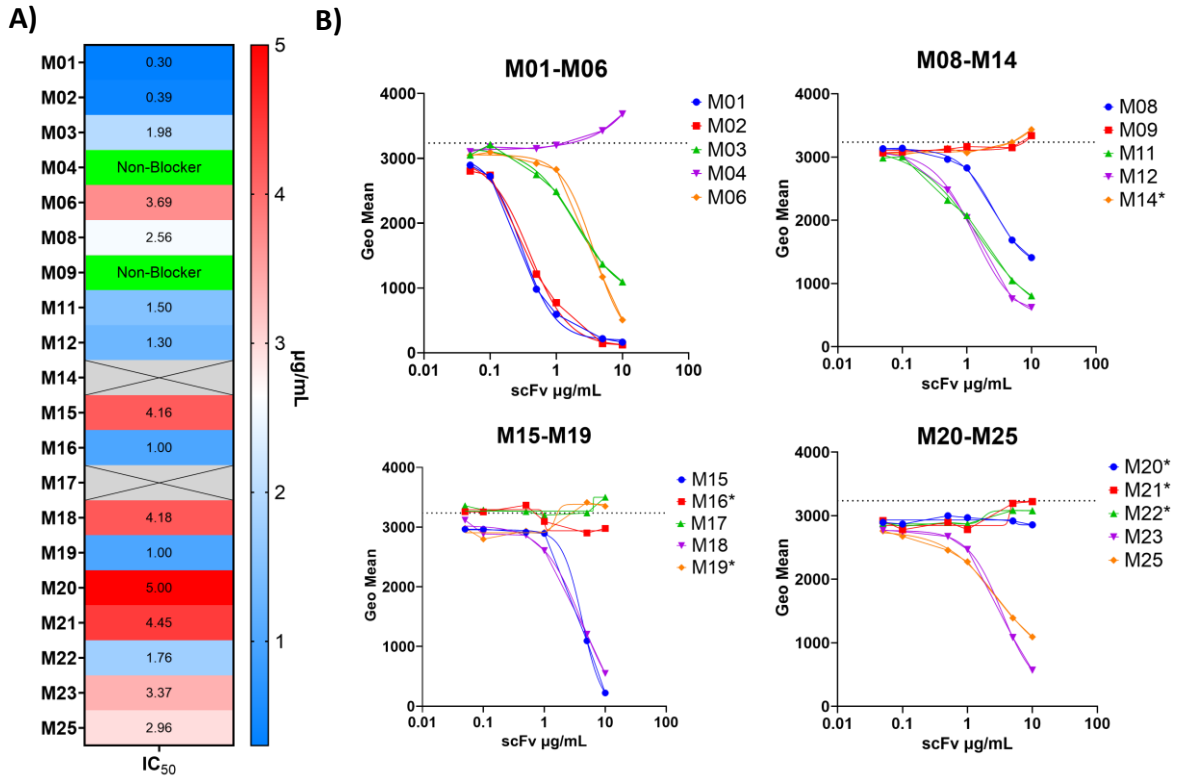

Figure 3.9 Mouse CD96 panned scFv blocking of mCD155 against RBL-mCD96

A) IC_{50} values for each scFv clone represented as a heatmap for each clone identified through phage-display panning against mCD96. IC_{50} values are coloured according to increasing inhibition - Blue represents low IC_{50} values, red indicates high IC_{50} values. **B)** Inhibition of mCD155 binding to RBL-mCD96 by titrated mCD96 specific scFv clones. Geometric mean shown highlights mCD155 binding, detected utilising fluorescently labelled Streptavidin against mCD155 avidin tag.

As with scFv clones panned against huCD96v2, understanding how the IC_{50} value of each scFv clone correlates with its corresponding EC_{50} value was of interest. Both values were again plotted against one another to generate an r^2 value to indicate whether the binding of mCD96 correlates with capacity to limit CD155 binding (Figure 3.10). Correlating the two groups of values resulted in an r^2 value of 0.0008, indicating that there is no correlation between scFv binding of mCD96 and its ability to block mCD155 binding. This correlation result is similar to that of scFv clones panned against huCD96v2.

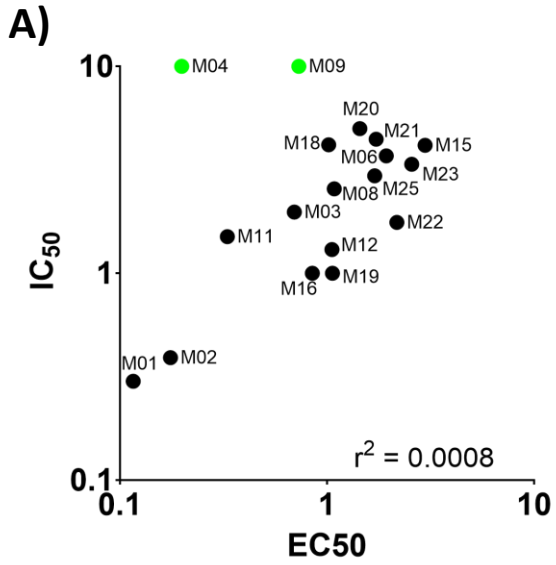

Figure 3.10 Correlation between the IC50 and EC50 values of mCD96 reactive scFv

A) The recorded IC_{50} and EC_{50} values for mCD96 panned scFv clones are plotted against each other to determine the correlation between the two values, represented by the calculated r^2 value. Green datapoints represent scFv clones which do not block the mCD96 interaction with mCD155.

3.3.3 Characterisation of scFv panned against both human and mouse CD96

To assess the binding characteristics of scFv clones generated by panning against both huCD96v2 and mCD96, scFv were again titrated and their binding of RBL-huCD96v2 quantified.

Binding of clones D01-D23 to RBL-huCD96v2 produced a broad range of binding affinities (Figure 3.11). Of the 23 scFv clones identified by phage-display to bind both huCD96v2 and mCD96, only 1 clone failed to bind RBL-huCD96v2 when quantifying scFv characteristics and was deemed a false-positive (D22). A further 2 clones were found to be poor binders of RBL-huCD96v2 (D09 and D21), exhibiting low B_{Max} values. Conversely, a greater number of scFv clones exhibited strong binding of RBL-huCD96v2. Clones D03 and D07 both have EC_{50} values below 0.5µg/mL, indicating that of the 22 clones which interact with huCD96v2, they represent the two clones which most strongly bind as a scFv.

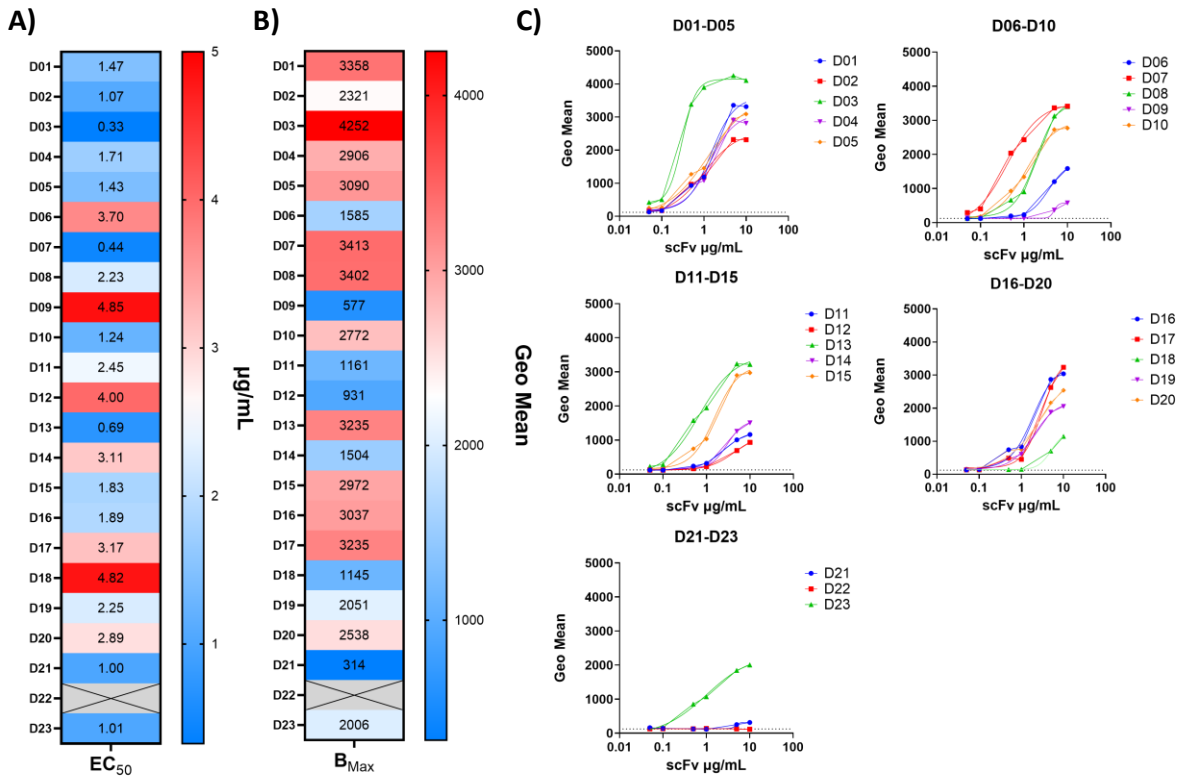

Figure 3.11 Dual-panned scFv binding of RBL-huCD96

A) EC_{50} values indicating binding of each dual-panned scFv clone panned against RBL expressed huCD96v2. EC_{50} values calculated using binding curve of each scFv to RBL expressed huCD96v2. **B)** B_{Max} values for each dual-panned scFv clone, highlighting the maximum geometric mean of each scFv to RBL expressed huCD96v2. **C)** Titration of each dual-panned scFv, highlighting binding to RBL-huCD96v2. Binding of scFv was detected through anti-His antibody and is represented by the geometric mean of each scFv concentration. Each scFv was assessed for binding of huCD96v2 once.

To quantify the ability of dual-panned scFv clones to inhibit the interaction of huCD96v2 with huCD155-Fc, binding of huCD155-Fc was quantified following the incubation of RBL-huCD96v2 cells with a titration of each scFv.

The limited binding of scFv clones D09 is reflected in their poor capacity to block huCD155 binding of huCD96v2 (Figure 3.12). However, whilst D21 was a poor binder of RBL-huCD96v2, its blockade of huCD155-Fc was greater than that of scFv clones with higher affinity. A number of scFv clones were found to be poor mediators of the inhibition of huCD155 binding. Clone D06 exhibited an IC_{50} value of 6.65 μg/mL, the highest IC_{50} value recorded with dual-panned scFv clones. This result again correlated with a high EC_{50} value, indicating that clone D06 is representative of a clone with weak binding and therefore weak blocking capacity. Clone D14 mirrored this result, although not to the same extent. Among this panel of dual-panned scFv clones however were a number which exhibit strong capacity to inhibit huCD155-Fc binding. Clones D03, D07 and D05 each exhibit IC_{50} values below 1 μg/mL, corresponding to simultaneous strong binding of RBL-huCD96v2 (Figure 3.11). Further to evidence presented in Figure 3.11 suggesting an inability to bind RBL-huCD96v2, clone D22 failed to inhibit huCD155 binding.

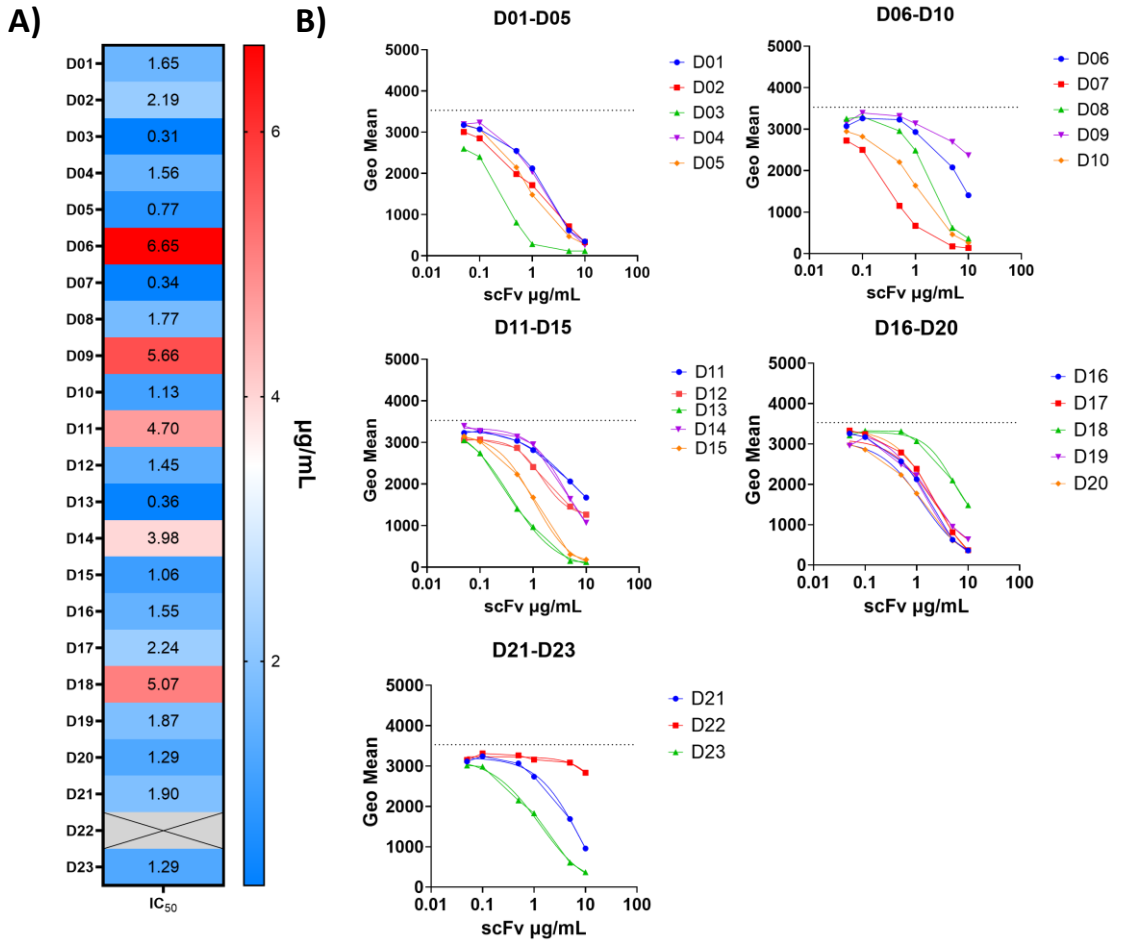

Figure 3.12 Dual-panned scFv blocking of huCD155 binding huCD96

A) The capacity for each dual-panned scFv to inhibit the binding of huCD155 with RBL expressed huCD96v2 is represented as a calculated IC_{50} value. A colour gradient heat-map is utilised to indicate variation in calculated IC_{50} value with blue representing low values and red representing large values. IC_{50} values are shown as the concentration (µg/mL) of each scFv clone required to limit huCD155 binding of huCD96v2 to 50% of the maximum binding. **B)** Binding curves of huCD155 to RBL expressed huCD96v2 with titrations of each dual-panned scFv. IC_{50} values were calculated utilising these binding curves. Each scFv titration inhibition of huCD155 binding was assessed once.

To better understand any correlation between dual-panned scFv binding of huCD96v2 and their capacity to inhibit huCD155 binding, the two measurements were compared to calculate an r^2 value (Figure 3.13A). The correlation between huCD96v2 binding and blocking utilising dual-panned scFv resulted in an r^2 value of 0.57, indicating a weakly positive correlation between the two factors. Whilst this correlation is weak, it is greater than the correlation between binding and blocking of scFv clones panned against either huCD96v2 or mCD96 alone (Figure 3.7, Figure 3.10)

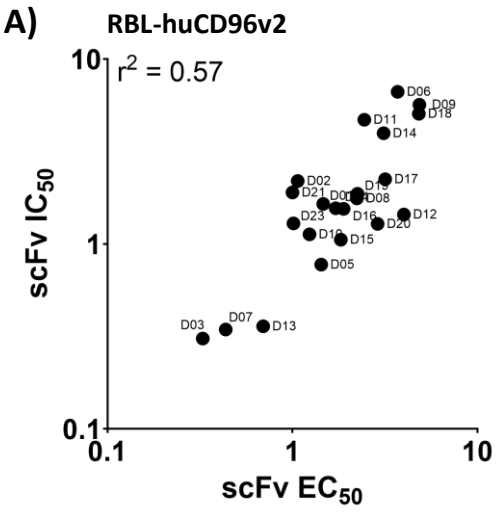

Figure 3.13 Correlation between binding and blocking capacity of dual-panned scFv against RBL expressed huCD96v2

A) The IC_{50} and EC_{50} values for RBL-huCD96v2 were plotted against each other for scFv clones panned against both huCD96v2 and mCD96 to determine the correlation between the two values, represented by the calculated r^2 value (0.57).

To further understand how these same dual-panned scFv clones both bind RBL-mCD96 and inhibit mCD96-Fc binding, an identical analytical approach was undertaken with RBL-mCD96 cells.

As with binding of RBL-huCD96v2, dual-panned scFv binding of RBL-mCD96 was varied. Binding curves of the 23 clones identified only 19 which were capable of binding RBL-mCD96. Clone D22 failed to bind RBL-huCD96v2 (Figure 3.11) and was found to also fail to bind RBL-mCD96 (Figure 3.14A). Additionally, clones D17, D21 and D23 were found to be incapable of binding RBL-mCD96 (Figure 3.14A) and were therefore false-positives. Of the remaining 19 scFv clones, a further 4 clones were weak binders, with EC_{50} values greater than 5 µg/mL (D04, D09, D12, D13) whilst the EC_{50} value of clone D18 was equivalently high at 4.99 µg/mL. Interestingly, a low affinity for mCD96 did not preclude certain scFv clones from binding a large number of target. Clone D04 for example exhibited a high EC_{50} value of 5.9 µg/mL but possessed a high B_{Max} value of 4565, indicative of broad antigen recognition with low affinity. Conversely, clones D12 and D13 exhibit high EC_{50} values and low B_{Max} values, indicating strong interaction but with decreased antigen recognition. A number of scFv clones noted for their strong binding of RBL-huCD96v2 were found to also interact with mCD96 strongly. scFv clone D01 exhibited a low EC_{50} value of 0.53 µg/mL (huCD96v2 = 1.47 µg/mL), representing a dual-panned scFv clone capable of binding strongly to both human and murine CD96.

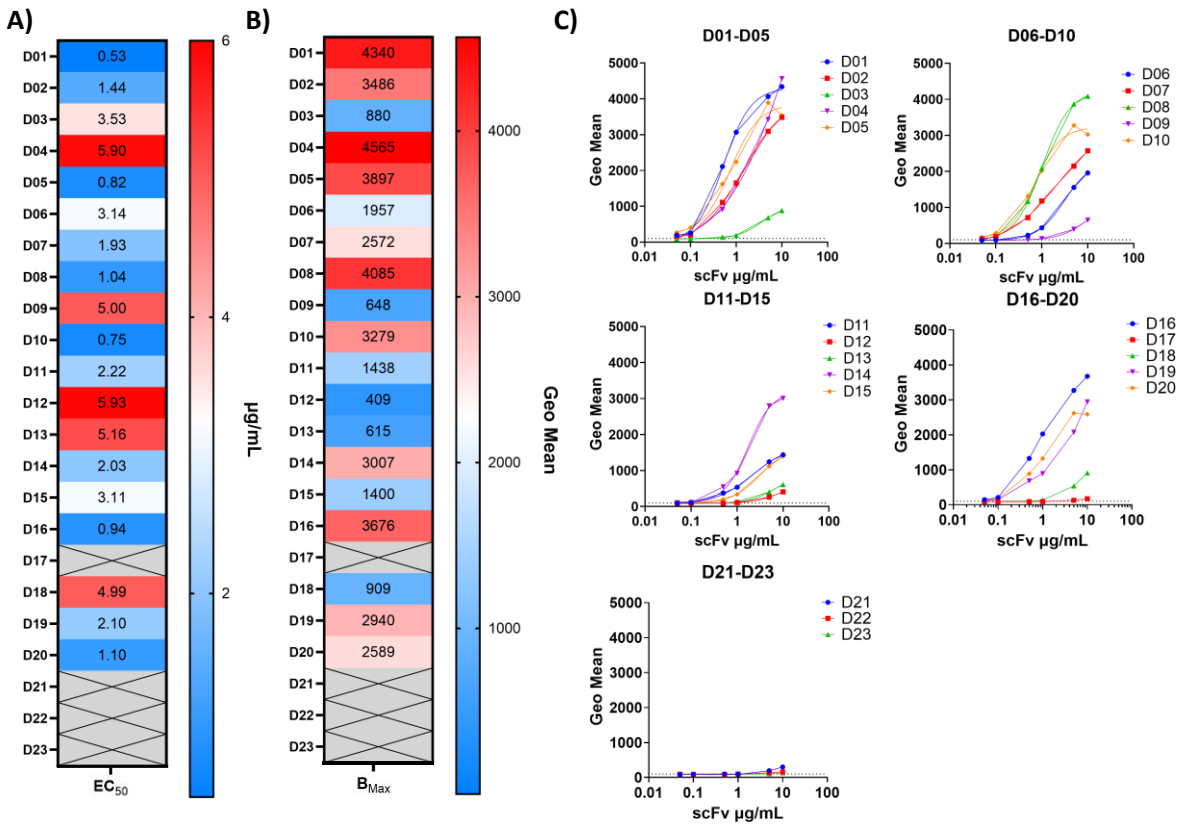

Figure 3.14 Dual-panned scFv binding of RBL-mCD96

A) EC_{50} binding values of each dual-panned scFv clone against RBL expressed mCD96. EC_{50} are calculated utilising the binding curve of each scFv clone titration to RBL-mCD96. **B)** B_{Max} values for each dual-panned scFv clone, highlighting the maximum geometric mean of each scFv to RBL expressed mCD96. **C)** Titration of each dual-panned scFv, highlighting binding to RBL-mCD96. Binding of scFv was detected through anti-His antibody and is represented by the geometric mean of each scFv concentration. Each scFv was assessed for binding of mCD96 once.

Blocking of mCD155-Fc binding to RBL-mCD96 by dual-panned scFv clones was varied, as with RBL-huCD96v2 cells (Figure 3.15). Clones which failed to bind RBL-mCD96 (D17, D21, D22 and D23) were noted again for the inability to block mCD155 binding of RBL-mCD96. Clone D21 did however exhibit a slight blockade of mCD96, however this was minimal and considering data highlighting its inability to bind mCD96, D21 was considered a non-binder and therefore non-blocker. Clones D09, D12, D13 and D18 failed to inhibit mCD155-Fc binding to a significant degree, reflective of limited RBL-mCD96 binding. However, a number of clones were found to be effective at blocking mCD155-Fc binding of RBL-mCD96, including clones D01, D10 and D16. Each of these scFv clones also exhibited strong binding of both huCD96v2 and mCD96.

These blocking data suggest a range of capacity for dual-panned scFv binding and blocking of mCD96 and suggest that a number of clones exhibit similar characteristics when bound to either human or mouse CD96.

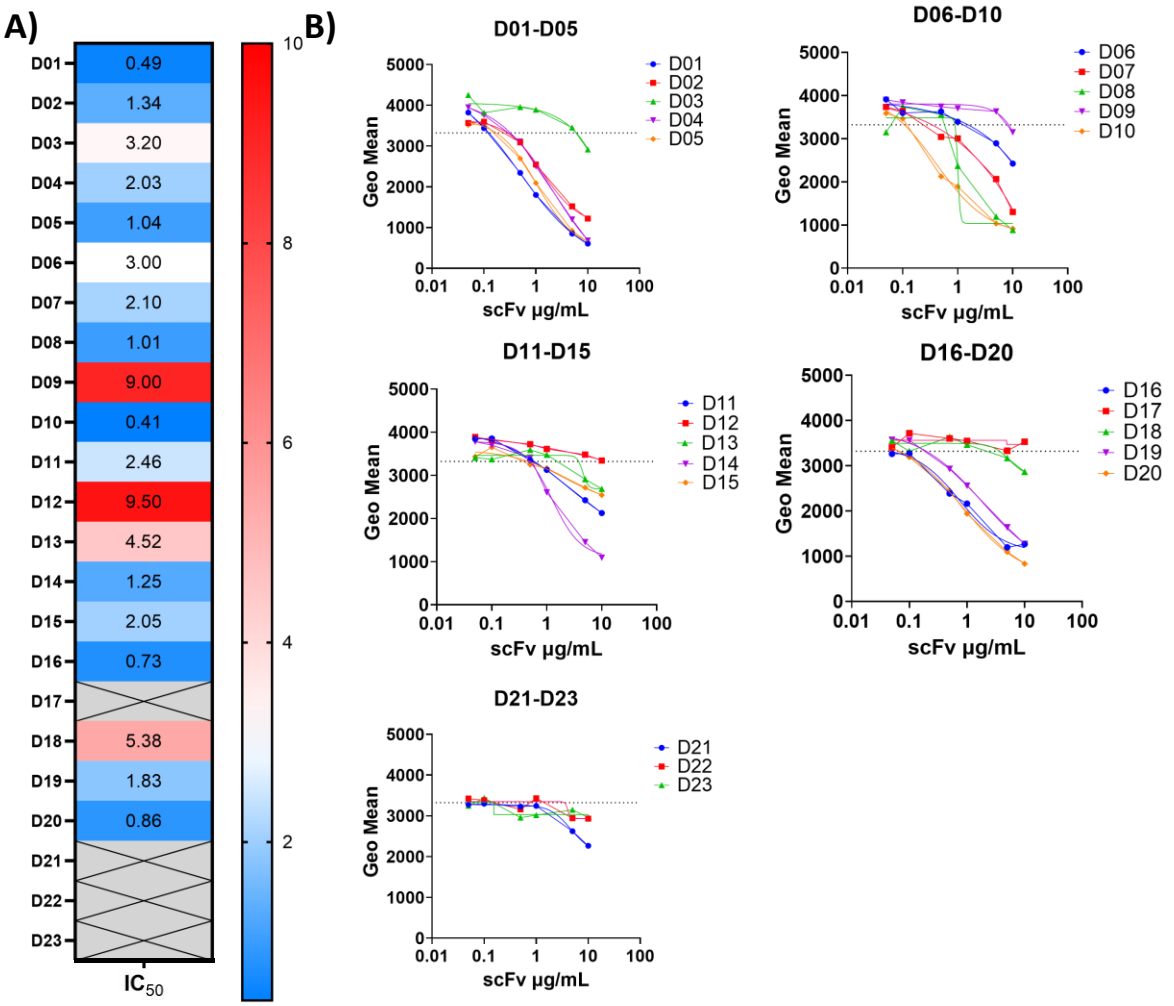

Figure 3.15 Dual-panned scFv blocking of RBL expressed mCD96

A) The capacity for each dual-panned scFv to inhibit the binding of mCD155 with RBL expressed mCD96 is represented as a calculated IC_{50} value. A colour gradient heat-map is utilised to indicate variation in calculated IC_{50} value with blue representing low values and red representing large values. IC_{50} values are shown as the concentration (µg/mL) of each scFv clone required to limit huCD155 binding of huCD96v2 to 50% of the maximum binding. **B)** Binding curves of mCD155 to RBL expressed mCD96 with titrations of each dual-panned scFv. IC_{50} values were calculated utilising these binding curves. Each scFv titration inhibition of huCD155 binding was assessed once.

To better understand how any correlation between dual-panned scFv clones ability to bind RBL-mCD96 and block binding of mCD155-Fc, each EC_{50} and IC_{50} value was plotted against one-another (Figure 3.16). A weakly positive correlation between the two factors was found, with an r^2 value of 0.63. This correlation was slightly higher than that of the same clones capacity to bind and block RBL-huCD96v2.

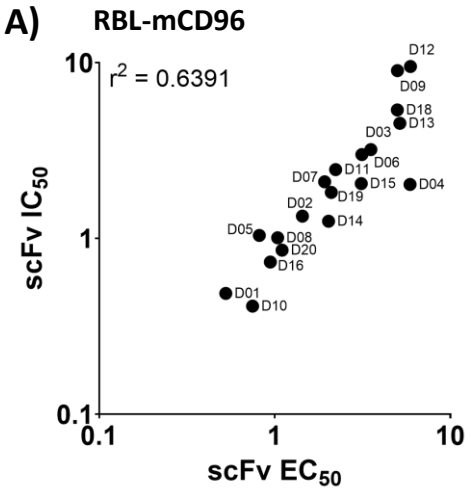

Figure 3.16 Correlation between binding and blocking capacity of dual-panned scFv against RBL expressed mCD96

A) The IC_{50} and EC_{50} values for RBL-mCD96 are plotted against each other for scFv clones panned against both huCD96v2 and mCD96 to determine the correlation between the two values, represented by the calculated r^2 value. Green datapoints represent scFv clones which do not block the mCD96 interaction with mCD155.

3.4 Mapping phage-display panned scFv to CD96 domains

CD96 consists of three extracellular domains, through which CD155 has been shown to interact with the most distal (D1) [174]. It has previously been shown that antibodies targeting CD96 can elicit anti-metastatic activity without blocking the CD96:CD155 interaction, therefore a better understanding of scFv clones and their domain-specific binding pattern was of interest [164]. For further investigation into how each CD96-targeting clone may induce T-cell activation and how the blocking of CD155 may impact this, understanding of the domain-specific binding characteristics for each scFv clone was of interest. Therefore, each clone was analysed for binding of truncated forms of recombinant huCD96v2 or mCD96 to determine which domain they are specific to. Truncated forms of CD96-Fc were generated, encompassing a loss of each domain before scFv binding was quantified utilising an ELISA approach. These truncated CD96-Fc consisted of either the full length extracellular domain (D1-3), domains 1 and 2 only (D1+2) or domains 2 and 3 only (D2+3), each with a C terminus human Fc domain. Binding of scFv to CD96-Fc-D1-3 and D1+2 but not D2+3 would suggest specificity to D1 of CD96. Similarly, binding of scFv to CD96-Fc-D1-3 and D2+3 but not D1+2 would indicate that the scFv is specific to D3 of CD96. Binding of all truncated variations of CD96-Fc would suggest a specificity for D2 of CD96. As each scFv contained a c-Myc tag, scFv binding was assessed utilising a biotinylated anti-c-Myc antibody and streptavidin-HRP, detailed in Figure 3.17.

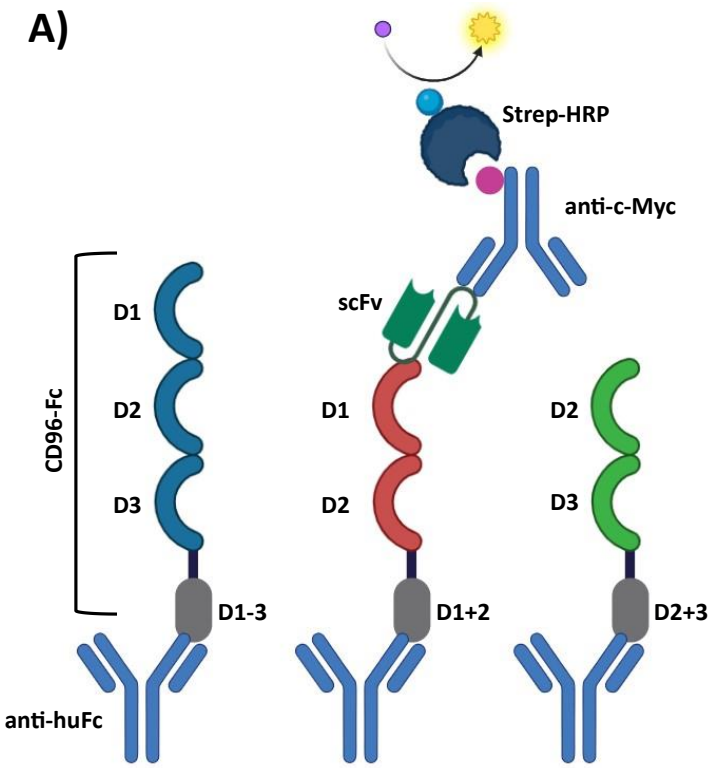

Figure 3.17 Schematic overview of truncated CD96 to determine scFv binding

A) Schematic overview of truncated recombinant CD96 bound to plate-bound anti-human Fc. scFv clones bound to truncated CD96 were detected with a biotinylated anti-c-Myc antibody and streptavidin-HRP. Signal detection of bound scFv to truncated CD96 protein was quantified by HRP chemical change and utilised to determine specificity of each clone for CD96 domains.

3.4.1 Human panned scFv binding of truncated CD96

To evaluate the domain-specific binding properties of scFv panned against human CD96v2, scFv clones were assessed for their binding of truncated forms of huCD96v2-Fc.

The binding characteristics of human-panned scFv clones to truncated huCD96v2-Fc was found to be diverse (Figure 3.18), reflective of scFv binding to RBL-huCD9v2 (Figure 3.5). Clones which indicate specificity for D1 of CD96 are indicated by effective binding of both plate-bound D1-3 and D1+2 huCD96v2 variants, but a distinct lack of binding to the D2+3 form. These include scFv clones H03, H11, H12, H22 and H24 among others. Each of these clones were shown in Figure 3.6 to be effective blockers of the RBL-huCD96v2 interaction with huCD155-Fc.

Clones exhibiting binding specificity for D2 were identified by their consistent binding to each form of huCD96v2, as D2 is present in each truncated protein (Figure 3.17). Clones H05, H09 and H10 each retain binding of all truncated huCD96v2 variants, suggesting that these clones bind the D2 region of CD96. When considering how these clones bind to our truncated proteins, it is important to consider that the removal of certain domains is likely to have an impact on the tertiary structure of the CD96 protein, potentially resulting in an altered scFv binding site and a change in epitope accessibility. This

may result in a binding site taking on a conformation that is not complementary to an scFv clone and therefore reduce the affinity of binding. The specific site each clone binds within the individual domains may also impact how they are affected by domain deletion. Clone H09 binding is more affected by the loss of D1, whilst clone H10 binding is more affected by the loss of D3. Whilst reduced, both retain their binding of truncated huCD96v2 variants suggesting binding of a D2 epitope which is sensitive to the removal of other domains.

Clones H02 and H08 were both found to not impede the binding of huCD155 when bound to RBL-huCD96v2 (Figure 3.6). Both clones binding of huCD96v2 was affected most by the loss of D3, however binding was recovered with the reintroduction of D3 and loss of D1. This, in combination with literature evidence for the role of D1 in CD155 interactions, suggests that both clones bind D3 or the border region between D2 and D3.

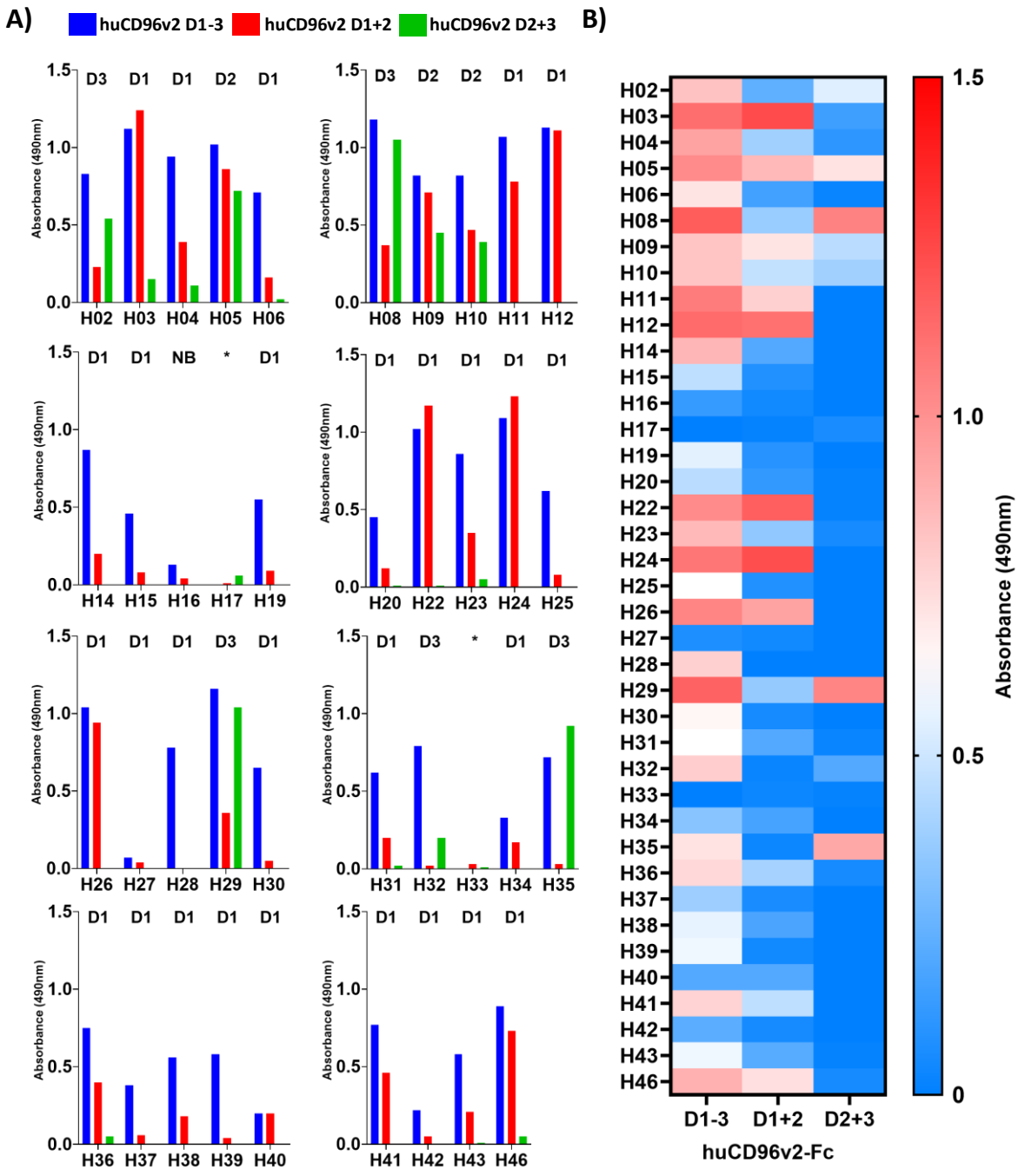

Figure 3.18 Binding of truncated huCD96 by human-panned scFv clones

A) Binding of human-panned anti-CD96 scFv clones to truncated variants of recombinant huCD96. scFv clones were bound to the extracellular domains of full-length mCD96 (D1-3), CD96 lacking domain 3 (D1+2) or CD96 lacking domain 1 (D2+3). Binding is quantified as absorbance (A490nm) of detected HRP chemical change following binding of a scFv c-Myc tag. **B)** Heatmap overview of absorbance values for each scFv clone binding to truncated huCD96.

3.4.2 Mouse Panned IgG Binding of Truncated mCD96

To assess the domain-specific binding properties of scFv panned against mCD96, an identical method to that used with human-panned scFv was initially used. However, the binding of mouse-panned scFv to truncated forms of recombinant mCD96 was poor and scFv clones failed to bind mCD96-Fc. At this

stage however, mouse-panned scFv had been converted to mIgG1 antibodies. Therefore, converted mIgG1 clones were utilised in an identical methodology to determine domain-specific binding. A biotinylated anti-mouse Fc antibody was used in place of an anti-c-Myc antibody to determine antibody binding of truncated mCD96.

A total of 12 mIgG1 clones were found to bind both D1-3 and D1+2 variants of mCD96-Fc whilst failing to bind D2+3, indicating clone specificity for D1 (Figure 3.19A/B). Antibody clone M04 binding of recombinant mCD96 variants was weak, but did suggest clone specificity for D3, with a lack of binding to D1+2 which was rescued by the removal of D1 and reintroduction of D3 (D2+3). Notably, clone M09 failed to bind recombinant mCD96 despite being shown to bind RBL-mCD96 (Figure 3.8). Interestingly, it is both of these clones which were shown to bind RBL-mCD96 and not impede binding of mCD155-Fc (Figure 3.9).

Binding of clones M16, M17, M19, M21 and M22 to RBL-mCD96 was previously shown to be weak, reflected in their limited binding of recombinant mCD96.

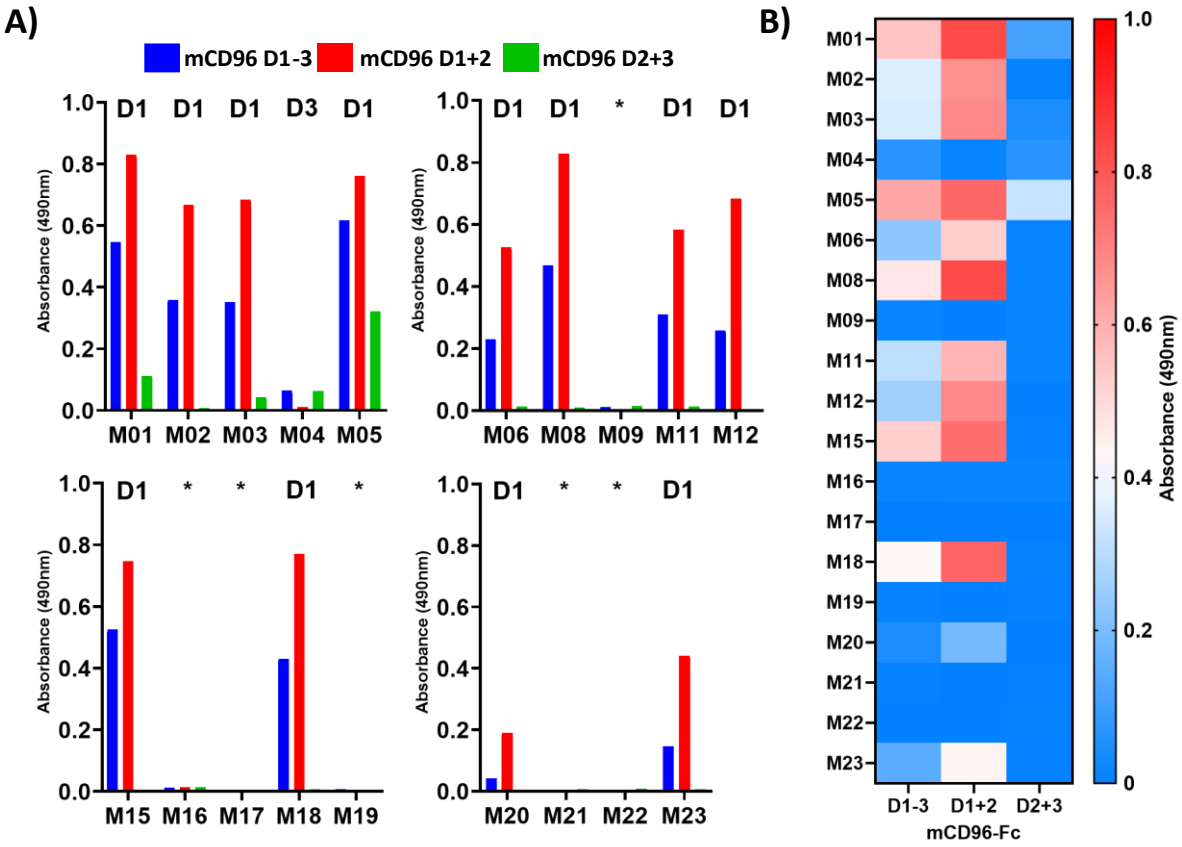

Figure 3.19 Binding of truncated mCD96 by mouse-panned scFv clones

A) Binding of mouse-panned anti-CD96 scFv clones to truncated variants of recombinant mCD96. scFv clones were bound to the extracellular domains of full-length mCD96 (D1-3), protein lacking domain 3 (D1+2) or protein lacking domain 1 (D2+3). Binding is quantified as absorbance (A490nm) of detected HRP chemical change following binding of a scFv c-Myc tag. **B)** Heatmap overview of absorbance values for each scFv clone binding to truncated mCD96.

3.4.3 Dual-panned anti-CD96 scFv binding of truncated CD96

As with scFv panned against either human or mouse CD96, scFv clones panned against both species were evaluated for their binding of truncated CD96. Considering that scFv clones recognise a single epitope which would be shared between huCD96v2 and mCD96, these dual-panned scFv were assessed for their binding of huCD96v2-Fc only.

Each dual-panned scFv exhibited a similar binding pattern across each truncated form of huCD96v2-Fc, with all scFv clones failing to bind a truncated form of CD96 lacking D1 (Figure 3.20A/B). The overall binding of scFv clones to full length recombinant huCD96v2 was consistent with the binding of scFv to RBL expressed huCD96v2 visualised in Figure 3.11C. Clones D21 and D22 were found to not bind RBL-huCD96v2 and is reflected in their inability to bind full length huCD96v2-Fc (Figure 3.20A). The binding of huCD96v2-Fc by a number of dual-panned scFv clones was also limited by the loss of D3, suggesting that whilst these scFv do each recognise D1 of huCD96v2, they are also reliant on other extracellular domains for effective binding. The requirement of domains 2 and 3 of CD96 for effective interactions with CD155 was highlighted previously by Meyer et al., where both domains were found to be required for optimal CD155 interactions [174].

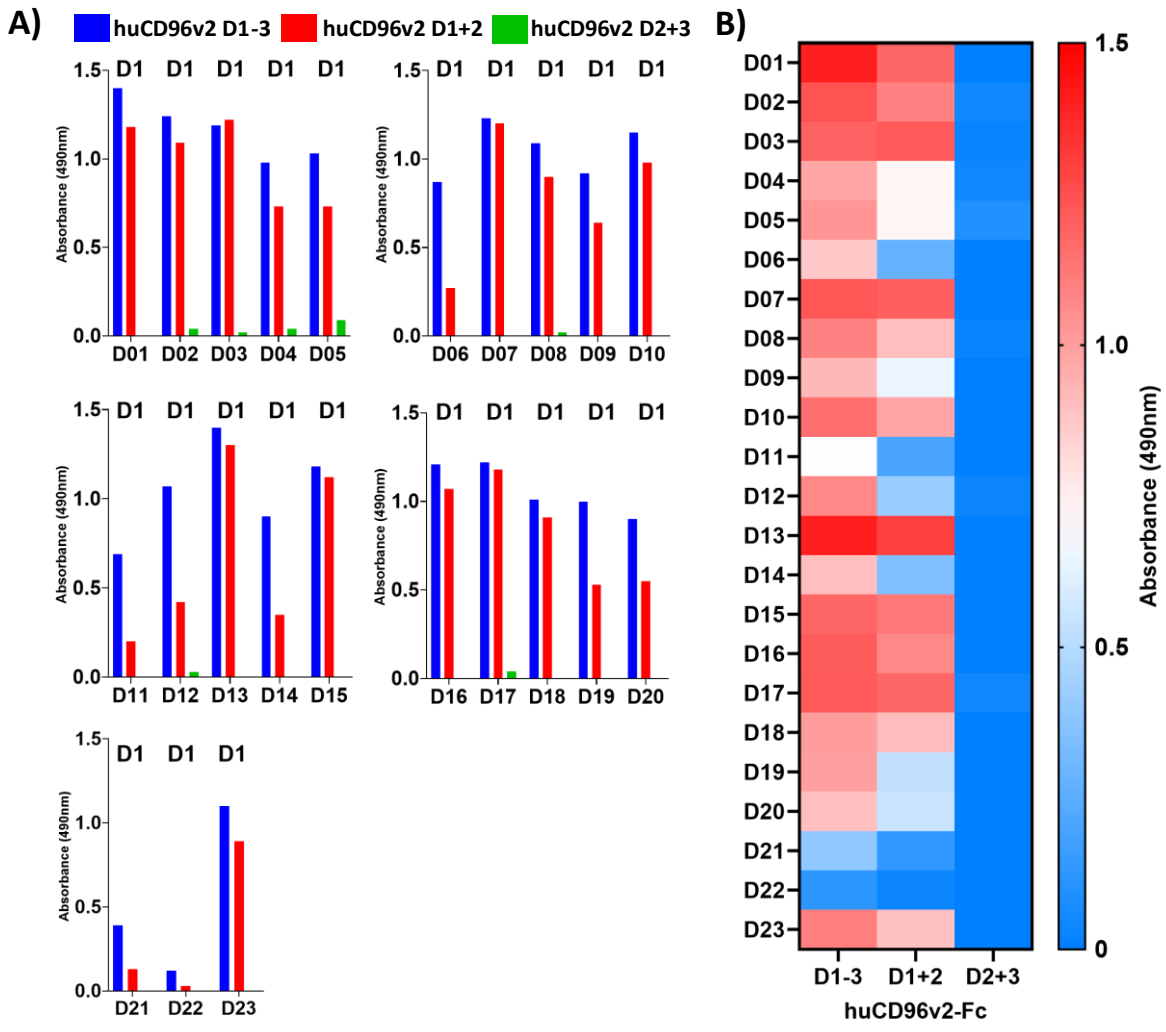

Figure 3.20 Mapping binding of dual-panned scFv to domains of huCD96v2

A) Specific domain binding of each cross-reactive scFv was assessed through a sandwich ELISA and indicates predominant binding of the huCD9v2 domain 1 by all dual-panned scFv clones. The loss of binding by scFv to CD96 D2+3 indicates that all scFv bind D1. **B)** Heatmap overview highlighting the comparative binding profile of each scFv to each truncated CD96. scFv binding of full-length or truncated forms of the CD96 extracellular domain are visualised as red, while a loss of binding is visualised as blue.

3.5 Phage-display isolated anti-CD96 antibody T-cell Proliferation

The ability of antibodies targeting human CD96 has been previously documented to augment T-cell proliferation. The provision of anti-human CD96 antibodies was shown by Rogel et al. to enhance T-cell proliferation, reliant on FcR-mediated antibody cross-linking. Antibodies induced T-cell proliferation when provided either in a soluble format with PBMCs, when directly plate-bound, or when in a soluble format with plate-bound recombinant FcR. The addition of soluble antibodies lacking the ability to interact with plate-bound recombinant FcR ablated the activation of T-cells through anti-CD96 antibodies, indicating that proficient cross-linking is essential to induce T-cell activity.

Considering that the panel of scFv clones identified by panning against both human and mouse CD96 (D01-D23) exhibited a pattern of strong binding to huCD96 (Figure 3.5), determining their capacity to augment T-cell activation was of interest. Human IgG1 mAbs were generated by BioInvent utilising the scFv complimentary-determining regions (CDR) from scFv clones D01-D23, before each was utilised in a human T-cell proliferation assay to evaluate their capacity to induce T-cell activation. Of the 23 scFv clones generated through phage-display, 1 was excluded for its reported non-binding of huCD96 (D22). Of the remaining 22 scFv clones, 7 failed to be generated as huIgG1 mAbs. This resulted in a total of 16 anti-CD96 antibodies with reported specificity for both human and mouse CD96 being available for characterisation as mAbs. These antibodies were cultured with PBMCs at 1 µg/mL with either 0.1 or 0.3 ng/mL of the CD3 antibody, OKT3. Similarly, they were also plate-bound at 2.5 µ/mL, again with both concentrations of OKT3. T-cell activation mediated by CD96 co-stimulation was evaluated by T-cell proliferation with respect to a matched huIgG1 isotype control, as well as the upregulation of T- cell expressed CD25.

3.5.1 Soluble anti-CD96 antibody induced human T-cell activation

To evaluate the ability of antibody clones identified by dual-panning of human and mouse CD96 to induce human T-cell activation, carboxyfluorescein diacetate succinimidyl ester (CFSE) stained PBMCs were cultured with anti-human CD96 antibodies at 1 µg/mL with either 0.1 (Low) or 0.3 ng/mL (High) OKT3 and proliferation assessed by CFSE dilution at day 4.

Incubation of PBMCs with a matched isotype control antibody (IC: huAT-171-2) and 0.1 or 0.3 ng/mL OKT3 induced 35 and 30% of CD3+CD4+ T-cells to undergo division, respectively. Conversely, CD4+ T-cells cultured with anti-CD96 antibodies with OKT3 underwent greater proliferation (Figure 3.21A). Proliferation of CD4+ T-cells above that of huAT-171-2 was limited at lower concentrations of OKT3, with clone D07 exhibiting the highest increase over control (49%). Only four clones induced significant proliferation over IC and low OKT3 (D08, D01, D21 and D07). However, proliferation in response to all anti-CD96 antibodies was increased dramatically when cultured with high OKT3. All antibody clones induced significant CD4+ T-cell proliferation with respect to isotype control, with clone D08 exhibiting the greatest increase (71%). Highlighted in Figure 3.21B is a representative example of clone D08 induced CD4+ T-cell proliferation with respect to isotype control with either 0.1 (Left histogram) or 0.3 ng/mL (Right histogram) OKT3. Increasing OKT3 concentration with IC had little effect on CD4+ T-cell proliferation, however when combined with anti-CD96 antibodies, dramatically increased T-cell proliferation.

As with CD4+ T-cell proliferation, CD8+ T-cell proliferation was weakly promoted by culture with IC and either low (32%) or high (23%) OKT3 (Figure 3.21C). CD8+ T-cell proliferation was only significantly augmented by clone D07 at low OKT3 concentrations with respect to IC + low OKT3. As with CD4+ T-cell proliferation, all antibody clones induced significant CD8+ T-cell proliferation with respect to IC when cultured with high OKT3. Clone D08 induced the greatest increase in CD8+ T-cell proliferation with high OKT3, and is highlighted in Figure 3.21D.

Overall, each dual-panned CD96-targeting antibody showed significant capacity to augment T-cell proliferation in solution with 0.3 ng/mL OKT3, however this proliferation was severely limited at lower concentrations of OKT3 to a small group of antibodies. At low concentrations of OKT3, clones which significantly augment T-cell proliferation over IC were those with lower scFv EC_{50} values.

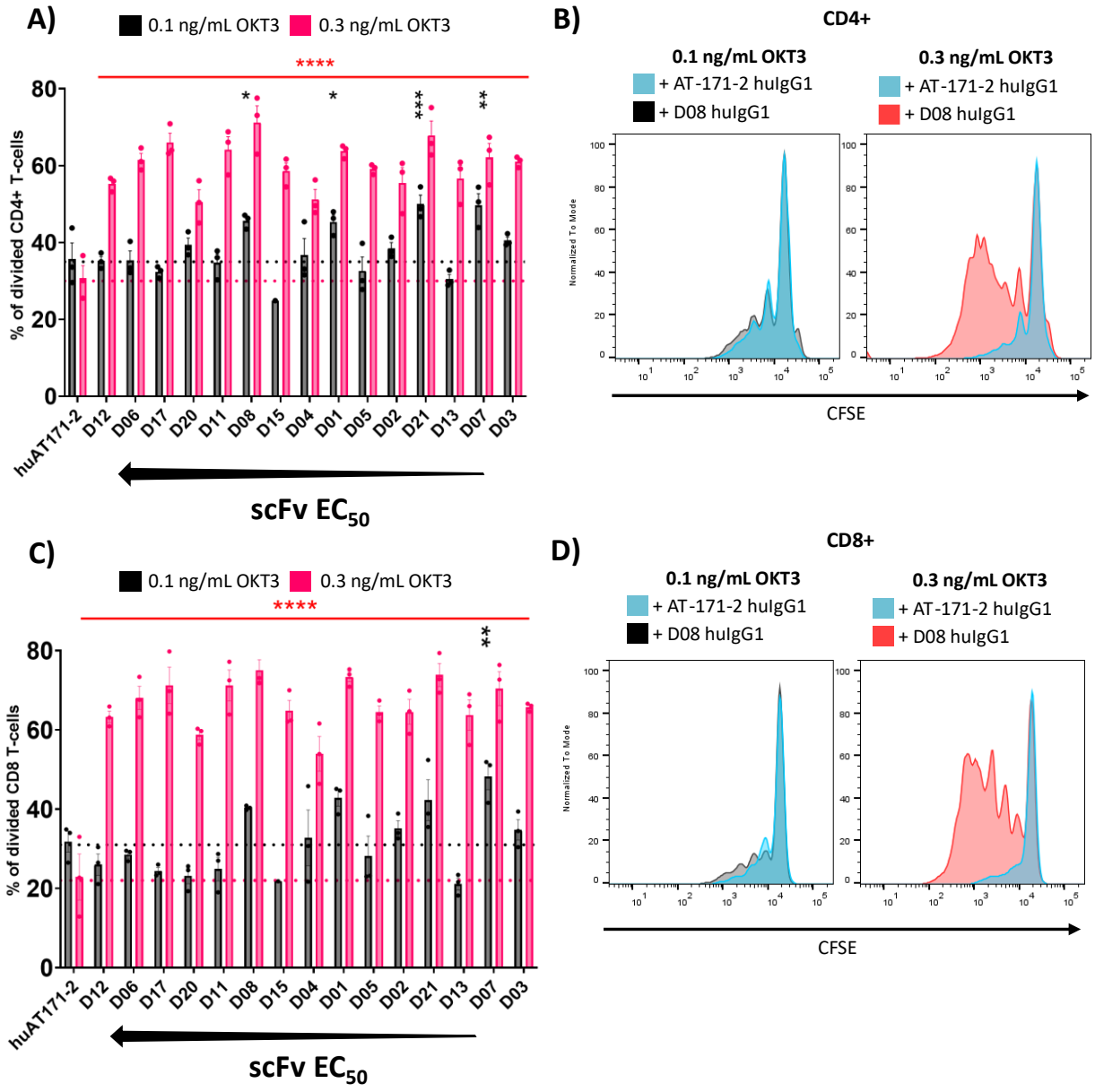

Figure 3.21 Soluble dual-panned anti-CD96 antibody induced T-cell proliferation

A) PBMCs cultured with low (0.1 ng/mL) or high (0.3 ng/m) concentrations of soluble OKT3 and 1 µg/mL soluble huIgG1 isotype control or anti-CD96 huIgG1 antibodies were evaluated at day 4 for proliferation of CD3+CD4+ T-cells. Black dashes represent mean proliferation induced by culture with low OKT3 with huIgG1 control antibody, red dashes represent mean proliferation induced by culture with high OKT3 and huIgG1 control antibody. Shown as percentage of gated CD3+CD4+ T-cells. Antibodies are ordered by their corresponding scFv clone EC_{50}, largest to smallest. **B)** Representative histograms highlight CD3+CD4+ T-cell CFSE-dilution induced by culture with low or high soluble OKT3 with 1 µg/mL huIgG1 isotype control antibody or D08 huIgG1 antibody. **C)** PBMCs cultured with low (0.1 ng/mL) or high (0.3 ng/m) concentrations of soluble OKT3 and 1 µg/mL soluble huIgG1 isotype control or anti-CD96 huIgG1 antibodies were evaluated at day 4 for proliferation of CD3+CD8+ T-cells. Black dashes represent mean proliferation induced by culture with low OKT3 with huIgG1 control antibody, red dashes represent mean proliferation induced by culture with high OKT3 and huIgG1 control antibody. Shown as percentage of gated CD3+CD4+ T-cells. Antibodies are ordered by their corresponding scFv clone EC_{50}, largest to smallest. **D)** Representative histograms highlight CD3+CD8+ T-cell CFSE-dilution induced by culture with low or high soluble OKT3 with 1 µg/mL huIgG1 isotype control antibody or D08 huIgG1 antibody. (**A+C** One donor with three technical replicates

using mixed-model analysis of each huIgG1 clones versus huAT171-2 IC. * = p<0.05, ** = p<0.005, **** = p<0.0001).

To further evaluate the ability of dual-panned CD96-targeting antibodies to activate both CD4+ and CD8+ T-cells, upregulation of IL-2RA (CD25) on proliferated T-cells was assessed. CD25 is upregulated on the surface of T-cells following activation and is indicative of an active T-cell phenotype.

Upregulation of CD25 on PBMCs in response to soluble huAT-171-2 isotype control in conjunction with either concentration of OKT3 was limited, with 29 and 32% of proliferated CD4+ T-cells expressing CD25 at day 4, respectively. Upregulation of CD25 was limited at lower concentrations of OKT3 (Figure 3.22A), with only clone D01 inducing significant upregulation of CD25 over IC (45%). Expression of CD25 on proliferated CD4+ T-cell increased across all clones when concentration of OKT3 was increased with respect to low OKT3. Of the 15 antibody clones, CD25 was significantly upregulated by 12 clones over IC + high OKT3. Representative histograms shown in Figure 3.22B of CD25 expression on CD4+ T-cells cultured with OKT3 and D08 highlight the clear increase in surface expression as a result of culture with anti-CD96 with increased OKT3 concentration.

Expression of CD25 was also evaluated on proliferated CD8+ T-cells. Upregulation of CD25 was limited following culture with IC with low (14%) or high OKT3 (24%). Culture of PBMCs with anti-CD96 clones with low concentration of OKT3 resulted in a range of CD25 upregulation. A greater number of anti-CD96 clones induced CD25 upregulation on proliferated CD8+ T-cells when combined with low OKT3, with 7 antibody clones inducing significant upregulation over IC. As with CD4+ T-cells cultured with high OKT3, CD25 was significantly upregulated by the same 12 clones with respect to IC and high OKT3 (Figure 3.22C). This is visualised in Figure 3.22D, whereby expression of CD25 induced by culture with soluble D08 antibody is augmented by increased OKT3.

Overall, expression of CD25 on proliferated T-cells was augmented by the provision of soluble anti-CD96 antibodies over a matched isotype control antibody, with expression increased when cultured with higher concentrations of anti-CD3 antibody. Considering the pattern of both T-cell proliferation and upregulation of CD25, these data suggest that the novel antibody clones identified through phage-display and shown to bind both human and mouse CD96 can augment human T-cell activation when provided as a soluble therapy.

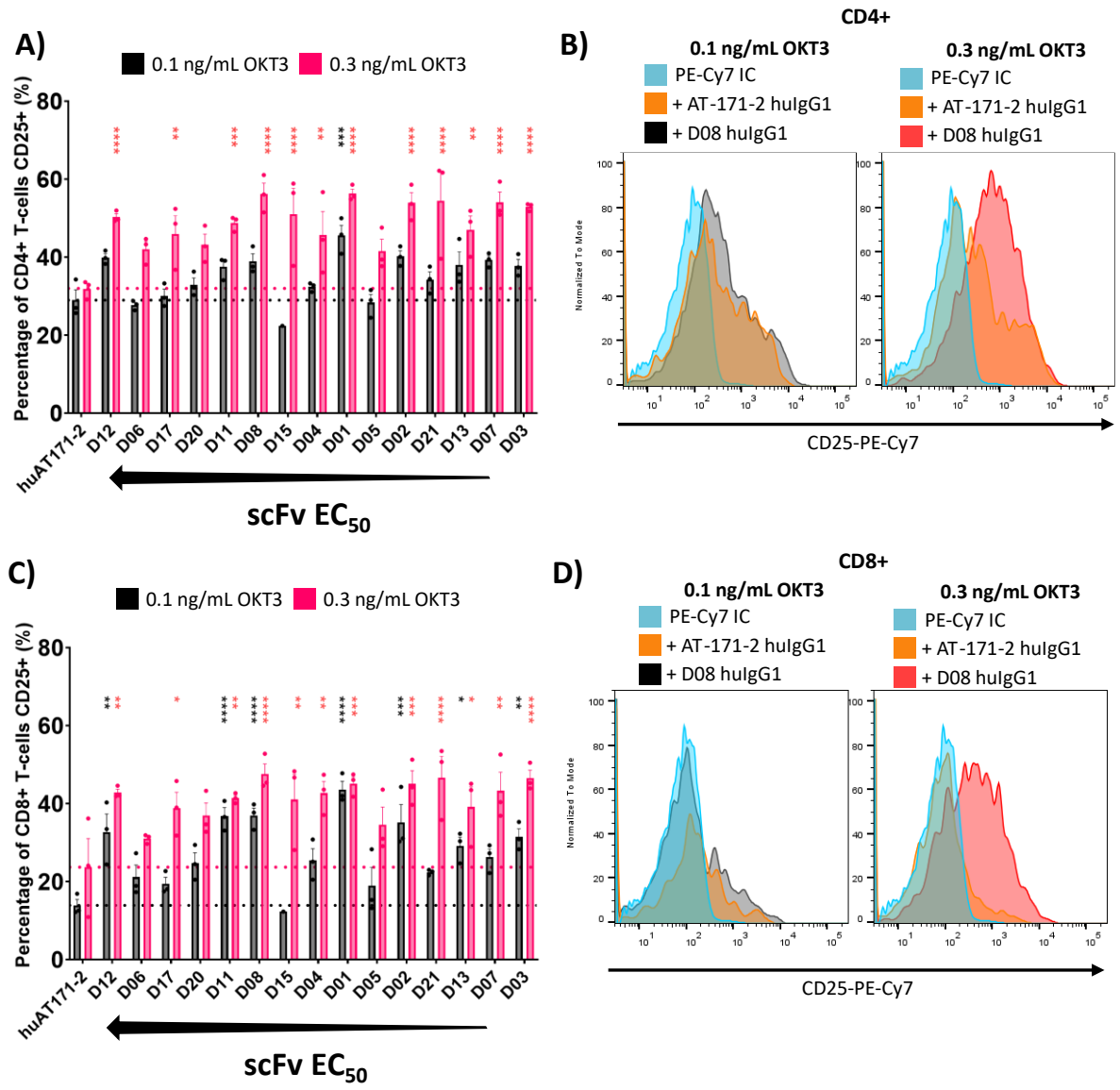

Figure 3.22 Soluble dual-panned anti-CD96 antibody induction of CD25 expression

A) Percentage of divided CD3+CD4+ T-cells expressing CD25 at day 4 following culture with low (0.1 ng/mL) or high (0.3 ng/mL) OKT3 with 1 µg/mL huIgG1 isotype control or huIgG1 anti-CD96 antibodies. Black dashed line represents mean CD25 expression of CD3+CD4+ T-cells cultured with low OKT3 and huIgG1 isotype control antibody, red dashed line represents mean CD25 expression of CD3+CD4+ T-cells cultured with high OKT3 and huIgG1 isotype control antibody. Antibodies are ordered by their corresponding scFv clone EC_{50}, largest to smallest. **B)** Representative staining of CD3+CD4+ T-cells cultured with low (Left) or high (Right)OKT3 in conjunction with huIgG1 isotype control antibody or huIgG1 D08 antibody. **C)** Percentage of divided CD3+CD8+ T-cells expressing CD25 at day 4 following culture with low (0.1 ng/mL) or high (0.3 ng/mL) OKT3 with 1 µg/mL huIgG1 isotype control or huIgG1 anti-CD96 antibodies. Black dashed line represents mean CD25 expression of CD3+CD8+ T-cells cultured with low OKT3 and huIgG1 isotype control antibody, red dashed line represents mean CD25 expression of CD3+CD8+ T-cells cultured with high OKT3 and huIgG1 isotype control antibody. Antibodies are ordered by their corresponding scFv clone EC_{50}, largest to smallest. **D)** Representative staining of CD3+CD8+ T-cells cultured with low (Left) or high (Right) OKT3 in conjunction with huIgG1 isotype control antibody or huIgG1 D08 antibody. (**A+C** One donor with three technical replicates using mixed-model analysis of each huIgG1 clones versus huAT171-2 IC. * = p<0.05, ** = p<0.005, *** = p<0.001, **** = p<0.0001).

3.5.2 Plate-captured anti-CD96 antibody induced human T-cell activation

To further assess how the panel of dual-panned anti-human CD96 antibodies may act to activate PBMC containing human T-cells, CD96 antibodies were directly bound to plates whilst OKT3 was provided as a soluble antibody at both low (0.1 ng/mL) and high (0.3 ng/mL) concentrations. Proliferation of T-cells was assessed at day 4.

Proliferation of T-cells in response to plate-bound IC with both low or high soluble OKT3 was limited and was reduced with respect to soluble IC (Figure 3.21A). CD4+ T-cell proliferation in response to plate-bound IC with low or high OKT3 was limited to 27% and 16%, respectively (Figure 3.23A). Three plate-bound anti-CD96 clones significantly augmented the provision of soluble low OKT3 (D12, D08, D13). Interestingly, only clone D08 significantly augmented CD4+ T-cell proliferation in plate-bound and soluble format at low OKT3 concentrations. Conversely, all clones when plate-bound significantly augmented CD4+ T-cell provision when cultured with soluble high OKT3.

Proliferation of CD8+ T-cells cultured with plate-bound IC with either low or high soluble OKT3 was reduced with respect to CD4+ T-cells. Only 15% and 7% of CD8+ T-cells proliferated in response to IC with low or high soluble OKT3, respectively. A greater number of clones induced significant increases in CD8+ T-cell proliferation when plate-bound (8 clones) when compared to soluble antibody provision (1 clone) (Figure 3.23C). As with soluble antibody provision, all anti-CD96 clones significantly augmented CD8+ T-cell proliferation when OKT3 concentration is increased. This effect is highlighted in Figure 3.23D, whereby clone D08 clearly promotes T-cell proliferation when combined with 0.3 ng/mL soluble OKT3 over 0.1 ng/mL.

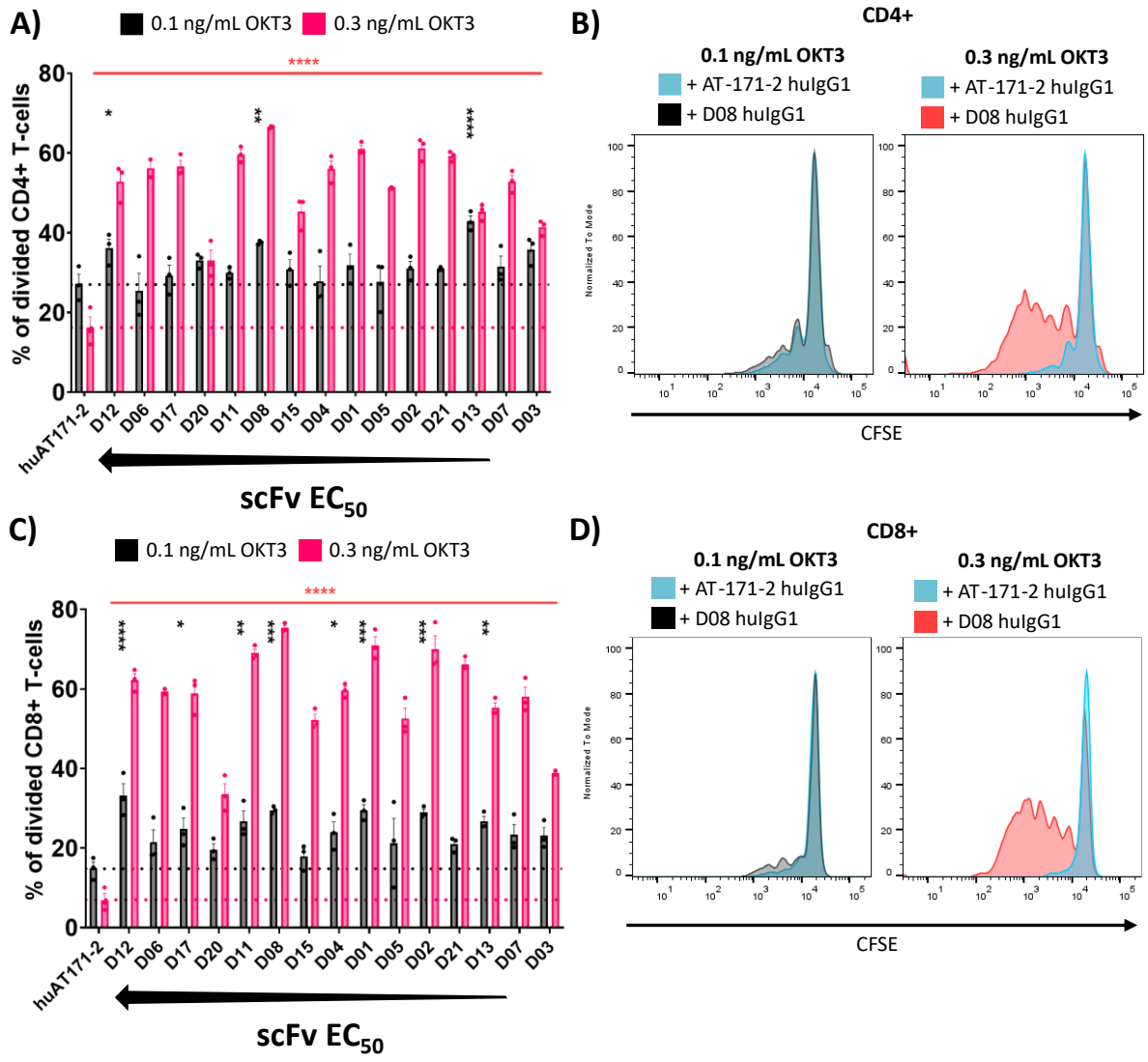

Figure 3.23 Plate-bound dual-panned anti-CD96 antibody induced T-cell proliferation

A) PBMCs cultured with low (0.1 ng/mL) or high (0.3 ng/m) concentrations of soluble OKT3 and 2.5 µg/mL plate-bound huIgG1 isotype control or anti-CD96 huIgG1 antibodies were evaluated at day 4 for proliferation of CD3+CD4+ T-cells. Black dashes represent mean proliferation induced by culture with low OKT3 with huIgG1 control antibody, red dashes represent mean proliferation induced by culture with high OKT3 and huIgG1 control antibody. Shown as percentage of gated CD3+CD4+ T-cells. Antibodies are ordered by their corresponding scFv clone EC_{50}, largest to smallest. **B)** Representative histograms highlight CD3+CD4+ T-cell CFSE-dilution induced by culture with low or high soluble OKT3 with 2.5 µg/mL huIgG1 isotype control antibody or D08 huIgG1 antibody. **C)** PBMCs cultured with low (0.1 ng/mL) or high (0.3 ng/m) concentrations of soluble OKT3 and 2.5 µg/mL plate-bound huIgG1 isotype control or anti-CD96 huIgG1 antibodies were evaluated at day 4 for proliferation of CD3+CD8+ T-cells. Black dashes represent mean proliferation induced by culture with low OKT3 with huIgG1 control antibody, red dashes represent mean proliferation induced by culture with high OKT3 and huIgG1 control antibody. Shown as percentage of gated CD3+CD8+ T-cells. Antibodies are ordered by their corresponding scFv clone EC_{50}, largest to smallest. **D)** Representative histograms highlight CD3+CD8+ T-cell CFSE-dilution induced by culture with low or high soluble OKT3 with 2.5 µg/mL huIgG1 isotype control antibody or D08 huIgG1 antibody. (**A+C** One donor with three technical replicates using mixed-model analysis of each huIgG1 clones versus huAT171-2 IC. * = p<0.05, ** = p<0.005, *** = p<0.001, **** = p<0.0001).

To evaluate the activation state of T-cells cultured with plate-bound anti-CD96 clones and soluble OKT3, upregulation of CD25 was assessed on proliferated CD4+ and CD8+ T-cells.

The upregulation of CD25 on proliferated CD4+ T-cells cultured with plate-bound IC and low or high soluble OKT3 was limited to 40% and 34%, respectively (Figure 3.24A). Of the 15 plate-bound antibody clones utilised, 3 significantly increased expression of CD25 when combined with low soluble OKT3 (D20, D07 and D03. Interestingly, none of these were clones which augmented low OKT3 induced CD4+ T-cell proliferation (Figure 3.23A). When plate-bound antibodies were combined with high OKT3, all increased CD4+ T-cell expression of CD25 above that of IC with high OKT3, each to varying significance. Whilst expression of CD25 induced by clone D08 was not significant with low OKT3, the increase induced when combined with high OKT3 over IC is clearly highlighted in Figure 3.24B.

The upregulation of CD25 on proliferated CD8+ T-cells in response to plate-bound anti-CD96 antibodies was also assessed (Figure 3.24C/D). As with CD4+ T-cells, only clones D20, D07 and D03 significantly increased CD8+ T-cell expression of CD25 over IC with low OKT3, whilst all anti-CD96 clones significantly augmented CD25 expression with high OKT3.

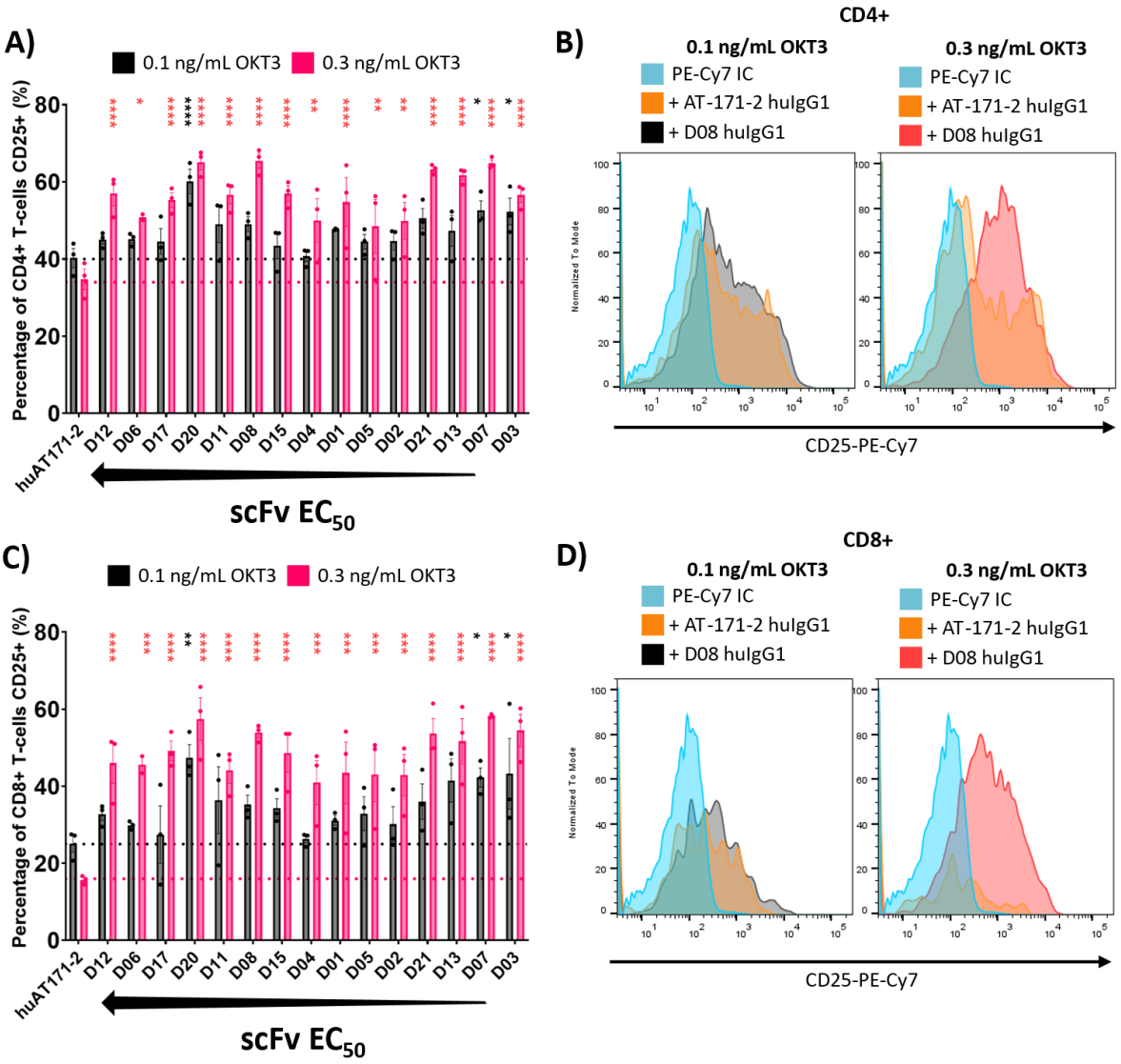

Figure 3.24 Plate-bound dual-panned anti-CD96 antibody induced CD25 expression

A) Percentage of divided CD3+CD4+ T-cells expressing CD25 at day 4 following culture with low (0.1 ng/mL) or high (0.3 ng/mL) OKT3 with 2.5 µg/mL plate-bound huIgG1 isotype control or huIgG1 anti-CD96 antibodies. Black dashed line represents mean CD25 expression of CD3+CD4+ T-cells cultured with low OKT3 and huIgG1 isotype control antibody, red dashed line represents mean CD25 expression of CD3+CD4+ T-cells cultured with high OKT3 and plate-bound huIgG1 isotype control antibody. Antibodies are ordered by their corresponding scFv clone EC_{50}, largest to smallest. **B)** Representative staining of CD3+CD4+ T-cells cultured with low (Left) or high (Right)OKT3 in conjunction with plate-bound huIgG1 isotype control antibody or huIgG1 D08 antibody. **C)** Percentage of divided CD3+CD8+ T-cells expressing CD25 at day 4 following culture with low (0.1 ng/mL) or high (0.3 ng/mL) OKT3 with 2.5 µg/mL plate-bound huIgG1 isotype control or huIgG1 anti-CD96 antibodies. Black dashed line represents mean CD25 expression of CD3+CD8+ T-cells cultured with low OKT3 and huIgG1 isotype control antibody, red dashed line represents mean CD25 expression of CD3+CD8+ T-cells cultured with high OKT3 and huIgG1 isotype control antibody. Antibodies are ordered by their corresponding scFv clone EC_{50}, largest to smallest. **D)** Representative staining of CD3+CD8+ T-cells cultured with low (Left) or high (Right) OKT3 in conjunction with huIgG1 isotype control antibody or huIgG1 D08 antibody. (**A+C** One donor with three technical replicates using mixed-model analysis of each huIgG1 clones versus huAT171-2 IC. * = p<0.05, ** = p<0.005, *** = p<0.001, **** = p<0.0001).

Considering both the variation in binding affinity for each scFv clone (Figure 3.11), understanding whether this correlated with T-cell proliferation was of interest. The proliferation of both CD4+ and CD8+ T-cells when cultured with either soluble or plate-bound CD96 antibodies and low or high OKT3 was plotted against corresponding scFv EC_{50} values to understand any relationship between T-cell proliferation and scFv affinity (Figure 3.25).

The proliferation of CD4+ T-cells induced by either soluble or plate-bound anti-CD96 antibodies had no relationship with clone affinity for huCD96v2 when cultured with high OKT3 (Figure 3.25A). However, when cultured with low OKT3, a weak relationship between EC_{50} value and CD4+ T-cell proliferation was found with soluble antibody ($r^2 = 0.11$) which was reduced when antibodies were directly plate-bound ($r^2 = 0.04$).

The relationship between scFv affinity and induced CD8+ T-cell proliferation was clearer. As with CD4+ T-cells, there was no correlation between scFv affinity and CD8+ T-cell proliferation when cultured with high OKT3 for either soluble or plate-bound anti-CD96 antibody. However, at low OK3 concentration, a stronger relationship between low EC_{50} value and greater CD8+ T-cell proliferation was found when utilising soluble antibody. Whilst this correlation was still weak ($r^2 = 0.23$), it was however greater than that of CD4+ T-cells and again was lost when antibodies were plate-bound ($r^2 = 0.015$) (Figure 3.25B).

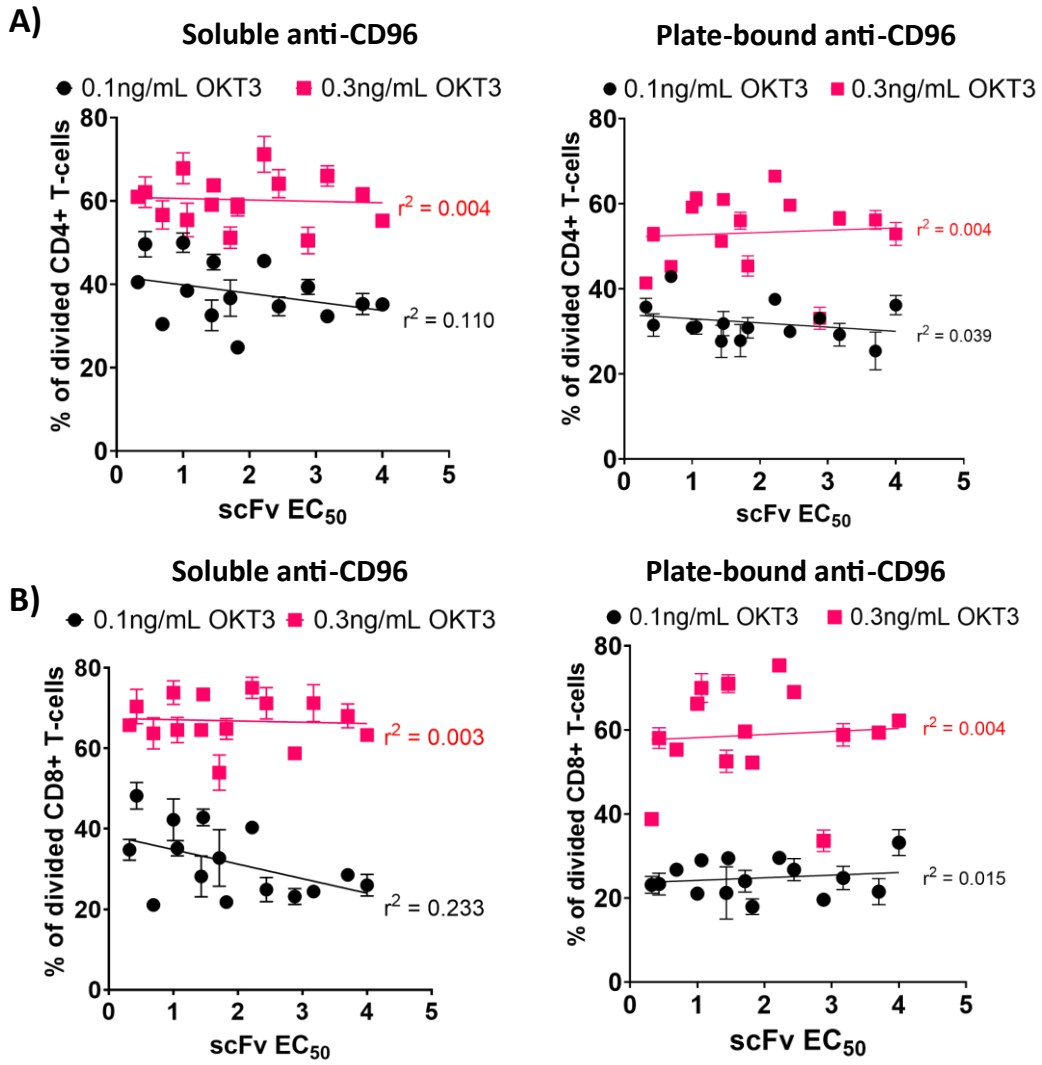

Figure 3.25 Relationship between scFv clone affinity and antibody induced T-cell proliferation

A) Proliferation of CD4+ T-cells by soluble (Left) or plate-bound (Right) dual-panned anti-CD96 huIgG1 antibodies with low or high OKT3 was plotted against each clones corresponding scFv EC_{50} value. Simple linear regression was performed to calculate an r^2 value for proliferation induced by either low or high OKT3. **B)** Proliferation of CD8+ T-cells by soluble (Left) or plate-bound (Right) dual-panned anti-CD96 huIgG1 antibodies with low or high OKT3 was plotted against each clones corresponding scFv EC_{50} value. Simple linear regression was performed to calculate an r^2 value for proliferation induced by either low or high OKT3.

3.6 Chapter Discussion

The aim of this chapter was to identify a panel of novel antibodies capable of targeting human or mouse CD96, as well as a group which could bind both. Currently there is only 1 anti-human CD96 immunotherapeutic in clinical trials, developed by GlaxoSmithKline (GSK6097608) [175]. This antibody has been developed to block the CD96 interaction with CD155, with the goal of increasing CD155 available to interact with CD226, a noted T-cell activation protein [72, 76]. The limited number of antibodies targeting CD96 with current clinical prospects, in conjunction with literature suggesting a stimulatory role for CD96 in human T-cells, highlights a necessity for the development of novel CD96 targeting therapeutics.

The identification of a panel of antibodies which recognise both human and murine CD96 was highly sought after. By panning against both huCD96v2 and mCD96, we have been able to generate therapeutics which can be utilised with both *in vivo* human PBMC assays, as well as *in vitro* mouse models. By utilising a phage-display panned approach against both huCD96v2 and mCD96, 23 novel scFv clones were generated (Table 3.1). Of these 23, one clone failed to bind huCD96v2 (D22), whilst two were generally poor binders. Further to this, 4 clones also failed to bind mCD96, including clone D22. Homology of D1 between huCD96v2 and mCD96 is 59%, whilst D2-3 is 66% [176]. Despite a greater similarity between D2-3 than D1, it was found that all scFv which bound did so to domain 1 of huCD96v2 (Figure 3.20). Whilst this characteristic may not be detrimental, it would have been beneficial to generate dual-panned scFv clones which did not act to impede CD155 binding so as to assess whether the blockade of CD155 may impact T-cell activation.

Table 3.1 Dual-panned scFv clone binding and blocking of human or mouse CD96

Number Of Dual-Panned Clones	Target	CD96 Binders	CD155 Blockers	CD155 Non-Blockers
23	huCD96v2	22	22	0
	mCD96	19	19	0

Of the 39 scFv clones identified by bacteriophage panning to bind huCD96v2, a total of 37 were found to effectively bind RBL-huCD96v2, indicating two scFv clones were false-positives. A range of binding affinity was calculated and presented as EC_{50} values for each individual clone. Whilst a number of clones did exhibit high affinity for huCD96v2, a number of these same clones had lower total binding, with limited B_{Max} values. Of huCD96v2 specific scFv clones, 2 were identified as binders of huCD96v2 whilst simultaneously not limiting interactions with the cognate binding partner of CD96, CD155. This characteristic of scFv clones was sought after, considering that CD155 can also

interact with the inhibitory receptor TIGIT. By blocking CD96, CD155 may instead be free to interact with TIGIT, limiting T-cell activity.

The extracellular domain of CD96 consists of 3 Ig-like domains, and whilst only D1 as the most distal is found to be directly involved in the binding of CD155, domains 2 and 3 are thought to contribute as their loss can limit effective CD155 binding [174]. Considering this, identifying the domains bound by each scFv clone was of interest to determine whether any blocking or non-blocking characteristic may be attributed to domain specificity. Anti-human CD96 scFv clones H02 and H08 both failed to inhibit binding of huCD155. In keeping with literature, neither clone was found to bind D1 of CD96. Both exhibited similar binding patterns to truncated forms of CD96, with their binding suggesting that they in fact bound D3. Of the 20 isolated scFv clones panned against mCD96, 18 exhibited clear binding to RBL-mCD96. Two clones, M04 and M09, were found to bind RBL-mCD96 but not limit binding of mCD155. However, when attempting to understand their specificity for distinct extracellular domains, neither were found to bind recombinant mCD96. Binding of M04 and M09 to both full-length and truncated forms of mCD96 in fact more closely matched that of clones found to not bind mCD96. This observation could be a result of the fact that both full-length and truncated versions of recombinant mCD96 were not forming the optimal conformations for these two clones to bind. Considering that both clones failed to inhibit mCD155 binding of RBL-mCD96 whilst both failed to bind recombinant mCD96, their binding of mCD96 is likely reliant on a similar epitope within either D2 or D3 of mCD96 which is not readily accessible in recombinant protein as a result of recombinant mCD96 misfolding. Overall, the identification of non-blocking scFv clones was limited, with our panning strategy instead appearing to have preference for CD96 blocking scFv clones.

The final goal of this chapter was to assess the ability of dual-panned anti-CD96 antibodies to induce T-cell activation following conversion from scFv to huIgG1 antibody. Previous work has detailed that either direct binding of anti-CD96 antibodies to tissue-culture plates or to beads can act to augment both human and mouse T-cell activation [167, 169]. The work detailed within this chapter aimed to culminate with further evidence that antibodies targeting CD96 were agonistic and could augment T-cell activation. This was carried out utilising scFv clones panned against both huCD96v2 and mCD96 before their conversion to huIgG1 antibodies, characterising their capacity to induce human T-cell activation by assessing both T-cell proliferation and upregulation of CD25. Across all antibodies, the ability to augment T-cell activation was substantially increased at higher concentrations of OKT3. Induction of both T-cell proliferation and upregulation of CD25 was increased by the provision of each anti-CD96 clone over a matched isotype control. This data provides further evidence for the role of CD96 as a mediator of stimulatory signalling to human T-cells, as well as providing ground-work for further work investigating both how these same antibodies may induce mouse T-cell activity both *in vitro* and *in vivo*. Whilst previous work has shown that treatment of *in vivo* models of cancer in mice with CD96 targeting antibodies can limit tumour progression, little evidence has been presented to

indicate whether the blockade of CD155 may affect therapeutic impact. Therefore, future work utilising these newly described antibodies will aim to better understand the impact of their use in treating models of cancer.

The application of both blocking and non-blocking antibody clones to certain tumour models such as MC38 or CT26 could provide greater insight into whether the provision of CD96 antagonistic antibodies may enhance T-cell mediated anti-tumour activity and whether blocking interaction with CD155 is beneficial. Both of these tumour models utilise murine colon carcinoma cell lines and can be used with immunocompetent mice to understand the biological action of immunotherapeutics in reducing tumour growth. Use of the CT26 model has previously been used to show that whilst the blockade or ablation of CD96 did not impact tumour growth, tumour infiltrated CD8+ T-cell function was impaired [167]. A second approach beneficial to understanding the role of CD96 would be utilising an immunisation model. CD8+ T-cells in OT-1 transgenic mice all encode a TCR specific against $Ovalbumin_{257-264}$ (SIINFEKL). OT-1 splenocytes may be cultured with SIINFEKL-loaded APCs, allowing peptide presentation and TCR activation which could be combined with CD96 targeting antibodies.

Further evidence has been presented here for the role of CD96 as a co-stimulatory receptor on human T-cells, as well as providing the foundation for a novel panel of CD96 targeting antibodies to be utilised in downstream tumour and immunisation models. However, how CD96 mediates this activation of T-cells has yet to be understood. Therefore, the next chapter seeks to understand the specific domains within the CD96 ICD which mediate T-cell activation, and the signalling pathways employed.

Chapter 4 CARs as a model system for investigating huCD96 signalling

4.1 Generating CAR T-cells containing a CD96 intracellular domain

To assess and characterise the signalling properties of CD96, the simultaneous provision of both CD3ζ and CD96 activation must be provided to T-cells, constituting Signal 1 and Signal 2 of the T-cell activation model. Whilst these could be provided utilising antibodies against both, the development of a model system which would induce activation of both through interaction with a single ligand was sought. By utilising a single ligand interaction to provide activation of both CD3ζ and CD96 simultaneously, better control over application of stimuli could be achieved. As such, a system whereby the intracellular domain (ICD) of huCD96 is incorporated into the ICD of a chimeric antigen receptor (CAR) was developed. CAR-T therapy constitutes a form of cell engineering, whereby T-cells are virally transduced to constitutively express an artificial receptor. CARs recognise and bind an extracellular ligand, acting to transduce stimulatory signalling through the use of specific incorporated ICDs, imparting T-cells with targeted anti-tumour activity in an MHC-independent fashion. CD19 is a transmembrane protein expressed on the surface of B-cells and commonly utilised as a target of CAR-T therapy, with the therapeutics Kymriah and Yescarta currently available for clinical treatment of B-cell leukaemia. Along with the ICD of CD3ζ, the ICD of 4-1BB or CD28 are commonly utilised for clinical CAR-T therapy, however for the purpose of this experimental model the ICD of huCD96 was used in place.

In this chapter, human CD19-recognising CAR-T cells were generated, utilising the ICD of CD96 and CD3ζ. Consensus sequences are present within the ICD of CD96 that are commonly found in other co-stimulatory proteins. These include a PRD, the consensus sequence for an inhibitory ITIM domain, and a YxxM motif. To understand the role of these sites in mediating CD96 activity, each was sequentially mutated. To examine the impact of introducing specific mutations on CD96-mediated signalling, two distinct methods were employed. Initially, how each mutation affected functional T-cell activity was assessed through the upregulation of CD69 and IL-2 release. Secondly, to understand how CD96 mediates downstream kinase activity, a kinomics approach utilising a predictive kinase platform was employed, with the aim of identifying specific kinases and signalling mediators activated by CD96.

4.1.1 Chimeric Antigen Receptor design

For the design of a CD19-targeting CAR, the scFv FMC63 was utilised. FMC63 originated from an anti-human CD19 mouse IgG2a antibody characterised in 1991 [3]. This scFv construct was fused to a CD8 stalk region followed by a CD8 transmembrane domain (TM) and the specific intracellular signalling domains detailed in Table 4.1. Each CAR construct was generated by Dr. Claude Chan (2.9).

Table 4.1 CAR constructs utilised and their corresponding ICD

ICD Group	CAR Construct	CAR Target	Detection Marker	Intracellular Domain
Wild-type	BBζ	Human CD19	RQR8	hu4-1BB + huCD3ζ
	96ζ	Human CD19	RQR8	huCD96 + huCD3ζ
Controls	ζ	Human CD19	RQR8	huCD3ζ
	BBnull	Human CD19	RQR8	No ICD
	AT-171-2	Non-Target Control	RQR8	hu4-1BB + huCD3ζ

Each CAR plasmid (MP13328) comprised of either the anti-human CD19 FMC63 scFv, or utilised a control non-target scFv, AT-171-2, previously generated in house for use as a control antibody. The AT-171-2 scFv was previously raised in-house against anti-human CD40 antibodies (ChiLob74), recognising the scFv region of these antibodies and as such does not recognise human CD19. Two constructs acted as 'wild-type' CARs - BBζ and 96ζ. These included either the ICD of hu4-1BB and huCD3ζ, commonly utilised for clinical therapy, or huCD96 and huCD3ζ. Both of these constructs contained the unaltered ICD from their respective wild-type proteins, outlined in Figure 4.1. Similarly, control CAR constructs were generated. The construct ζ contained only the ICD of huCD3ζ, acting as a baseline control for any co-stimulatory effects induced by 96ζ. Finally, two non-signalling constructs were also generated – BBnull recognised huCD19 while lacking an ICD. On the other hand, AT-171-2 incorporated the 4-1BB and CD3ζ ICD design of BBζ, but utilised the control scFv incapable of recognising CD19.

Each CAR construct was placed under the control of an EF1α promoter, following which was an RQR8 detection tag (Figure 4.1A). This was followed by a T2A self-cleaving peptide, allowing for ribosomal skipping during CAR translation and translation of two final products, the CAR and the RQR8 detection tag [177, 178]. The inclusion of the RQR8 detection tag enabled for indirect confirmation of CAR expression through the use of either anti-human CD20 (Rituximab) or CD34 (QBend10) antibodies. The RQR8 tag combined the binding epitopes of CD20 and CD34 on a CD8α stalk and transmembrane domain, highlighted in Figure 4.1B, therefore was readily detected with the anti-human CD20

antibody, Rituximab [5]. As both the RQR8 and CAR were under the control of the same promoter and so transcribed together before being cleaved during RNA translation, expression of RQR8 could indicate the concurrent translation and expression of CAR.

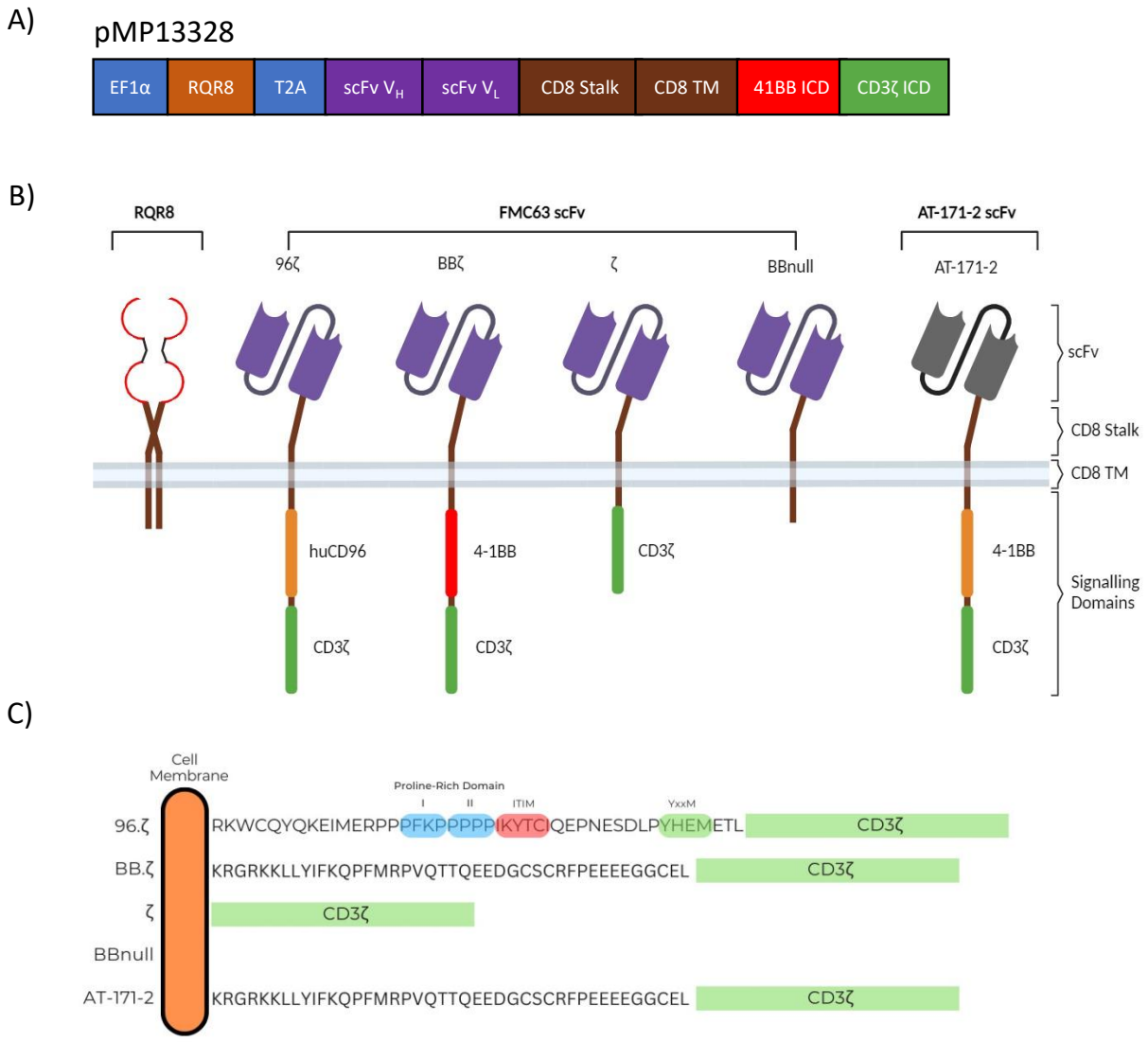

Figure 4.1 Schematic representation of utilised CAR constructs

A) Plasmid map of MP13228 plasmid utilising a 4-1BB intracellular domain for generating CAR lentivirus. Labelled in the EF1α promoter sequence, followed by the RQR8 detection tag and T2A site. Following this is the heavy and light chains of the FMC63 scFv, the CD8α stalk and transmembrane domains and the 4-1BB and CD3ζ intracellular domains. **B)** Schematic representation of the RQR8 transduction marker and CD19 (or non-targeting AT-171-2 control) targeting CARs and their respective intracellular domains. RQR8 was expressed as an independent protein and contained epitopes for both the anti-human CD20 (Rituximab) and anti-human CD34 (QBend10) antibodies. From left to right: CD19-recognising CARs (96ζ, BBζ, ζ, Bβnull) and non-targeting AT-171-2 control CAR, with their respective intracellular domains. **C)** Schematic representation of the intracellular sequence for each CAR construct. Highlighted within the huCD96 sequence were the predicted signalling domains including both Class I and Class II proline-rich domains, the consensus sequence for an ITIM, and a YxxM motif. (Images generated using both BioRender and InkScape).

4.1.2 Generating CAR lentivirus for transduction of Jurkat T-cells

To generate CAR-T cells, a lentivirus transduction method was utilised (2.11). The use of lentivirus for CAR-T generation has been shown to be an effective approach for efficient gene transfer into target cells due to their ability to transduce both dividing and non-dividing cells [179]. To generate suitable lentivirus for the transduction of target cells, a third-generation lentivirus production method was used, whereby 293FT cells were transfected with the MP13328 plasmid containing each CAR construct, two packaging plasmids (pMDLg/pRRE and pRSV.Rev), and an envelope plasmid (pMDG.1) for a total of four individual plasmids (2.11). The packaging plasmid pMDLg/pRRE contained the *Gag* gene responsible for intra-viral matrix, capsid and nucleocapsid, alongside the *Pol* gene, a polyprotein which is broken down to form reverse transcriptase, protease, RNAse H and integrase. Additionally, the pRSV.Rev plasmid encoding a *Rev* element was used, which acts to bind the Reverse Response Element (RRE) site in unspliced transcripts and allowing for nuclear export [6]. Finally, the envelope plasmid pMDG.1 encoding for the VSVG element (Vesicular stomatitis virus G glycoprotein) was included, allowing the generated lentivirus to be pseudotyped and rendered as replication incompetent. The use of this VSVG element as an envelope enabled generated lentivirus particles to enter target cells through the binding of the low-density lipoprotein receptor (LDL-R), expressed on T-cells.

4.1.3 Generated CAR expressing Jurkat cells

To generate a cell line which could be utilised to assess the signalling properties of CD96, lentivirus was used to transduce Jurkat T-cells (J-CAR cells). Retronectin, a recombinant human fibronectin protein, was used to enhance co-localisation of virus and target cells. Retronectin contains a Heparin-binding domain which binds to the envelope of viruses, whilst also containing two cell binding domains to bind T-cell expression Very Late antigen-4 and -5 (VLA-4 /5). This interaction is hypothesised to bring both the virus and cell into close proximity, increasing cellular uptake of virus to increase Jurkat transduction [180].

To assess the transduction efficacy of J-CAR cells, J-CAR were stained against either the RQR8 marker protein using Rituximab, or the CAR using an anti-FMC63 antibody against the CAR scFv region as detailed in the methods. All transduced J-CAR exhibited successful transduction as assessed through expression of both CAR and RQR8, with small variability of both RQR8 and CAR expression between each transduction (Figure 4.2A). In addition, there was a positive correlation between CAR and RQR8 marker expression (Figure 4.2B). Whilst all CARs presented high expression, CAR-ζ transduction was reduced, resulting in a second population of CAR negative Jurkat cells. To ensure expression of each CAR was consistent across each J-CAR cell line, cells were magnetically sorted according to their expression of RQR8 (Figure 4.2C). J-CAR were stained with low concentrations of biotinylated

Rituximab (0.05µg/mL) to select for J-CAR cells expressing high RQR8, before RQR8^{HI} J-CAR were isolated utilising MACs (2.11). The positive correlation between CAR and RQR8 expression ensured that these sorted RQR8^{HI} cells would be CAR+, removing low or non-expressing Jurkats. Following the removal of non-expressors, all transduced J-CAR cells presented expression of both CAR and RQR8 at more similar levels, allowing for comparison between J-CAR (Figure 4.2D/E).

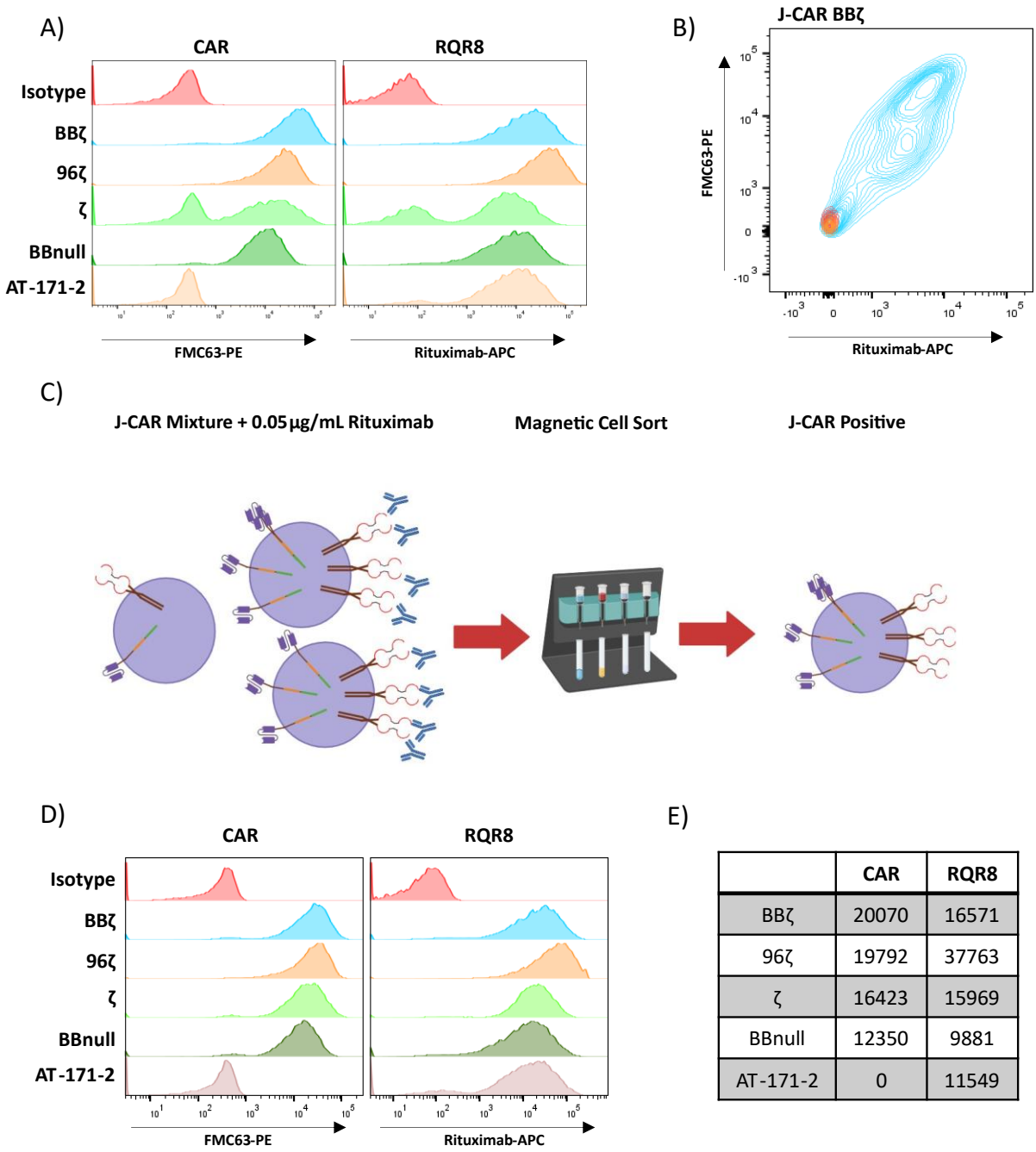

E)

	CAR	RQR8
BBζ	20070	16571
96ζ	19792	37763
ζ	16423	15969
BBnull	12350	9881
AT-171-2	0	11549

Figure 4.2 Transduction efficiency of Jurkat T cells utilising CAR construct containing lentivirus

A) Jurkat T-cells transduced with lentivirus to express CAR were stained with anti-FMC63 (0.5 µg/mL, Left panel) and Rituximab (0.5 µg/mL Right panel) to determine transduction efficacy. Anti-huIgG1-APC was utilised to detect Rituximab binding (1/200). Matched isotype controls are shown as top histograms (Red). **B)** Representative staining of J-CAR BBζ cells with anti-FMC63-PE (0.5 µg/mL) and Rituximab (0.5 µg/mL, + anti-huIgG1-APC 1/200). (J-CAR BBζ cells. Red = mIgG2a IC, Orange = huIgG1 IC, Blue = anti-FMC63-PE + Rituximab). **C)** Schematic overview of MACs sorting method isolating

RQR8 expressing J-CAR cells from negative population. **D)** MACs sorted J-CAR cells stained with anti-FMC63 (Left panel) and Rituximab (Right panel) as previous, to determine CAR and RQR8 expression of MACs sorted J-CAR. **E)** Geometric mean values of CAR+ and RQR8+ populations following MACs sort.

4.2 Investigating the sub-optimal activation of J-CAR cells

Following confirmation of equal CAR expression across J-CAR cells, pilot assays were carried out to assess the most effective method for activating J-CAR cells through huCD19-recognising CAR. A number of methodologies were assessed including culture with plate-bound recombinant huCD19 (rhuCD19), capture and presentation of rhuCD19 on plate-bound anti-huFc antibodies, and co-culture with huCD19 expressing B cells.

4.2.1 Activation of J-CAR with recombinant human CD19

To evaluate the capacity of plate-bound rhuCD19 to activate J-CAR cells, rhuCD19 was assessed for both its capacity to bind Jurkat expressed CAR, and its ability to activate J-CAR cells. Tissue culture plates were coated with rhuCD19 in coating buffer, utilising a similar method to that employed for plate-bound antibodies. Also assessed was the pre-coating of plates with an anti-human Fc antibody, SB2H2, to capture recombinant rhuCD19 and potentially mediate a more physiological presentation profile.

To first confirm that J-CAR cells could in fact bind rhuCD19, binding of the J-CAR BBζ cell line was quantified using a rhuCD19 titration. BBζ expressing J-CAR cells capably bound soluble rhuCD19, with a calculated EC_{50} value of 2.76 µg/mL (Figure 4.3A/B).

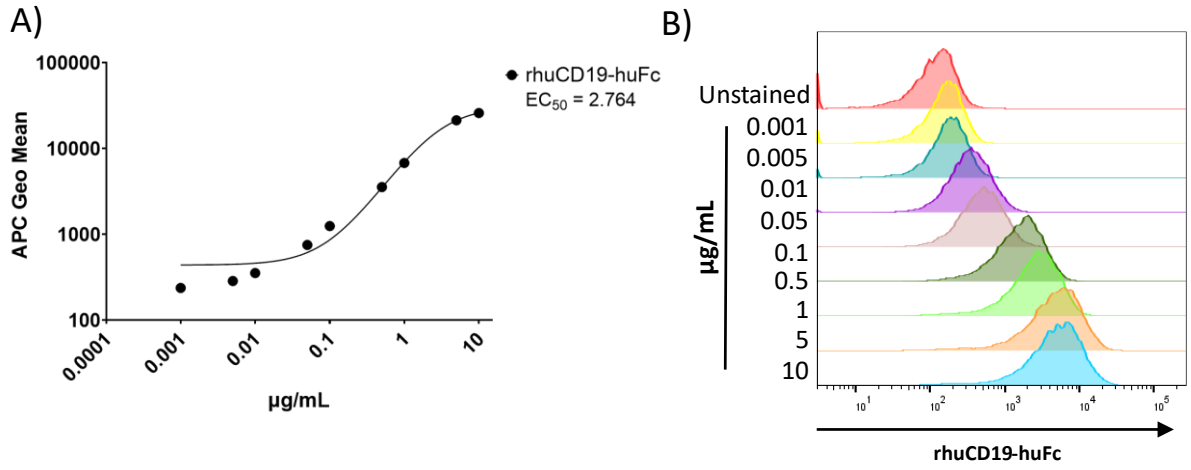

Figure 4.3 Recombinant Human CD19 binding of BBζ expressing J-CAR cells

A) Titration of rhuCD19 binding to BBζ expressing J-CAR cells (EC_{50} = 2.764 µg/mL). rhuCD19 was detected utilising an APC labelled anti-huFc antibody. **B)** Histograms of rhuCD19 titration against BBζ expressing J-CAR cells. Unstained J-CAR cells were used as a negative control (Red histogram).

CD69 is a T cell activation marker, upregulated upon T-cell activation [181]. To confirm Jurkat T-cell upregulation of CD69 upon activation, wild-type Jurkats were stimulated with the anti-human CD3 antibody, OKT3, in a plate-bound conformation (Figure 4.4A). CD69 was upregulated strongly by 24 hours, with a gradual downregulation by 48 and 72 hours. Therefore, the upregulation of CD69 over the course of 48-72 hours could be utilised as an indicator of Jurkat activation.

To assess the capacity of rhuCD19 to activate Jurkats through their CAR, a number of concentrations of rhuCD19 were used. rhuCD19 was either plate-bound directly to tissue-culture plates, or as a soluble protein to wells pre-coated with an anti-human IgG antibody (SB2H2). For this initial pilot, J-CAR BBζ cells were used, while the AT-171-2 non-binding J-CAR cells were used as a control. When rhuCD19 was directly bound to plates, no indication of J-CAR activation through BBζ CAR was identified, with expression of CD69 consistent over 72 hours regardless of increased rhuCD19 concentration (Figure 4.4B). This lack of CD69 upregulation was similar with AT-171-2 J-CAR cells, indicating that rhuCD19 is incapable of providing a stimulatory signal when bound to tissue culture plates.

To assess whether capturing soluble rhuCD19 on SB2H2-coated plates would allow for J-CAR activation, J-CAR cells were cultured as above and CD69 expression was assessed over 72 hours (Figure 4.4C). Similar to direct coating of rhuCD19 to plates, capture of rhuCD19 with SB2H2 failed to induce T-cell activation. No increase in CD69 expression over the baseline (0 hrs) was observed over the course of 72 hours.

Together these data suggested that rhuCD19, while capable of binding CAR, was not capable of inducing J-CAR activation when either plate-bound or Fc captured. Consequently, other alternatives were investigated to achieve optimal J-CAR activation.

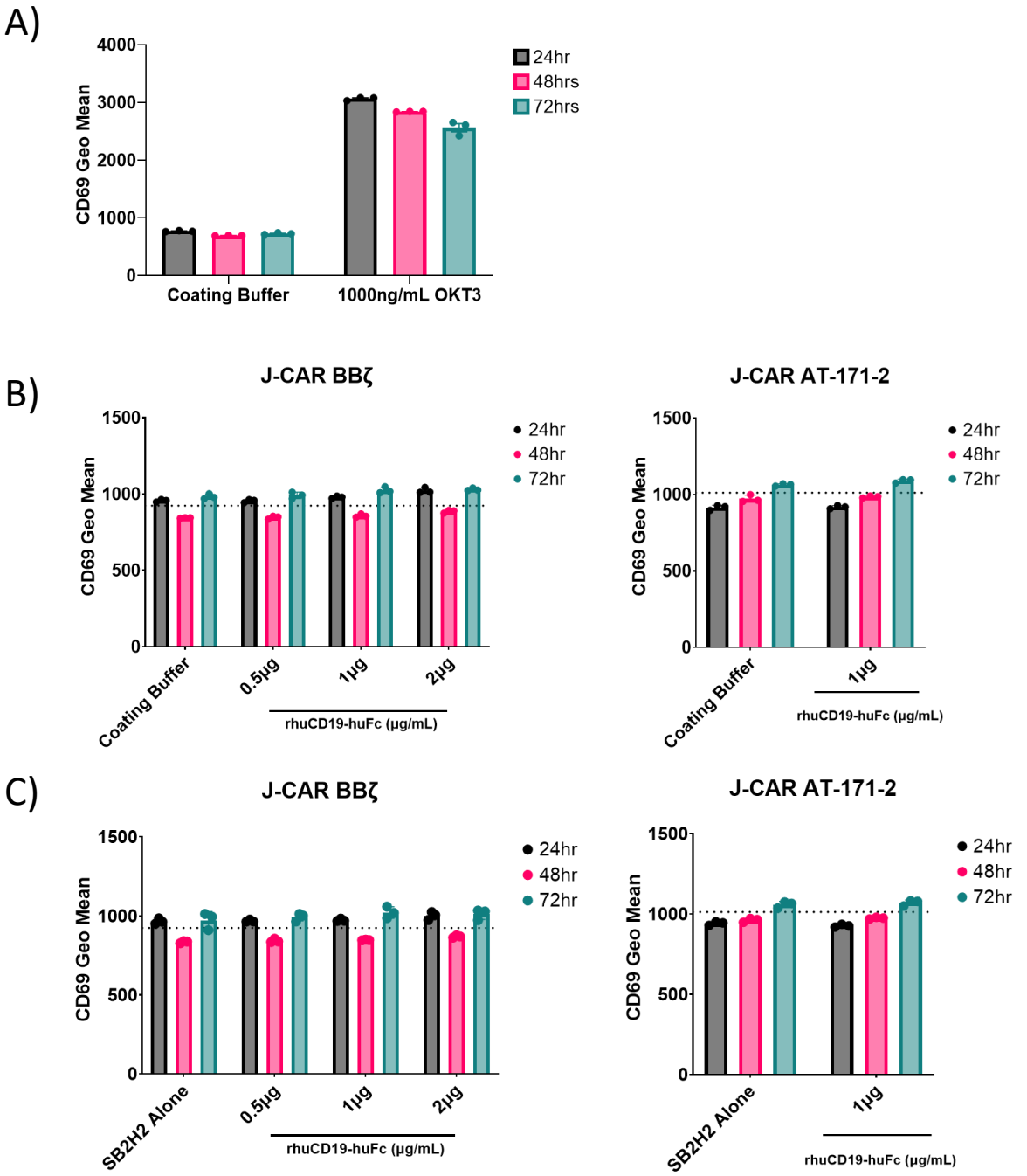

Figure 4.4 Recombinant huCD19 effectively binds J-CAR but fails to induce cell activation

A) Expression of CD69 at 24, 48 and 72 hours on wild-type Jurkat T-cells cultured in tissue-culture plates coated overnight with coating buffer alone or coating buffer containing anti-human CD3 (OKT3) at 1000 ng/mL. **B)** Upregulation of CD69 at 24, 48 and 72 hours on CAR-BBζ (Left graph) and CAR-AT-171-2 (Right graph) when cultured in rhuCD19 coated tissue-culture plates at 0.5, 1 or 2 µg/mL. **C)** Expression of CD69 at 24, 48 and 72 hours on CAR-BBζ (Left graph) and CAR-AT-171-2 (Right graph) cultured with soluble rhuCD19 at corresponding concentrations in SB2H2-coated plates. (Graphs B/C dashed line represents baseline J-CAR CD69 expression at prior to culture).

4.2.2 Activation of J-CAR with huCD19 expressing target cells

As a common clinical target of CAR-T therapeutics, CD19+ B cells represented the next logical choice for activating J-CAR cells [182]. The physiological high expression of CD19 on B cells could potentially offer a greater number of available ligands for CAR binding and subsequent J-CAR activation. Therefore, a co-culture approach was used whereby J-CAR cells were co-cultured with Ramos B cells before J-CAR activation assessed through CD69 upregulation and IL-2 release.

Initially, to confirm that the Ramos B-cell line expressed the CD19 CAR target, as well as CD20 to enable differentiation of Ramos from J-CAR, expression of both targets was evaluated by flow-cytometry. Ramos B-cells showed clear expression of both CD19 and CD20 (Figure 4.5A). As a B cell lineage marker, CD20 is not expressed on T-cells and therefore Jurkat cells were CD20 negative. Ramos target cells were also distinguishable from Jurkat cells through expression of CD20 (Figure 4.5B). As a result, J-CAR specific upregulation of CD69 in response to co-culture with CD19+ Ramos cells could be assessed.

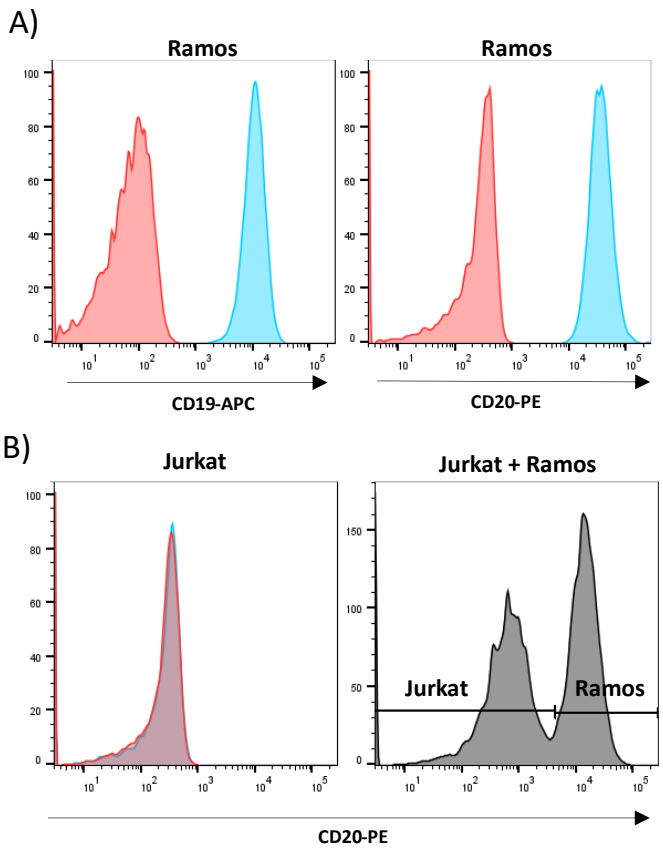

Figure 4.5 CD20 expression on Ramos target cells distinguishes target cell from Jurkat

A) Staining of Ramos B cells against CD19 (Left blue histogram, 2 µg/mL) and CD20 (Right blue histogram, 2 µg/mL). Ramos B cells were stained with equivalent isotype control antibodies (2 µg/mL) (Red histograms). **B)** Jurkat T-cells (Left) or Jurkat cultured with Ramos B cells (Right) stained for CD20 expression (2 µg/mL).

To assess the optimal ratio of effector J-CAR cells to target Ramos cells (E:T), the number of target Ramos cells was gradually increased, ranging from E:T ratios of 100:1, 10:1 and 1:1. As a positive control of J-CAR activation, plate-bound OKT3 was used as described in 4.2.1. The control CAR AT-171-2 was utilised as a negative control. Each J-CAR was cultured with plate-bound OKT3, or co-cultured with Ramos B cells at the indicated ratios.

J-CAR BBζ cells activated with plate-bound OKT3 strongly upregulated CD69 by 24 hours, with gradual upregulation by 48 and 72 hours. Conversely, J-CAR BBζ cells cultured in coating buffer treated plates failed to upregulate CD69 (Figure 4.6A/B). Upregulation of CD69 on J-CAR BBζ cells co-cultured with Ramos cells was limited at an E:T ratio of 100:1. However, at 10:1 upregulation of CD69 was similar to that of sub-optimal CD3 stimulation. CD69 upregulation was greatest when cultured at a 1:1 ratio, peaking at 48 hours before decreasing by 72 hours (Figure 4.6A/C).

J-CAR AT-171-2 cells exhibited increased CD69 expression when activated with plate-bound OKT3 whilst failing to respond when cultured in coating buffer treated tissue-culture plates (Figure 4.6D/E). As expected, J-CAR cells expressing an AT-171-2 CAR did not upregulate CD69 when co-cultured with Ramos B cells (Figure 4.6D/F).

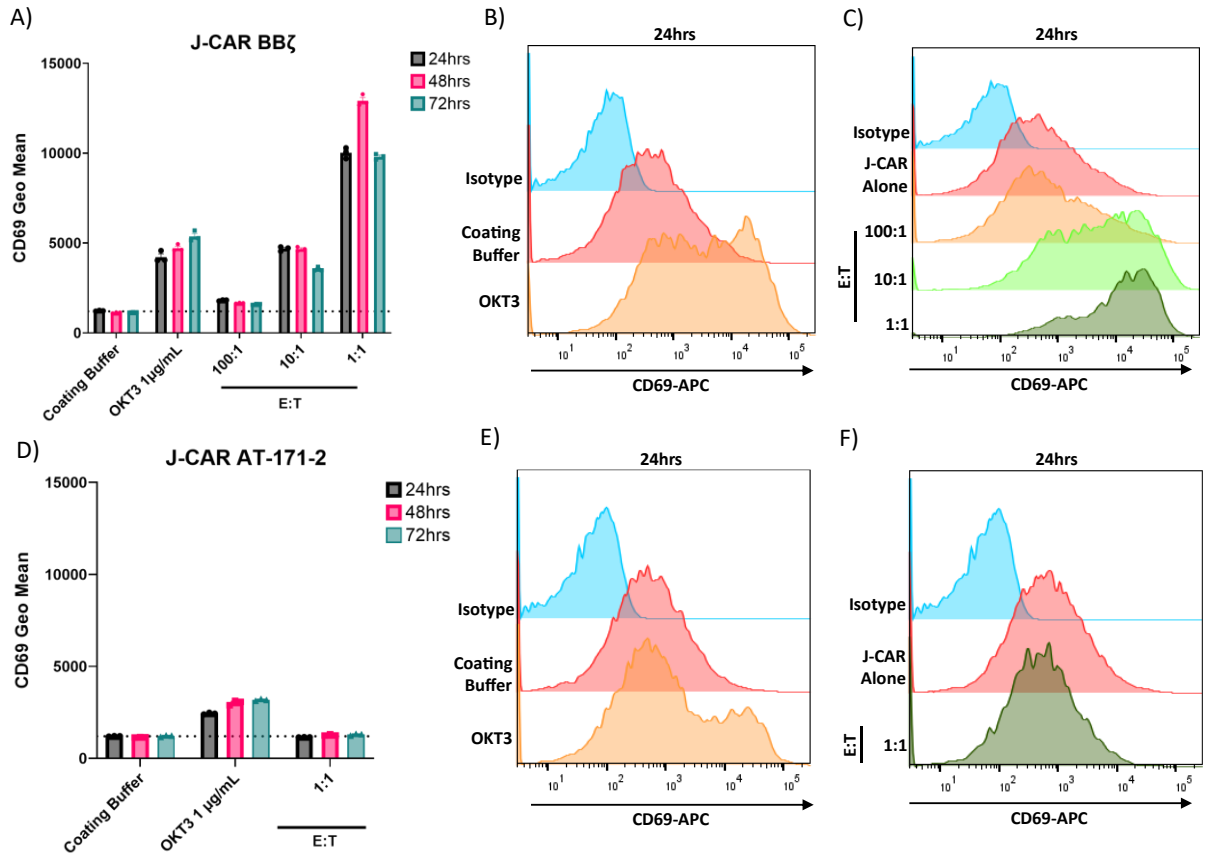

Figure 4.6 J-CAR upregulation of CD69 upon co-culture with CD19+ Ramos B cells.

A) CAR-BBζ Jurkat cells were plated in wells treated with either coating buffer or plate-bound OKT3 (1 µg/mL). J-CAR were also co-cultured with Ramos B cells at ratios of 100:1, 10:1 or 1:1. Expression of CD69 (2 µg/mL) was assessed at 0 hours (Dashed line) and over the course of 72 hours. **B)**

Representative histograms of CD69 expression on BBζ expressing J-CAR cells cultured in tissue-culture plates coated with coating buffer alone (Red) or with 1 µg/mL OKT3 (Orange). Matched isotype control staining of J-CAR BBζ cells is shown in blue. **C)** Representative histograms of CD69 staining (2 µg/mL) of BBζ expressing J-CAR cells cultured alone (Red) or co-cultured with Ramos B cells at 100:1 (Orange), 10:1 (Green) or 1:1 (Dark green). Matched isotype control staining of J-CAR BBζ cells is shown in blue. **D)** CAR-AT-171-2 Jurkat cells were plated in wells treated with either coating buffer or plate-bound OKT3 (1 µg/mL). J-CAR were also co-cultured with Ramos B cells at a ratio of 1:1. Expression of CD69 (2 µg/mL) was assessed at 0 hours (Dashed line) and over the course of 72 hours. **E)** Representative histograms of CD69 expression on AT-171-2 expressing J-CAR cells cultured in tissue-culture plates coated with coating buffer alone (Red) or with 1 µg/mL OKT3 (Orange). Matched isotype control staining of J-CAR BBζ cells is shown in blue. **F)** Representative histograms of CD69 staining (2 µg/mL) of AT-171-2 expressing J-CAR cells cultured alone (Red) or co-cultured with Ramos B cells at a 1:1 ratio (Dark green). Matched isotype control staining of J-CAR BBζ cells is shown in blue. (**A+D** Data shown is mean of triplicates.)

To further assess whether the activation of J-CAR through Ramos co-culture enhanced IL-2 secretion, ELISA was utilised (Figure 4.7). BBζ expressing J-CAR cells produced low levels of IL-2 when activated with CD3 targeting antibody (OKT3) (Figure 4.7A). BBζ J-CAR cells co-cultured with Ramos cells at a ratio of 100:1 produced similar levels of IL-2. IL-2 released by BBζ J-CAR cells cultured with Ramos at 10:1 was increased, peaking at 24 hours. Release of IL-2 was further increased by BBζ J-CAR cells when cultured with Ramos at a 1:1 ratio, with the highest recorded IL-2 at 72 hours. Culture of Jurkat expressing AT-171-2 CAR in OKT3-coated plates increased IL-2 release over culture in plates with coating buffer alone (Figure 4.7B). However, co-culture of AT-171-2 J-CAR cells with target Ramos failed to induce IL-2 release.

These data indicated that for effective activation of CD19-specific J-CAR T-cells, a co-culture with CD19+ B cells was optimal. Upregulation of CD69 and IL-2 release could also be effectively measured to assess J-CAR activation in response to target co-culture, with a minimum E:T ratio of 10:1 required to elicit a similar response to that of the anti-human CD3 antibody, OKT3.

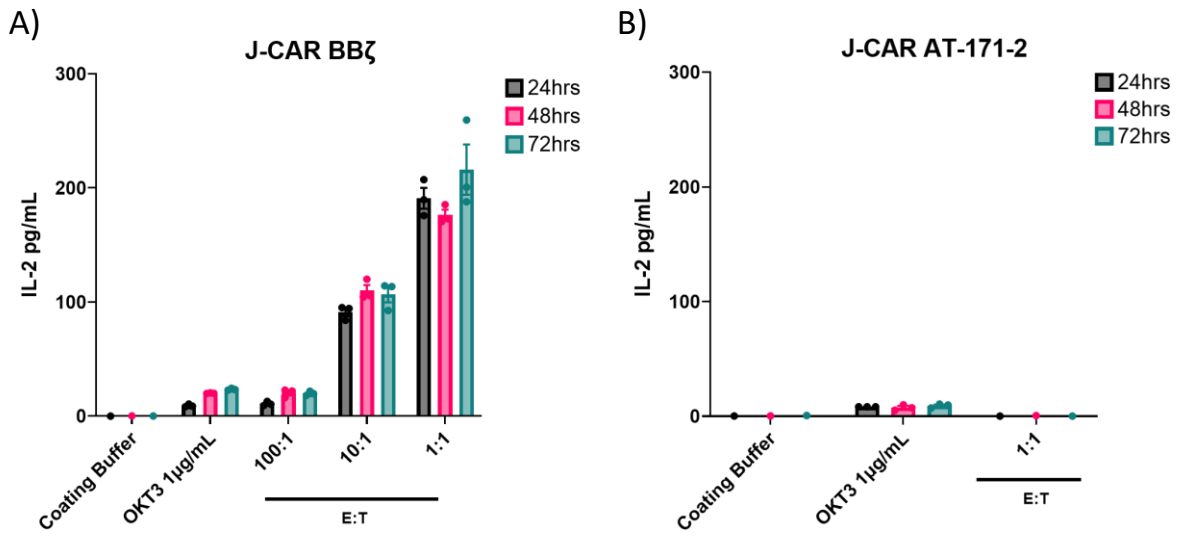

Figure 4.7 J-CAR IL-2 production increases in response to increased target co-culture

A/B) Supernatant containing IL-2 was quantified by ELISA to determine BBζ (A) or AT-171-2 (B) expressing J-CAR cytokine release in response to plate-bound OKT3 (Or coating buffer control) and decreasing ratios of Ramos co-culture. Supernatant was collected at 24, 48 and 72 hours. (Data shown were technical triplicate values of one experiment, +/- SEM).

4.3 Dissecting the source of CD96 stimulatory signalling

Within the data presented in this chapter, it has been shown that utilising a Ramos co-culture methodology is the most optimal method for inducing J-CAR activation (Figure 4.6). In addition, upregulation of CD69 and release of IL-2 could both serve as indicators of Jurkat activation. Within this next subchapter, the capacity of the CD96 ICD to impart stimulatory signalling will be investigated.

4.3.1 The CD96 ICD enables effective cell activation in the context of CARs

To determine how the inclusion of the CD96 ICD may augment CD3ζ signalling, a co-culture T:E ratio of 10:1 was utilised. At this ratio, J-CAR BBζ co-cultured with target Ramos cells resulted in similar J-CAR activation to that of plate-bound OKT3 antibody. Considering that CD69 expression in response to either plate-bound OKT3 or co-culture with Ramos cells peaked at between 24 and 48 hours, expression was assessed at 6, 24 and 48 hours. Similarly, supernatant was collected at these timepoints to quantify IL-2 release. As a control for CD96 induced signalling, J-CAR ζ was tested alongside J-CAR 96ζ. Both J-CAR AT-171-2 and BBnull served as negative controls, with both lacking the capacity to induce J-CAR activation (Figure 4.1).

When assessing the expression of CD69 on J-CAR T-cells cultured alone, small variations of background CD69 expression were recorded. Background expression of CD69 was also found to vary over the course of the assay (Figure 4.8A/B). However, this change in expression was limited to J-CAR AT-171-2, BBζ, and 96ζ. To account for these small changes in background J-CAR CD69 expression, expression of CD69 on J-CAR cells cultured alone was measured at each time point. The geometric mean of background CD69 expression was then removed from the geometric mean of co-cultured J-CAR cells to give a more accurate assessment of CD69 upregulation. Going forward, all representation of CD69 geometric mean was calculated this way.

$$CD69\ Geo\ Mean =$$

$$CD69\ Geometric\ Mean\ (Cells\ Alone) - CD69\ Geometric\ Mean\ (Co - Culture)$$

Interestingly, when quantifying the background expression of CD69 on unstimulated J-CAR cells, the inclusion of the 4-1BB ICD conferred a higher baseline expression of CD69 (Figure 4.8A). Both the control CAR (AT-171-2) and the BBζ CAR utilised the ICD of 4-1BB. Expression of CD69 was highest at 6 hours on both J-CAR AT-171-2 and BBζ cells cultured alone. Conversely, the control BBnull J-CAR,

lacking an ICD, had the lowest CD69 expression at 6 hours. Expression of CD69 on J-CAR ζ and 96ζ was similar across all timepoints when cultured alone. All J-CAR cells experienced downregulation of CD69 over the course of 72 hours. This data implied that tonic signalling, a noted characteristic of CARs utilising the 4-1BB ICD, may be reduced in CAR that utilises CD96 as a co-stimulatory domain [183].

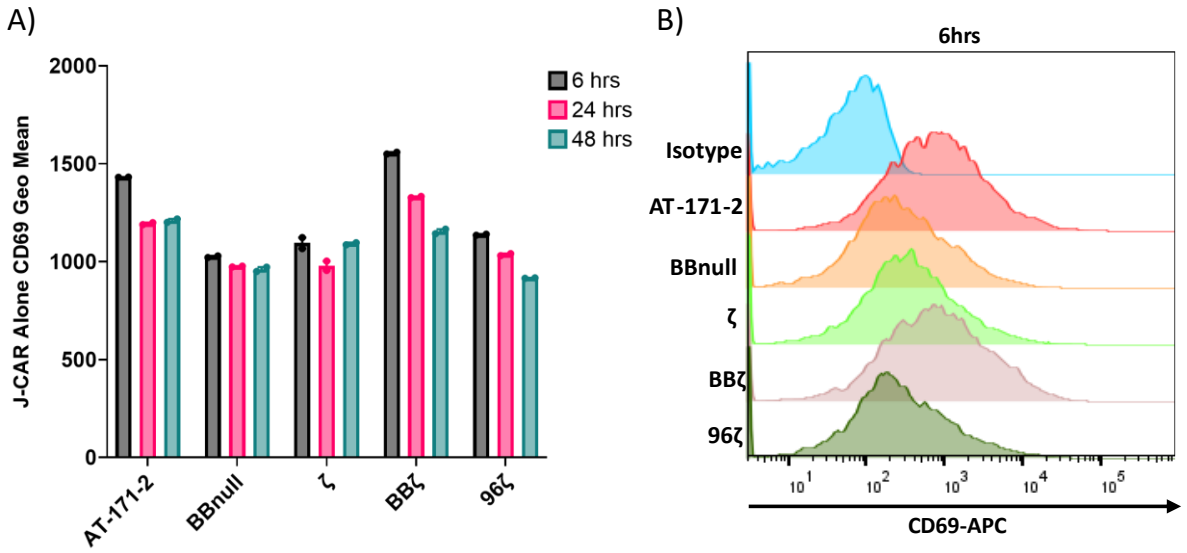

Figure 4.8 Background expression of CD69 across J-CAR cell lines

A) Expression of CD69 on J-CAR T-cells cultured alone, assessed at 6, 24 and 48 hours by flow-cytometry (anti-human CD69, 2 µg/mL). **B)** Representative histogram staining of CD69 on J-CAR T-cells cultured alone for 6 hours.

To evaluate the potential for each CAR described above to induce Jurkat activation, J-CAR were co-cultured at an E:T ratio of 10:1 and assessed for CD69 and IL-2 release.

Co-culture of Ramos cells with J-CAR expressing either AT-171-2 or BBnull CAR resulted in no upregulation of CD69 over the course of 48 hours (Figure 4.9A/B). Co-culture of J-CAR ζ with Ramos cells resulted in minimal upregulation of CD69, peaking at 24 hours. In contrast, J-CAR BBζ co-culture resulted in strong CD69 upregulation, again peaking at 24 hours. Notably, J-CAR 96ζ exhibited significant capacity to induce Jurkat activation over J-CAR ζ, with CD69 upregulation peaking at 24 hours (Figure 4.9A/B). This upregulation of CD69 by J-CAR 96ζ indicated that the ICD of CD96 combined with ζ was capable of transmitting stimulatory signals in the context of a CAR.

Furthermore, supernatant was collected at each timepoint to quantify IL-2 release by ELISA. As previously reported, neither control J-CAR (AT-171-2 or BBnull) released IL-2 in response to co-culture with Ramos target cells (Figure 4.9C). Release of IL-2 by J-CAR ζ cells co-cultured with Ramos was minimal. Comparatively, IL-2 release by both J-CAR BBζ and 96ζ cells was significantly increased over J-CAR ζ at all timepoints. Interestingly, IL-2 release by J-CAR 96ζ was significantly increased over J-CAR BBζ at both 6 and 24 hours.

Overall, these data provided evidence for the co-stimulatory role of CD96 in the context of J-CAR cells. Whilst the inclusion of the 4-1BB ICD served as a positive control, it has also shown that Jurkat activation through a 96ζ CAR may differ from that of a 4-1BB CAR. While CD69 upregulation was stronger in BBζ expressing Jurkat cells, release of IL-2 occurred much quicker in 96ζ cells, and generally outperformed 4-1BB.

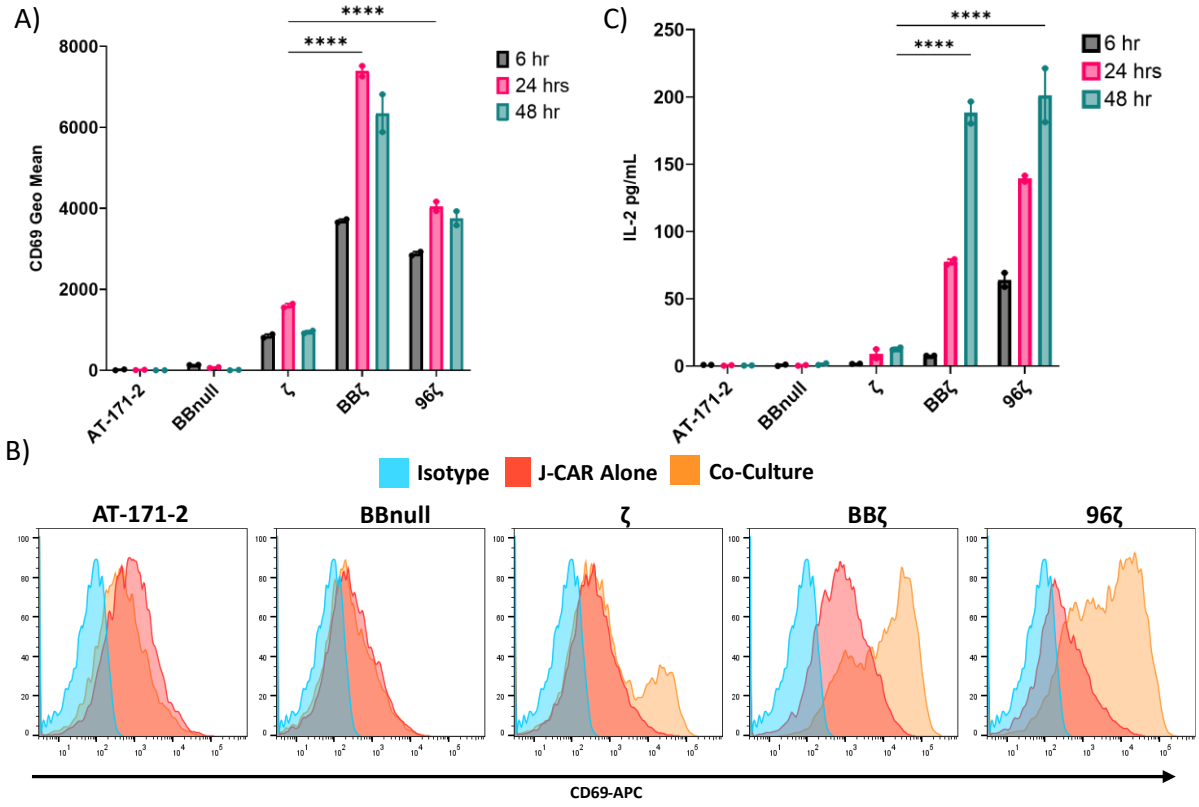

Figure 4.9 Inclusion of the CD96 ICD imparts strong J-CAR activation over CD3ζ signalling alone.

A) Geometric mean of J-CAR CD69 expression when co-cultured with target Ramos B cells at an E:T ratio of 10:1. CD69 expression was assessed at 6, 24 and 48 hours. **B)** Representative histograms of J-CAR CD69 expression at 24 hours. J-CAR and Ramos co-culture was stained against CD20 (2 µg/mL) and J-CAR identified as CD20-negative. Cells were stained against CD69 (2 µg/mL). Matched mIgG1 isotype control antibody is shown as blue histogram. **C)** Supernatant collected at each timepoint was assessed for IL-2 by ELISA. (**A+C** ±SEM of 1 independent experiment and assessed with a 2-way Anova with Tukey's test for multiple comparisons. **** = p<0.0001)

4.3.2 Point mutations of the CD96 ICD

Within the ICD of huCD96, a number of hypothesised signalling domains exist which are commonly found in other co-stimulatory proteins, however their role and contribution to signalling mediated by CD96 is not yet fully elucidated [184]. These domains include a proline rich domain (PRD), a consensus sequence for an ITIM, as well as a YxxM domain which can act as the binding target of SH2-domain containing proteins [63, 185]. Considering the contribution of these domains to signalling in other co-stimulatory proteins, it was hypothesized that these domains may also influence the stimulatory effect of CD96. In an analysis of SH3 binding motifs, Teyra et. al presented a number of consensus sequences for potential PRDs, of which two are present in CD96 as a Class I PRD (PRDI) and a Class II PRD (PRDII) [158]. These PRDs are centred around a core PxxP sequence, with Class I PRDs predicted to have a $^{-3}RxxP^{0}xxP^{+3}$ consensus sequence, while Class II PRD are predicted to have a consensus sequence of $^{0}PxxP^{+3}xR/K^{+5}$. These are present in CD96 as RPPPFKP (PRDI) and PPPPIK (PRDII). A third consensus sequence described by Teyra et. also exists ($^{-6}RxxxxxP^{0}$, Class III) in CD96 as RPPPFKP, overlapping with the Class I sequence.

Table 4.2 Site-directed mutations of the CD96 ICD utilised for CAR-96ζ

CD96 CAR Construct	CD96 ICD Sequence	CD3ζ
96ζ	RKWCQYQKEIMERPPPFKPPPPPIKYTCIQEPNESDLPYHEMETL (PRDI, PRDII, ITIM, YxxM, PRDIII)	Y
96-P3Aζ	RKWCQYQKEIMERAAAFKPPPPPIKYTCIQEPNESDLPYHEMETL	Y
96-P4Aζ	RKWCQYQKEIMERAPFKAAPPAIKYTCIQEPNESDLPYHEMETL	Y
96-Y566Aζ	RKWCQYQKEIMERPPPFKPPPPAIKYTCIQEPNESDLPYHEMETL	Y
96-YXXMζ	RKWCQYQKEIMERPPPFKPPPPPIKYTCIQEPNESDLAHEAETL	Y
96	RKWCQYQKEIMERPPPFKPPPPPIKYTCIQEPNESDLPYHEMETL	N

Consequently, to identify which of the domains within CD96 are responsible for mediating J-CAR activation, specific point-mutations were introduced at key sites through site-directed mutagenesis (Table 4.2). J-CAR cells were generated utilising these mutated forms of 96ζ CAR (2.9). To inhibit the Class I PRD, the first 3 prolines of the proline-rich region were mutated to alanine, generating a P3A mutant. To target Class I, Class II and Class III PRDs, a more targeted approach was utilised, mutating four core prolines that would target all three PRDS and generate a P4A mutant. An initial CD96 PRD mutation was designed, broadly mutating the 8 prolines which constitute the PRD, however this drastic change produced a CAR which failed to express. To assess the functionality of the ITIM consensus sequence, the tyrosine residue was mutated to alanine, whilst both the tyrosine and

methionine of the YxxM domain were also mutated to alanine in an effort to understand its contribution.

Considering that antibody targeting of CD96 alone fails to induce T-cell activation, a CAR with only the ICD of CD96 was included as a negative control [169]. With this approach, the contribution of each signalling domain could be evaluated utilising both J-CAR ζ and J-CAR 96 as controls.

4.3.3 Mutations of the CD96 ICD PRD impair J-CAR activation

Initially, the role of the YxxM motif (96-YxxMζ), the ITIM consensus sequence (96-Y566Aζ), and the Class I PRD (96-P3Aζ) were investigated. To assess the impact of these mutations, the same assays utilised for the J-CAR pilot studies were carried out, measuring upregulation of CD69 and release of IL-2.

Co-culture of J-CAR 96 cells with Ramos resulted in no upregulation of CD69. As found with pilot assays, J-CAR ζ co-culture with Ramos induced low upregulation of CD69, peaking at 24 hours (Figure 4.10A). Co-culture of J-CAR 96ζ however induced strong J-CAR activation, increasing CD69 expression to peak at 48 hours. On the other hand, mutations of either the YxxM or ITIM motif resulted in limited ablation of CD96-mediated CD69 upregulation. Only at 48 hours did the introduction of the YxxM mutation significantly affect J-CAR 96ζ induced CD69 upregulation. Similarly, only at 6 and 48 hours did the introduction of an ITIM mutation affect CD69 upregulation. Conversely, mutation of PRD1 (P3A) significantly reduced 96ζ induced CD69 upregulation at all timepoints. While CD69 expression was reduced with respect to 96ζ, none of these mutations limited activation to that induced by CD3ζ signalling alone.

Furthermore, the impact of CD96 ICD mutations on IL-2 release was assessed. J-CAR activation through CD3ζ alone induced low-level secretion of IL-2, peaking at 24 hours, while the inclusion of the CD96 ICD significantly increasedIL-2 production (Figure 4.10B). Mutagenesis of the YxxM motif had little impact on total IL-2 release, however mutation of the ITIM sequence significantly reduced IL-2 production at both 24 and 48 hours with respect to 96ζ. J-CAR 96-P3Aζ induced similar IL-2 release to that of 96ζ. Overall, no site-directed mutagenesis of the CD96 ICD supressed IL-2 release to that of CD3ζ.

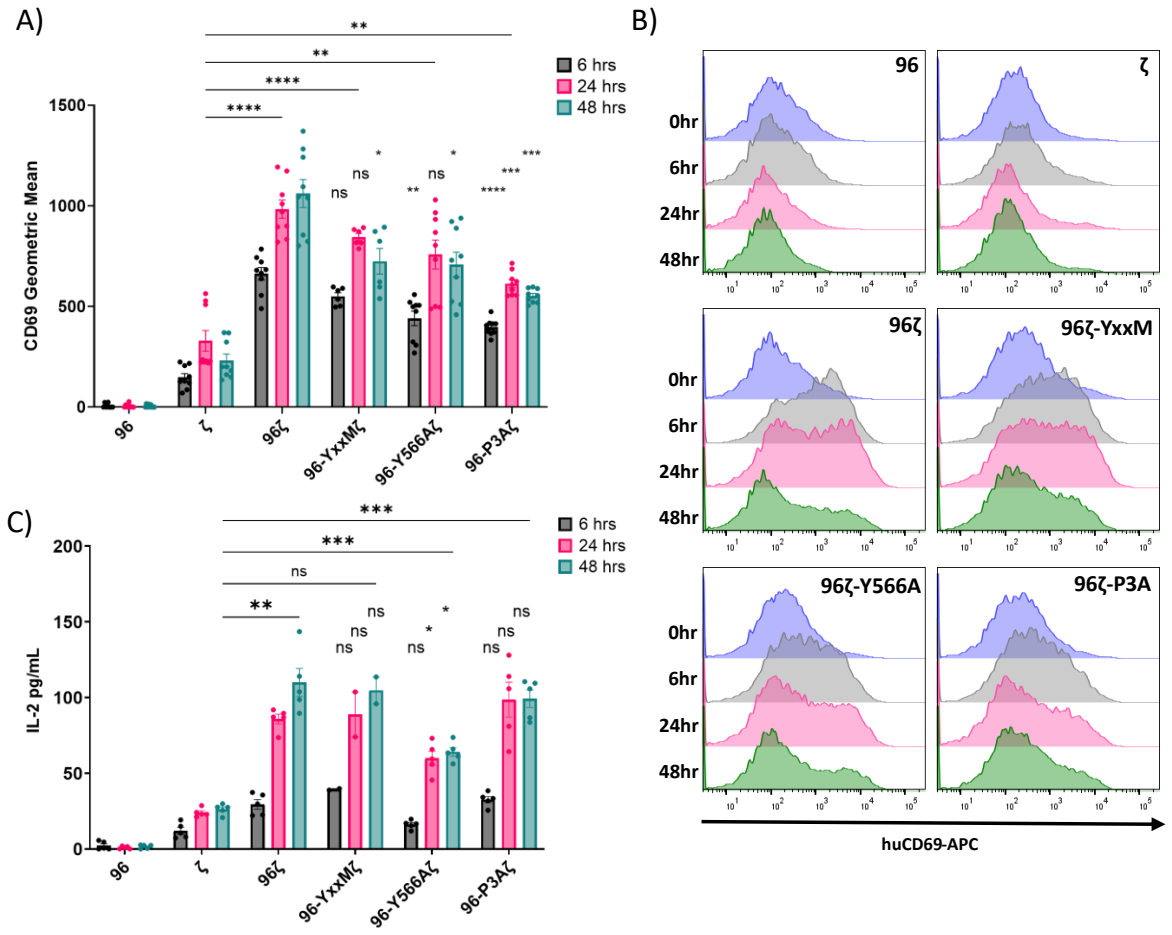

Figure 4.10 Mutation of CD96 PRDI limits CD69 upregulation but not IL-2 production

A) CD69 expression of J-CAR cells co-cultured with Ramos B cells at a ratio of 10:1 was assessed through flow-cytometry over the course of 48 hours. **B)** Representative histograms of CD69 expression on J-CAR cells when co-cultured with Ramos cells at a ratio of 10:1. J-CAR and Ramos co-culture were stained against CD20 (2 µg/mL) and J-CAR identified as CD20-negative. Cells were stained against CD69 (2 µg/mL) **C)** IL-2 production by J-CAR cells cultured with Ramos B cells in panel A was quantified using ELISA at 6, 24 and 48 hours. (**Panels A-C** ±SEM of 3 independent experiments and assessed with 2-way Anova with Tukey's test for multiple comparisons. Values above CD96 mutations are statistical significance with respect to equivalent timepoint of 96ζ. ns = non-significant, **p<0.01, ***p<0.001, ****p<0.0001)

4.3.4 Targeted mutations of four core prolines ablates stimulatory capacity of CD96

Considering that the P3A mutation of PRDI limited CD69 upregulation with respect to 96ζ at all timepoints, a more specific mutation of the PRD was designed to target both PRDs (Table 4.2). As a method of targeting the three PRDs present within the CD96 ICD, a P4A mutation was utilised which encompassed core prolines common to each motif.

To assess the impact of mutating these four core prolines, 96-P4Aζ was assessed compared to J-CAR utilising either the ICD of CD96 alone, CD3ζ, or 96ζ. As previous, CAR 96 failed to induce CD69 upregulation, whilst CAR ζ induced low upregulation of CD69 (Figure 4.11A/B). CAR 96ζ significantly increased upregulation of CD69 with respect to CAR ζ. Interestingly, CAR 96-P4Aζ failed to induce

significant CD69 expression with respect to CAR ζ, with CD69 upregulation significantly decreased with respect to CAR 96ζ at both 24 and 48 hours (Figure 4.11A/B).

J-CAR expressing 96-P4Aζ were assessed for their release of IL-2 following Ramos co-culture. CAR ζ induced limited IL-2 release, whilst CAR 96ζ increased release of IL-2 as previously noted. Conversely, CAR 96-P4Aζ failed to induce IL-2 release above that of the control CAR ζ (Figure 4.11C).

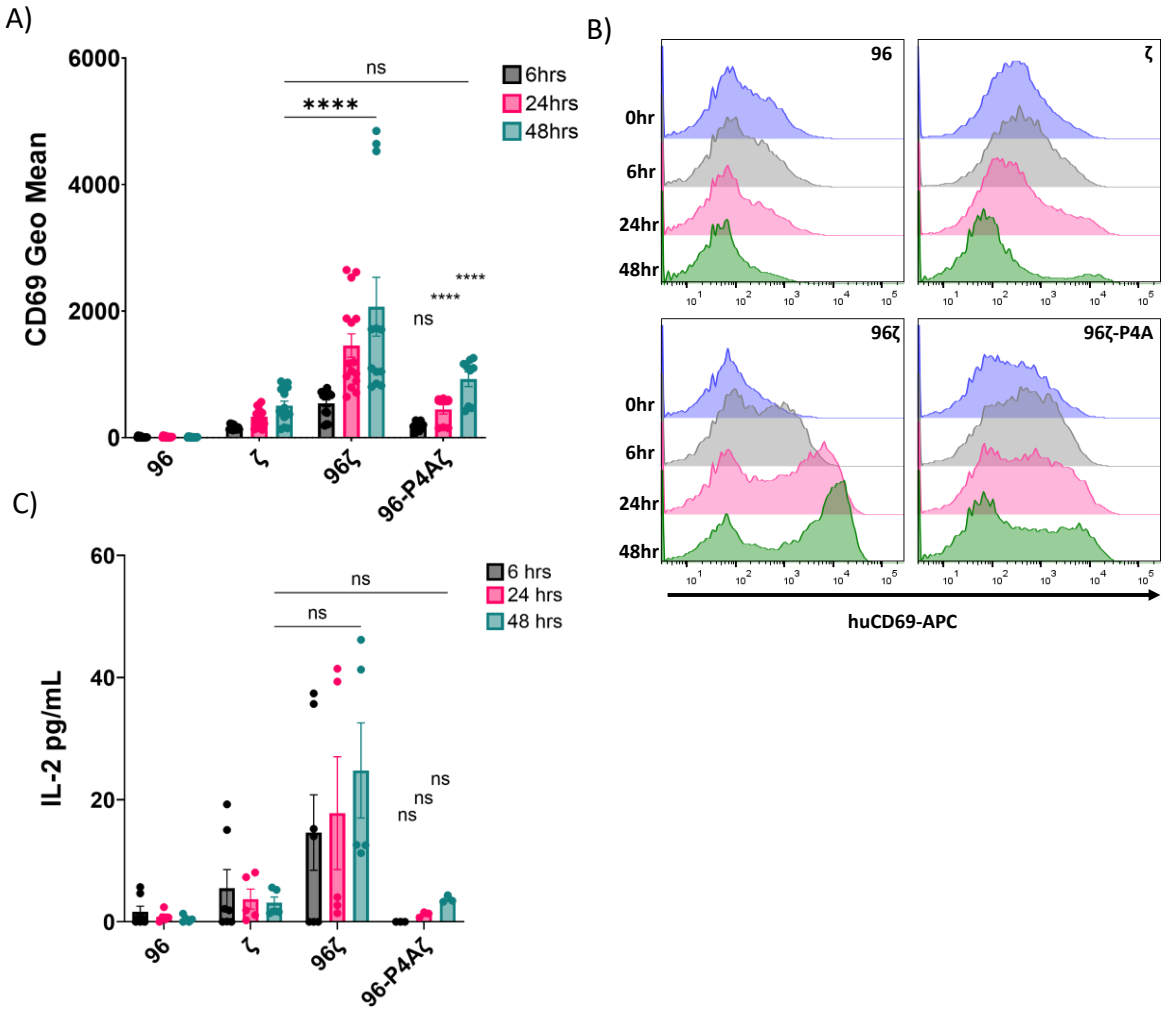

Figure 4.11 Mutation of CD96 PRDI and PRDII limits both CD69 upregulation and IL-2 production

A) CD69 expression of J-CAR cells co-cultured with Ramos B cells at a ratio of 10:1 was assessed by flow-cytometry over the course of 48 hours. **B)** Representative histograms of CD69 expression on J-CAR cells when co-cultured with Ramos cells at a ratio of 10:1. J-CAR and Ramos co-culture were stained against CD20 (2 µg/mL) and J-CAR identified as CD20-negative. Cells were stained against CD69 (2 µg/mL) **C)** Supernatant IL-2 collected at 6-, 24-, 48- and 72-hours from J-CAR cells co-cultured with Ramos B cells and quantified by ELISA. (**Panels A+C** ±SEM of 3 independent experiments (With exception of 96-P4Aζ IL-2 which is 1) and assessed with 2-way Anova with Tukey's test for multiple comparisons. Statistical significance above CD96 P4A mutation are statistical significance with respect to equivalent timepoint of wild-type CD96. ns = non-significant, ****p<0.0001)

4.4 Downstream kinase activity of the CD96 intracellular domain

Considering that the stimulatory capacity of huCD96 was mapped to the intracellular proline-rich domain of huCD96, work was carried out to further understand the overall signalling pathways and specific kinases utilised by huCD96. To visualise and understand which kinases were activated or inhibited by CD96 signalling, a peptide-based array set-up contained within disposable chips (PamChips) was utilised, whereby kinase substrates present within a porous chip are phosphorylated by active kinases within the lysate of co-cultured J-CAR cells (Figure 4.12). PamChip phosphosites consist of a wide range of known kinase targets, with each peptide target consisting of the 10-20 amino acids surrounding the site of phosphorylation. Using two distinct PamChip layouts to allow both phospho-tyrosine (PTK) or serine/threonine (STK) kinase activity to be quantified, an identical co-culture method utilised previously with Ramos B cells as a CD19 expressing target was employed to activate J-CAR T-cells. J-CAR cells expressing either CAR-ζ, CAR-96ζ, CAR-96-P3Aζ or CAR-96-P4Aζ were co-cultured with Ramos cells before kinase activity assessed using the PamGene Kinase profiling platform.

To understand the pattern of kinase activity induced by CAR signalling, immobilised peptide phosphorylation patterns were utilised to predict activated kinases using an Upstream Kinase Analysis system (UKA). Log-fold changes (LogFC) in PamChip substrate phosphorylation relative to a control sample are initially measured prior to UKA. UKA utilises the LogFC of substrate phosphorylation and known kinase-substrate relationships with a functional class scoring system to determine the predicted kinase activity within cell lysate.

Initial data-output consists of substrate phosphorylation LogFC with respect to a control CAR (ζ or 96ζ), allowing for an indication of the overall phosphorylation trend of each sample prior to UKA. Comparison against ζ allowed for the visualisation of phospho-activity above or below that of CD3ζ alone, whilst comparison against 96ζ allowed further assessment of how PRD mutations affected huCD96 signalling. To identify the significance of phosphosite activity changes between each CD96 J-CAR and either control CAR, a two-sided Student t-test was used for each test, resulting in a phosphosite LogFC value and the $-\log_{10}(p)$ significance value.

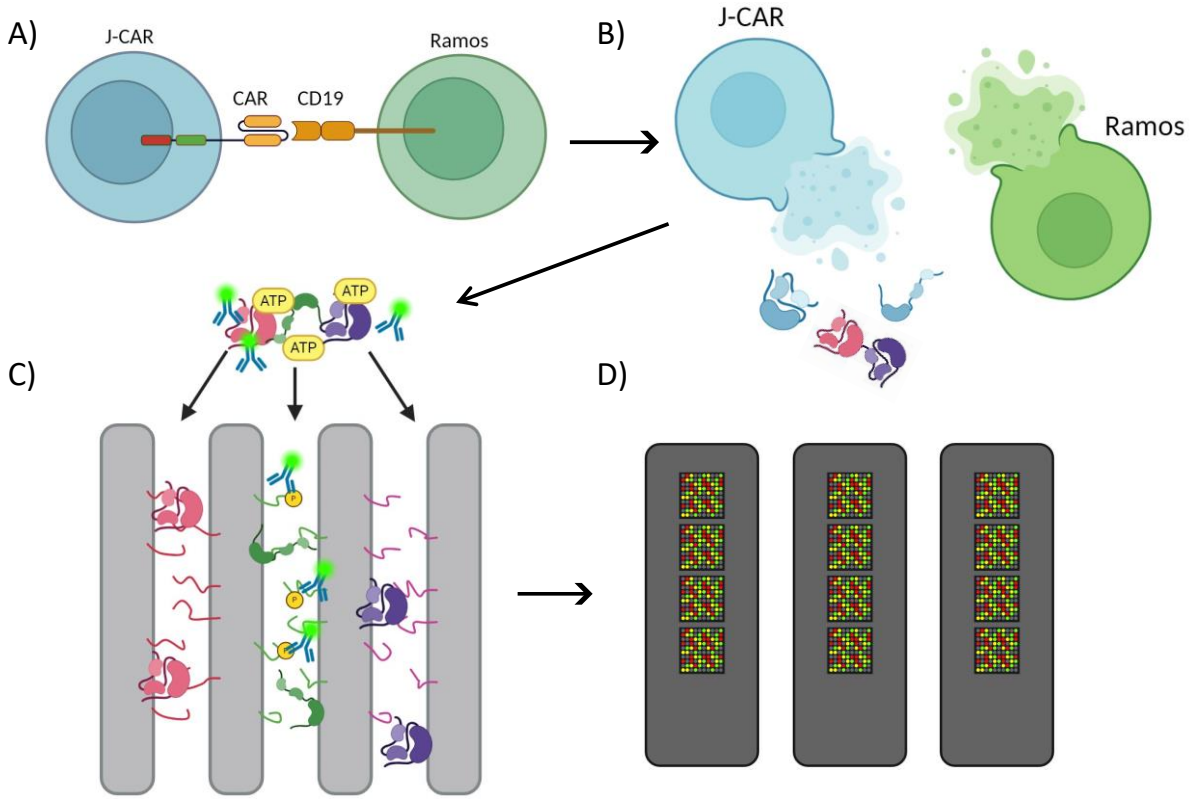

Figure 4.12 Experimental workflow for kinase analysis utilising PamChips

A) J-CAR cells were co-cultured with target Ramos cells to activate Jurkat cells through their CAR. **B)** Co-cultured cells were collected and lysed to attain kinase containing lysate. **C)** Co-culture lysate was combined with GFP labelled phopho-tyrosine or phospho-serine/threonine specific antibodies and ATP before being passed through PamChip arrays containing channels of immobilised kinase substrates. Active kinases phosphorylated substrates, while GFP-tagged anti-phospho antibody detected phosphorylation of phosphosites within each channel. **D)** Imaging of PamChip over the course of the assay allowed signal intensity to be measured over time, indicating the quantitative level of kinase activation.

4.4.1 Upstream kinase analysis scoring system

To understand the pattern of kinase activity induced by CAR signalling, immobilised peptide phosphorylation patterns were utilised to predict activated kinases using an Upstream Kinase Analysis system (UKA). UKA utilises known kinase-substrate relationships, as well as a functional class scoring system, to determine which kinases are active within our cell lysate according to the pattern of peptide phosphorylation. UKA results in a number of scoring outputs, including the Median Kinase Statistic, the Significance Score, the Specificity Score, and the Median Final Score.

The Median Kinase Statistic is a representation of the change in kinase activity with respect to a control sample. Using known kinase-substrate relationships and a class ranking system based on known kinase activity against each peptide it may act upon, changes in the activity of predicted kinases are scored. Median Kinase Statistic values larger than 0 indicate that kinase activity is greater in a test condition than in a control. A value of less than 0 indicates that the predicted kinase is more active in the control (Figure 4.13A/B). Further data processing (Significance and Specificity Score) utilises the Median Kinase Statistic to assess the significance of kinase activity changes, as well as confirming that observed changes are due to phosphorylation of specific peptides.

The Significance Score assesses the significance of a sample by rearranging sample data to generate a new Median Kinase Statistic before assessing how this differs from the original score. A high Significance Score indicates that the difference between our test and control CAR is significant and that we do not observe a similar significant difference between test and control when sample data is randomised. This permutation of data is repeated 500 times to generate a large number of test and control Median Kinases Scores (Figure 4.13C).

Similarly, the Specificity Score relies on the rearranging of peptide phosphorylation data to randomly assigned kinases and assessing whether the Median Kinase Statistic is significantly different to that achieved through each kinase's original peptide group. By assigning peptide phosphorylation values to different kinases and calculating a test Median Kinase Statistic, it is possible to evaluate whether randomized peptide phosphorylation could produce a comparable Median Kinase Statistic. A Median Kinase Statistic utilising permuted data which results in a score similar to that of the original data indicates that this score could also be achieved with randomised data and therefore has a low Specificity Score. A high Specificity Score relies on randomised data generating a Median Kinase Statistic different to that of the original, implying that the Median Kinase Statistic could only be achieved through the phosphorylation of those specific peptides (Figure 4.13D).

Finally, the *p*-value, or Median Final Score, is achieved through the sum of the Significance Score and Specificity Score. Kinases are then ranked by their Median Final Score, with kinases therefore ordered by the sum of their significance and specificity. Those scoring less than the predetermined

cutoff of 1.3 (-*log*10(0.05)) are removed, before finally being ranked according to Median Kinase Statistic, highlighting kinases that are significantly active due to specific CAR induced signalling, and in order of activity or inhibition with respect to a control.

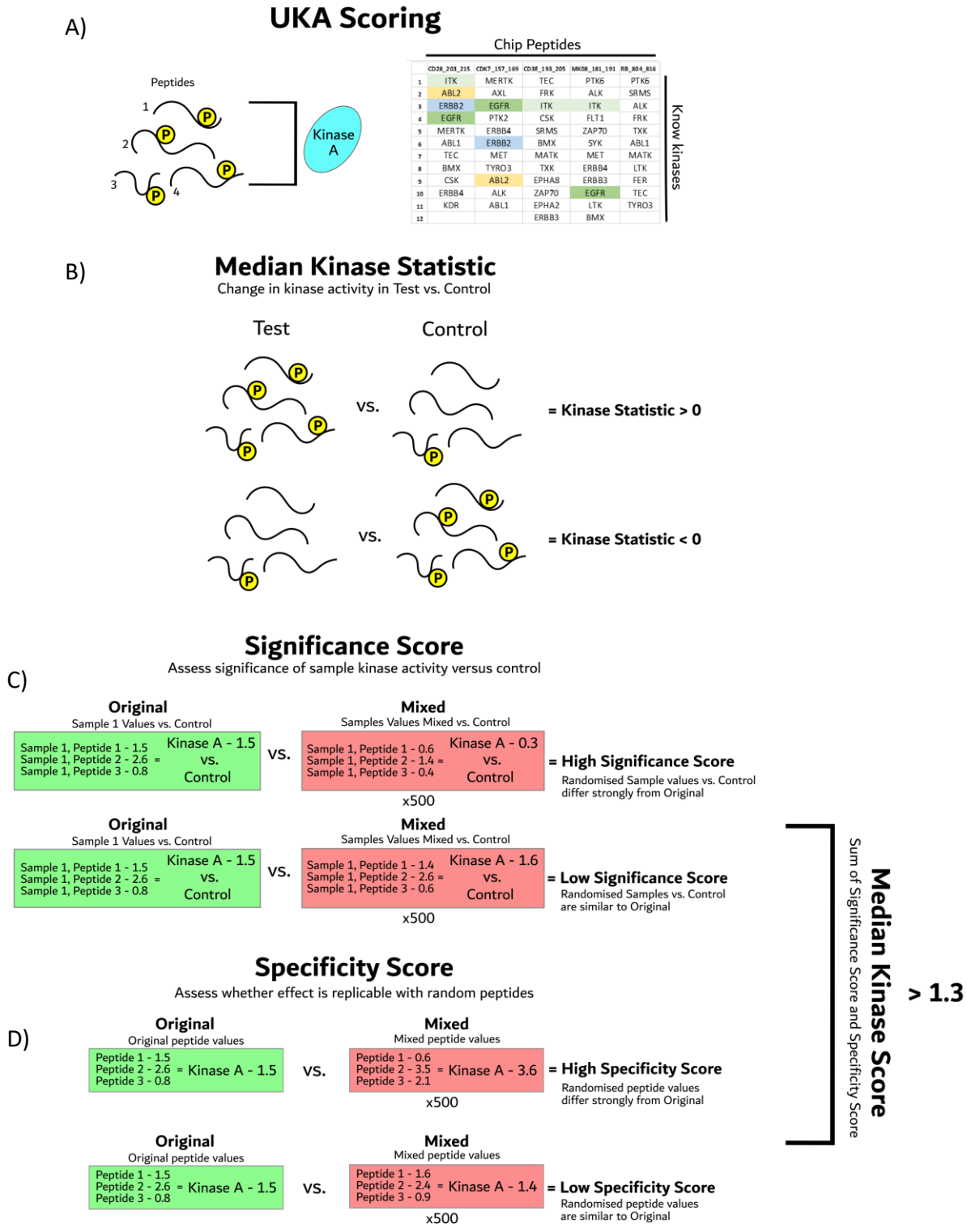

Figure 4.13 Upstream Kinase Analysis scoring systems utilised to class significance and specificity of kinase activity

A) PamGene Kinase Analysis overview. Phosphorylation of peptide substrates for individual kinases is assessed, matching peptide phosphorylation data under test conditions to known peptide-kinase

relationships. **B)** The Median Kinase Statistic was generated by assessing peptide phosphorylation and UKA of phosphorylation with respect to control activity. A Median Kinase Statistic > 0 indicates greater specific kinase activity under test conditions versus control, while a score < 0 indicates greater kinase activity under control conditions versus test. **C)** Significance Scoring assesses the significance of sample Median Kinase Statistics vs. control by randomising peptide phosphorylation values, generating new Median Kinase Statistic values and assessing how test vs. control Statistics differ. High Significance Scores result from strong differences, low Significance Scores from limited differences. **D)** Specificity Scoring assesses whether Median Kinase Statistics calculated could be achieved utilising randomised peptide phosphorylation values. High Specificity Scores result from randomised values differing to original Median Kinase Statistics, low Specificity Scores result from randomised data generating similar Median Kinase Statistic values. Median Kinase Scores are the sum of Significance and Specificity scoring, with a cutoff value of 1.3.

4.4.2 CD96 PRD mutations limit tyrosine kinase targeted substrate phosphorylation

Cell lysate from co-cultured 96ζ J-CAR increased phosphorylation of tyrosine kinases substrate targets with respect to ζ J-CAR. The phosphorylation of 36 PTK substrates was increased over ζ activity, while the phosphorylation of 33 PTK substrates was decreased with respect to ζ. LogFC of 96ζ induced phosphosite phosphorylation ranged from 0.08 (PRRX2) to 0.44 (DCX) for increased substrate phosphorylation, and -0.06 (KIT) to -0.46 (LAT) for reduced substrate phosphorylation (Figure 4.14A/D).

Cell lysate from co-cultured 96-P3Aζ J-CAR similarly increased phosphorylation of tyrosine kinase substrates. However, a total of 10 substrates phosphorylated by 96ζ lysate had no significant activity with respect to ζ lysate. Phosphorylation of the substrate RB_804_816 was reduced with respect to ζ following the introduction of a P3A mutation. Among the substrates with reduced phosphorylation, 6 showed a complete loss of activity, while phosphorylation of RBL2_99_111, where previously reduced by 96ζ, was increased (Figure 4.14B/D).

The introduction of a P4A mutation further limited phosphorylation of tyrosine kinase substrates. Of the 36 substrates with increased phosphorylation by 96ζ over ζ alone, 17 exhibited no significant phospho-activity following the introduction of a P4A mutation. Furthermore, phospho-activity of 15 substrates previously limited by 96ζ exhibited no significant difference with respect to ζ (Figure 4.14C/D).

In summary, 96ζ signalling induced strong activation of tyrosine kinases over ζ alone, as evidenced by strong phosphorylation of a large number of immobilised tyrosine kinase substrates. The introduction of sequential mutations within the PRD of 96ζ limited activity of tyrosine kinases, resulting in limiting substrate phosphorylation. Targeting of Class I, II and III PRDs with a P4A mutation limited 96ζ induced tyrosine kinase beyond that of a Class I targeting P3A mutation. Interestingly, 96ζ also acted to inhibit a proportion of tyrosine kinase mediated phosphorylation with respect to ζ.

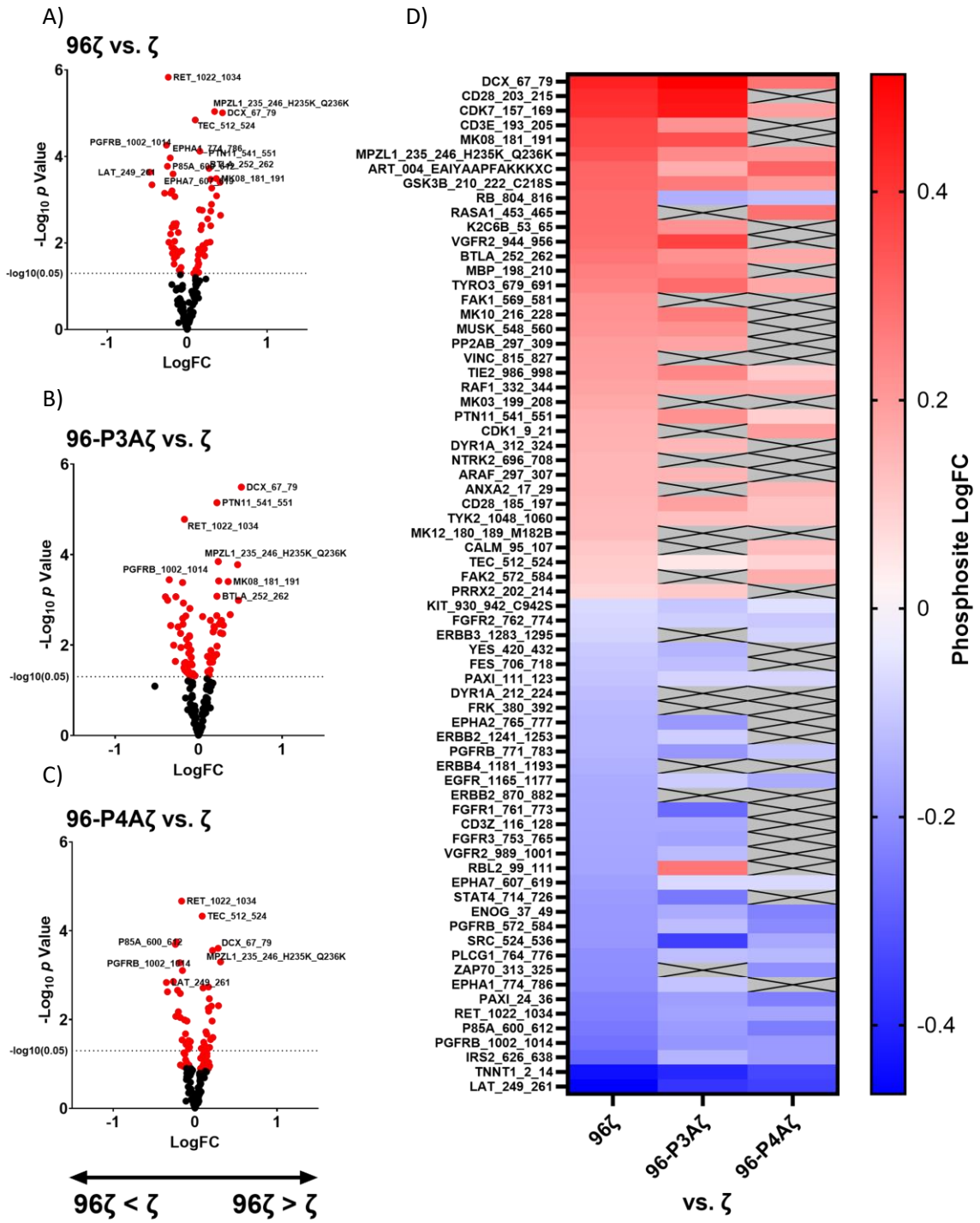

Figure 4.14 Tyrosine kinase substrate phosphorylation is inhibited by a PRD mutation of CD96

A-C) Volcano plots visualising the LogFC in PamChip phosphosite activity versus a control CAR, ζ. Named phosphosites represented the top 12 phosphosites by *p* value in 96ζ vs. ζ (Top plot) and their reduction or loss of significant activity by either P3A (B) or P4A (C) mutations of the CD96 ICD. Red datapoints represent substrates with $-\log_{10}(p)$ values greater than 1.3. Black datapoints represented substrates with $\log_{10}(p)$ values less than 1.3. **D)** Heatmap visualising all statistically significant ($-\log_{10}(p<1.3)$) tyrosine kinase mediated phosphosite changes in 96ζ, 96-P3Aζ or 96-P4Aζ vs. ζ.

4.4.3 Upstream Kinase Analysis of CD96 induced tyrosine kinase targeted peptide phosphorylation

To better understand the specific tyrosine kinases activated by 96ζ signalling in J-CAR cells, as well as assess the impact of PRD mutations on kinase activity, the peptide phosphorylation data highlighted in Figure 4.14 was utilised to assess active kinases. Using this data, UKA was carried out to interpret the pattern of substrate phosphorylation. As described in 4.4.1, UKA results in a number of scoring outputs including a median kinase statistic to report the direction of kinase activity changes, and a final kinase score to report the significance of kinase activity.

A total of 16 tyrosine kinases exhibited significantly increased activity by 96ζ J-CAR co-culture compared to a ζ control, while 24 were found to be inhibited, for a total of 41 differentially active kinases (Figure 4.15A/D). The top 10 differentially changed kinases are labelled in Figure 4.15A. Of these, MAP3K5, MAP3K8, MAP2K7, MAP2K4 and FLT4 were significantly activated by the inclusion of the huCD96 ICD, while EPHA1, BLK, HCK, LCK and ERBB3 were inhibited (Figure 4.15A/D).

Kinase activity induced by 96-P3Aζ is shown in Figure 4.15B/D. The total number of differentially active kinases induced by 96-P3Aζ signalling decreased to 31 kinases. The number of kinases with significantly increased activity reduced from 16 to 15, with the activity of only JAK3 ablated (Figure 4.15B/D). Of the 24 kinases predicted to be inhibited by CAR-96ζ signalling, the introduction of a P3A mutation resulted in a reduction to 16 kinases.

Finally, kinase activity induced by 96-P4Aζ co-culture is assessed in Figure 4.15C/D. Total tyrosine kinase activity was further reduced again, from 41 kinases to 19. Amongst these, only 9 of the 16 kinases activated by 96ζ retained their activity with respect to ζ, whilst only 10 of the initial 24 kinases inhibited by 96ζ retained significance (Figure 4.15C/D).

Overall, 96ζ is shown to mediate the activation of 16 PTK and inhibition of 24 PTK, with respect to ζ. The introduction of a P3A mutation shown previously to partially limit J-CAR activation (Figure 4.10) predominantly limited the inhibition of tyrosine kinases by 96ζ, with only JAK3 activity limited of kinases with increased activity. However, the use of a broader P4A mutation, shown to ablate 96ζ mediated J-CAR activation (Figure 4.11), resulted in the widespread loss of both activated and inhibited kinases.

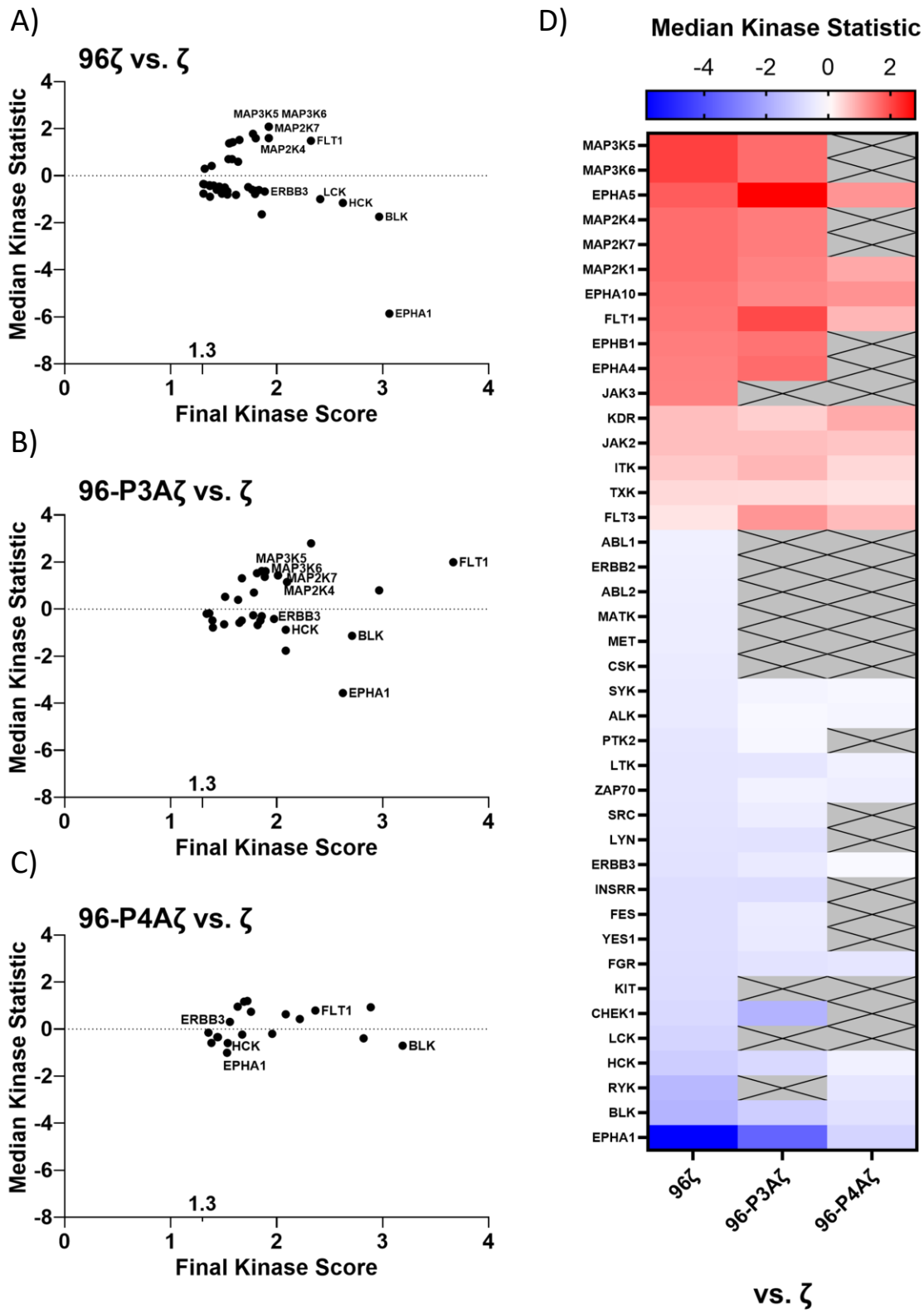

Figure 4.15 Upstream kinase analysis of 96ζ highlights progressive loss of PTK activity through PRD mutations

A-C) Upstream Kinase Analysis of J-CAR co-culture lysate utilising LogFC of substrate phosphorylation. Median Kinase Statistic with respect to ζ is plotted against Final Kinase Score, utilising a Kinase Score cutoff of 1.3. Top 10 kinases according to Final Kinase Score are labelled for 96ζ vs. ζ, with these kinases labelled for 96-P3Aζ and 96-P4Aζ vs. ζ to indicate change or loss of kinase activity. **D)** Heatmap visualising Median Kinase Scores of kinases with Final Kinase Scores greater than 1.3,

ordered by greatest increase in kinase activity over ζ to greatest decrease in kinase activity over ζ. Grey boxes indicate loss of kinase significance, with Final Kinase Scores less than 1.3.

4.4.4 CD96 PRD mutations ablate serine/threonine kinase substrate phosphorylation

As previously described for analysis of PTK-specific substrate phosphorylation, lysate from 96ζ J-CAR co-cultured with Ramos B cells was also analysed for phosphorylation of substrates targeted by serine/threonine kinases (STK). Lysate utilised for STK analysis was collected from the same J-CAR co-culture used for PTK analysis. As before, STK substrate phosphorylation was assessed as a LogFC from that of a ζ, allowing for initial analysis of total STK activity.

A total of 25 STK substrates exhibited an increased LogFC of phosphorylation by 96ζ over control ζ CAR (Figure 4.16A). Increases in STK substrate phospho-activity ranged from a 0.12 LogFC (ESR1) to 0.84 (ERBB2). Conversely, the phosphorylation of 21 STK substrates was decreased by the presence of CD96 within the CAR ICD. Decreases in STK substrate phosphorylation ranged from a -0.14 LogFC (FRAP) to -0.53 LogFC (GPSM2) (Figure 4.16A/D).

The inclusion of a P3A mutation had a substantial impact on STK mediated substrate phosphorylation (Figure 4.16B/D). The total number of substrates with increased phosphorylation over control decreased from 25 to 11, with all phosphorylated substrates exhibiting either a reduced or similar LogFC value. The inhibitory action of 96ζ on a number of substrates was also affected by the inclusion of a P3A mutation. Of the 21 STK substrates with reduced activity with respect to control, 10 retained a significant change. Interestingly, the inhibition of a small number of substrate phosphorylation was increased by a P3A mutation. Inhibition of FRAP phosphorylation with respect to control for example, increased from a LogFC of -0.14 (96ζ) to -0.21 (96-P3Aζ) (Figure 4.16A/B).

Finally, the use of a P4A mutation within the CD96 ICD severely ablated changes in STK substrate phosphorylation (Figure 4.16C/D). The total number of STK substrates with increased phosphorylation over ζ was limited to 4, with the LogFC of substrates ERBB2, PLEK and NCF1 retained regardless of a P3A or P4A mutation. Interestingly, the P3A-mediated ablation of FIBA phosphorylation is regained by a P4A mutation.

The inhibition of STK substrate phosphorylation by 96ζ was also impacted by a P4A mutation. Of the 21 substrates with reduced phospho-activity, only 3 retained significant change over ζ. Of these 3, only the PLM substrate remained significantly inhibited in both 96ζ CAR and PRD mutated derivatives. Inhibition of substrates NFKB1 and KPB1 phosphorylation was lost upon P3A mutation, however, was restored when a P4A mutation was assessed (Figure 4.16C/D).

Overall, initial analysis of STK substrate phosphorylation indicated that 96ζ signalling drove activation of a large number of serine/threonine kinases. By introducing a P3A mutation within the CD96 Class I

PRD, the increase and decrease of STK mediated phosphorylation induced by ζ was limited. By mutating four core proline residues, 96ζ STK activity with respect to CAR-ζ was almost fully ablated.

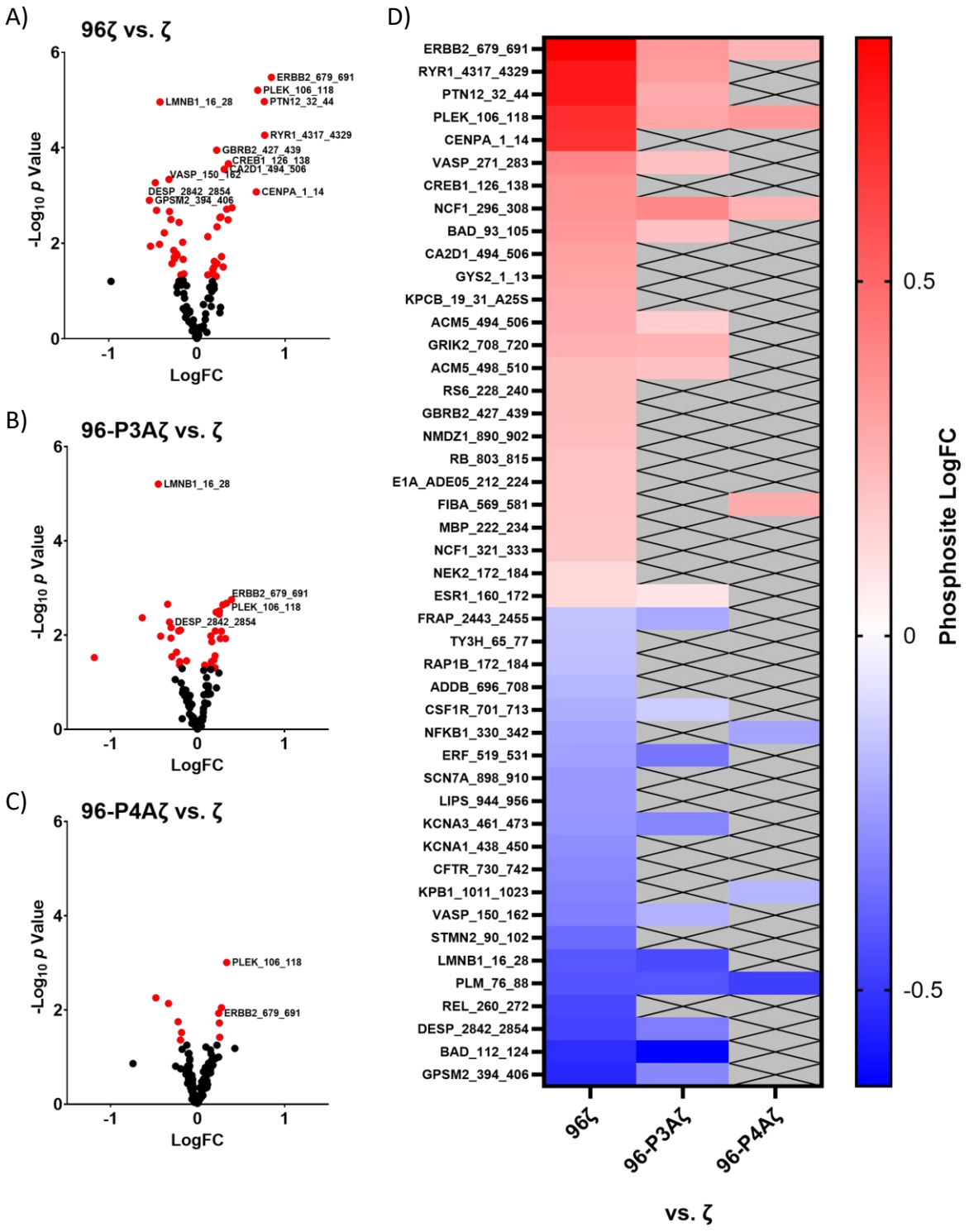

Figure 4.16 96ζ induced STK substrate phosphorylation is largely ablated by PRD mutations

A-C) Volcano plots visualising the LogFC in PamChip serine/threonine substrate phosphorylation versus control ζ. Named phosphosites represent the top 12 phosphosites by *p* value in 96ζ vs. ζ (Top plot) and their reduction or loss of significant activity by either P3A (B) or P4A (C) mutations of the CD96 ICD. Red datapoints represented substrates with $-\log_{10}(p)$ values greater than 1.3. Black datapoints represented substrates with $\log_{10}(p)$ values less than 1.3. **B)** Heatmap highlighting all statistically significant ($-\log_{10}(p<1.3)$) serine/threonine kinase mediated phosphosite changes in 96ζ, 96-P3Aζ or 96-P4Aζ vs. ζ.

4.4.5 The CD96 PRD drives activation and inhibition of key serine/threonine kinases

To determine the activation or inhibition of serine/threonine kinases, UKA was utilised using STK substrate phosphorylation data (Figure 4.16). As with UKA of PTK activity, Median Kinase Statistic and Final Kinase Scores for STK are reported and shown in Figure 4.17.

The total number of differentially active STK was increased over total active PTK. A total of 63 STK had significant differential activity over ζ. The activity of 29 STK was increased by 96ζ over ζ, whilst 34 exhibited decreased activity (Figure 4.17A/D). Top 10 kinases according to their Final Kinase Score for 96ζ are labelled in Figure 4.17A. Of these top 10 differentially active kinases, PRKCQ, COQ8A, PRKAB1, RAF1, PRKCZ and PRKCB were more active than ζ alone. The kinases CAMK2A, CAMK2D, CDK15 and CDLK1 were found to be less activate (Figure 4.17A/D).

The introduction of a P3A mutation limited the activity of a large number of kinases, with kinases activated by 96ζ preferentially affected. Of the 29 kinases activated by 96ζ, a total of 13 remained active following the introduction of a P3A mutation. 96ζ signalling limited the activity of 34 kinases with respect to ζ. Of these, the inhibition of 24 kinases was retained with a P3A mutation (Figure 4.17B/D).

Finally, the impact of a P4A mutation was assessed. The introduction of a P4A mutation had a greater impact on the activity of inhibited kinases. Only 22% (14) of differentially active kinases which were activated by 96ζ retained their activity with a P4A mutation, whilst two kinases inhibited by 96ζ gained slight increases in activity (MAPK9 and MAPK13) (Figure 4.17C/D). Of the kinases initially inhibited by 96ζ, only two retained differential activity with respect to ζ, with both retaining an inhibitory profile (RPS6KB2 and CDK15) (Figure 4.17D). Notably, the Protein Kinase C family members PRKCZ, PRKCB and PRKCQ retained 96ζ-mediated activity in both PRD mutations.

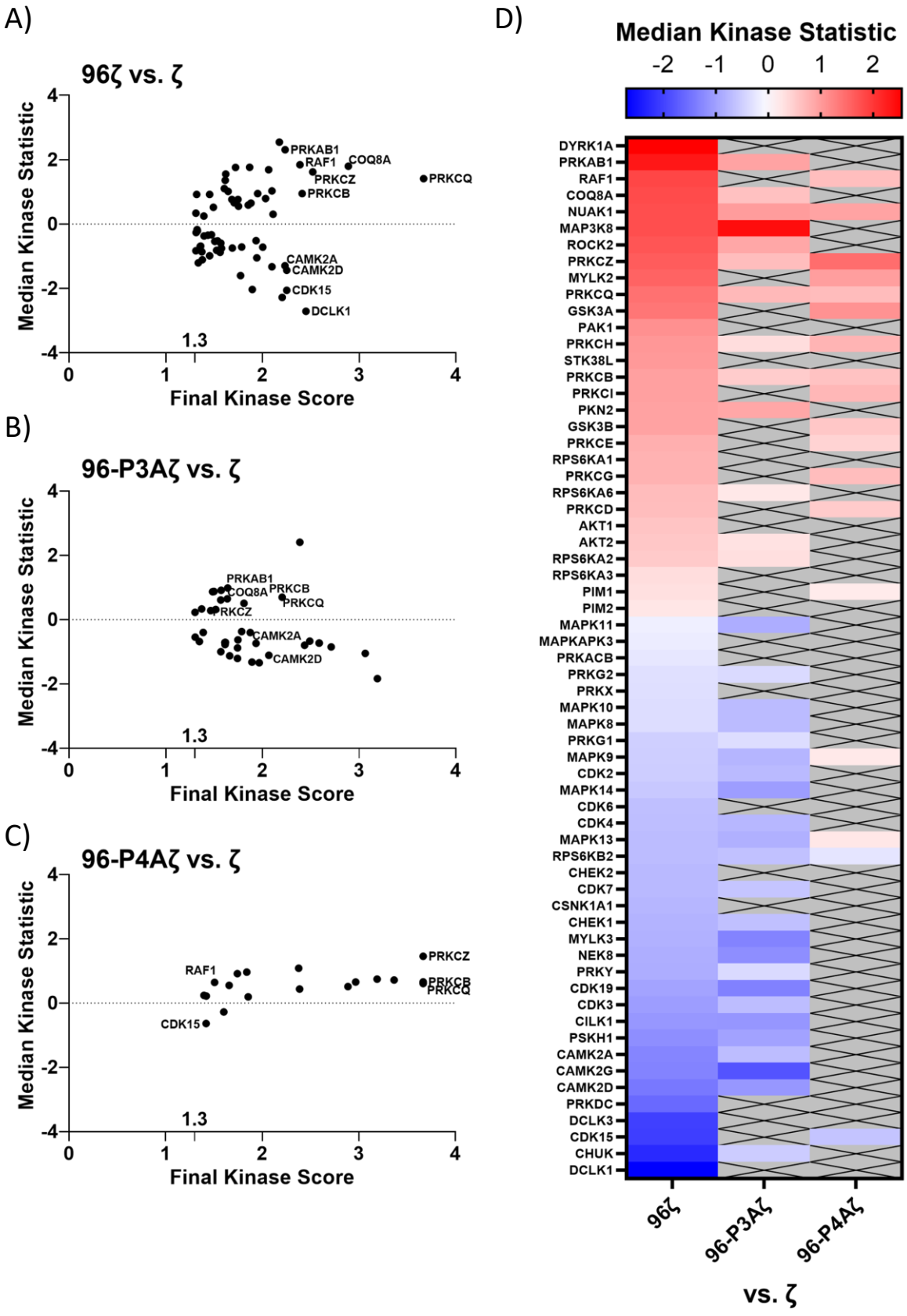

Figure 4.17 CD96 PRD mutations ablates the activity of serine/threonine kinases

A-C) Upstream Kinase Analysis of J-CAR co-culture lysate utilising LogFC of STK substrate phosphorylation. Median Kinase Statistic with respect to ζ is plotted against Final Kinase Score, utilising a Kinase Score cutoff of 1.3. Top 10 kinases according to Final Kinase Score are labelled for 96ζ vs. ζ, with these kinases labelled for 96-P3Aζ and 96-P4Aζ vs. ζ to indicate change or loss of kinase

activity. **D)** Heatmap visualising Median Kinase Scores of kinases with Final Kinase Scores greater than 1.3, ordered by greatest increase in kinase activity over ζ to greatest decrease in kinase activity over ζ. Grey boxes indicate loss of kinase significance, with Final Kinase Scores less than 1.3.

4.4.6 PRD mutations limits key tyrosine kinase activation by CD96

UKA of 96ζ activation has previously utilised ζ as a baseline to assess kinase activity. However, to further examine how PRD mutations limited 96ζ-mediated J-CAR activation, analysis was carried out utilising 96ζ as a baseline control for each mutation as opposed to ζ. This approach allows for greater understanding of how the introduction of PRD mutations impacted CD96 specific activity, rather than merely assessing how PRD mutations affect signalling with respect to ζ. The analysis utilised the same datasets as examined previously, using 96ζ as a control rather than ζ.

UKA of 96-P3Aζ activity with respect to 96ζ resulted in a total of 18 differentially changed tyrosine kinases, whilst UKA of 96-P4Aζ activity with respect to 96ζ resulted in 30 tyrosine kinases differentially activated. This data is shown in Figure 4.18A/B.

Of the 18 tyrosine kinases found to be significantly differentially activated by 96-P3Aζ with respect to 96ζ, 6 exhibited increased activity, whilst the activity of 12 was diminished (Figure 4.18A). Similarly, comparison of 96-P4Aζ with 96ζ highlighted 22 PTK exhibiting increased kinase activity, whilst the activity of 9 was reduced (Figure 4.18B). Interestingly, the overlap of tyrosine kinases with significant changes with respect to 96ζ in either 96-P4Aζ or 96-P3Aζ was minimal, with only 5 kinases present in both datasets (Figure 4.18C). Of the tyrosine kinases which exhibit reduced activity with respect to 96ζ following the introduction of a P4A mutation, many are heavily implicated in the transduction of TCR signalling including ITK, BTK, JAK3 and a number of MAPK . Whilst initial analysis of tyrosine kinase activity with respect to ζ alone highlighted that each CAR induced upregulation of ITK activity compared to ζ alone, it is only by comparing PRD mutations to 96ζ that the loss of ITK activity by PRD mutations can be visualised.

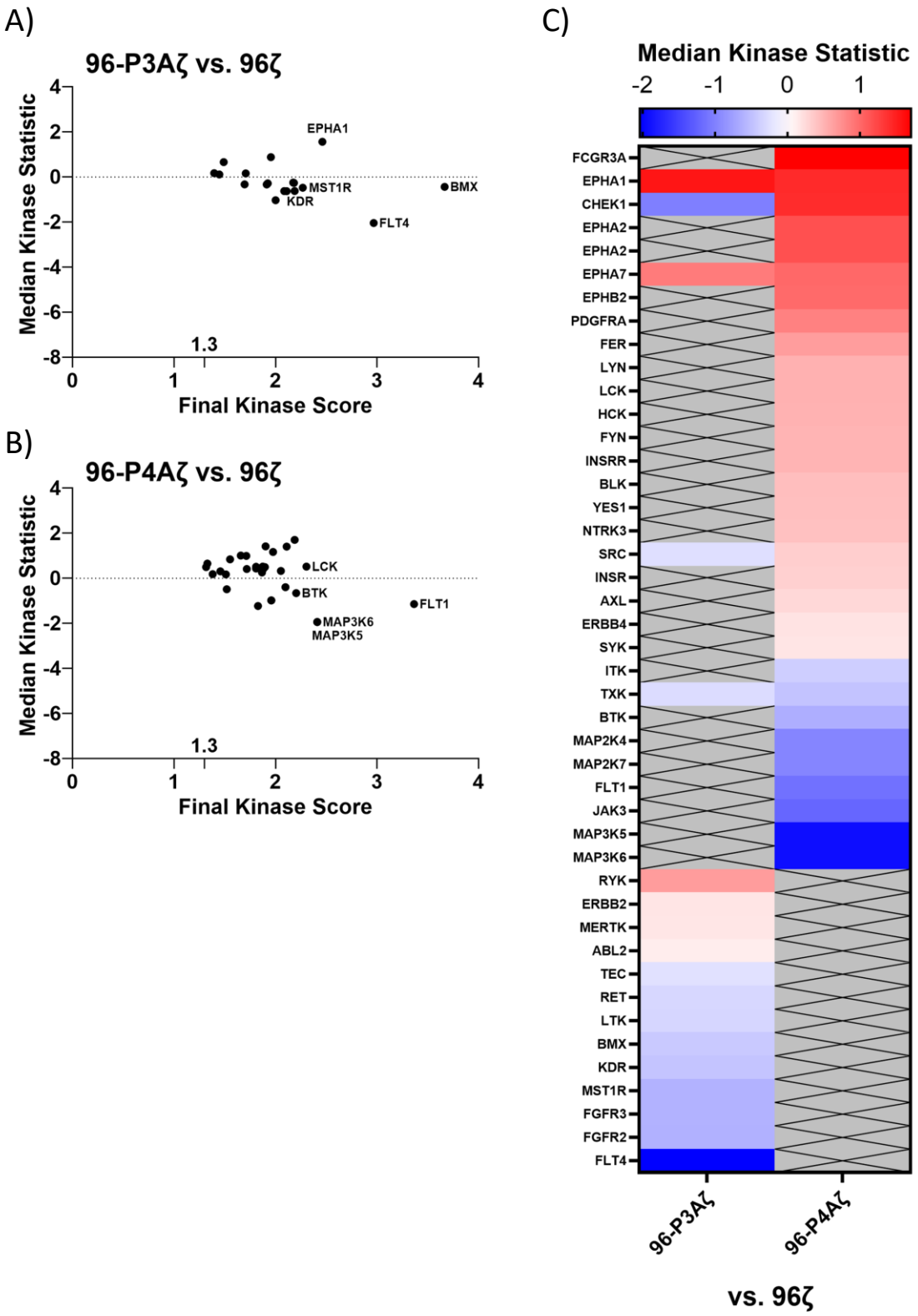

Figure 4.18 CD96 PRD mutation induced loss of tyrosine kinase activity and implicates key Src family members

A-B) Upstream Kinase Analysis of J-CAR co-culture utilising PTK substrate phosphorylation data. Median Kinase Statistic of tyrosine kinases with respect to 96ζ are shown against corresponding Final Kinase Scores, utilising a Final Kinase Score cutoff of 1.3. Top 5 kinases according to Final Kinase Score are labelled for both comparisons. **C)** Heatmap of active tyrosine kinases with Final Kinase Score greater than 1.3 with respect to 96ζ. Grey boxes indicate kinases with Final Kinase Scores less than 1.3.

4.4.7 Mutations of the CD96 PRD alters CD96-mediated serine/threonine kinases activity

To further understand the activation of serine/threonine kinases by the CD96 PRD, UKA was employed to assess STK activity induced by 96-P3Aζ and 96-P4Aζ with respect to 96ζ. As before, the same dataset utilised for comparisons against ζ was used. Changes in serine/threonine kinase activity was similar to that of tyrosine-kinase activity (Figure 4.18), with the introduction of PRD mutations resulted in widespread changes in CD96-mediated serine/threonine kinase activity.

The introduction of a P3A mutation resulted in a total of 49 serine/threonine kinases exhibiting differential activity with respect to 96ζ, while the introduction of a P4A mutation increased this to a total of 60 (Figure 4.19). Of the 60 serine/threonine kinases with differential activity induced by 96-P4Aζ, 26 were common also to 96-P3Aζ. Those serine/threonine kinases common to both datasets predominantly retained changes in activity regardless of PRD mutation. However, a number of kinases which exhibited reduced activity with a P3A mutation in fact reversed to exhibit increased activity with a P4A mutation. These included a number of cyclin-dependent kinases (CDK) such as CDK5, CDK19 and CDK9 (Figure 4.19A/B).

Of the 49 serine/threonine kinases with differential activity induced by 96-P3Aζ with respect to 96ζ, 19 exhibited increased activity, whilst 30 were reduced (Figure 4.19C). A number of serine/threonine kinases which were limited with a P3A mutation were heavily implicated in the MAPK signalling pathway, including ARAF, BRAF and RAF1, each acting upstream of MEK1/2. Each of these kinase activities was lost with a P4A mutation. Similarly, utilising 96-P3Aζ resulted in both AKT1 and AKT2 exhibiting decreased activity with respect to 96ζ, reducing further with a P4A mutation.

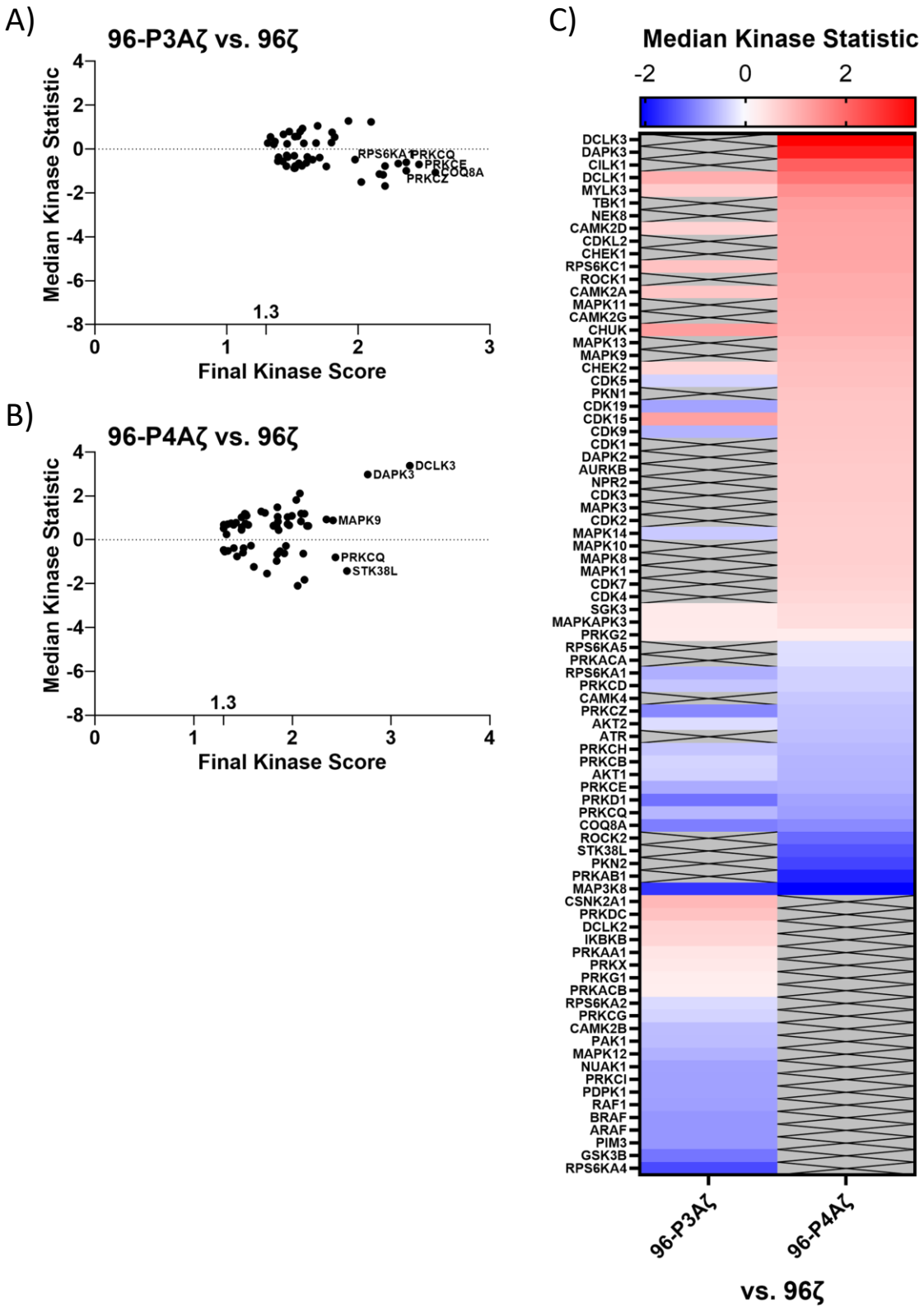

Figure 4.19 PRD mutation induced loss of serine/threonine kinase activity implicates both MAPK and PI3K/Akt pathways

A-B) Upstream Kinase Analysis of J-CAR co-culture utilising STK phosphorylation data. Median Kinase Statistic of serine/threonine kinases with respect to 96ζ are shown against their corresponding Final Kinase Scores, utilising a Kinase Score cutoff of 1.3. Top 5 kinases according to Final Kinase Score are labelled for both comparisons. **C)** Heatmap of active serine/threonine kinases with Final Kinase Score greater than 1.3 with respect to 96ζ. Grey boxes indicate kinases with Final Kinase Scores less than 1.3.

4.4.8 Proline mutations of CD96 ablate Akt phosphorylation

UKA of activated J-CAR indicated that the serine/threonine kinase AKT was activated by 96ζ and was severely limited by the introduction of either a P3A or P4A mutation. PI3K/AKT signalling acts immediately downstream of the TCR, reliant on the activity of the PDK1 (PDPK1) kinase. In UKA of J-CAR activity, PDK1 was active in 96ζ J-CAR cells however exhibited a Final Kinase Score below 1.3, indicating low confidence in the prediction of kinase activity (Data not shown). PDK1 activity in 96-P4Aζ was ablated, however again exhibited a low Final Kinase Score and was not shown.

To assess how kinase activation of J-CAR identified by UKA correlated with individual kinase activation, AKT phosphorylation was quantified by western blot. A control CD96 CAR lacking CD3ζ (96) was utilised alongside ζ as a negative control. An identical method of J-CAR activation was utilised as with PamGene analysis. J-CAR cells were cultured with target Ramos cells at a T:E ratio of 10:1, before cells were lysed and probed for phosphorylated AKT and total AKT. To normalise for variations in protein loading, gels were probed for α-Tubulin and final values normalised to this. AKT activation is presented as a ratio of phospho-Akt (pAkt) over total Akt (tAkt).

Activation of J-CAR cells expressing 96 failed to induce phosphorylation of AKT, with a pAkt/tAkt value of 0.74 (Figure 4.20A/B). In contrast, AKT phosphorylation was increased by the control CAR, ζ (pAkt/tAkt: 0.99). 96ζ augmented AKT phosphorylation over ζ, raising the pAkt/tAkt ratio to 1.14. The introduction of the P3A mutation ablated the increased AKT phosphorylation induced by both ζ and 96ζ (pAkt/tAkt: 0.69). Furthermore, the use of a P4A mutation resulted in reduced AKT phosphorylation, however, was slightly raised over P3A (pAkt/tAkt: 0.82) (Figure 4.20A+B).

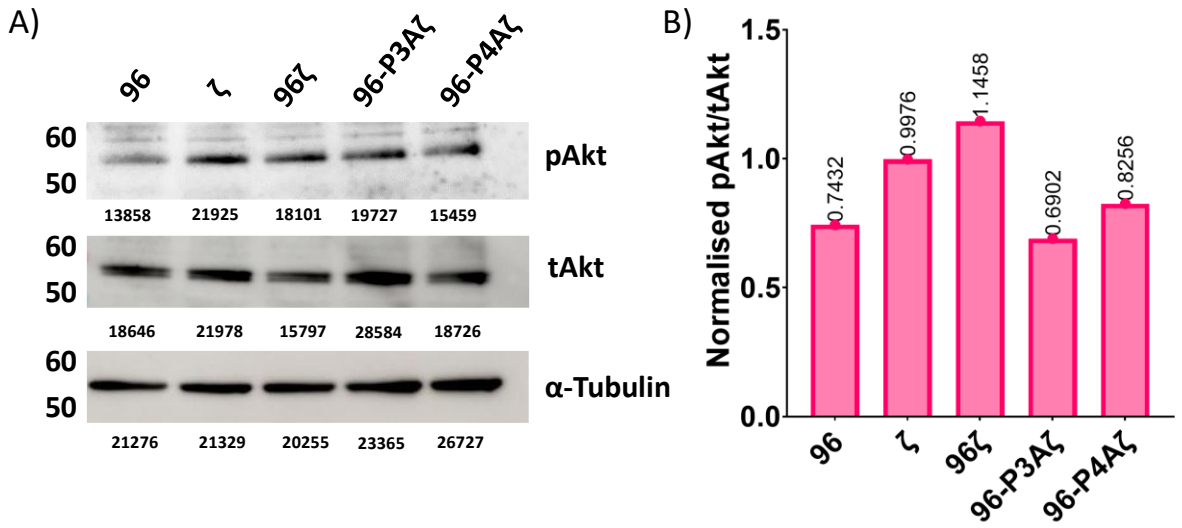

Figure 4.20 Western Blot of J-CAR lysate indicates Akt activation is mediated by CD96 PRDs

A) Western Blot staining of lysate from co-cultured J-CAR cells. From left to right, CAR containing the CD96 ICD alone (96), CD3ζ alone (ζ), CD96 and CD3ζ (96ζ), CD96 containing a P3A mutation and CD3ζ (96-P3Aζ) or a P4A mutation and CD3ζ (96-P4Aζ) were assessed. Gels were stained against phospho-Akt1/2 (Top gel), total Akt1/2 (Middle gel) and control α-Tubulin (Bottom gel). **B)** Quantification of CAR induced Akt phosphorylation, shown as phospho-Akt over total-Akt (pAkt/tAkt). Bands were quantified as AUC values utilising ImageJ and normalised to α-Tubulin to account for protein loading variation. Data shown from one experiment.

4.5 Inclusion of the CD96 ICD in primary CAR-T

Considering data presented in 4.3.1, it is suggested that the ICD of CD96 can augment the activation of T-cells. The targeting of CD96 on primary human T-cells by antibodies, as well as the inclusion of the CD96 ICD within CAR-T has provided strong evidence for the role of CD96 as a co-stimulatory molecule. Considering this data, further analysis was carried out to assess how the inclusion of the CD96 ICD within a primary T-cell expressed CAR could affect T-cell activation and induced capacity for targeted killing. Whilst the use of a 96ζ CAR in the Jurkat T-cell line has indicated that T-cells can be activated through 96ζ, cell lines intrinsically contain certain mutations that may contribute to differential activity with respect to primary human T-cells [186]. Consequently, considering the stimulatory capacity of CD96 when included within a J-CAR cell, assessing how CD96 could both activate T-cells and induce targeted cell killing compared to a clinically used 4-1BB CAR was of interest.

4.5.1 Transduction of primary CAR-T

To generate primary CAR-T cells, an identical method of lentivirus generation and T-cell transduction was utilised as with the production of CAR-T Jurkat cells (2.14). Transduction efficiency of donor T-cells was assessed 48-72 hours post-transduction. The transduction of each CAR was assessed against

non-transduced control primary T-cells. Whilst activity of CAR-96ζ was assessed against CD3ζ across three independent experiments, the 4-1BB CAR was only used in two of these comparisons.

Transduction of donor primary T-cells was overall poorer than the transduction of Jurkat T-cells. Transduction efficacy utilising a control ζ CAR was 32.6% across 3 independent experiments (Figure 4.21B/C). BBζ transduction efficacy was increased at 47.75% over 2 independent experiments. Transduction efficacy of 96ζ was also increased with respect to ζ over 3 independent experiments (37.1%). Highlighted in Figure 4.21B is the average total CAR transduction efficacy of T-cells across each construct, as well as the matched transduction efficacy for each individual experiment. Considering the range of transduction efficiency between CAR constructs, the total number of CAR+ T-cells was normalised to that of the lowest transduction efficacy with untransduced (UTR) donor T-cells to ensure total number of cells per well would remain consistent across each CAR construct.

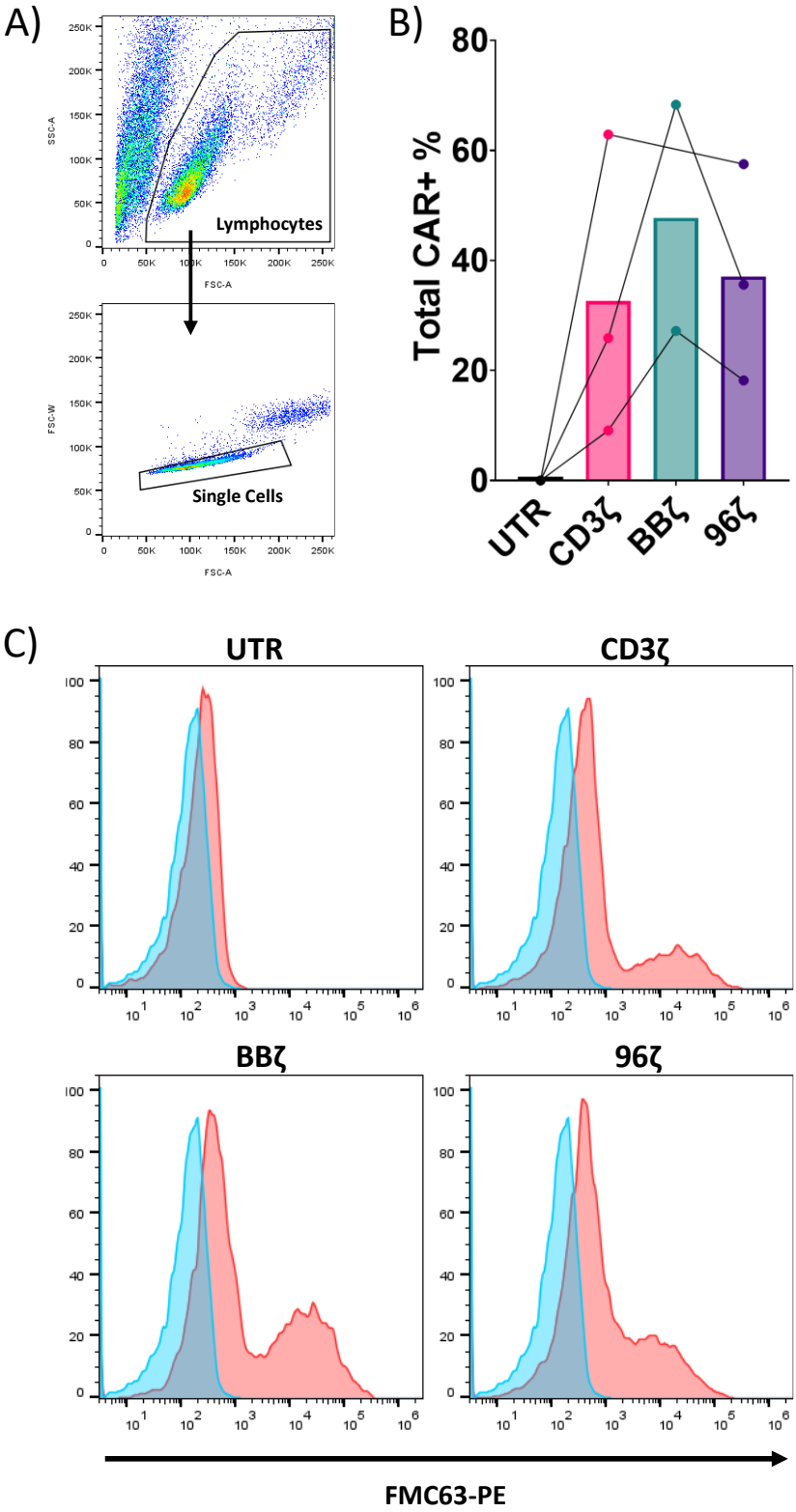

Figure 4.21 CAR transduction of donor primary T-cells

A) Gating strategy utilised for assessing the transduction of donor primary T-cells. Cells were gated on SSA-A vs. FSC-A to identify lymphocytes (Top) and FSC-W vs. FSC-A to identify single cells. **B)** Average transduction efficiency of each CAR construct across 3 independent experiments (2 experiments for BBζ). Data shown is a percentage of total cells. Data points joined represent matched independent experiments. **C)** Representative histograms of primary untransduced and CAR-T cells stained with anti-FMC63-PE (Red, 2 µg/mL) at or matched mIgG1-PE isotype control (Blue, 2 µg/mL).

4.5.2 Impact of the CD96 ICD upon primary CAR-T cell expansion

To assess the capacity of a CD96 CAR-T to induce T-cell activation, expansion of 96ζ primary CAR-T was assessed with respect to either control ζ or BBζ CAR. The percentage of CAR+ T-cells was normalised using untransduced cells to match the lowest transduction efficacy, before being co-cultured with target CD19+ Raji cells at an E:T ratio of 1:1. Total CD4+CAR+ and CD8+CAR+ cells were counted at time of seeding (0hrs) and every 24 hours up to 72 hours, with data presented as CAR+ cells per µL for both CD4+ or CD8+ T-cells. To account for minor variations in the number of CAR-T cells between constructs, data was also presented as fold change relative to each 0-hour timepoint.

The expression of CAR on UTR T-cells was lacking, therefore the total count of CD4+ CAR+ T-cells was 0 at all timepoints. ζ expressing CD4+ T-cells exhibited slow expansion between 0 and 24 hours, with expansion greatest between 24 and 48 hours, peaking at 198 CD4+CAR+ T-cells per µL at 48 hours (Figure 4.22A). Initial expansion of BBζ T-cells was reduced at 24 hours with respect to ζ, however expansion increased to peak at 48 hours with 175 CD4+CAR+ cells per µL (Figure 4.22A). Overall, expansion of 96ζ CD4+ T-cells followed a similar trend to that of ζ. 96ζ CAR+ T-cells expanded slowly between 0 hours and 24 hours, peaking at 48 hours with 160 CD4+CAR+ (Figure 4.22A).

Fold expansion of CD4+ ζ T-cells was limited within the first 24 hours of co-culture, before increasing to a peak fold increase of x4 by 48 hours (Figure 4.22B). Fold expansion of BBζ T-cells was similar to that of ζ, with a small increase by 24 hours before expanding to a peak fold increase by 48 hours of x5 (Figure 4.22B). Fold increase in CD4+ BBζ T-cells showed no statistical difference compared to CAR-ζ. Initial fold increase by 24 hours of CD4+ 96ζ T-cells was greater than both ζ or BBζ, with a x2.2-fold increase. Similarly, 96ζ exhibited the largest fold increase of each CAR, peaking at 48 hours with a x5.6-fold increase. This increase was statistically significant relative to ζ, but not to BBζ (Figure 4.22B).

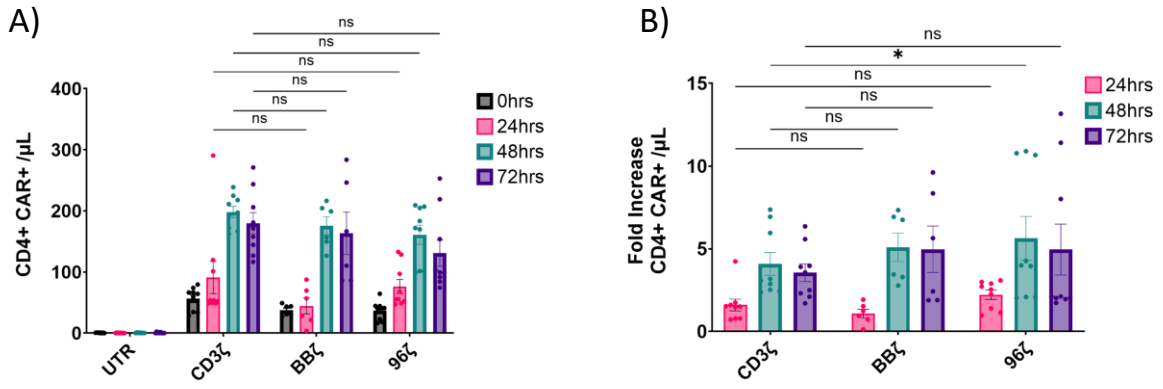

Figure 4.22 Expansion of CD4+CAR+ primary T-cells co-cultured with Raji target cells

A) Untransduced and CAR expressing primary T-cells were co-cultured with Raji B cells at an E:T ratio of 1:1. CD4+ CAR+ T-cells were counted at the time of plating utilising flow-cytometry counting beads, and every 24 hours thereafter. Data was shown as total CD4+CAR+ T-cells present per µL. **B)** Fold increase in CD4+CAR+ T-cells per µL was shown over the average number of CD4+CAR+ T-cells present at 0 hours. (Panels A+B Cell count mean ±SEM of 3 independent experiments (BBζ data was included in 2 experiments) and assessed with a mixed effects analysis with Tukey's test for multiple comparisons. ns = non-significant, *p<0.05

Alongside CD4+CAR+ T-cell expansion, CD8+CAR+ T-cell expansion was assessed. As with CD4+ T-cells, UTR CD8+ lacked CAR expression and therefore CD8+CAR+ cell counts were 0 at each timepoint. The reduced number of CD8+CAR+ T-cells across each construct compared to CD4+CAR+ T-cells is reflective of a smaller CD8+ T-cell population. Whilst the initial number of CD4+ CAR+ T-cells per µL ranged from 56 to 37 cells per µL at 0 hours, CD8+ T-cells ranged from 17 to 13 CAR+ cells per µL.

Although expansion of CD8+CAR+ ζ T-cells was limited following 24 hours of target co-culture, expansion increased substantially to peak at 79 CD8+CAR+ T-cells by 48 hours (Figure 4.23A). BBζ CD8+ T-cells failed to expand up to 24 hours. As with ζ, there was strong expansion of CD8+CAR+ BBζ T-cells between 24 and 48 hours, peaking at 48 hours with 75 CD8+CAR+ T-cells per µL (Figure 4.23A). As with both ζ and BBζ, initial expansion of 96ζ T-cells was limited up to 24 hours. Expansion drastically increased at 48 hours, peaking at 76 CD8+CAR+ T-cells per µL (Figure 4.23A). No statistically significant difference was noted in this initial expansion between either BBζ or 96ζ and the control CAR, ζ.

As with CD4+CAR+ T-cell expansion, fold-increase in CD8+CAR+ expansion was analysed (Figure 4.23B). No significant fold-increase was recorded by 24 hours of co-culture for any CAR construct. CD8+ ζ T-cells exhibited a x5.3-fold increase in CAR+ T-cells per µL between 0 and 48 hours. Similarly, CD8+ BBζ T-cells expanded x5.5-fold by 48 hours. Expansion of BBζ was not significantly different to that of ζ at any timepoint assessed. Fold increase of 96ζ was greater than both ζ and BBζ, with an average fold increase of x8.7 by 48 hours. This fold-increase expansion was significantly increased

over that of ζ and BBζ, however the range of fold-expansion between replicates was more varied with 96ζ than with either ζ or BBζ (Figure 4.23B).

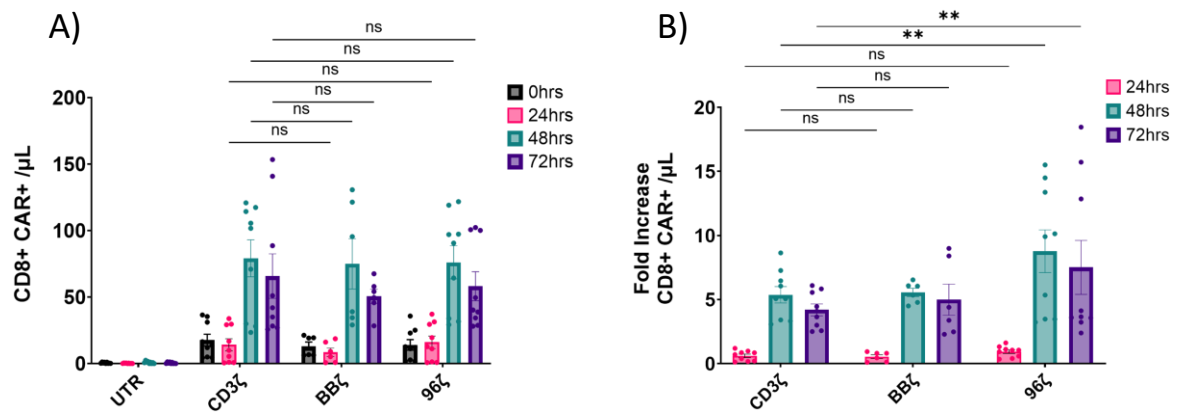

Figure 4.23 Expansion of CD8+ CAR+ primary T-cells co-cultured with Raji target cells

A) Untransduced and CAR expressing primary T-cells were co-cultured with Raji B cells at an E:T ratio of 1:1. CD8+ CAR+ T-cells were counted at the time of plating utilising flow-cytometry counting beads, and every 24 hours thereafter. Data was shown as total CD8+CAR+ T-cells present per µL. **B)** Fold increase in CD8+CAR+ T-cells per µL was shown over the average number of CD8+CAR+ T-cells present at 0 hours. (Panels A+B Cell count mean ±SEM of 3 independent experiments (BBζ data was included in 2 experiments) and assessed with a mixed effects analysis with Tukey's test for multiple comparisons. ns = non-significant, **p<0.005)

4.5.3 Cytokine secretion by primary CAR-96ζ is reduced with respect to CAR-BBζ

To assess whether activation of primary CAR T-cells could induce the secretion of IL-2 or IFN-γ cytokines in response to Raji target co-culture, supernatant collected from CAR-T expansion assays was analysed utilising ELISA.

Secretion of IL-2 by UTR primary T-cells in response to co-culture with target Raji cells was limited (Figure 4.24A). Conversely, IL-2 secretion by ζ T-cells was increased by 24 hours of co-culture, peaking at 23 pg/mL (Figure 4.24A). IL-2 release by BBζ expressing T-cells was increased compared to ζ and progressively increased over the course of the co-culture, peaking at 74 ng/mL at 72 hours (Figure 4.24A). IL-2 release by 96ζ T-cells was limited and did not differ from control ζ T-cells. As with ζ expressing T-cells, 96ζ IL-2 release peaked at 24 hours (17 ng/mL) and remained consistent throughout the course of the co-culture (Figure 4.24A). This was significantly reduced compared to BBζ, however was not significantly different from ζ.

IFN-γ release by each CAR construct was similar in trend to that of IL-2 secretion (Figure 4.24B). UTR T-cells co-cultured with target Raji cells failed to release significant IFN-γ with respect to any CAR transduced T-cells, peaking at 72 hours (2.79 ng/mL) (Figure 4.24B). Release of IFN-γ by control ζ T-cells progressively increased over the course of the co-culture assay, peaking at 72 hours (32 ng/mL) (Figure 4.24B). IFN-γ release by BBζ T-cells was significantly increased over ζ, peaking at 72 hours

with 114 pg/mL (Figure 4.24B). As with CAR-mediated release of IL-2, IFN-γ release induced by 96ζ was limited with respect to BBζ and in line with control ζ. 96ζ IFN-γ release peaked at 72 hours with 26 pg/mL (Figure 4.24B). This cytokine release exhibited no statistical difference when compared to ζ, indicating that the inclusion of the CD96 ICD within a CAR does not promote IFN-γ release to the extent that 4-1BB does.

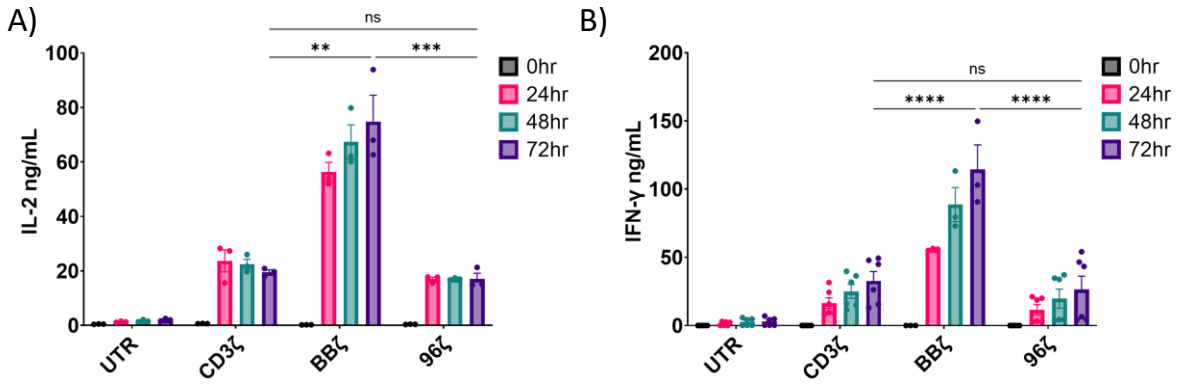

Figure 4.24 Cytokine production by primary CAR-T

A) IL-2 secretion from CAR+ primary T-cell expansion assays was quantified with ELISA. Supernatant was collected at each indicated timepoint before assessed for IL-2. (Data shown is one independent experiment +/- SEM with 2-way Anova and Tukey's test for multiple comparisons.) **B)** IFN-γ secretion from CAR+ primary T-cell expansion assays was quantified with ELISA. Supernatant was collected at each indicated timepoint before assessed for IFN-γ. Data shown is two independent experiments (BBζ data is one experiment). (+/- SEM with mixed-effects analysis and Tukey's test for multiple comparisons. ns = non-significant, **p<0.005, ***p<0.001, **** p<0.0001)

4.5.4 Killing capacity of CD96 ICD primary CAR-T

Considering evidence presented within this chapter using a primary T-cell expressed CAR containing the ICD of CD96 suggested that while the presence of CD96 does not inhibit ζ activity, it does fail to induce significant cytokine release. To evaluate the ability of primary T-cell expressed CAR utilising the ICD of CD96 to kill target cells, CAR+ T-cells were cultured with target Raji cells to quantify target cell death. CAR+ T-cells were co-cultured with Raji target cells at an E:T ratio of 1:1. GFP+ Raji B cells (Raji-GFP) were utilised to distinguish from CAR+ T-cells (Figure 4.25A). Membrane integrity of Raji B cells was assessed utilising Propidium Iodide (PI) staining of Raji-GFP at 6 and 24 hours as an indicator of CAR-mediated target cell killing (Figure 4.25B). The percentage of CAR+ T-cells was normalised to the lowest percentage CAR+ utilising UTR T-cells to ensure an equal number of T-cells used across the assay. Finally, cytokine release by CAR-T cells was evaluated to confirm CAR-T activation.

To confirm CAR+ T-cell activation cytokine release was quantified at both 6 and 24 hours. IL-2 release in response to culture with UTR T-cells was minimal (Figure 4.25C). IL-2 release by all CAR constructs was minimal at 6 hours, but significantly increased by 24 hours. As with IL-2, IFN-γ release was limited at 6 hours, increasing significantly by 24 hours in each CAR+ T-cell co-culture (Figure 4.25D).

These data mirror data presented in Figure 4.24, indicating CAR+ T-cell activation within this specific killing assay.

Having confirmed activation of CAR+ T-cells within this co-culture assay, specific killing of Raji-GFP T-cells was analysed. Non-specific killing of GFP+ target Raji cells by UTR T-cells was limited at both 6 and 24 hours (Figure 4.25E). At 6 hours, 10% of Raji-GFP target cells cultured with UTR T-cells stained positive for PI, indicating membrane integrity had been disrupted and that the cells were undergoing cell death. By 24 hours, this increased to 14% of Raji-GFP. Conversely, Raji-GFP cells co-cultured with control ζ expressing T-cells were killed at a significantly higher rate than that of UTR. By 6 hours, 18% of target Raji-GFP were undergoing cell death, increasing to 46% of Raji-GFP by 24 hours. Cell death induced by ζ co-culture was significantly increased over co-culture with UTR T-cells at both 6 and 24 hours.

Co-culture with BBζ expressing T-cells induced a similar pattern of target cell death. At 6 hours, 22% of target cells were undergoing cell death, increasing to 45% by 24 hours (Figure 4.25E). BBζ induced Raji-GFP death was significantly increased over that induced by UTR-mediated non-specific killing, however there was no significant increase in killing over ζ at either 6 or 24 hours. As with both ζ and BBζ, Raji-GFP co-culture with 96ζ T-cells resulted in significant increase in Raji-GFP cell death at both 6 and 24 hours compared to co-culture with UTR T-cells. At 6 hours, 17% of target Raji-GFP cells were undergoing cell death, increasing to 38% by 24 hours. Whilst this reduction in killing mediated by 96ζ was small, it was significant with respect to BBζ at both 6 and 24 hours, and ζ at 24 hours only.

In conclusion, the inclusion of the CD96 ICD within primary T-cell expressed CAR induced greater expansion of CD8+CAR+ T-cell than either ζ or BBζ expressing T-cells. However, release of both IL-2 and IFN-γ was not significantly increased over that of T-cells expressing ζ CAR, whilst killing of target Raji B cells similarly was limited compared to BBζ CAR-T.

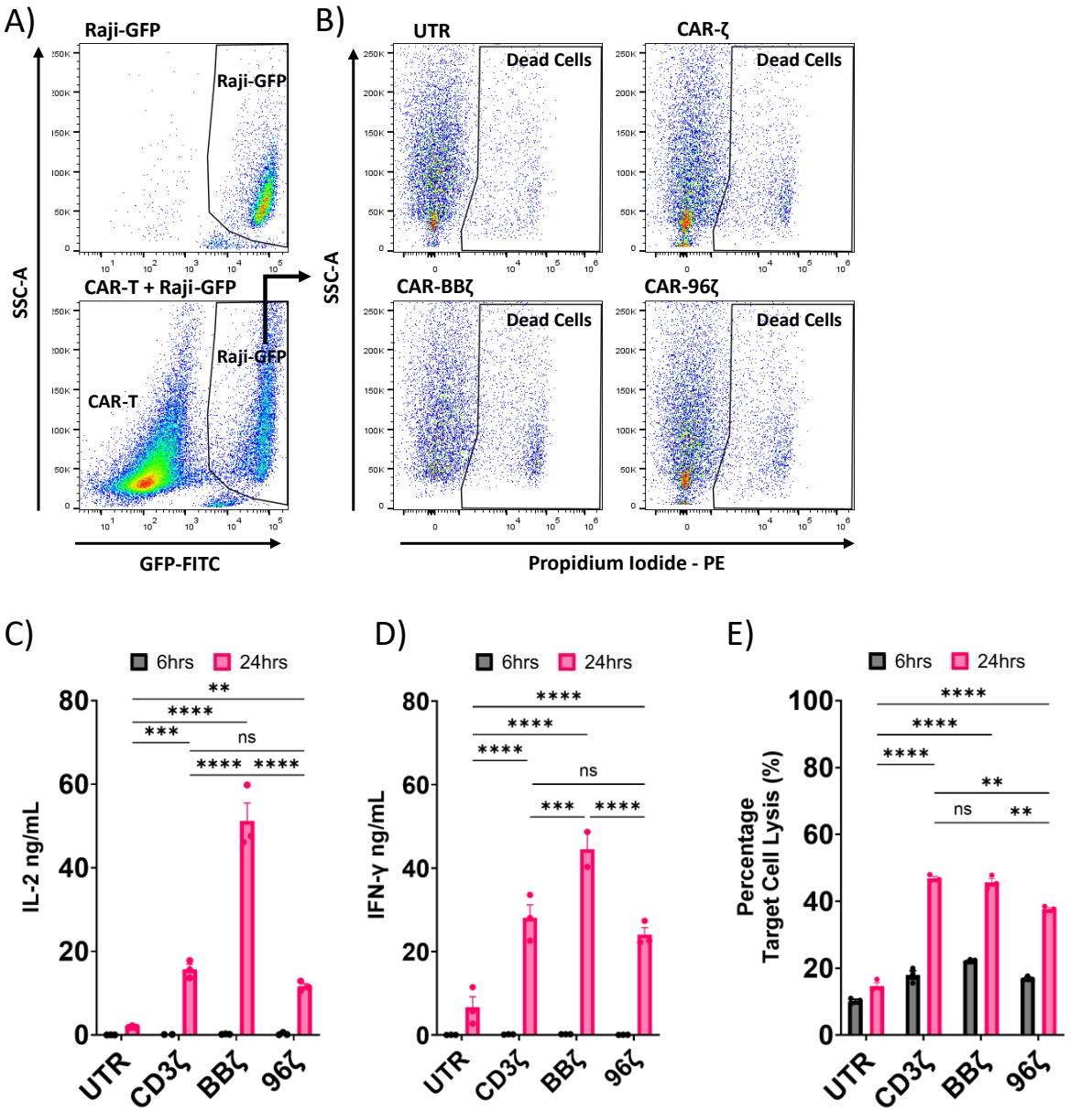

Figure 4.25 Target cell lysis by primary CAR-T cells

A) Gating strategy utilised to identify Raji-GFP cells (Top panel) in culture with either untransduced or CAR+ T-cells (Bottom panel). Cells were gated as SSC-A vs. FITC to identify GFP+ Raji. **B)** Representative PI staining of Raji-GFP cells co-cultured with either UTR, ζ, BBζ or 96ζ CAR-T cells at 6 hours. Cells were stained with propidium iodide at 0.4 µg/mL and shown as SSC-A vs. PE. **C)** ELISA quantified IL-2 release by UTR or CAR-T expressing primary T-cells co-cultured with Raji-GFP cells at an E:T ratio of 1:1 at 6 or 24 hours. **D)** ELISA quantified IFN-γ release by UTR or CAR-T expressing primary T-cells co-cultured with Raji-GFP cells at an E:T ratio of 1:1 at 6 or 24 hours. **E)** Raji-GFP killing by UTR or CAR-T expressing T-cells. Raji-GFP killing indicated by percentage of GFP+PI+ cells. (Panels C-E +/- SEM of 1 independent experiments with 3 technical triplicates and assessed with 2-way Anova with Tukey's test for multiple comparisons. ns = non-significant, **p<0.005, ***p<0.0005, ****p<0.0001)

4.6 Chapter 4 Discussion

While the data presented in Chapter 3 demonstrated that antibody-mediated targeting of huCD96 can induce T-cell activation, the underlying signalling pathways and source of CD96 signalling remain unclear. To address this, CAR-expressing Jurkat T-cells were used as a model system, enabling both CD3ζ and CD96 activation through interaction with a single extracellular ligand. Additionally, site-directed mutations in specific CD96 ICD domains were introduced to gain deeper insight into how CD96 augments CD3ζ-mediated T-cell activation.

To understand the role of the CD96 ICD in T-cell activation, 96ζ expressing J-CAR cells were co-cultured with target Ramos B-cells. The inclusion of the CD96 ICD within a CAR was found to augment T-cell activation, analogous to the impact of anti-human CD96 antibody crosslinking previously published and further detailed in Chapter 3 (Figure 4.9) [167, 169]. Whilst the inclusion of the CD96 ICD imparted greater upregulation of CD69 than that of ζ CAR, J-CAR activation was still reduced when compared against the clinically utilised BBζ CAR. However, CAR utilising the CD96 ICD as a co-stimulatory domain did in fact induce quicker and more pronounced IL-2 release than BBζ (Figure 4.9). The mechanism mediating this rapid expression of IL-2 was less clear. As a key mediator of T-cell activation, IL-2 mRNA undergoes constitutive expression and decay. Following T-cell co-stimulation with CD28, IL-2 mRNA has been shown be stabilised by the RNA-binding protein, NF90 [187, 188]. AKT activated by CD28 co-stimulation was shown by Pei et al. to colocalise within the nucleus with NF90 and mediate NF90 phosphorylation, promoting IL-2 mRNA stability and subsequent translation. Considering functional data presented within this chapter indicates a loss of IL-2 release following mutations of the CD96 PRD, as well as the loss of AKT activity, a similar method of IL-2 mRNA stabilization may be employed by CD96 (Figure 4.11, Figure 4.17).

The ICD of CD96 contains consensus sequences for a number of signalling domains common to both stimulatory and inhibitory molecules. The presence of common activating and inhibitory domains has resulted in a lack of agreement for the role of CD96 in human T-cell activation. The presence of an ITIM consensus sequence, coupled with the inhibitory action of CD96 described by Chan et al. in their work with NK cells, would suggest that given the correct cues or environment, CD96 can function to inhibit immune cell activity [154]. Within the data presented by Chan et al., NK cell expressed CD96 was found to limit release of IFN-γ and NK-cell mediated tumour control, directly opposing the stimulatory role of NK-cell expressed CD226. Conversely, human CD96 also contains a YxxM consensus sequence, pivotal for CD28-mediated T-cell activation [189]. However, mutations introduced into either of these domains failed to significantly alter the activity of CD96 in the context of CAR-mediated T-cell activation (Figure 4.10). In the initial mutational design, only by mutating the Class I PRD with a P3A mutation did CD69 upregulation significantly reduce from that of 96ζ at each time

point. IL-2 release however was unaffected by either YxxM or P3A mutations. Mutation of the ITIM consensus sequence reduced IL-2 release at 24 and 48 hours.

The disparity between limiting CD69 upregulation through a Class I PRD mutation, and the lack of significant change in IL-2 release suggests these two T-cell responses are mediated through different signalling domains. To account for this, a broader PRD mutation was designed, encompassing two core PxxP domains to target PRDI, PRDII and PRDIII. Utilising a broader PRD mutation, upregulation of CD69 and IL-2 release was ablated (Figure 4.11), limiting J-CAR activation to more closely resemble ζ induced activity. This data suggests that the stimulatory action of CD96 when in the context of T-cell expressed CAR is mediated through the PRD as a whole.

Teyra et al. describe a wide number of SH3 domain interactions with PRDs, covering Class I, II and III PRDs, each of which is present with CD96 [158]. Whilst their analysis was not exhaustive, they did indicate that a number of Src family kinases show specificity for the proline-rich consensus sequences present within the CD96 ICD. Binding of the LCK kinase is predicted to interact with both Class I and Class II PRDs through its SH3 domain. LCK activity was found to be limited by 96ζ J-CAR, however this limitation was ablated with either P3A or P4A mutations (Figure 4.15). Both the ITK and LCK kinases have been shown previously to interact with the PRD of the T-cell specific adapter protein (TSAD) [190]. In this context, Anderson et al. proposed that the consensus sequence for ITK SH3 domain binding of TSAD is *x***P***x***P***xx***R/K***, correlating with the CD96 PRD, P**P**P**P**PI**K** (Figure 4.26A). This consensus sequence has also been shown to be present as a binding site within the CD28 ICD for the SH3 domain of ITK [191]. ITK and LCK binding of the TSAD PRD through their SH3 domains was hypothesised to result in phosphorylation of local tyrosine residues, allowing further binding of kinase SH2 domains. Considering the same PRD consensus sequences is found within the CD96 ICD, it is plausible a similar system is utilised by CD96. Whilst ITK activity was not ablated by mutations of the PRD when tyrosine kinase activity was compared to ζ signalling (Figure 4.15), activity was significantly diminished by the introduction of a P4A mutation when compared to 96ζ (Figure 4.18). A caveat to this hypothesis is the intrinsic loss of the phosphatase PTEN in the Jurkat cell line [186]. PTEN mediates the dephosphorylation of cell membrane bound PIP_3 to PIP_2, opposing PI3K activity and limiting the membrane recruitment of kinases through their pleckstrin homology (PH) domains. Whilst ITK is found predominantly as a cytosolic protein within primary T-cells, ITK is largely localised to the cell membrane in the Jurkat T-cell line due to constitutive PIP_3 recruitment of ITK. The impact of PTEN loss was apparent in western blot analysis of AKT phosphorylation, with J-CAR expressing a 96 CAR exhibiting enhanced AKT phosphorylation in the absence of a ζ ICD. This accumulation of ITK to the cell membrane may inflate the apparent contribution of ITK to 96ζ-mediated J-CAR activation, skewing analysis of ITK activity.

Inhibition of ITK within J-CAR T-cells was attempted utilising the small-molecule inhibitor, Ibrutinib [192]. However, this resulted in complete inhibition of T-cell activation due to the intrinsic role of ITK in CD3ζ signalling (Data not shown). Considering the implication of ITK in CD96 signalling highlighted within this data, further investigation of its activity and role would be beneficial.

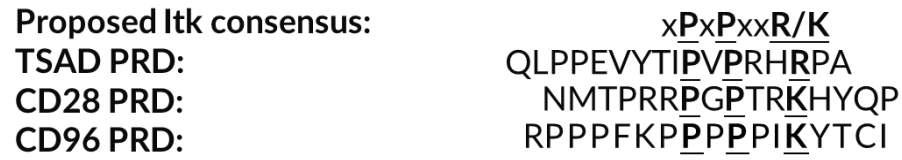

Figure 4.26 Alignment of TSAD, CD28 and CD96 indicates an Itk consensus sequence

A) Amino acid alignment of the PRD present within the T-cell specific Adapter Protein, CD28 and CD96. Underlined and in bold are the amino acids defined in literature to be the consensus sequence for binding of the ITK SH3 domain to each PRD. Proposed consensus sequence is adapted from Anderson et al.

Interestingly, differences in loss of AKT activity were found between P3A and P4A mutations of the PRD. Whilst activation of both AKT1 and AKT2 is increased by 96ζ, AKT1 activity was ablated by both P3A and P4A mutations, while AKT2 was only limited by a P4A mutation (Figure 4.17). This further suggests that that the different PRD classes within the CD96 ICD contribute to T-cell activation in distinctly different ways.

Both AKT1 and AKT2 are key for sustained response of CD8+ T-cells to antigen, driving T-cell effector function in response to PI3K signalling [193, 194]. PI3K has been shown to recognise YxxM motifs through a p85 subunit. An analogous example of this is contained within the CD28 YxxM domain, YMNM, which interacts with both PI3K and the scaffold protein Grb2, although binding of Grb2 is shown to be also reliant on the presence of the Asparagine residue [185]. Considering AKT activity was limited by PRD mutations within CD96, it is plausible that activity of the CD96 PRD also involves kinase activity mediated through the YxxM motif. Whilst mutating the YxxM domain of CD96 failed to result in a significant reduction in CD69 or IL-2 upregulation, it may in fact act in a dispensable manner downstream of the PRD to augment T-cell activity. One hypothesis is that the CD96 YxxM is acted upon by kinases recruited by the PRD, giving explanation to the fact that only by mutating the PRD was CD96 activity limited (Figure 4.11). Phosphorylation of the tyrosine residue contained within the YxxM motif by kinases recruited to the PRD may allow binding of PI3K and downstream activity of AKT. This kinase recruitment to the PRD may be the dominant method of CD96 mediated signalling and be capable of AKT activation independent of YxxM.

Previous literature has identified that members of the MAPK family are activated following the antibody-mediated cross-linking of CD3 and CD96 on CD8+ human T-cells, with activation of both MEK and ERK proposed as downstream mediators of CD96 T-cell activation [167]. Considering this, focus was drawn to members of this signalling pathway in an attempt to understand the signalling cascade

induced by CD96. A large number of intermediary kinases were found to be activated, each with diverse functions. Key among these were members of the MAPK signalling pathway. These include the serine/threonine kinases RAF-1, ARAF and BRAF (Figure 4.17). These three kinases each act directly upstream of MEK1/2 and ERK and can themselves be activated through ITK phosphorylation of PLCγ1. T-cell activation through 96ζ was found to increase RAF-1 activity with respect to a ζ control (Figure 4.17), whilst RAF-1, ARAF and BRAF all exhibited decreased activity following PRD mutations (Figure 4.19).

PAK1 represents a serine/threonine kinase with increased activation following 96ζ mediated T-cell activation, which is ablated with either PRD mutation (Figure 4.17). Intrinsically involved in TCR signalling and subsequent cytoskeletal cell remodelling, PAK1 is reliant on CD3ζ associated ZAP-70 and LCK [195]. Downstream, PAK1 can mediate the activation of MEK1/2 and subsequently, ERK, through direct activation of MAP3K8 [196]. Within the analysis of kinase activity, MAP3K8 was found to be highly activated with respect to ζ, yet both PRD mutations inhibited activity with respect to the 96ζ (Figure 4.19). Taken together with the pattern of PAK1 activity, MAP3K8 may be a downstream mediator of CD96 signalling through PAK1 which results in enhanced activation of MEK1/2 and ERK [196, 197]. A proposed model detailing the hypothesised signalling cascade of 96ζ CAR is detailed in Figure 4.27A, utilising kinases shown to be activated by 96ζ mediated J-CAR activation. Kinases indicated in green were shown specifically to be activated by 96ζ and either inhibited or lost significance with respect to ζ following a PRD mutation.

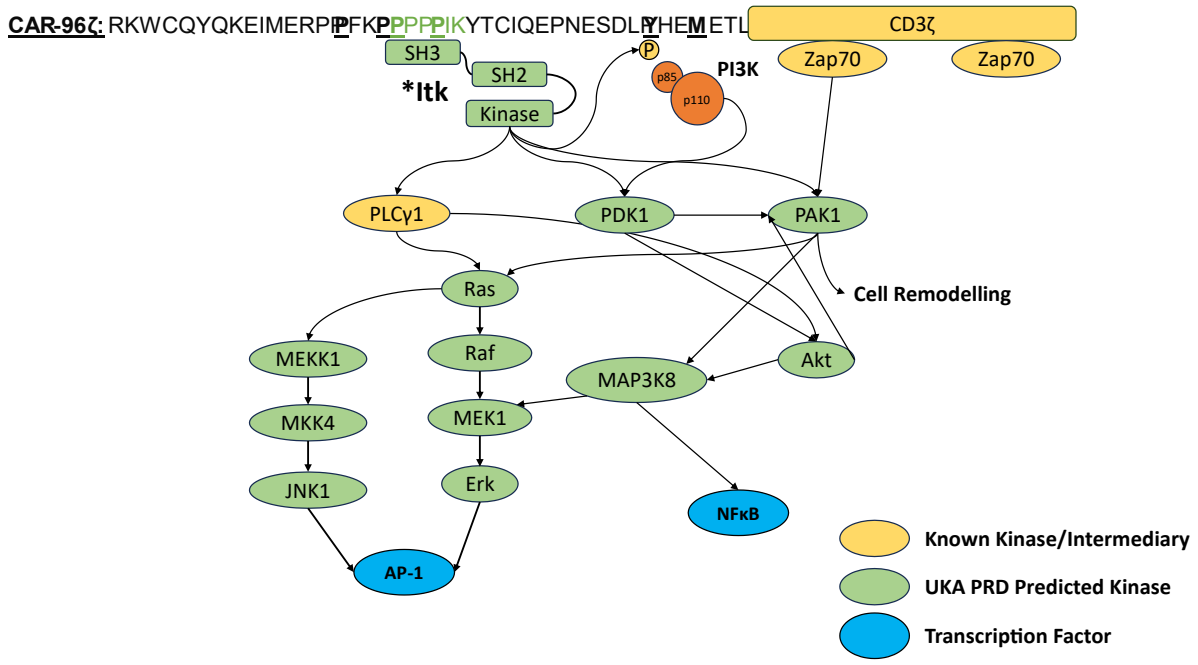

Figure 4.27 Proposed signalling pathway of CD96 in the context of CAR-T utilising UKA data

A) Schematic overview of the predicted signalling pathway of 96ζ. ITK interacts with the 96ζ PRD through its SH2 domain, mediating potential phosphorylation of the adjacent YxxM motif and recruitment of PI3K. ITK may act directly on PLCγ1, PDK1 and PAK1, whilst PI3K can directly phosphorylate PDK1. Downstream, both PLCγ1 and PDK1 may act to phosphorylate AKT, ultimately

activating MAP3K8 and NFκB. Both PAK1 and PLCγ1 can mediate activation of RAS, resulting in RAF and MEK/ERK activation, as well as MEKK1, MKK4 and JNK1. Both of these signalling pathways can result in the formation of the AP-1 transcription factor complex, facilitating nuclear localisation and T-cell activation. Kinases labelled in green are predicted to be upregulated by 96ζ signalling and inhibited by PRD mutations. Kinases listed are not exhaustive of kinases with differential activity. Not all kinase interactions are shown for simplicity. Blue icons indicate transcription factors which act downstream of noted kinases. * = ITK accumulation at Jurkat cell surface may skew interpretation of ITK as the primary mediator of CD96 PRD activity.

Considering evidence presented for CD96 as a co-stimulatory molecule utilised CAR-T as a model system, the final focus was on how the inclusion of the CD96 ICD in primary human T-cell CARs would compare to that of the clinically used 4-1BB CAR. Primary CAR-T utilising 96ζ was compared against either UTR T-cells, or primary T-cells utilising either ζ or BBζ CAR. The capacity of these CARs to induce T-cell expansion, as well as their production of key cytokines and ability to kill target cells was assessed.

In vivo expansion of CAR-T cells in response to target is associated with positive clinical responses, and the ability of CAR-T cells to expand is determinant in their capacity to control disease. For CAR-T therapy to achieve a positive clinical outcome, CAR-T cells must sufficiently expand in response to target [198]. To initially assess the capacity of CAR-T cells to respond to target, expansion was quantified over 72 hours of target co-culture (Figure 4.22, Figure 4.23).

Fold increase of CD4+CAR+ T-cells was augmented by the presence of either the 4-1BB or CD96 ICD, however a significant advantage over ζ was only achieved by 96ζ at 48 hours. Fold increase of CD8+ CAR+ T-cells was however increased by the inclusion of the CD96 ICD with respect to both a BBζ or ζ CAR at both 48 and 72 hours. This subtle but distinct difference between expansion of CD4+ and CD8+ T-cells may suggest that the functional capacity of CD96 is more prominent in CD8+ T-cells. Considering that analysis of the CD96 ICD has been carried out predominantly in the CD8+ Jurkat cell line, further characterisation of CD96 utilising CD4+ T-cells may be beneficial to identify any cell-subtype differences in CD96 activity. Overall, differences in initial CD4+ or CD8+ T-cell expansion in response to target was minimal between each CAR suggesting that the inclusion of 4-1BB does not promote initial T-cell proliferation beyond that of CD3ζ and that CD96 does not inhibit initial T-cell activation.

Tonic signalling within T-cells occurs due to the constant low-quality engagement of TCR with self-peptides. Whilst this engagement is not sufficient to activate T-cells, it does drive cell homeostasis and survival [199]. This ligand-independent tonic signalling also occurs in CAR-T cells, often driven by aggregation of CAR [200, 201]. This tonic signalling in CAR-T cells is attributed to be a cause of cell exhaustion, limiting anti-tumour responses and restraining the therapeutic efficacy of CAR-T treatment. The use of the 4-1BB ICD within CARs has been shown to result in continuous TRAF2-

mediated NFκB activation [183]. Whilst not directly within the scope of this study, data presented here may give an indication as to the effect of the CD96 ICD on CAR-T tonic signalling. When assessing basal background expression of CD69 for Jurkats expressing CAR, two CAR designs which utilised the intracellular domain of 4-1BB (AT-171-2 & BBζ) both exhibited the highest level of surface CD69 on non-activated cells, whilst CAR either lacking an ICD or which utilised CD3ζ with or without CD96 showed comparatively reduced CD69 expression (Figure 4.8). Whilst other factors also contribute to T-cell tonic signalling, considering the impact of CD96 on T-cell fitness and whether its inclusion may reduce tonic-signal induced exhaustion would be beneficial.

Clearer differences could be attributed to the inclusion of specific ICDs when assessing primary CAR-T release of both IL-2 and IFN-γ. CAR utilising the 4-1BB ICD were much more active in their release of pro-inflammatory cytokines at each timepoint quantified, however as with the measurement of T-cell expansion, the inclusion of the CD96 ICD did not act to inhibit ζ mediated release of either IL-2 or IFN-γ. Both of these cytokines are found to be elevated in the systemic inflammatory response that can occur following CAR-T therapy. CRS is characterised by the sudden and widespread release of cytokines such as IL-2, IL-6 and IFN-γ from both infused CAR-T cells, as well as from activated bystander cells. Whilst the use of the 4-1BB ICD is thought to limit CRS due to reduced expansion, risk of CRS is still prominent [202]. This lack of strong pro-inflammatory cytokine release, coupled with comparable initial proliferation of CAR+ T-cells, may indicate that CD96 would be a beneficial alternative to 4-1BB as an ICD of choice with CAR-T.

Finally, the primary function of CAR-T therapy focusses on their capacity to kill target cells. Upon recognition of a ligand in an MHC-independent manner, CAR-T utilises multiple mechanisms of killing, including the release of perforin and granzymes [203]. Co-culture of primary CAR-T utilising the CD96 ICD in fact reduced cytotoxicity with respect to CD3ζ (Figure 4.25).

To better understand the long-term implications of utilising CD96 as an ICD for CAR-T, further analysis of T-cell response to repeated antigen exposure would be beneficial. Dobrin et al. describe a method of repeated target exposure, enabling the authors to assess how T-cell fitness and cytolytic capacity is maintained over longer periods. Utilising a similar methodology to compare the CD96 and 4-1BB ICDs may better allow for differences between the two to become clearer [204]. Similarly, there are a multitude of other indicators of T-cell function which would have been beneficial to assess in characterising our CAR-T. Upregulation of the IL-2 receptor alpha chain (CD25) is common to activated T-cells and may have been beneficial to quantify. Similarly, CD107a expression can be utilised as an indicator of T-cell degranulation and would give a greater indication of the specific T-cell cytotoxic capacity following CAR-T engagement [205].

Overall, data presented within this chapter has shown that activating signals mediated through CD96 are reliant on the intracellular PRD in the context of a CAR, and that the ITIM and YxxM motifs are

largely dispensable. The signalling cascade induced by CD96 predominantly utilises serine/threonine kinases which are limited by the mutation of the CD96 PRD. Finally, the inclusion of a CD96 ICD within a primary CAR-T does not act to significantly inhibit CAR-mediated T-cell activation, in fact augmenting the proliferation of CD8+CAR+ T-cells. Considering the stimulatory function of CD96 described both within this chapter and the previous, understanding how CD96 functions interacting with its cognate ligand, CD155, is of interest. Considering that CD96 competes for binding with both TIGIT and CD226, understanding how this may affect T-cell activation was investigated.

Chapter 5 The role of CD96 in primary human T-cell activation

5.1 T-cell activation utilising bacterial superantigens

In both this thesis and previous literature, cross-linking of CD96 targeting antibodies has been shown to augment the activation and proliferation of human T-cells. Similarly, it has been shown here that augmenting human T-cell activation utilising a huCD96-incorporating CAR is reliant on the presence of the PRD within the huCD96 ICD. However, no conclusive evidence has been presented to show that the interaction of huCD96 with its cognate receptor, huCD155, can also mediate T-cell activation. Antibody blockade of mCD96 on CD8+ T-cells is found to limit antigen-specific T-cell responses, however this work was carried out in mice and failed to take into account the potential redirection of CD155 to either TIGIT or CD226 as a result of blocking CD96 [167]. This effort to better understand the role of huCD96 is complicated by its competition for receptor binding with both TIGIT and CD226. To better understand how huCD96 may mediate T-cell activation, an experimental system was designed to utilise a recombinant antigen in place of an anti-CD3 antibody. In this proposed system, a recombinant antigen can be loaded onto CD155 expressing APC, providing physiological TCR activation. This model has previously been utilised with both TIGIT or CD226 expressing Jurkat T-cells, whereby CD155 expressing Raji B-cells were used to present the *Staphylococcal* Enterotoxin E (SEE) [89, 206]. This model provides an antigen:TCR interaction to induce initial Signal 1 TCR-mediated T-cell activation, whilst the provision of APC-expressed CD155 allows for the investigation of how CD96 may augment TCR activation.

Staphylococcal enterotoxin superantigens (sAgs) encompass a class of bacterial peptides with specificity for MHCII, however do not require the uptake and intracellular processing typically associated with exogenous antigens, instead directly binding surface MHC. This can result in widespread activation of T-cells and result in both toxic shock syndrome (TSS) and CRS. sAgs act to bind the Vβ domain of the TCR, enabling the activation of T-cells independent of antigen-specificity, with SEE found to have preference for the binding of Vβ8 TCR, as well as HLA-DR [207-210]. To enable the activation of human T-cells utilising SEE as Signal 1, Raji or Raji-CD155 target cells were peptide-loaded with recombinant SEE (rSEE) prior to being co-cultured with isolated primary T-cells. T-cell activation was then assessed by measuring their proliferation and cytokine release.

5.1.1 Confirmation of HLA-DR expression on Raji B-cells

Previous work has determined that the sAg SEE has strong specificity for MHC-II HLA-DR [207, 208]. To confirm that both Raji and Raji-CD155 B-cells express this class of MHCII, cells were stained for

expression of HLA-DR. Both Raji and Raji-CD155 cells were found to express HLA-DR at equivalent levels (Figure 5.1). Considering strong expression on both cell types, both cell lines were utilised in the proposed model for primary T-cell activation.

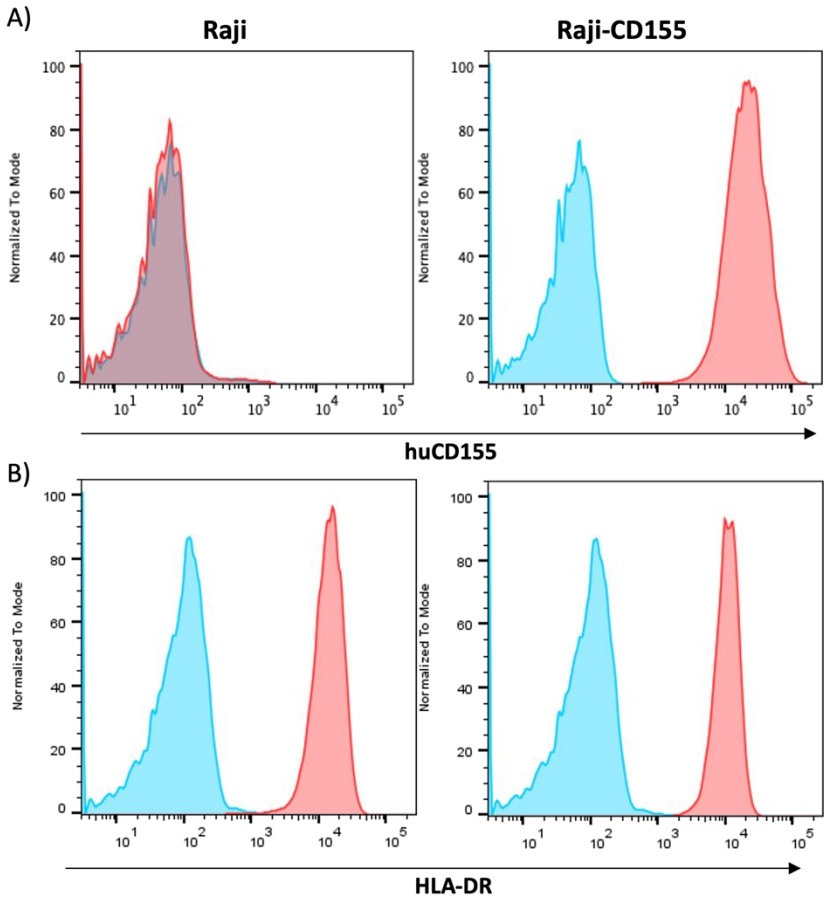

Figure 5.1 Raji and Raji-CD155 expression of MHC-II HLA-DR and CD155

A) Staining of Raji and Raji-CD155 B-cells utilising an anti-human CD155 antibody (Red), confirming CD155 expression is limited to Raji-CD155 cells. Cells were also stained with a matched isotype control antibody (Blue). **B)** Staining of Raji and Raji-CD155 B-cells utilising an anti-HLA-DR antibody (Red). Cells were also stained with a matched isotype control antibody (Blue).

5.1.2 Raji presented SEE induces strong primary T-cell proliferation

Before proceeding to assess how CD155 provision may augment T-cell activation by Raji presented superantigen, determining the appropriate ratio of effector T-cell to peptide-loaded target Raji cells (E:T) was required. Previous work has highlighted that loading Raji cells with between 30-60 ng/mL of SEE is adequate to activate Jurkat T-cells, therefore Raji cells were loaded with 60 ng/mL SEE before being co-cultured with T-cells at increasing ratios. A titration reducing the number of target Raji cells was assessed to determine the minimum ratio required to induce T-cell activation, utilising TransAct (Soluble CD3/CD28 antibodies) as a positive control. The total number of T-cells remained constant whilst the number of Raji B-cells was reduced.

CD4+ T-cells proliferated strongly when co-cultured with sAg-loaded Raji cells, with 62% of CD4+ T-cells proliferating when co-cultured at a ratio of 1:1 E:T. Conversely, co-culture with unloaded Raji cells induced only 17% of CD4+ T-cells to proliferate. T-cell proliferation was reduced in line with reduced target cell ratio. At an E:T ratio of 100:1, CD4+ T-cell proliferation in response to sAg-loaded Raji was limited to only 6.2%, compared to only 2.2% of CD4+ T-cells cultured with unloaded Raji (Figure 5.2B+D). Culture of T-cells with TransAct resulted in 45% of CD4+ T-cell to proliferate, exceeded only by T-cells cultured with sAg-loaded Raji at either a 5:1 or 1:1 ratio.

Contrary to the proliferation of CD4+ T-cells in response to sAg-loaded Raji cells, CD8+ T-cells failed to respond to SEE presentation (Figure 5.2C). While CD8+ T-cells classically recognise peptides in the context of MHC-I rather than MHC-II, sAgs are capable of cross-linking the TCR of either CD4 or CD8+ T-cells due to sAg specificity for TCR Vβ domains (Vβ8). Conversely, T-cells activated with soluble TransAct CD3/CD28 induced 26% of CD8+ T cell to proliferate (Figure 5.2C+D).

Based on the results of CD4+ T-cell proliferation in response to sAg-loaded Raji, SEE induces T-cell proliferation comparable to that of soluble CD3/CD28 stimulation when co-cultured at ratios between 10:1 and 1:1. Considering this, peptide-loading of Raji cells with SEE at 60 ng/mL was determined to be adequate for the activation of isolated T-cells, and that proceeding with a E:T ratio of between 10:1 and 1:1 was suitable for a sAg model utilising primary T-cells.

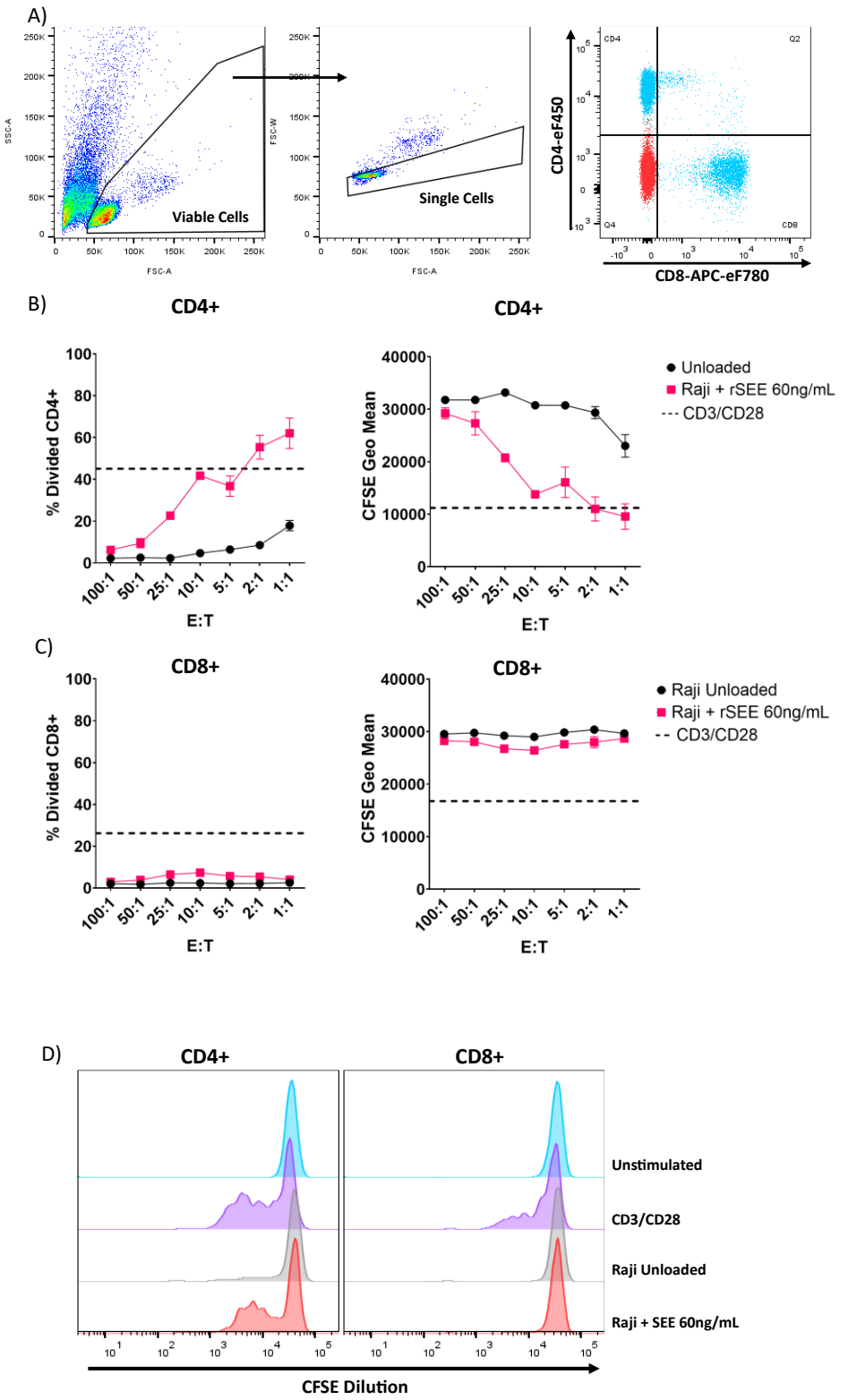

Figure 5.2 sAg-loaded Raji induce strong primary T-cell activation

A) Gating strategy for determining CD4+ and CD8+ populations of isolated T-cells. Gates determining CD4+ or CD8+ T-cells were based on FMO controls for CD4-eF450 and CD8-APC-eF780. Non-stained T-cells are shown in red, isolated T-cells stained against CD4 and CD8 in blue. **B)** Percentage (Left) and CFSE geometric mean (Right) of CD4+ T-cells co-cultured with sAg-loaded Raji B cells at increasing titration. T-cells cultured with TransAct are represented by a dashed line. **C)** Percentage (Left) and CFSE geometric mean (Right) of CD8+ T-cells co-cultured with sAg-loaded Raji B cells at increasing titration. T-cells cultured with TransAct are represented by a dashed line. **D)** Representative histograms of CD4+ (Left) and CD8+ (Right) T-cell proliferation. T-cells were cultured

alone (Blue), with TransAct (Purple), with unloaded Raji B cells (Grey) or with sAg-loaded Raji B cells (Red). (B+C ±SEM 3 technical repeats)

5.2 Expression of CD155 receptors across T-cell donors

CD155 acts as the receptor for three T-cell receptors, CD96, TIGIT and CD226, each of which compete for binding with distinctly different affinity. TIGIT binds CD155 with the greatest affinity, followed by CD96, while CD226 binds with the weakest (TIGIT: K_D = 3.15 nM, CD96: K_D = 37.6 nM, CD226: K_D = 119 nM) [88]. As such, determining the baseline expression of these three receptors on primary donor T-cells, as well as how their expression is altered following sAg-mediated T-cell activation, is imperative to accurately interpret the proliferative response of T-cells.

CD96 expression was limited across all four donor CD4+ T-cells, ranging from less than 1% to 1.3%. TIGIT expression on CD4+ T-cells was similarly low across three of four donors, with an average expression of 6.24%. Donor 4 exhibited the highest TIGIT expression on CD4+ T-cells, with 16.1% of CD4+ T-cells being TIGIT+. Of CD4+ T-cells, an average of 16.85% were CD226+. Expression was varied between donors, with only 2% of CD4+ T-cells from donor 2 expressing CD226, whilst 30.6% of T-cells from donor 4 were CD226+ (Figure 5.3A/B).

The variation of receptor expression between donors was similar in CD8+ T-cells (Figure 5.3C/D). Expression of CD96 was negligible across all four donors, however TIGIT was highly expressed on CD8+ T-cells from both donors 2 and 4 (27.5 and 27.1%, respectively). Conversely, less than 4% of donors 1 and 3 CD8+ T-cells were TIGIT+. CD226 expression was highest with donors 3 and 4, with 21 and 10.7% of CD8+ T-cells expressing CD226. Donors 1 and 2 expressed 6.5 and 0%, respectively.

Overall, these data highlight wide variation of receptor expression between T-cell donors. Receptor expression does however allow the proposed sAg-mediated model to be utilised with Raji-CD155 target cells, presenting CD155 to cells expressing varying levels of initial TIGIT and CD226. However, low initial expression of CD96 across all donors suggests that any early T-cell interaction with CD155 is unlikely to be through CD96. Given that previous literature suggests that CD96 is a late marker of activation, and that expression is induced 4-5 days post stimulation, assessing T-cell responses over an extended period would be beneficial [153].

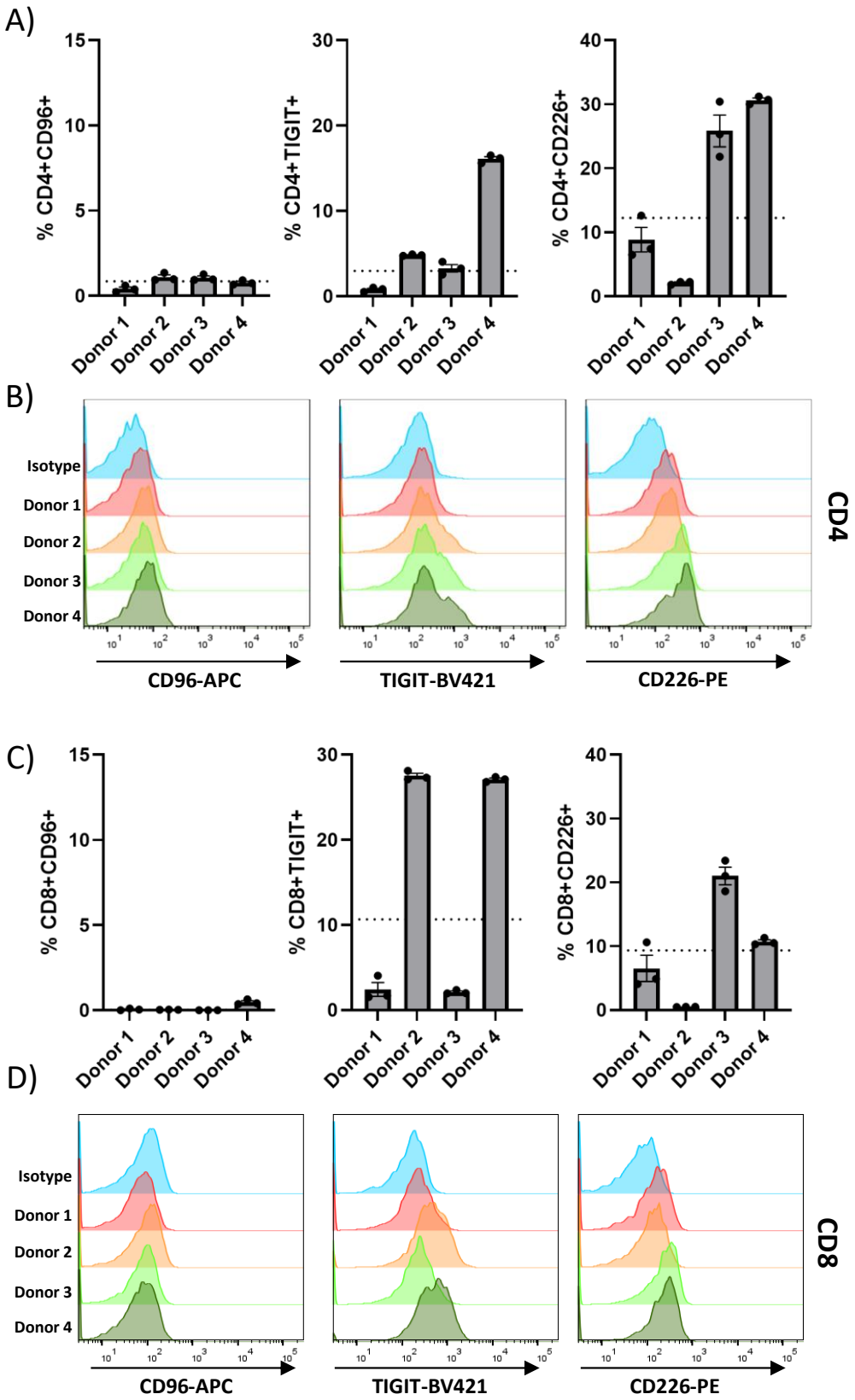

Figure 5.3 Expression of CD96, TIGIT and CD226 on isolated T-cells is varied between donors

A) Expression of CD96, TIGIT and CD226 on isolated CD4+ T-cells. Average receptor expression across four donors is represented by a dashed line. **B)** Representative histograms from each donor, highlighting staining of CD96, TIGIT and CD226 on isolated CD4+ T-cells. A matched isotype control antibody is shown in blue. **C)** Expression of CD96, TIGIT and CD226 on isolated CD8+ T-cells. Average receptor expression across four donors is represented by a dashed line. **D)** Representative histograms from each donor, highlighting staining of CD96, TIGIT and CD226 on isolated CD8+ T-cells.

A matched isotype control antibody is shown in blue. (Data shown is three technical replicates ±SEM).

5.3 CD155 augments sAg-mediated T-cell proliferation

To initially determine how isolated primary T-cells respond to sAg-loaded Raji-CD155 target cells, an initial investigation was carried out to assess whether expression of CD155 on sAg-presenting target cell would augment sAg-mediated T-cell proliferation. To better understand the role CD96 may play in augmenting this activity, an Fc-silenced anti-human CD96 antibody was used to assess whether the blockade of CD96 would impact any CD155-mediated effect. By using an Fc-silenced isotype (N297S) of the 19-134 anti-human CD96 antibody (19-134 N297S), CD96 could be blocked whilst inhibiting any cross-linking between antibody and B-cell expressed FcγR [169].

5.3.1 CD155 receptor upregulation in response to sAg stimulation in TIGIT^{LO}CD226^{LO} T-cells

Considering that CD155 interacts with CD96, TIGIT and CD226, understanding how these three receptors are upregulated in response to sAg-mediated T-cell activation is pivotal. T-cells have been shown previously to proliferate in response to antibody mediated CD96 stimulation, however our donors all express limited CD96. Therefore, for CD96 to mediate any activity in T-cells, it must be upregulated in response to TCR stimulation. As such, CD155 receptor expression was assessed over the course of 5 days in response to Raji or Raji-CD155 (sAg-loaded or unloaded) co-culture at a ratio of 10:1 (E:T). This study utilised the first T-cell donor, shown in Figure 5.3 as Donor 1.

CD4+ T-cell upregulation of CD96 was greatest in T-cells cultured with either sAg-loaded Raji or Raji-CD155 cells than unloaded target cells. Upregulation of CD96 was gradual, however increased substantially between days 4 and 5, with expression peaking at 38% and 32% for Raji and Raji-CD155, respectively. Unloaded Raji cells similarly induced gradual CD96 upregulation till day 3, beyond which expression stagnated at 13.5% of CD4+ T-cells. T-cell culture with unloaded Raji-CD155 cells resulted in reduced CD96 expression on CD4+ T-cells compared to culture with unloaded Raji, with 7.2% of CD4+ T-cells expressing surface CD96 by day 5 (Figure 5.4A).

CD8+ T-cell upregulation of CD96 was lower than that of CD4+ T-cells. Culture with sAg-loaded Raji and Raji-CD155, as well as unloaded Raji, all resulted in similar CD96 expression trends on CD8+ T-cells. All three resulted in surface expression of ~15% by day 5. Unloaded Raji-CD155 co-culture resulted in reduced CD8+ T-cell CD96 expression of 5% by day 5 (Figure 5.4B).

TIGIT expression on unstimulated CD4+ T-cells was minimal (0.77%). Expression was increased in response to sAg presentation by both Raji and Raji-CD155, with 20% of CD4+ T-cell cultured with Raji expressing TIGIT by day 5, and 15% in those cultured with Raji-CD155. Unloaded Raji or Raji-CD155

induced modest upregulation, with TIGIT expression limited to 4.6 and 3.1% respectively (Figure 5.4C). CD8+ T-cell TIGIT upregulation was similarly increased in response to sAg-loaded Raji or Raji-CD155 co-culture (24 and 19%), however culture with non-loaded Raji was similarly raised (21%) suggesting this TIGIT upregulation is a result of T-cell recognition of allogenic MHC rather than specific response to sAg. Non-loaded Raji-CD155 induced lower TIGIT expression with 8.5% of CD8+ T-cells presenting as TIGIT+ (Figure 5.4D).

Expression of CD226 on T-cells was low, with 8.8% of CD4+ T-cells expressing CD226 (Figure 5.4E). Expression was increased in response to sAg-loaded Raji co-culture, with 50% of CD4+ T-cells expressing CD226 by day 5. Co-culture with sAg-loaded Raji-CD155 limited CD226 upregulation to 34%. Non-loaded Raji and Raji-CD155 co-culture induced lower expression, resulting in 13.7 and 3.9% of CD4+ T-cells being CD226+ by day 5. CD8+ T-cell expression of CD226 was similarly low at 6.5% of cells (Figure 5.4F). Both non-loaded and sAg-loaded Raji cells induced similar upregulation of CD226, however 24.7% of CD8+ T-cells cultured with sAg-loaded Raji were CD226+ by day 5, while only 15.3% of those cultured with non-loaded Raji were. sAg-loaded Raji-CD155 induced similar expression to non-loaded Raji by day 5, however CD226 expression only began to increase between days 3 and 4. Non-loaded Raji-CD155 failed to induce CD226 upregulation, with expression limited to 1.8% of CD8+ T-cells at day 5.

Overall, T-cells from donor 1 exhibited no expression of CD96 and low expression of both TIGIT and CD226 prior to their activation. As such, donor 1 T-cells were deemed to be $TIGIT^{LO}CD226^{LO}$.

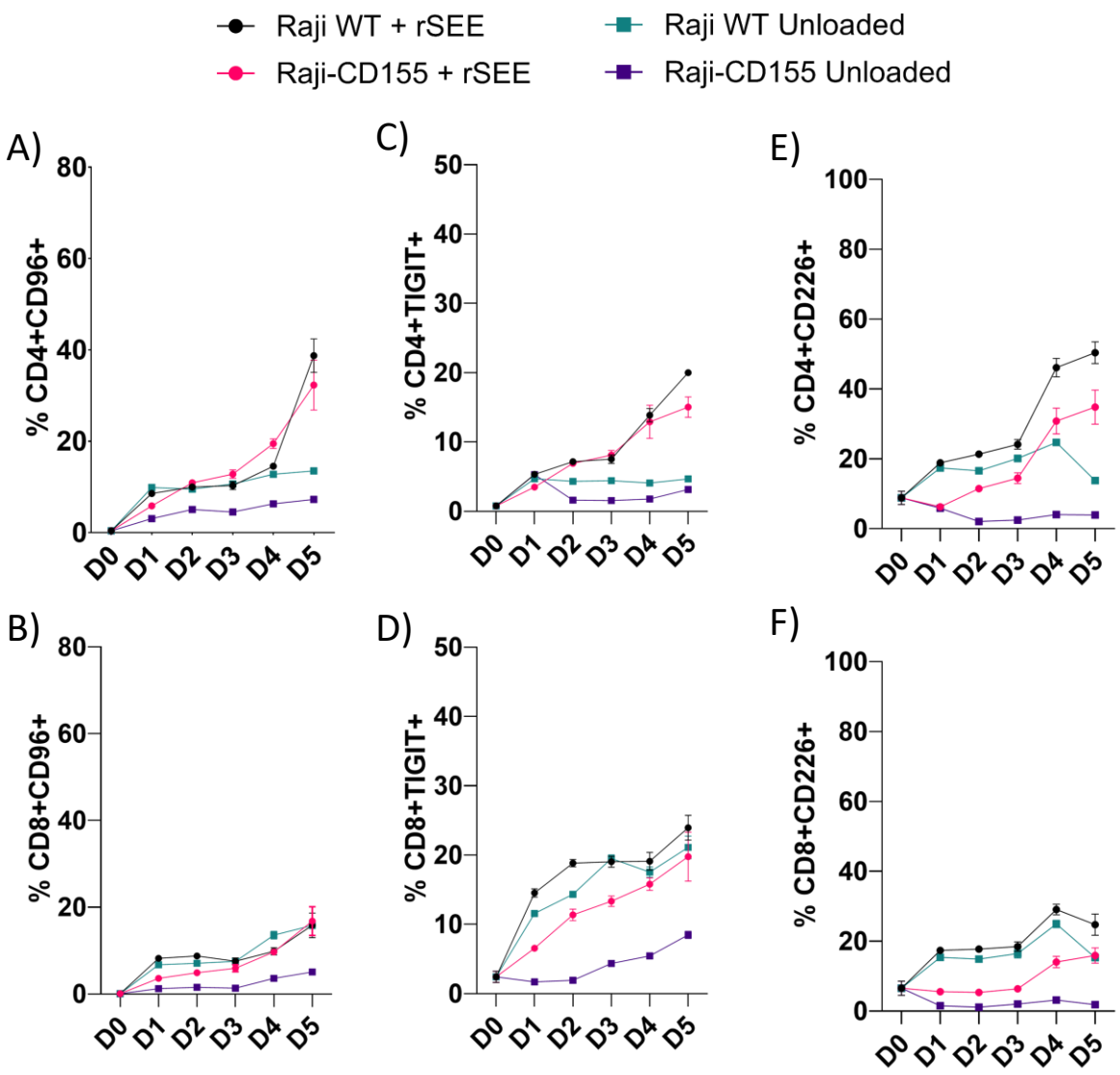

Figure 5.4 CD155 receptor expression changes upon sAg stimulation of TIGIT^{LO}CD226^{LO} T-cells

A/B) Expression of CD96 on TIGIT^{LO}CD226^{LO} CD4+ (A) or CD8+ (B) T-cells cultured with sAg-loaded Raji (Black), sAg-loaded Raji-CD155 (Red), unloaded Raji (Green) or unloaded Raji-CD155 (Purple) at a ratio of 10:1. Expression was assessed daily from day 0 to day 5 and is presented as a percentage of CD4+ or CD8+ T-cells. **C/D)** Expression of TIGIT on TIGIT^{LO}CD226^{LO} CD4+ (C) or CD8+ (D) T-cells cultured with sAg-loaded Raji (Black), sAg-loaded Raji-CD155 (Red), unloaded Raji (Green) or unloaded Raji-CD155 (Purple) at a ratio of 10:1. Expression was assessed daily from day 0 to day 5 and is presented as a percentage of CD4+ or CD8+ T-cells. **E/F)** Expression of CD226 on TIGIT^{LO}CD226^{LO} CD4+ (C) or CD8+ (D) T-cells cultured with sAg-loaded Raji (Black), sAg-loaded Raji-CD155 (Red), unloaded Raji (Green) or unloaded Raji-CD155 (Purple) at a ratio of 10:1. Expression was assessed daily from day 0 to day 5 and is presented as a percentage of CD4+ or CD8+ T-cells. (Data points represent three technical replicates ±SEM)

5.3.2 CD4+ TIGIT^{LO}CD226^{LO} proliferation is unaffected by CD96 blockade

To determine the impact of CD96 expression upon T-cell activation and proliferation, primary T-cells were co-cultured in the same conditions as utilised to monitor the upregulation of CD155 receptors, detailed in Figure 5.4. To determine what role CD96 exerted over T-cell activation, the capacity of CD96 to bind CD155 was inhibited utilising a previously defined Fc-silenced anti-human CD96 blocking antibody, 19-134 N297S [169]. CFSE-labelled T-cell were cultured with SEE-loaded Raji or Raji-CD155 cells at 1:1, 5:1 or 10:1 (E:T) in the presence of excess Fc-silent CD96 blocking antibody (19-134 N297S, 25 μg/mL) or matched non-binding isotype control antibody (IC N297S, 25 μg/mL), before CD4+ and CD8+ T-cell proliferation was assessed through dilution of CFSE.

CD4+ TIGIT^{LO}CD226^{LO} T-cells from donor 1 responded strongly to sAg presentation by Raji B cells at all E:T ratios assessed whether in the presence of a non-blocking isotype antibody or a CD96 blocking antibody (Figure 5.5). At a ratio of 1:1, 84.8 and 85.3% of CD4+ T-cells had undergone proliferation in response to sAg-loaded Raji in the presence of Fc-silent isotype or CD96 blocking antibody (19-134 N297S). Conversely, 93.8 and 93.3% had proliferated when cultured with sAg-loaded Raji-CD155 and isotype or 19-134 antibody, indicating that whilst CD155 increased T-cell activation, the blockade of CD96 failed to limit proliferation (Figure 5.5A/B).

Reducing the total number of B-cell targets (5:1 E:T) reduced CD4+ T-cell proliferation. Of CD4+ T-cells cultured with sAg-loaded Raji, proliferation was reduced to 81.7 and 83.9% (Isotype vs. 19-134). As previous, CD4+ proliferation in response to sAg-loaded Raji-CD155 was increased to 92.8 and 92.5%, again indicating that blockade of CD96 at a 5:1 E:T ratio had no impact on CD155-mediated CD4+ T-cell proliferation (Figure 5.5C/D).

Further decreasing the total number of B-cell targets to 10:1 again limited CD4+ T-cell proliferation in response to sAg-loaded Raji with no change when blocking CD96 (76.8 vs. 77.9%, Isotype vs. 19-134). Culture with sAg-loaded Raji-CD155 again promoted CD4+ T-cell proliferation over Raji, with 90.2 of CD4+ T-cells having proliferated (Figure 5.5E/F). Culture with 19-134 N297S reduced CD4+ T-cell proliferation slightly to 85.9%, however this decrease was not significant with respect to culture with an equivalent isotype.

Overall, CD4+ TIGIT^{LO}CD226^{LO} T-cells exhibited strong proliferation in response to sAg-loaded Raji cells, while Raji expression of CD155 augmented this proliferative activity. Blockade of CD96 through an Fc-silent blocking antibody had no significant impact on CD155 induced TIGIT^{LO}CD226^{LO} T-cell proliferation. CD4+ T-cell upregulation of CD96 in response to sAg was relatively low by day 4 (14%), while expression of the stimulatory receptor, CD226, was high (50%) (Figure 5.4). This pattern of CD226 and the lack of response to CD96 blockade may account for the strong stimulatory reaction to CD155 observed.

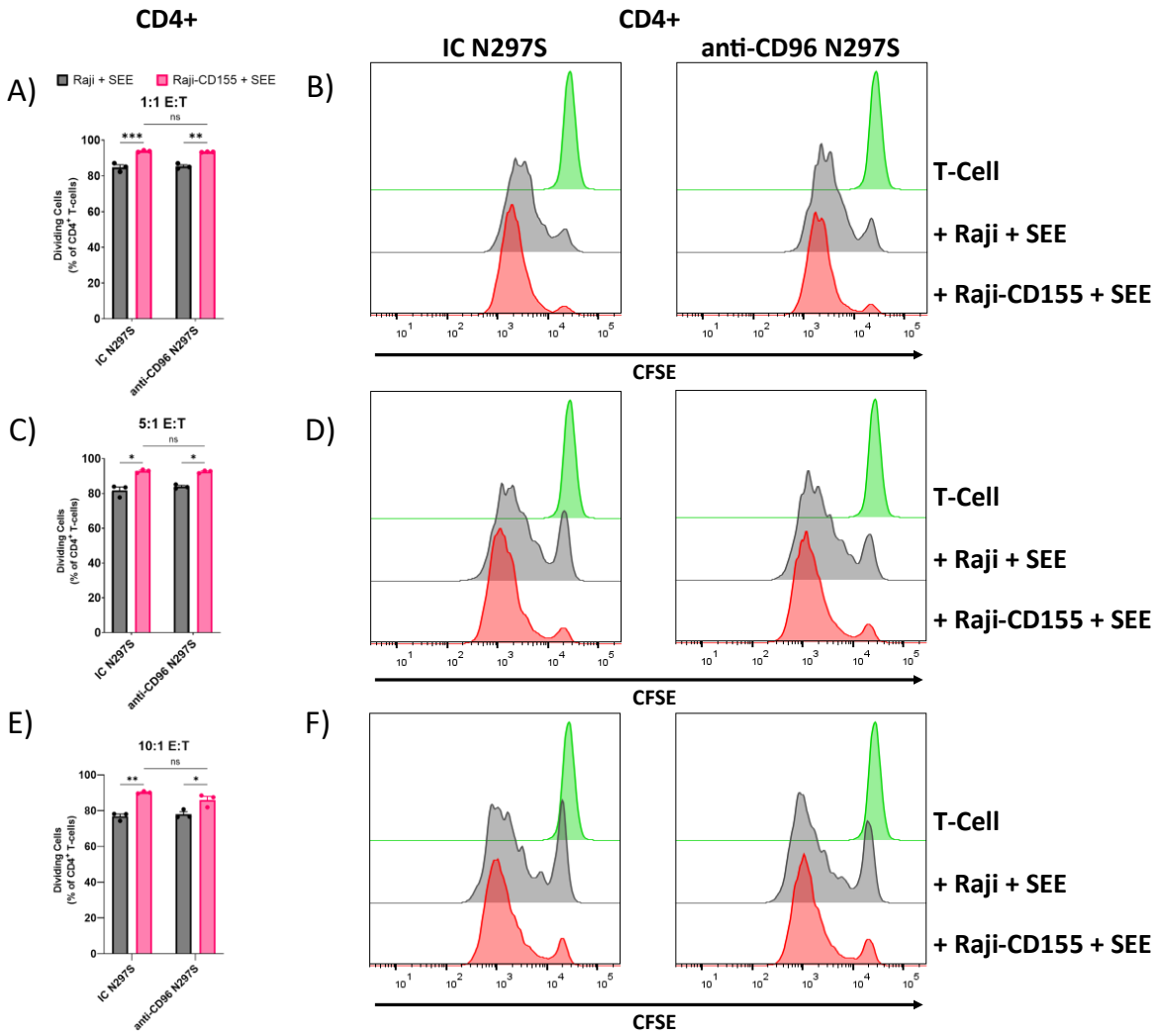

Figure 5.5 CD155 enhancement of CD4+ TIGIT^{LO}CD226^{LO} proliferation is not impacted by CD96 blockade.

A) Proliferation of CD4+ TIGIT^{LO}CD226^{LO} T-cells cultured with sAg-loaded Raji or Raji-CD155 at a ratio of 1:1 E:T. Proliferation assessed at day 4. **B)** Representative histogams of CD4+ TIGIT^{LO}CD226^{LO} T-cell CFSE dilution when cultured at a 1:1 E:T ratio with non-blocking control antibody (IC N297S) (Left) or CD96 blocking antibody (19-134 N297S) (Right). T-cells cultured alone are shown in green, T-cells cultured with sAg-loaded Raji in grey and T-cells cultured with sAg-loaded Raji-CD155 in red. **C)** Proliferation of CD4+ TIGIT^{LO}CD226^{LO} T-cells cultured with sAg-loaded Raji or Raji-CD155 at a ratio of 5:1 E:T. Proliferation assessed at day 4. **D)** Representative histogams of CD4+ TIGIT^{LO}CD226^{LO} T-cell CFSE dilution when cultured at a 5:1 E:T ratio with non-blocking control antibody (IC N297S) (Left) or CD96 blocking antibody (19-134 N297S) (Right). T-cells cultured alone are shown in green, T-cells cultured with sAg-loaded Raji in grey and T-cells cultured with sAg-loaded Raji-CD155 in red. **E)** Proliferation of CD4+ TIGIT^{LO}CD226^{LO} T-cells cultured with sAg-loaded Raji or Raji-CD155 at a ratio of 1:1 E:T. Proliferation assessed at day 4. **F)** Representative histogams of CD4+ TIGIT^{LO}CD226^{LO} T-cell CFSE dilution when cultured at a 10:1 E:T ratio with non-blocking control antibody (IC N297S) (Left) or CD96 blocking antibody (19-134 N297S) (Right). T-cells cultured alone are shown in green, T-cells cultured with sAg-loaded Raji in grey and T-cells cultured with sAg-loaded Raji-CD155 in red. (A, C & E data points are the mean of three technical replicates of 1 TIGIT^{LO}CD225^{LO} donor, ±SEM. 2-way ANOVA, * = $p < 0.05$, ** = $p < 0.005$, *** = $p < 0.0005$)

5.3.3 CD8+ TIGIT^{LO}CD226^{LO} proliferation is limited by CD96 blockade

In contrast to results from the pilot study assessing the suitability of utilising sAg-loaded Raji cells to induce T-cell proliferation (Figure 5.2), CD8+ T-cells originating from donor 1 were sufficiently activated by sAg-loaded Raji and Raji-CD155 target cells (Figure 5.6), undergoing extensive proliferation. Total CD8+ T-cell proliferation was however reduced with respect to that of CD4+ T-cell proliferation.

As with CD4+ T-cells cultured with sAg-loaded Raji at an E:T ratio of 1:1, blockade of CD96 had no impact on CD8+ T-cell proliferation (51.8 vs. 51.5%, Isotype vs. 19-134). Target expression of CD155 again imparted a strong stimulatory effect on CD8+ T-cells, increasing T-cell division to 68.7% when cultured with a non-blocking isotype antibody. The addition of CD96 blocking antibody had little impact, with CD155 induced T-cell proliferation remaining increased at 66% of CD8+ T-cells (Figure 5.6A/B).

Reduction of total sAg-loaded Raji or Raji-CD155 to a 5:1 E:T ratio reduced CD8+ T-cell proliferation. As with co-culture at a 1:1 ratio, sAg-loaded Raji induced comparable proliferation when cultured with either isotype or CD96 blocking antibody (44.1 vs. 44.7%, respectively). Target cell expression of CD155 augmented CD8+ T-cell proliferation at a 5:1 ratio, increasing CD8+ proliferation to 61.7% in the presence of an isotype antibody, and 58.4% in the presence of a CD96 blocking antibody (Figure 5.6C/D).

The further reduction of co-cultured target cells to a 10:1 ratio again reduced CD8+ T-cell proliferation. CD8+ T-cell proliferation when cultured with sAg-loaded Raji was similar whether cultured with isotype or CD96 blocking antibody (44.96 vs. 42.93%). However, while the addition of an isotype antibody did not impact the increase in proliferation of CD4+ T-cells in response to sAg-loaded Raji-CD155, antibody blockade of CD96 ablated CD155-mediated T-cell proliferation, reducing proliferation of CD8+ T-cells from 61% to 46.7% (Figure 5.6E/F).

These data examining CD4+ and CD8+ T-cell response to target expression of CD155 emphasize that CD155 can act to augment sAg-mediated T-cell proliferation. Of note within this data is that at a ratio of 10:1 E:T, the CD155-mediated stimulatory effect upon CD8+ T-cells was ablated by the addition of a CD96 blocking antibody. Considering the increased expression of surface TIGIT on CD8+ T-cells over CD4+ T-cells over the course of the assay (Figure 5.4), as well as the impact that this expression relative to CD226 may have on the impact of CD96 blockade, assessing this model utilising a different donor and subsequently, a different pattern of receptor expression was important.

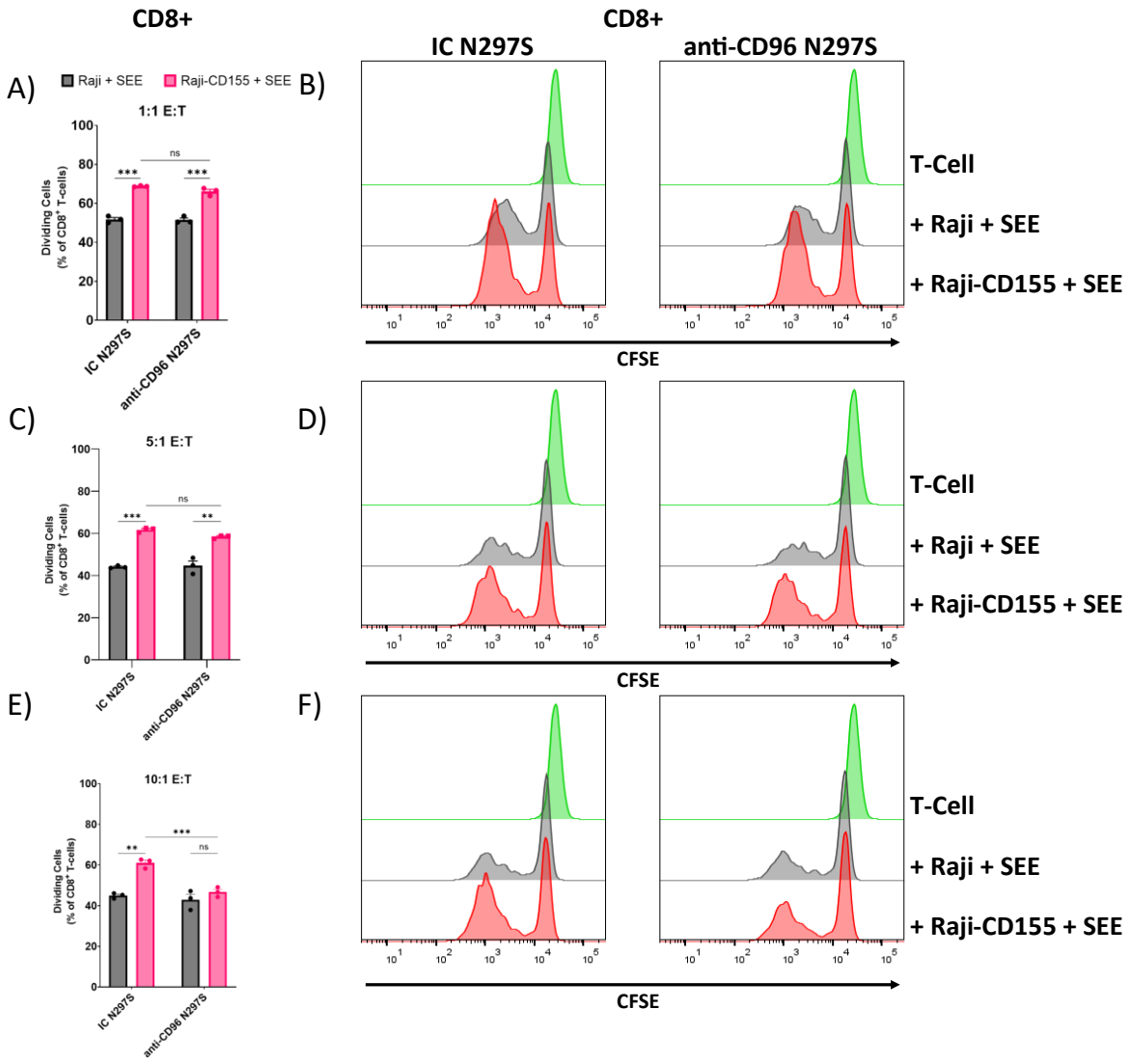

Figure 5.6 CD96 augments CD155 mediated proliferation of TIGIT^{LO}CD226^{LO} CD8+ T-cell proliferation **A)** Proliferation of CD8+ TIGIT^{LO}CD226^{LO} T-cells cultured with sAg-loaded Raji or Raji-CD155 at a ratio of 1:1 E:T. Proliferation assessed at day 4. **B)** Representative histogams of CD8+ TIGIT^{LO}CD226^{LO} T-cell CFSE dilution when cultured at a 1:1 E:T ratio with non-blocking control antibody (IC N297S) (Left) or CD96 blocking antibody (19-134 N297S) (Right). T-cells cultured alone are shown in green, T-cells cultured with sAg-loaded Raji in grey and T-cells cultured with sAg-loaded Raji-CD155 in red. **C)** Proliferation of CD8+ TIGIT^{LO}CD226^{LO} T-cells cultured with sAg-loaded Raji or Raji-CD155 at a ratio of 5:1 E:T. Proliferation assessed at day 4. **D)** Representative histogams of CD8+ TIGIT^{LO}CD226^{LO} T-cell CFSE dilution when cultured at a 5:1 E:T ratio with non-blocking control antibody (IC N297S) (Left) or CD96 blocking antibody (19-134 N297S) (Right). T-cells cultured alone are shown in green, T-cells cultured with sAg-loaded Raji in grey and T-cells cultured with sAg-loaded Raji-CD155 in red. **E)** Proliferation of CD8+ TIGIT^{LO}CD226^{LO} T-cells cultured with sAg-loaded Raji or Raji-CD155 at a ratio of 1:1 E:T. Proliferation assessed at day 4. **F)** Representative histogams of CD8+ TIGIT^{LO}CD226^{LO} T-cell CFSE dilution when cultured at a 10:1 E:T ratio with non-blocking control antibody (IC N297S) (Left) or CD96 blocking antibody (19-134 N297S) (Right). T-cells cultured alone are shown in green, T-cells cultured with sAg-loaded Raji in grey and T-cells cultured with sAg-loaded Raji-CD155 in red. (A, C & E data points are the mean of three technical replicates of 1 TIGIT^{LO}CD225^{LO} donor, ±SEM. 2-way ANOVA, * = $p < 0.05$, ** = $p < 0.005$, *** = $p < 0.0005$)

5.4 CD96 augments the activation of TIGIT^{INT}CD226^{HI} T-cells

To determine how isolated primary T-cells expressing low levels of TIGIT but high levels of CD226 respond to Raji presentation of sAg, T-cells from Donor 3 (Figure 5.3) were co-cultured with sAg-loaded Raji cells and receptor expression changes assessed over 5 days. Concurrently, T-cells were co-cultured with sAg target cells as with Donor 1 to ascertain whether the presence of CD155 would bear any impact on receptor upregulation. Data shown in Figure 5.5 and Figure 5.6 indicated that a ratio of 10:1 E:T was effective to induce suboptimal T-cell proliferation. As such, Raji target cells were loaded with 60ng/mL of SEE sAg and co-cultured at a ratio of 10:1 E:T.

5.4.1 TIGIT^{INT}CD226^{HI} T-cells upregulate CD155 receptors upon activation

Expression of CD96 on both CD4+ and CD8+ T-cells from donor 3 was low prior to co-culture on day 0. Culture with unloaded Raji cells resulted in low upregulation, with 16% of CD4+ and 5% of CD8+ T-cells expressing CD96 by day 5. Similarly, unloaded Raji-CD155 induced 9% of CD4+ T-cells to upregulate CD96 by day 5, and 2.5% of CD8+ T-cells. Culture with sAg-loaded Raji cells promoted strong CD96 upregulation in both CD4+ and CD8+ T-cells (51% and 20%, respectively), whilst culture with sAg-loaded Raji-CD155 cells induced greater CD96 expression, with 60% of CD4+ and 40% of CD8 T-cell expressing CD96+ by day 5 (Figure 5.7A/B).

TIGIT expression on T-cells from donor 3 was low at day 0, with TIGIT expressed on 3.2% and 2% of CD4+ and CD8+ T-cells. Non-specific response to unloaded Raji and Raji-CD155 resulted in small upregulation of TIGIT, similar to that of CD96. While unloaded Raji co-culture resulted in 20% of CD4+ and 17% of CD8+ T-cells expressing TIGIT by day 5, expression induced by unloaded Raji-CD155 was comparatively reduced (16% and 10% of CD4+ and CD8+, respectively). TIGIT upregulation in response to sAg-loaded Raji cells was increased, with 39% of CD4+ and 35% of CD8+ T-cells being TIGIT+ by day 5. Culture with sAg-loaded Raji-CD155 further increased TIGIT expression by day 5, resulting in 42 and 45% of CD4+ and CD8+ T-cells expressing TIGIT (Figure 5.7C/D).

Expression of CD226 was relatively high on donor 3 cells prior to co-culture, with 26% of CD4+ and 21% of CD8+ T-cells expressing CD226. Allogenic induced expression of CD226 was strong, with unloaded Raji cells promoting expression of CD226 on 51% of CD4+ T-cells by day 4. CD4+ expression of CD226 induced by this allogenic response reduced by day 5 to 37%, a trend mirrored in CD8+ T-cells where expression peaked at day 4 before dropping to 31%. Unloaded Raji-CD155 induced limited CD226 upregulation in both CD4+ and CD8+ T-cells, peaking at day 4 with 23% and 20% respectively. Co-culture with sAg-loaded Raji induced CD226 expression in both CD4+ and CD8+ T-cells, resulting in upregulation to 76 and 52% of cells, respectively. Whereas CD155 presence on sAg-

loaded Raji cells promoted both CD96 and TIGIT expression, CD226 expression was reduced at early timepoints when cultured with Raji-CD155 before expression increased by day 5 (Figure 5.7E/F).

T-cells have been shown here to upregulate CD155 receptors in response to B-cell presentation of sAg, with upregulation of both CD96 and TIGIT enhanced by the expression of CD155 on sAg presenting Raji cells. This CD155-mediated increase in receptor expression was greater in CD8+ T-cells. CD96 expression was limited in both CD4+ and CD8+ T-cells, with expression rapidly increasing by day 3, concurrent with literature suggesting a role as a late activation marker [153]. Prior to activation, expression of TIGIT on T-cells from donor 3 was greater than that of donor 1, however was still low. As such, T-cells from donor 3 were deemed to be TIGIT^{INT}CD226^{HI}.

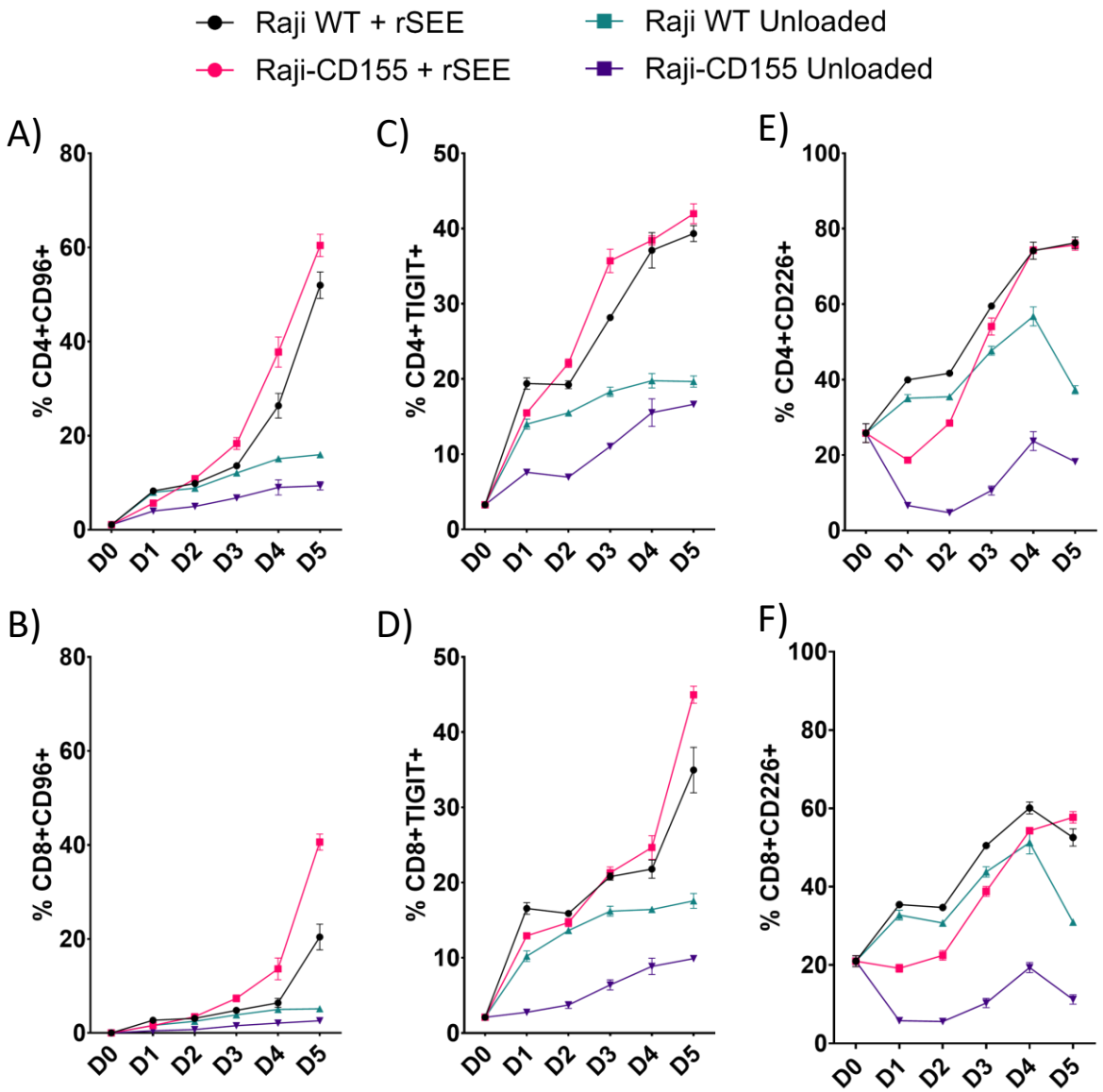

Figure 5.7 TIGIT^{INT}CD226^{HI} T-cells upregulate each CD155 receptor in response to CD155

A/B) Expression of CD96 on TIGIT^{INT}CD226^{HI} CD4+ (A) or CD8+ (B) T-cells cultured with sAg-loaded Raji (Black), sAg-loaded Raji-CD155 (Red), unloaded Raji (Green) or unloaded Raji-CD155 (Purple). Expression was assessed daily from day 0 to day 5 and is presented as a percentage of CD4+ or CD8+ T-cells. **C/D)** Expression of TIGIT on TIGIT^{INT}CD226^{HI} CD4+ (C) or CD8+ (D) T-cells cultured with sAg-

loaded Raji (Black), sAg-loaded Raji-CD155 (Red), unloaded Raji (Green) or unloaded Raji-CD155 (Purple). Expression was assessed daily from day 0 to day 5 and is presented as a percentage of CD4+ or CD8+ T-cells. **E/F)** Expression of CD226 on TIGIT^{INT}CD226^{HI} CD4+ (C) or CD8+ (D) T-cells cultured with sAg-loaded Raji (Black), sAg-loaded Raji-CD155 (Red), unloaded Raji (Green) or unloaded Raji-CD155 (Purple). Expression was assessed daily from day 0 to day 5 and is presented as a percentage of CD4+ or CD8+ T-cells. (Data points represent three technical replicates ±SEM)

5.4.2 Raji expression of CD155 promotes sAg mediated TIGIT^{INT}CD226^{HI} T-cell activation through CD96

Considering the variation in CD155 receptor expression on T-cells from donor 3 (Figure 5.7), as well as differences in receptor upregulation between donors 1 and 3 (Figure 5.4, Figure 5.7), understanding how this change in expression pattern may impact proliferation in response to sAg and CD155 was of interest. Donor 3 (TIGIT^{INT}CD226^{HI})T-cells were prepared as previously described and co-cultured at a 10:1 ratio with sAg-loaded Raji or Raji-CD155 cells before proliferation was assessed at day 4. CD96 interaction with CD155 was again blocked utilising a CD96 blocking antibody or matched isotype control antibody.

Primary T-cells proliferated strongly in response to culture with non-blocking isotype antibody and sAg-loaded Raji cells, with 40% of CFSE labelled CD4+ T-cells and 12% of labelled CD8+ T-cells undergoing division. Similarly, T-cells cultured with a CD96 blocking antibody and SEE-loaded Raji were also robustly activated, with 42% of CD4+ T-cells (Figure 5.8A/B) and 12.2% of CD8+ T-cells undergoing division (Figure 5.8C/D). Proliferation of T-cells cultured with a non-blocking control antibody and SEE-loaded Raji-CD155 cells was increased over wild-type Raji cells, increasing proliferation to 57.6% of CD4+ and 26.5% of CD8+ T-cells. This increase in cell division was ablated by the addition of the blocking CD96 antibody, limiting T-cell proliferation to 38% and 12% for CD4+ and CD8+ T-cells, respectively. This significant reduction in proliferation induced by the blockade of CD96 returned cell division to that induced by SEE-loaded wild-type Raji cells, ablating CD155-mediated augmentation of sAg-mediated T-cell activation. Neither CD4+ nor CD8+ T-cells cultured with SEE unloaded Raji and Raji-CD155 cells underwent any significant proliferation (Appendix 10).

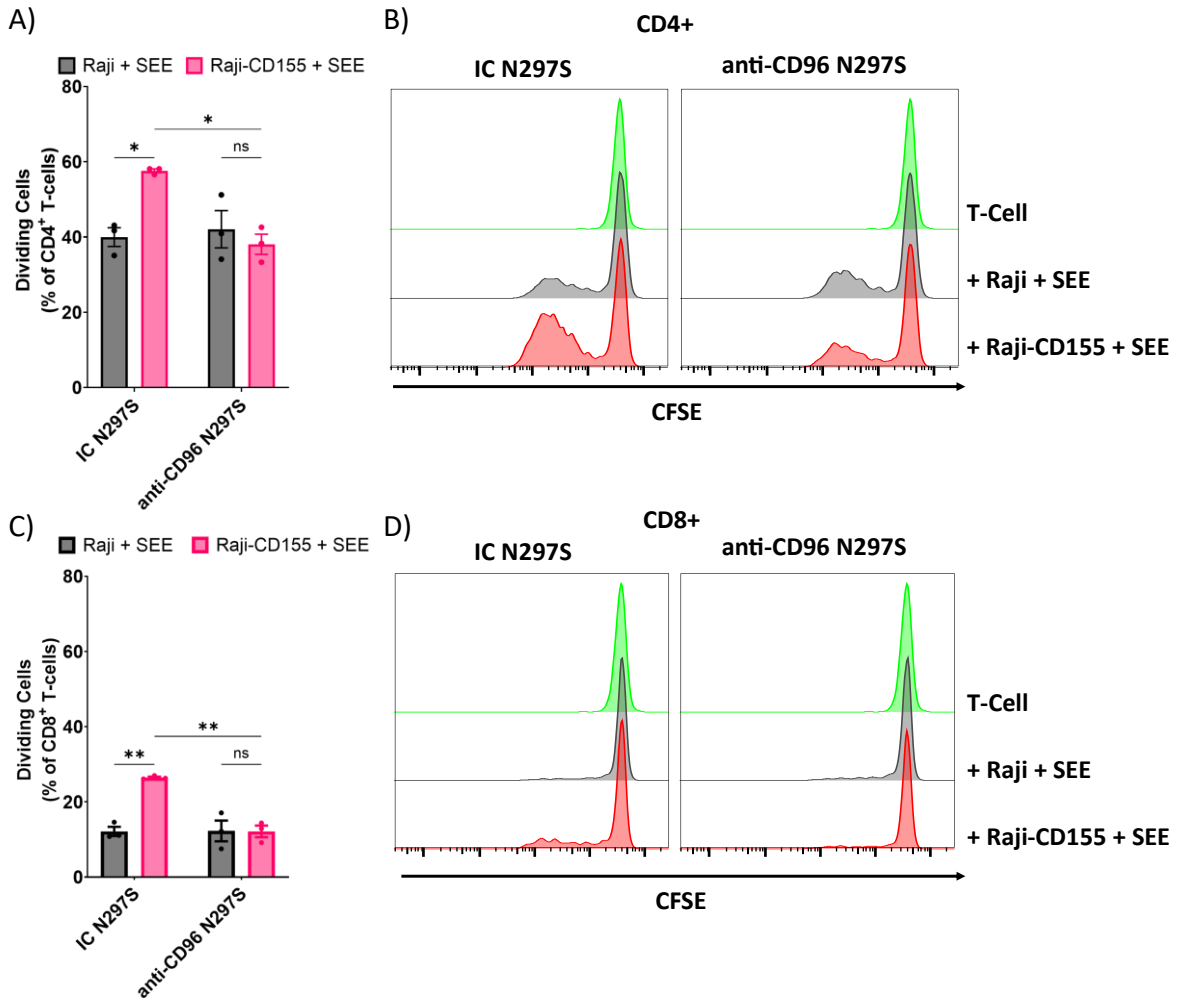

Figure 5.8 TIGIT^{INT}CD226^{HI} T-cell proliferation is enhanced by CD96 expression

A) Proliferation of CD4+ TIGIT^{INT}CD226^{HI} T-cells cultured with sAg-loaded Raji or Raji-CD155 B cells at a ratio of 10:1. Cells were cultured with either non-blocking isotype control antibody (IC N297S) or CD96 blocking antibody (19-134 N297S), and proliferation assessed at day 4. **B)** Representative histograms of CD4+ T-cell CFSE dilution when cultured with non-blocking antibody (Left) or CD96 blocking antibody (Right). Conditions shown are T-cells alone (Green), with sAg-loaded Raji (Grey) or with sAg-loaded Raji-CD155 (Red). **C)** Proliferation of CD8+ TIGIT^{INT}CD226^{HI} T-cells cultured with sAg-loaded Raji or Raji-CD155 B cells at a ratio of 10:1. Cells were cultured with either non-blocking isotype control antibody (IC N297S) or CD96 blocking antibody (19-134 N297S), and proliferation assessed at day 4. **D)** Representative histograms of CD8+ T-cell CFSE dilution when cultured with non-blocking antibody (Left) or CD96 blocking antibody (Right). Conditions shown are T-cells alone (Green), with sAg-loaded Raji (Grey) or with sAg-loaded Raji-CD155 (Red). (Data points are the mean of three technical replicates of 1 TIGIT^{LO}CD225^{HI} donor, ±SEM. 2-way ANOVA, ns= non-significant, * = $p < 0.05$, ** = $p < 0.005$)

To assess cytokine production by TIGIT^{INT}CD226^{HI} T-cells in response to sAg-loaded Raji and Raji-CD155 cells, IL-2 and IFN-γ in supernatant collected from the T-cell proliferation assay shown in Figure 5.8 was collected at 48 and 72 hours.

TIGIT^{INT}CD226^{HI} T-cells production of IL-2 was increased by culture with sAg-loaded Raji-CD155 cells over wild-type Raji in the presence of a non-blocking isotype antibody (Figure 5.9A). Interestingly, the culture of T-cells with sAg-loaded wild-type Raji with a CD96 blocking antibody increased IL-2 release with respect to the use of a control antibody. Antibody aggregation may account for the apparent stimulatory role observed in the absence of CD155, however the addition of sAg-loaded Raji-CD155 ablated increased IL-2 release in the presence of a blocking antibody. By 72 hours, total supernatant IL-2 decreased across each condition (Figure 5.9A), likely a result of increased T-cell activity. Despite this, a similar trend to that of 48-hour IL-2 release was recorded. No change in IL-2 release was found to be significant.

IFN-γ secretion by TIGIT^{INT}CD226^{HI} T-cells was limited at 48 hours, however the addition of Raji-CD155 promoted its secretion (Figure 5.9B). Culture of T-cells with sAg-loaded Raji-CD155 increased IFN-γ release over wild-type Raji in the presence of a non-blocking control antibody. As with T-cell proliferation, the addition of a CD96 blocking antibody increased IFN-γ release when cultured with wild-type Raji. Culture with sAg-loaded Raji-CD155 with CD96 blocking antibody had no impact on IFN-γ release. By 72 hours, the expression of CD155 on target Raji cells promoted IFN-γ release. As before, the addition of blocking CD96 antibody with sAg-loaded Raji increased IFN-γ with respect to a non-blocking antibody. The use of a CD96 blocking antibody in the presence of CD155 expressing Raji cells however did not limit supernatant IFN-γ, with supernatant IFN-γ increasing further again. As with IL-2, no changes in IFN-γ release was found to be significant.

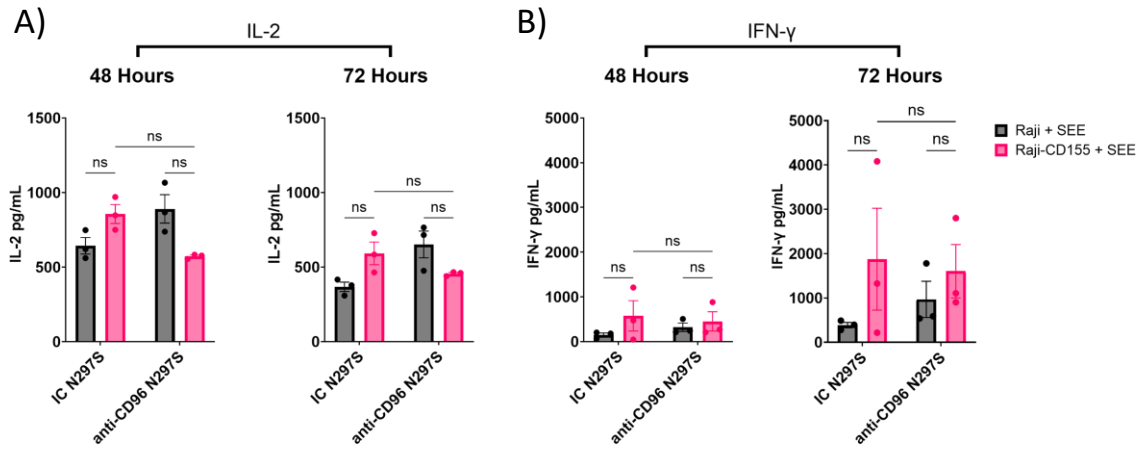

Figure 5.9 IL-2 but not IFN-γ secretion by TIGIT^{INT}CD226^{HI} T-cells is promoted by CD96

A/B) Supernatant was collected at 48 (A) or 72 hours (B) from isolated primary T-cells cultured with sAg-loaded Raji or Raji-CD155 with either non-blocking isotype control (IC N297S) antibody or CD96 blocking antibody (19-134 N297S). Supernatant IL-2 was quantified used ELISA and is presented as pg/mL. **C/D)** Supernatant IFN-γ was collected at 48 (A) or 72 hours (B) from isolated primary T-cells

cultured with sAg-loaded Raji or Raji-CD155 with either non-blocking isotype control (IC N297S) antibody or CD96 blocking antibody (19-134 N297S). Supernatant IFN-γ was quantified used ELISA and is presented as pg/mL. (Data points are the mean of three technical replicates of 1 $TIGIT^{LO}CD225^{HI}$ donor proliferation assay, ±SEM. 2-way ANOVA, ns= non-significant)

5.5 $TIGIT^{INT}CD226^{LOW}$ T-cells exhibit reduced activation potential

While the co-culture of Raji-CD155 target cells with $TIGIT^{INT}CD226^{HI}$ T-cells from donor 3 has been found to mediate the robust upregulation of CD96, TIGIT and CD226, assessing how T-cells from donor 2 with a distinctly different TIGIT and CD226 phenotype would respond to sAg stimulation, with or without the presence of CD155, was of interest. As before, the upregulation of CD96, TIGIT and CD226 on both CD4+ and CD8+ T-cells from donor 2 (Figure 5.3) was investigated.

5.5.1 $TIGIT^{INT}CD226^{LOW}$ T-cells exhibit reduced sAg-mediated CD155 receptor upregulation

Both CD4+ and CD8+ T-cells from donor 2 express negligible levels of CD96 on non-activated T-cells. T-cell expression of CD96 increased to 20% of CD4+ T-cells by day 5 when cultured with wild-type sAg-loaded Raji cells, and to 17% in CD8+ T-cells. However, the expression of CD96 on T-cells cultured with sAg-loaded Raji-CD155 was limited to 12.4% and 4.7% of CD4+ and CD8+ T-cells, respectively. Culture with unloaded Raji cells induced higher CD96 upregulation on CD4+ T-cells than CD8+, however this was limited to 10 and 2.5% respectively. Unloaded Raji-CD155 further limited CD96 expression to 5 and 0.5% in CD4+ and CD8+ T-cells (Figure 5.10A/B). Upregulation of CD96 in donor 2 is in contrast to that of donor 3, with CD96 upregulation restricted across the 5 days examined.

Prior to B-cell co-culture, TIGIT expression was reduced on CD4+ T-cells with respect to CD8+, with 4.8% of CD4+ T-cells expressing TIGIT compared to 27% of CD8+ T-cells (Figure 5.10C/D). CD4+ T-cells cultured with sAg-loaded wild-type Raji increased expression of TIGIT to 17% versus 6.5% for T-cells cultured with Raji-CD155. CD8+ T-cells increased TIGIT expression to 48% when cultured with sAg-loaded wild-type Raji, and whilst co-culture with sAg-loaded Raji-CD155 induced initial expression of TIGIT on CD8+, expression returned to 24% by day 5. Unloaded Raji cells induced similar initial TIGIT upregulation in both CD4+ and CD8+ T-cells, however expression change from day 0 was limited by day 5. CD4+ T-cell TIGIT expression peaked at days 2-3 regardless of unloaded Raji or Raji-CD155 before returning to 8 and 3% respectively. CD8+ TIGIT expression similarly peaked at day 3 before returning to 29% and 11% for unloaded Raji or Raji-CD155 co-cultures (Figure 5.10C/D).

Initial CD226 expression was negligible in both CD4+ and CD8+ T-cells (Figure 5.10E/F). This is in direct contrast to donor 3, where CD226 expression prior to B-cell co-culture was high (Figure 5.7E/F). While CD4+ T-cells cultured with sAg-loaded wild-type Raji increased CD226 expression from 2% to 37% by day 5, those cultured with sAg-loaded Raji-CD155 increased expression to only 13%. Unloaded wild-type Raji induced higher CD226 expression than that of sAg-loaded Raji-CD155,

indicating a mild allogeneic response against Raji cells. However, reduced surface expression of CD226 could also be a result of receptor internalisation following binding of CD155 rather than a lack of upregulation. CD8+ T-cells were limited in their upregulation of CD226 when CD155 was present, increasing from 0.5% to 27% with wild-type Raji and to 6.73% with Raji-CD155. Again, CD8+ T-cells cultured with unloaded wild-type Raji exhibited marginally higher CD226 expression than sAg-loaded Raji-CD155, while only 1% of T-cells cultured with unloaded Raji-CD155 were CD226+ by day 5.

Considering the increased TIGIT expression of donor 2 CD8+ T-cells with respect to both donors 1 and 3, as well as the negligible expression of CD226 across both CD4+ and CD8+ T-cells, T-cells from donor 2 were deemed to be TIGIT^{INT}CD226^{LO}.

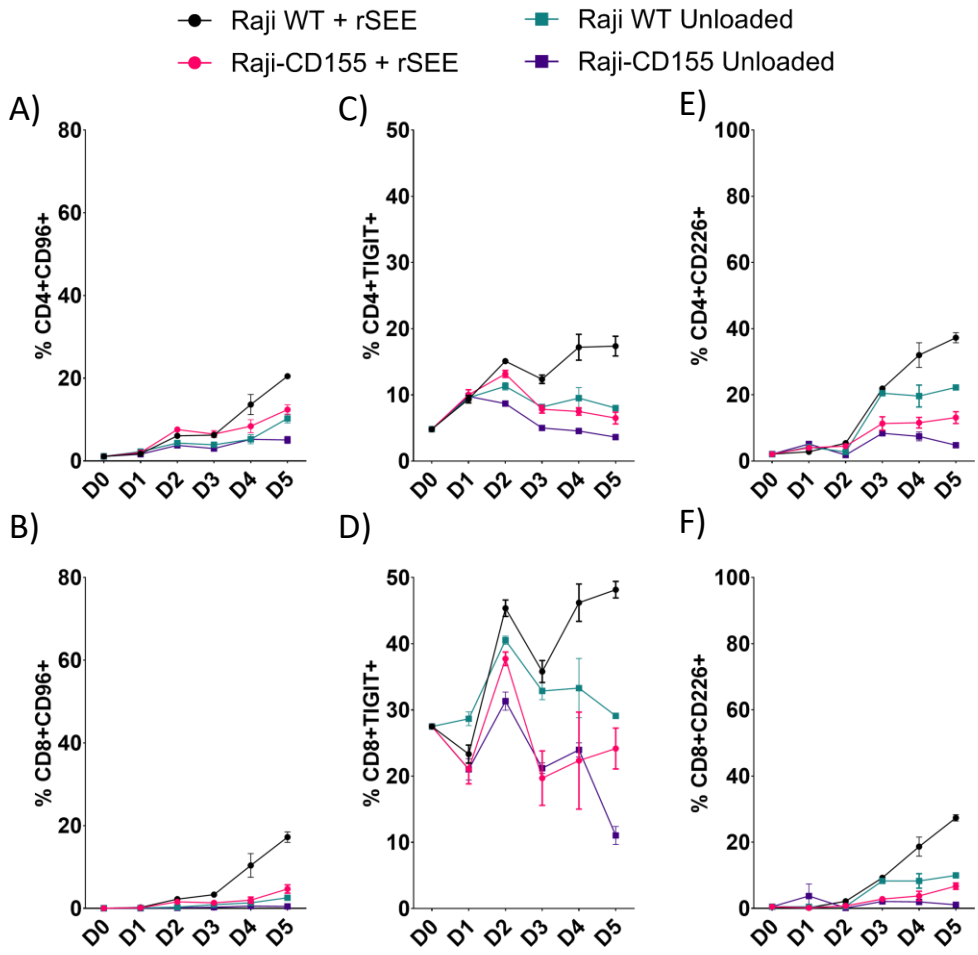

Figure 5.10 TIGIT^{INT}CD226^{LO} T-cells (Donor 2) upregulate CD155 receptors in response to CD155

A/B) Expression of CD96 on TIGIT^{INT}CD226^{LO} CD4+ (A) or CD8+ (B) T-cells cultured with sAg-loaded Raji (Black), sAg-loaded Raji-CD155 (Red), unloaded Raji (Green) or unloaded Raji-CD155 (Purple). Expression was assessed daily from day 0 to day 5 and is presented as a percentage of CD4+ or CD8+ T-cells. **C/D)** Expression of TIGIT on TIGIT^{INT}CD226^{LO} CD4+ (C) or CD8+ (D) T-cells cultured with sAg-loaded Raji (Black), sAg-loaded Raji-CD155 (Red), unloaded Raji (Green) or unloaded Raji-CD155 (Purple). Expression was assessed daily from day 0 to day 5 and is presented as a percentage of CD4+ or CD8+ T-cells. **E/F)** Expression of CD226 on TIGIT^{INT}CD226^{LO} CD4+ (C) or CD8+ (D) T-cells cultured with sAg-loaded Raji (Black), sAg-loaded Raji-CD155 (Red), unloaded Raji (Green) or unloaded Raji-CD155 (Purple). Expression was assessed daily from day 0 to day 5 and is presented as a percentage of CD4+ or CD8+ T-cells. (Data points represent three technical replicates ±SEM)

5.5.2 TIGIT^{INT}CD226^{LO} T-cells proliferation is inhibited by B-cell presentation of CD155

Considering the distinct difference in expression of both TIGIT and CD226 between donors 2 and 3, understanding whether an initial TIGIT^{INT}CD226^{LO} phenotype may subsequently impact T-cell activation in response to culture with sAg-loaded Raji or Raji-CD155 was assessed. Considering the limited upregulation of CD96 in response to sAg-loaded Raji co-culture by donor 3 T-cells, how the addition of a CD96 blocking antibody would impact T-cell activation was similarly relevant.

As previous, TIGIT^{INT}CD226^{LO} T-cell proliferation was assessed at day 4, at which point 27% of CD4+ T-cells cultured with non-blocking control antibody and sAg-loaded Raji had undergone cell division (Figure 5.11A/B). In direct contrast to the response of donor 3 T-cells (Figure 5.8), the proliferation of TIGIT^{INT}CD226^{LO} CD4+ T-cells cultured with sAg-loaded Raji-CD155 and non-blocking control antibody was reduced, with 12.6% undergoing division.

Proliferation of CD4+ T-cells cultured with sAg-loaded Raji cells in the presence of a CD96 blocking antibody was comparable to those cultured with a non-blocking control, with 24% of CD4+ T-cells having undergone division (Figure 5.11A/B). Proliferation of CD4+ T-cells cultured with sAg-loaded Raji-CD155 and a CD96 blocking antibody was further reduced to 8%, however this reduction from CD4+ T-cells cultured with a non-blocking antibody was not significant.

CD8+ T-cells from donor 2 co-cultured with sAg-loaded Raji cells exhibited similar proliferation, regardless of culture with either non-blocking control or CD96 blocking antibody (17 and 12%, respectively) (Figure 5.11C/D). CD8+ T-cell division was reduced when cultured with sAg-loaded Raji-CD155 in the presence of a non-blocking control antibody (10%), with proliferation further reduced with the blockade of CD96 (7%). Again, this decrease in proliferation when cultured with CD96 blocking antibody was not significant with respect to culture with a non-blocking antibody. Unloaded Raji and Raji-CD155 failed to induce T-cell proliferation (Appendix 11).

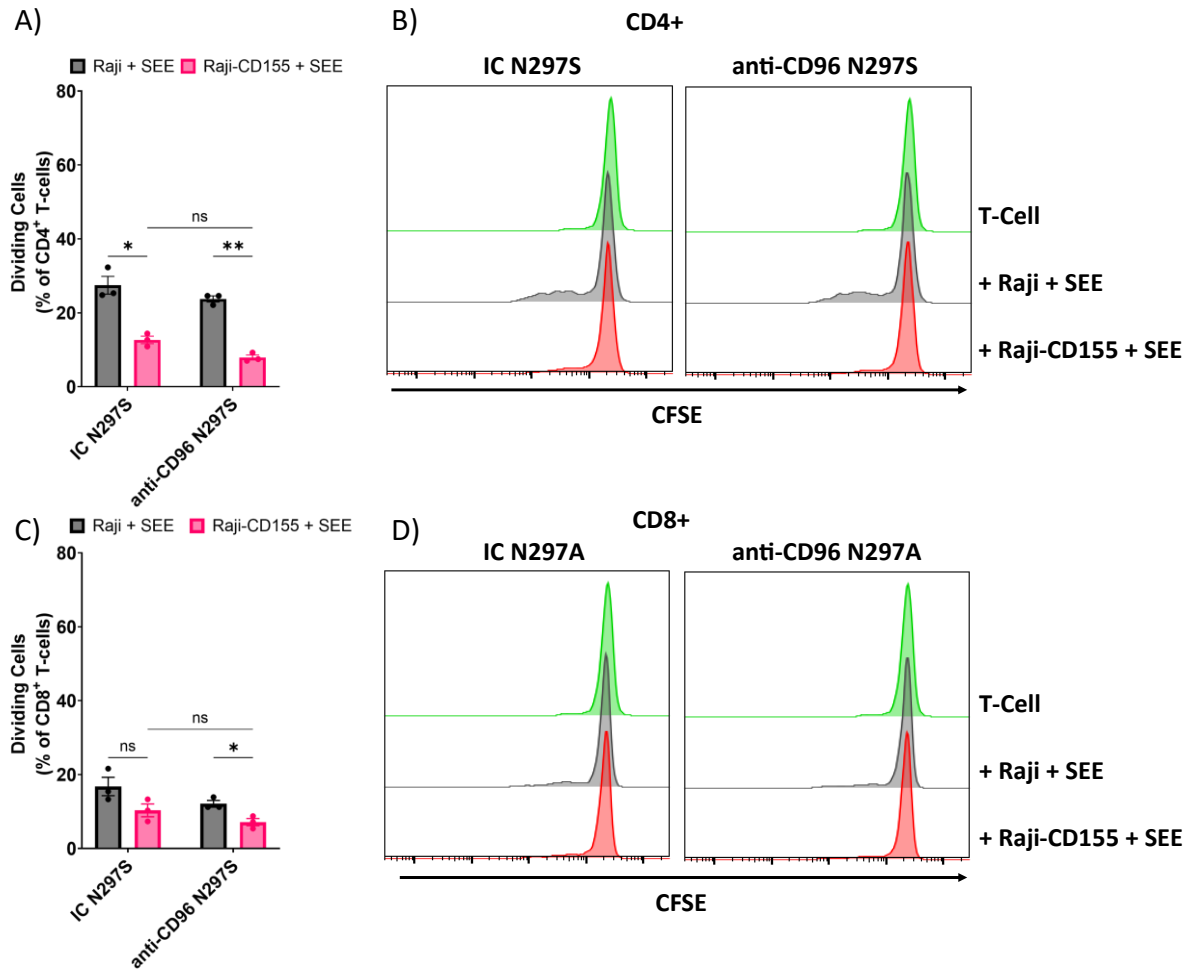

Figure 5.11 TIGIT^{INT}CD226^{LO} T-cell proliferation is inhibited by APC presentation of CD155

A) Proliferation of CD4+ TIGIT^{INT}CD226^{LO} T-cells cultured with sAg-loaded Raji or Raji-CD155 B cells at a ratio of 10:1. Cells were cultured with either non-blocking isotype control antibody (IC N297S) or CD96 blocking antibody (19-134 N297S), and proliferation assessed at day 4. **B)** Representative histograms of CD4+ TIGIT^{INT}CD226^{LO} T-cell CFSE dilution when cultured with non-blocking antibody (Left) or CD96 blocking antibody (Right). Conditions shown are T-cells alone (Green), with sAg-loaded Raji (Grey) or with sAg-loaded Raji-CD155 (Red). **C)** Proliferation of CD8+ TIGIT^{INT}CD226^{LO} T-cells cultured with sAg-loaded Raji or Raji-CD155 B cells at a ratio of 10:1. Cells were cultured with either non-blocking isotype control antibody (IC N297S) or CD96 blocking antibody (19-134 N297S), and proliferation assessed at day 4. **D)** Representative histograms of CD8+ TIGIT^{INT}CD226^{LO} T-cell CFSE dilution when cultured with non-blocking antibody (Left) or CD96 blocking antibody (Right). Conditions shown are T-cells alone (Green), with sAg-loaded Raji (Grey) or with sAg-loaded Raji-CD155 (Red). (Data points are the mean of three technical replicates of 1 TIGIT^{HI}CD226^{LO} donor, ±SEM. 2-way ANOVA, ns= non-significant, * = $p < 0.05$, ** = $p < 0.005$)

Considering the inhibitory impact that target expression of CD155 has been found to exert on TIGIT^{INT}CD226^{LO} T-cell proliferation, determining whether this effect was reflected in T-cell cytokine release was investigated.

IL-2 release by TIGIT^{INT}CD226^{LO} T-cells in response to sAg-loaded Raji was noticeably reduced at 48 hours with respect to donor 3 TIGIT ^{LO} CD226^{HI} T-cells (Figure 5.9). Culture of T-cells with sAg-loaded Raji-CD155 and a non-blocking control antibody significantly reduced T-cell release of IL-2 with respect to sAg-loaded wild-type Raji co-culture. Co-culture with a CD96 blocking antibody significantly enhanced this reduction (Figure 5.12A). By 72 hours, total supernatant IL-2 had decreased, reflecting T-cell activation. As at 48 hours, the provision of Raji expressed CD155 with a non-blocking control antibody limited T-cell release of IL-2, whilst the blockade of CD96 further curbed IL-2 release.

As with IL-2 release, IFN-γ secretion was reduced with respect to donor 3 TIGIT ^{LO}CD226^{HI} T-cells. Co-culture with sAg-loaded Raji-CD155 limited IFN-γ release at 48 hours regardless of culture with non-blocking or CD96 blocking antibody (Figure 5.12B). By 72 hours, total supernatant IFN-γ increased substantially. As at 48 hours, target expression of CD155 significantly limited T-cell IFN-γ release. Antibody blockade of CD96 had negligible impact on IFN-γ release.

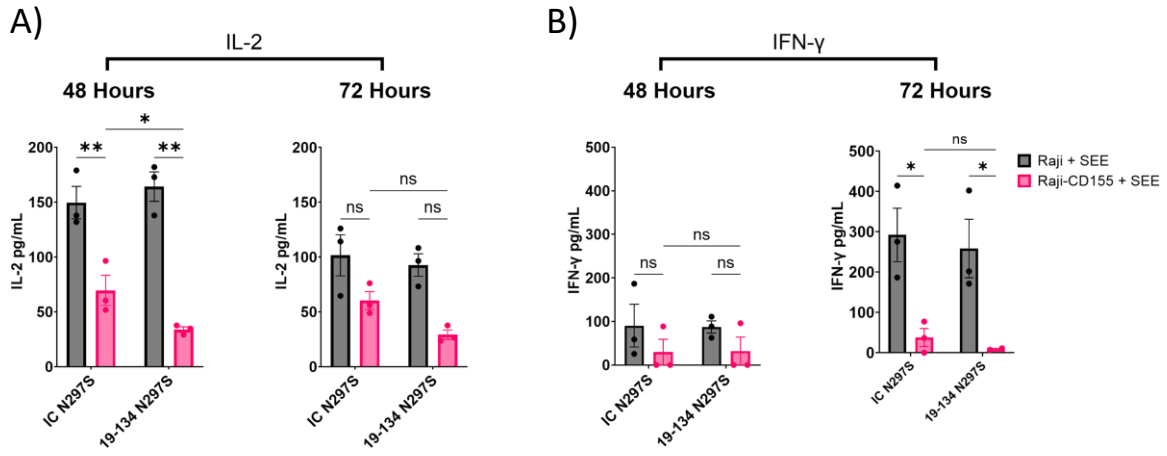

Figure 5.12 TIGIT^{INT}CD226^{LO} IL-2 and IFN-γ secretion is limited by CD155 provision and CD96 blockade

A/B) Supernatant was collected at 48 (A) or 72 hours (B) from isolated primary T-cells cultured with sAg-loaded Raji or Raji-CD155 with either non-blocking isotype control (IC N297S) antibody or CD96 blocking antibody (19-134 N297S). Supernatant IL-2 was quantified used ELISA and is presented as pg/mL. **C/D)** Supernatant IFN-γ was collected at 48 (A) or 72 hours (B) from isolated primary T-cells cultured with sAg-loaded Raji or Raji-CD155 with either non-blocking isotype control (IC N297S) antibody or CD96 blocking antibody (19-134 N297S). Supernatant IFN-γ was quantified used ELISA and is presented as pg/mL. (Data points are the mean of three technical replicates of 1 TIGIT^{INT}CD225^{LO} donor proliferation assay, ±SEM. 2-way ANOVA, ns= non-significant, * = $p < 0.05$, ** = $p < 0.005$)

These data from donor 2 T-cells exhibiting a $TIGIT^{INT}CD226^{LO}$ phenotype are in contrast to results from a donor with either a $TIGIT^{LO}CD226^{LO}$ (Donor 1) or $TIGIT^{INT}CD226^{HI}$ (Donor 3) phenotype. Whereas data examined previously highlighted a stimulatory role for the provision of Raji presented CD155, this data suggests that increased baseline T-cell expression of TIGIT may mediate an inhibitory signal that limits the upregulation and subsequent activity of both CD96 and CD226. As a result, T-cell proliferative responses to B-cell expression of CD155 are reduced.

5.6 CD96 blockade has limited impact on $TIGIT^{HI}CD226^{HI}$ T-cells

T-cells from donor 4 exhibited high baseline expression of both TIGIT and CD226 across both CD4+ (16.1 and 30.6%, respectively) and CD8+ T-cells (27.1 and 10.7%, respectively) with respect to our previous donors (Figure 5.3). As previous, determining how T-cell expression of CD96, TIGIT and CD226 was altered in response to sAg-mediated T-cell activation was first assessed, as well as the impact of B-cell CD155 expression.

As with each previous donor, initial CD96 expression was negligible across both CD4+ and CD8+ T-cells. CD4+ T-cell expression of CD96 increased substantially by day 5 in response to co-culture with both sAg-loaded wild-type Raji or Raji-CD155 (42.2 and 49.1%, respectively) (Figure 5.13A). CD96 upregulation on CD8+ T-cells similarly increased when cultured with sAg-loaded Raji or Raji-CD155, peaking at day 5 (23.9 and 41.6%, respectively) (Figure 5.13B). Upregulation of CD96 on either CD4+ or CD8+ T-cells cultured with unloaded target cells was limited, regardless of CD155 expression (Figure 5.13A/B).

Expression of TIGIT at day 0 on CD4+ T-cells (16.1%) was the highest across all phenotyped donors, while CD8+ TIGIT expression (27.1%) matched that of donor 2 (27.5%). CD4+ T-cell expression of TIGIT increased gradually over 5 days when cultured with either sAg-loaded Raji or Raji-CD155, resulting in similar TIGIT expression by day 5 (47.8% and 46.5%, respectively) (Figure 5.13C). TIGIT expression on CD8+ T-cells remained constant when cultured with sAg-loaded Raji cells, increasing after day 3. Conversely, TIGIT expression was marginally reduced by target expression of CD155, before expression increased after day 3. CD8+ T-cell TIGIT expression was similar by day 5 regardless of target CD155 expression (Raji: 58.7%, Raji-CD155: 61.6%) (Figure 5.13D). Culture with non-loaded Raji target cells had little impact on CD4+ or CD8+ TIGIT expression, while culture with non-loaded Raji-CD155 reduced both CD4+ and CD8+ surface TIGIT expression.

Baseline expression of CD226 on CD4+ T-cells was highest amongst all donors assessed (30.6%). CD4+ T-cell expression of CD226 was increased by day 5 in response to both sAg-loaded Raji (75%) or Raji-CD155 co-culture (74%) (Figure 5.13E). CD8+ T-cell expression of CD226 increased from day 3 in response to sAg-loaded Raji and Raji-CD155, likewise peaking at day 5 (Figure 5.13F). Both CD4+ and

CD8+ T-cells cultured with non-loaded Raji retained their expression of CD226, whereas T-cells cultured with non-loaded Raji-CD155 exhibited significant loss of CD226 expression.

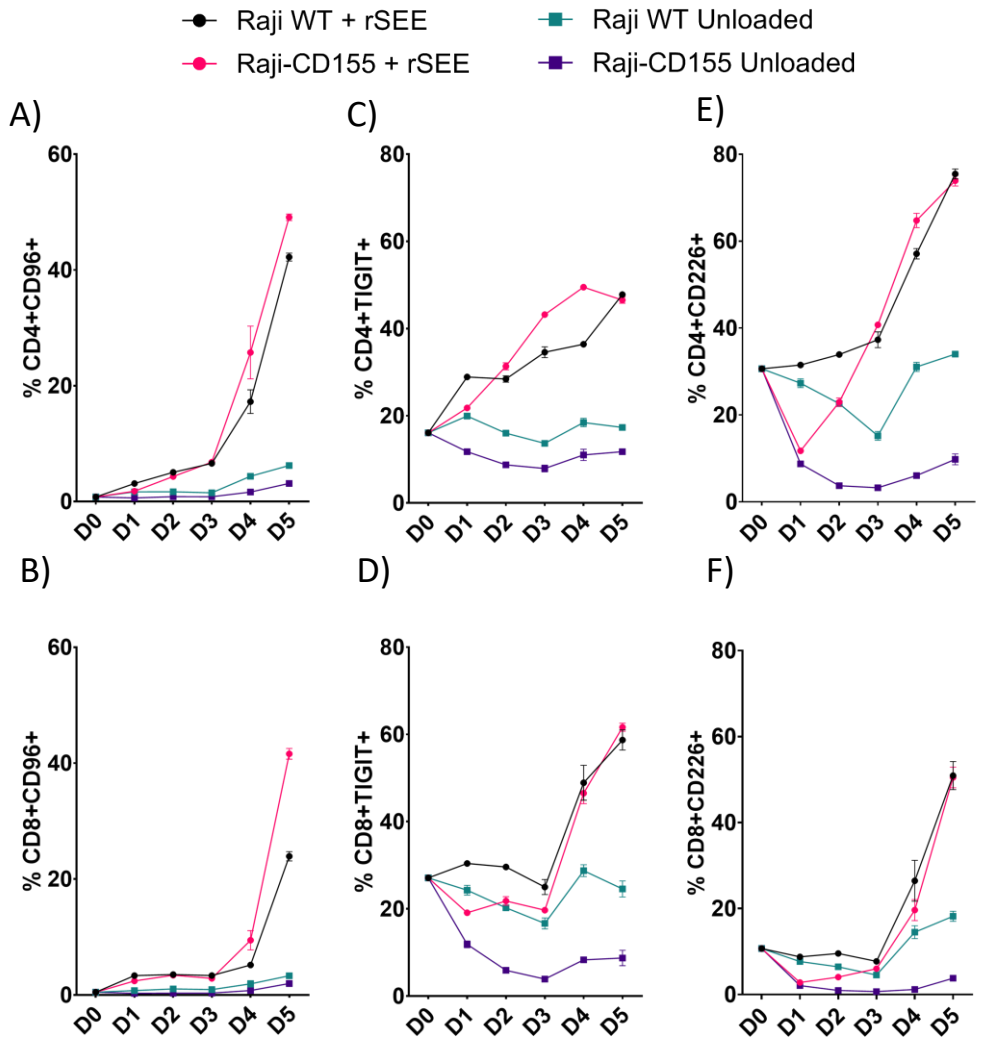

Figure 5.13 TIGIT^{HI}CD226^{HI} T-cells increase CD96 upregulation in response to target expression of CD155

A/B) Expression of CD96 on TIGIT^{HI}CD226^{HI} CD4+ (A) or CD8+ (B) T-cells cultured with sAg-loaded Raji (Black), sAg-loaded Raji-CD155 (Red), unloaded Raji (Green) or unloaded Raji-CD155 (Purple). Expression was assessed daily from day 0 to day 5 and is presented as a percentage of CD4+ or CD8+ T-cells. **C/D)** Expression of TIGIT on TIGIT^{HI}CD226^{HI} CD4+ (C) or CD8+ (D) T-cells cultured with sAg-loaded Raji (Black), sAg-loaded Raji-CD155 (Red), unloaded Raji (Green) or unloaded Raji-CD155 (Purple). Expression was assessed daily from day 0 to day 5 and is presented as a percentage of CD4+ or CD8+ T-cells. **E/F)** Expression of CD226 on TIGIT^{HI}CD226^{HI} CD4+ (C) or CD8+ (D) T-cells cultured with sAg-loaded Raji (Black), sAg-loaded Raji-CD155 (Red), unloaded Raji (Green) or unloaded Raji-CD155 (Purple). Expression was assessed daily from day 0 to day 5 and is presented as a percentage of CD4+ or CD8+ T-cells. (Data points represent three technical replicates ±SEM)

5.6.1 CD155-mediated TIGIT^{HI}CD226^{HI} T-cell proliferation is partially reliant on CD96

To understand how target expression of CD155 may impact the activation of TIGIT^{HI}CD226^{HI} T-cells, T-cells from donor 4 were co-cultured with sAg-loaded Raji or Raji-CD155 and the proliferation of CD4+ and CD8+ T-cells assessed at day 4.

TIGIT^{HI}CD226^{HI} CD4+ T-cell proliferation in response to sAg-loaded Raji cell co-culture was high, with 55.1% of CD4+ T-cell having undergone proliferation in the presence of a non-blocking control antibody. CD4+ T-cell proliferation was significantly increased when T-cells were co-cultured with sAg-loaded Raji-CD155 target cells with a non-blocking antibody (68.9%). The addition of a CD96 blocking antibody had no impact on the proliferation of CD4+ T-cell proliferation in response to wild-type Raji cells (56%), however culture with sAg-loaded Raji-CD155 target cells and a CD96 blocking antibody reduced proliferation of CD4+ T-cells to 61.5%. The decrease in proliferation when cultured with CD96 blocking antibody was not significant with respect to a non-blocking control antibody (Figure 5.14A/B).

TIGIT^{HI}CD226^{HI} CD8+ T-cell proliferation was also increased in response to sAg-loaded Raji co-culture (Figure 5.14C/D). Of CD8+ T-cells, 36.6% had undergone division in response to sAg-loaded Raji cells when cultured with a non-blocking control antibody, whilst Raji expression of CD155 significantly increased CD8+ proliferation to 48.5%. CD8+ T-cell proliferation in response to sAg-loaded Raji in the presence of a CD96 blocking antibody was similar to that of cells cultured with control antibody (33.5%). As with CD4+ T-cell proliferation, CD8+ T-cell proliferation was augmented by target expression of CD155 even when cultured with a CD96 blocking antibody (41.8%). However, this increase was significantly reduced with respect to culture with control antibody. Neither unloaded Raji or Raji-CD155 induced significant TIGIT^{HI}CD226^{HI} T-cell proliferation (Appendix 12).

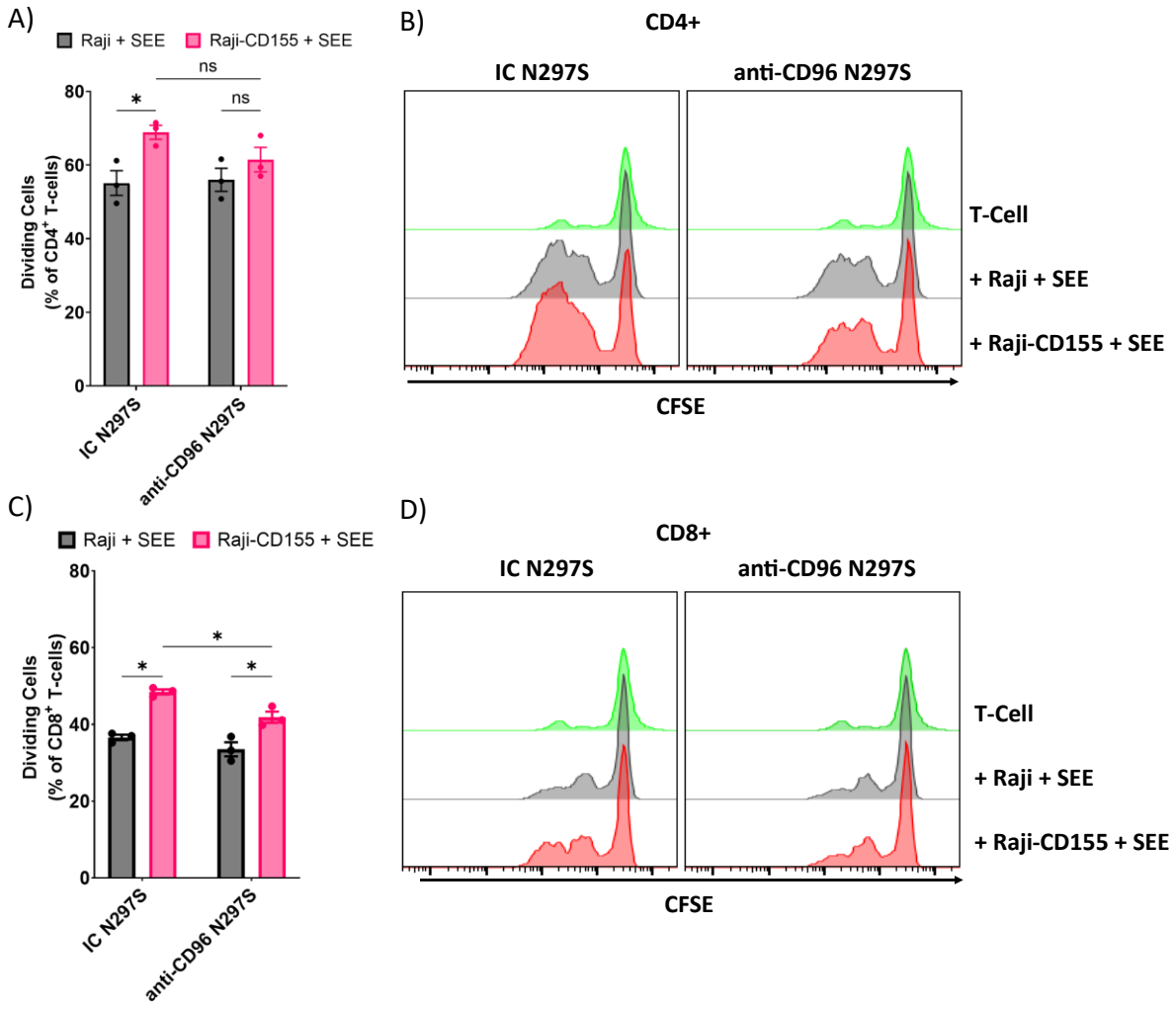

Figure 5.14 TIGIT^{HI}CD226^{HI} T-cell proliferation is not affected by CD96 blockade

A) Proliferation of CD4+ TIGIT^{HI}CD226^{HI} T-cells cultured with sAg-loaded Raji or Raji-CD155 B cells at a ratio of 10:1. Cells were cultured with either non-blocking isotype control antibody (IC N297S) or CD96 blocking antibody (19-134 N297S), and proliferation assessed at day 4. **B)** Representative histograms of CD4+ TIGIT^{HI}CD226^{HI} T-cell CFSE dilution when cultured with non-blocking antibody (Left) or CD96 blocking antibody (Right). Conditions shown are T-cells alone (Green), with sAg-loaded Raji (Grey) or with sAg-loaded Raji-CD155 (Red). **C)** Proliferation of CD8+ TIGIT^{HI}CD226^{HI} T-cells cultured with sAg-loaded Raji or Raji-CD155 B cells at a ratio of 10:1. Cells were cultured with either non-blocking isotype control antibody (IC N297S) or CD96 blocking antibody (19-134 N297S), and proliferation assessed at day 4. **D)** Representative histograms of CD8+ TIGIT^{HI}CD226^{HI} T-cell CFSE dilution when cultured with non-blocking antibody (Left) or CD96 blocking antibody (Right). Conditions shown are T-cells alone (Green), with sAg-loaded Raji (Grey) or with sAg-loaded Raji-CD155 (Red). (Data points are the mean of three technical replicates of 1 TIGIT^{HI}CD226^{HI} donor, ±SEM. 2-way ANOVA, ns= non-significant, * = $p < 0.05$)

As with each previous donor, supernatant from TIGIT^{HI}CD226^{HI} T-cell was collected at 48 and 96 hours and cytokine presence assessed utilising IL-2 and IFN-γ ELISA.

Supernatant collected at 48 hours from TIGIT^{HI}CD226^{HI} T-cells cultured with sAg-loaded Raji cells contained similar concentration of IL-2 regardless of the presence of a non-blocking control antibody or CD96 blocking antibody. T-cells secreted increased IL-2 when cultured with sAg-loaded Raji-CD155 in the presence of a non-blocking control antibody, however this increase was ablated when cultured

with CD96 blocking antibody (Figure 5.15A). Supernatant IL-2 at 96 hours was reduced with respect to 48 hours, indicative of increased T-cell activation. As with 48 hours, culture of TIGIT^{HI}CD226^{HI} T-cells with sAg-loaded Raji-CD155 increased IL-2 release over wild-type Raji when cultured with a non-blocking antibody. This increase in IL-2 secretion was ablated at 96 hours when cultured with a CD96 blocking antibody, as at 48 hours (Figure 5.15A).

As with IL-2, supernatant IFN-γ was quantified at both 48 and 96 hours (Figure 5.15B). Secretion of IFN-γ by TIGIT^{HI}CD226^{HI} T-cell was less clean than IL-2 at the same timepoints. At 48 hours, culture of T-cells with sAg-loaded Raji-CD155 and non-blocking isotype control antibody induced similar release of IFN-γ, however the blockade of CD96 increased IFN-γ secretion. At 96 hours, sAg-loaded Raji-CD155 induced similar increase of IFN-γ in the presence of a non-blocking antibody. However, the provision of a CD96 blocking antibody increased IFN-γ release induced by sAg-loaded Raji cells despite the lack of CD155. The provision of Raji-CD155 with CD96 blocking antibody reduced IFN-γ release with respect to wild-type Raji. No change in IFN-γ release between conditions was significant.

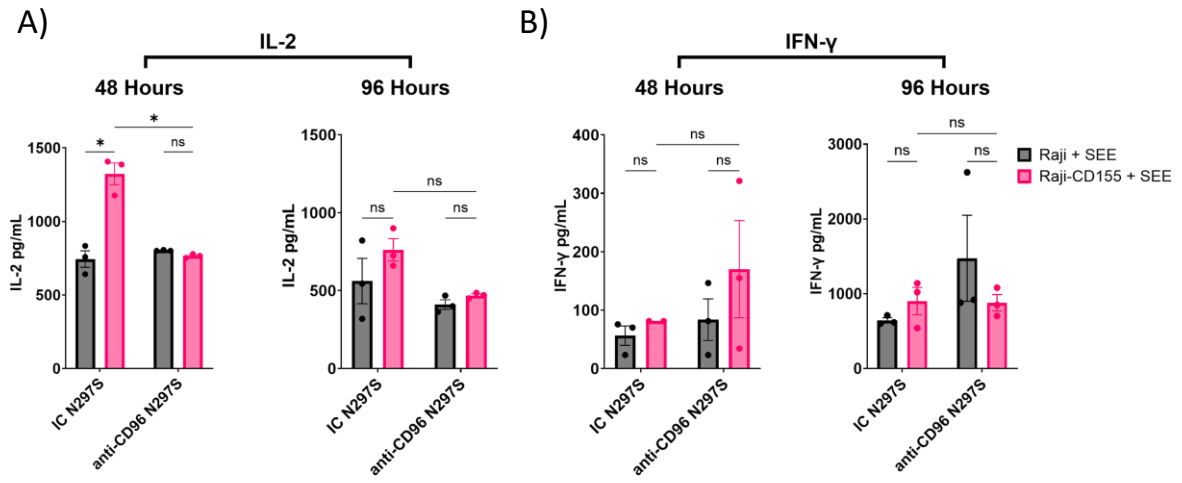

Figure 5.15 TIGIT^{HI}CD226^{HI} IL-2 release is promoted by CD96-CD155 interactions

A/B) Supernatant IL-2 was collected at 48 (A) or 96 hours (B) from isolated primary TIGIT^{HI}CD226^{HI} T-cells cultured with sAg-loaded Raji or Raji-CD155 with either non-blocking isotype control (IC N297S) antibody or CD96 blocking antibody (19-134 N297S). Supernatant IL-2 was quantified used ELISA and is presented as pg/mL. **C/D)** Supernatant IFN-γ was collected at 48 (A) or 72 hours (B) from isolated primary TIGIT^{HI}CD226^{HI} T-cells cultured with sAg-loaded Raji or Raji-CD155 with either non-blocking isotype control (IC N297S) antibody or CD96 blocking antibody (19-134 N297S). Supernatant IFN-γ was quantified used ELISA and is presented as pg/mL. (Data points are the mean of three technical replicates of 1 TIGIT^{HI}CD226^{HI} donor proliferation assay, ±SEM. 2-way ANOVA, ns= non-significant, * = $p < 0.05$)

5.7 Discussion

Previous work to determine the function of CD96 in human T-cells has focussed on the provision of targeted antibodies to induce T-cell activation. However, evidence for the interaction of CD96 with CD155 mediating a similar stimulatory response is limited. While the provision of a CD96 targeting antibody has been demonstrated both in literature and within this thesis to augment OKT3 induced T-cell activation, whether CD96 interaction with its cognate ligand provides a comparably stimulatory signal in the context of pMHC driven T-cell activation is unclear [167, 169]. To create a T-cell activation model more closely resembling that of the physiological process of T-cell activation, we have utilised the bacterial sAg SEE as an artificial peptide, allowing peptide presentation in the context of B-cell expressed MHC-II. To understand how the provision of CD155 during pMHC interactions may dictate T-cell activation, both wild-type Raji and Raji-huCD155 cells were utilised as APCs.

Notable of importance was variation of CD155 receptor expression on donors, resulting in donor-specific patterns of CD96, TIGIT and CD226 expression. Expression of CD96 was limited across all donors, therefore donors were phenotyped according to expression of TIGIT and CD226 on non-activated T-cells prior to co-culture (Figure 5.3). Given that CD96 expression across all donors was negligible prior to T-cell activation, a result mirrored in the original description of CD96 by Wang et al., initial T-cell interaction with CD155 is likely defined by T-cell expression of TIGIT and CD226 [153]. These phenotypic descriptions of donors are not absolute however and are based on expression relative to other donors assessed. Considering the varied expression of receptors across donors, analysis of proliferation was done on a donor-by-donor basis rather than the grouping donors to assess an overall response. Donor expression of TIGIT and CD226 across both CD4+ and CD8+ T-cells are summarised in Table 5.1, as well their given phenotype. Also highlighted is how the provision of Raji expressed huCD155 affected T-cell proliferation in the presence of a non-blocking control antibody. Of the four donors, Raji expression of CD155 augmented T-cell proliferation in three donors, whilst only acting to inhibit the activation of donor 2 T-cells with a $TIGIT^{INT}CD226^{LO}$ phenotype.

Table 5.1 Donor T-cell pre-activation phenotyping of TIGIT and CD226 expression

Expression of TIGIT and CD226 across CD4+ and CD8+ T-cells from the four donors utilised, as well as the given phenotype. Also listed is the stimulatory or inhibitory effect mediated by CD155 presence in presence of a non-blocking isotype antibody (IC).

Donor	CD4+ TIGIT %	CD4+ CD226 %	CD8+ TIGIT %	CD8+ CD226 %	Day 0 Phenotype	CD155 Effect (IC)
1	0.77	8.84	2.42	6.52	$TIGIT^{LO}CD226^{LO}$	Stimulatory
2	4.82	2.10	27.50	0.51	$TIGIT^{INT}CD226^{LO}$	Inhibitory
3	3.28	25.83	2.10	21.00	$TIGIT^{INT}CD226^{HI}$	Stimulatory
4	16.10	30.60	27.10	10.70	$TIGIT^{HI}CD226^{HI}$	Stimulatory

Important to consider during the analysis of these data is the consideration of T-cell subsets, notably that of memory T-cells present within circulating lymphocytes. Memory T-cells form an integral part of the adaptive immune system and are characterised by a low activation threshold with strong effector functionality. These cells recirculate through non-lymphoid tissue and therefore constitute a substantial proportion of donor PBMCs. Memory T-cells subsets such as T_{CM}, T_{EM} and T_{EMRA} are common amongst these circulating cells. Specifically of relevance is the T_{EMRA} T-cell subset, terminally differentiated CD8+ effector T-cells found to re-express CD45RA. T_{EMRA} cells exhibit strong cytotoxic capacity and the expression of exhaustion genes [211]. Phenotypic characterisation of T_{EMRA} cells has shown that gene and surface marker expression across this population of cells is not homogenous amongst donors, with expression of effector molecules associated with T-cell cytotoxicity being varied [212]. Analysis of T-cell subsets from melanoma patients found that the majority of T_{EMRA} cells were found within the group of T-cells expressing TIGIT, indicating that this subset of terminally differentiated T_{EMRA} may be resistant to activation by CD155 expressing target cells [213]. The specific subsets of donor T-cells was not assessed prior to their use in the co-culture assays described but is important to consider during their analysis.

Our initial study utilising T-cells from donor 1 sought to determine whether the provision of CD155 on sAg-loaded B-cells could augment T-cell activation, as well as the optimal ratio of effector T-cells to sAg-loaded target B-cells. At each E:T ratio assessed, it was found that sAg-loaded B-cells could activate $TIGIT^{LO}CD226^{LO}$ T-cells of donor 1, whilst the provision of CD155 could in fact augment T-cell proliferation (Figure 5.5, Figure 5.6). Interestingly however, the addition of a CD96 blocking antibody only limited CD155-mediated CD8+ T-cell proliferation at a high E:T ratio of 10:1 and had no impact on CD4+ T-cell proliferation at any ratio, or CD8+ T-cells at either a 1:1 or 5:1 ratio. The increased availability of CD155 at low co-culture ratios may allow for CD155 to outcompete the CD96 blocking antibody, enabling more frequent interaction with CD96. TIGIT binds CD155 with greatest affinity

with respect to CD96 and CD226. Co-culture at low ratios where available CD155 is likely to be saturating enables interaction with both TIGIT and CD226 when CD96 interaction is blocked. By reducing CD155 availability whilst blocking CD96, CD155 will preferentially interact with TIGIT over CD226 due to increased affinity.

Whilst the provision of CD155 augmented CD4+ T-cell proliferation in donor 1, blockade of CD96 did not impact proliferation at a ratio of 10:1 as it did with CD8+ T-cells. To explain this discrepancy, the differences between CD4+ and CD8+ T-cell expression of TIGIT and CD226 may be considered. The expression of CD226 on CD8+ T-cells was lower by day 4 than on CD4+ T-cells, whilst expression of TIGIT was increased. By blocking CD96 on CD8+ T-cells in the context of low CD155 availability, CD155 interactions are preferentially with TIGIT. This early work suggests that both ligand availability, as well as the specific pattern of receptor expression on T-cells, may heavily dictate T-cell responsiveness to target expression of CD155.

The next donor to be assessed was donor 3, which was characterised as $TIGIT^{INT}CD226^{HI}$. Considering that the activity of CD96 was only inhibited at a high ratio with donor 1, an E:T ratio of 10:1 was utilised. The upregulation of each receptor on $TIGIT^{INT}CD226^{HI}$ T-cells was more pronounced than that of donor 1, with high expression of each by day 4 across both CD4+ and CD8+ T-cells (Figure 5.7). Therefore, by blocking CD96, any redirection of CD155 to TIGIT or CD226 is likely to be primarily driven by ligand affinity for CD155 rather than cell surface abundance of receptor as with donor 1.

The blockade of CD96 on $TIGIT^{INT}CD226^{HI}$ T-cells ablated the CD155 mediated increase in T-cell proliferation (Figure 5.8). Interestingly, despite high relative expression, CD226 did not appear to promote T-cell activity when CD96 was blocked. Considering the inhibitory role of TIGIT coupled with the stimulatory role of CD226, it is plausible that their activity counteracts one another in the absence of CD96 to have limited tangible impact on T-cell proliferation. Worboys et al. have previously shown that TIGIT and CD226 coalesce together within the immune synapse during pMHC interactions, with TIGIT acting to disrupt the stimulatory signalling of CD226. This occurs through both direct competition for ligand, and the inhibition of CD226 homodimerisation within the TCR synapse [89, 206]. No evidence has been presented to suggest that it has any similar effect on CD96. In fact, CD96 is found to be excluded from the immediate TCR synaptic area [89]. Considering this, in the absence of CD96 signalling by antibody blockade, CD226 activity is likely ablated by high expression of TIGIT, limiting CD226-mediated T-cell activation.

The responsiveness of $TIGIT^{INT}CD226^{LO}$ T-cells from donor 2 was in direct contrast to both donors 1 and 3. Upregulation of CD155 receptors was limited across both CD4+ and CD8+ T-cells, whilst total proliferation of T-cells was reduced, potentially reflective of T-cells which are predominantly T_{EMRA} (Figure 5.10). A proportion of T_{EMRA} cells have been shown to primarily express TIGIT, often representing a subset which are terminally exhausted and less predisposed to activation [212, 214].

Considering these T-cells are TIGIT^{INT}, they may in fact fall into this reported spectrum of T-cells. Amongst both CD4+ and CD8+ T-cells, receptor upregulation was greatest when co-cultured with sAg-loaded wild-type Raji cells, suggesting that the early provision of CD155 to T-cells with a predominantly TIGIT phenotype may act to limit the upregulation of both CD96 and CD226, likely mediated by direct inhibition of TCR signalling by TIGIT [215]. Josefsson et al. have shown previously that TIGIT+ T-cells can mediate the downregulation of CD226, supporting this observation that CD226 upregulation is limited in TIGIT^{INT}CD226^{LO} T-cells [215].

The provision of CD155 on target B-cells was found to inhibit the proliferation of TIGIT^{INT}CD226^{LO} T-cells from donor 2 (Figure 5.11). Considering that TIGIT was the most predominant receptor across both CD4+ and CD8+ T-cells from donor 2 prior to B-cell co-culture, TIGIT interactions with target CD155 likely acted to impede TCR signalling. The addition of a CD96 blocking antibody mediated no substantial effect on this inhibition, however the upregulation of CD96 in response to sAg-loaded Raji-CD155 was limited. IL-2 secretion by TIGIT^{INT}CD226^{LO} T-cells by 24 hours was also inhibited by target expression of CD155. Interestingly however was that the blockade of CD96, even at this early time point where CD96 expression is limited, appeared to further inhibit IL-2 release (Figure 5.12). Considering the limited availability of CD155 at a 10:1 ratio, and limited expression of CD226, this result is likely driven by the redirection of available CD155 towards TIGIT as a result of its increased affinity.

Donor 2 represents the only donor T-cells to be clearly inhibited by B-cell expression of CD155. T-cell expression of TIGIT and concurrently low expression of CD226 is likely a contributing factor to this. Considering the expression of other key markers prior to T-cell co-culture would have been beneficial to gain a better understanding of how the specific T-cell subset may be responsible. This may have included assessing expression of both CD45RA and CCR7 to determine whether these TIGIT expressing T-cells in fact fall into the T_{EMRA} subset (CD45RA+CCR7-) [212]. Expression of PD-1 alongside TIGIT has been implicated in the suppression of CD8+ TILS [216]. Both of these molecules can act to inhibit CD226, and whilst our target Raji cells do not express the PD-1 ligands PD-L1/2, the expression of PD-1 alongside TIGIT may give an indication to the responsiveness of donor T-cells to activation.

Ligand upregulation and the subsequent proliferation of T-cells from our final donor, donor 4, was most similar to donors 1 and 3 than donor 2. Despite increased initial expression of TIGIT, CD96 upregulation was pronounced over the course of 5 days, with greater expression on CD4+ T-cells (Figure 5.13). This upregulation was likely due in part to increased expression of CD226 prior to T-cell activation, limiting the inhibitory impact of increased TIGIT expression. Interestingly, whilst the provision of CD155 mediated an increase in both T-cell proliferation and IL-2 release, blockade of CD96 did not limit T-cell proliferation as substantially as it did with donor 3 (Figure 5.12). Whilst proliferation of TIGIT^{HI}CD226^{HI} T-cells was reduced, CD155 provision still mediated an increase in

proliferation despite the inhibition of CD96, most notably on CD8+ T-cells. This result may be explained by the fact that upregulation of CD96 by day 4, the point that proliferation was assessed, was greater on CD4+ T-cells than CD8+ T-cells (Figure 5.13).

Previous evidence presented to suggest an inhibitory role for CD96 has primarily focused on its observed inhibition of mouse NK cell activation [154]. This work highlighted that CD96 knockout or blockade of the CD96:CD155 interaction in LPS or cytokine stimulated mouse NK cells alleviated CD155-mediated suppression of IFN-γ release but did not impact the capacity of primed NK cells to kill. Interestingly, this study found that NK expression of TIGIT *in vivo* had little impact on NK functionality. However, this work failed to consider the impact that co-expression of both TIGIT and CD226 may have when CD155 is provided as a target expressed ligand, or how by removing or blocking CD96 may mediate increased CD155 interaction with TIGIT. Similarly, this work relied on NK activation through external provision of LPS or cytokines, whereby CD96 interacts with CD155 outside of a typical TCR synapse. Considering that CD96 has been shown to require initial TCR activation to mediate antibody-induced T-cell activation, it would be of interest to determine whether providing an pMHC event and CD96:CD155 signal from two distinct cells would result in the inhibitory result recorded with NK cells, or whether increased spatial separation of CD96 from TCR would still result in T-cell activation.

Within this chapter, sAg-loaded Raji presentation of CD155 has been shown to both enhance and limit the proliferation and activation of human donor T-cells. Whilst initial expression of both TIGIT and CD226 may mediate some control over T-cell responses to CD155-mediated activation by directly acting upon the TCR to enhance or limit T-cell activity, response to CD155 was not homogenous amongst donors. T-cell phenotypes beyond their expression of CD155 receptors is certain to have a direct impact on their responsiveness to sAg-mediated activation, regardless of the provision of CD155. Circulating memory T-cells exhibiting an exhausted phenotype commonly express specific markers of exhaustion, including PD-1, LAG-3 and TIGIT [217]. Considering that expression of these markers was not assessed prior to the use of donor T-cells, it cannot be excluded that donor responsiveness to sAg, whether in the presence of CD155 or not, was not at least partially affected by the activation state of T-cells. To better understand the role of CD96 utilising this model of donor T-cell activation, a more expansive design would be beneficial. Concurrent blocking of both TIGIT and CD226 would allow a more in-depth investigation into the impact of CD96 activation on T-cell activation, allowing for CD155 interactions with CD96 to be independent of both TIGIT and CD226 signalling.

In conclusion, the blockade of CD96 on donor T-cells has been shown to limit T-cell proliferation in certain donors, however these results are potentially impacted by factors not assessed. As a result,

while these data indicate a role for CD96 in mediating the activation of human T-cells, further work is required to provide more conclusive evidence that accounts for other variables.

Chapter 6 Discussion

6.1 Developing a panel of novel anti-CD96 antibodies

The activation of T-cells is reliant on a broad and complex network of surface expressed immunostimulatory and inhibitory receptors which act to mediate control over T-cell responses. However, tumours can often evolve to promote an immunosuppressive TME, limiting both immune infiltration and cytotoxic activity. Ongoing research into therapeutics against checkpoint inhibitors such as PD-1 or CTLA-4 has resulted in a clinically successful class of immunomodulatory antibodies such as ipilimumab and nivolumab, acting to disrupt the inhibitory signalling mediated by both tumour and immunoregulatory cells [133, 134]. This class of antibodies has proven effective in the treatment of previously unresponsive cancers, however the lack of response in certain patients, or refractory response in others, has meant that the identification and targeting of new immune checkpoints is critical. Immunostimulatory antibodies represent a class of immunotherapeutics which aim to directly enhance immune responses against tumours by targeting immunostimulatory receptors. Urelumab, a huIgG4 mAb against hu4-1BB, has been shown extensively to augment T-cell activation. However, the clinical benefits of Urelumab, whether as a monotherapy or in combination with other immunotherapeutics, have been shown to be limited [137, 138]. Targeting of the OX40 receptor, a member of the TNF family of receptors upregulated on activated CD4+ and CD8+ T-cells, has been shown to enhance T-cell survival and proliferation following interaction with its ligand, OX40L [218]. Agonistic antibodies against OX40 have also been shown to enhance anti-tumour activity in some murine tumour models [219, 220]. These results targeting stimulatory receptors expressed on T-cells highlight both that immunostimulatory antibodies may be utilised to enhance immune responses against cancer, whilst also indicating that work exploring alternative targets is necessary.

CD96 forms an integral component of the TIGIT/CD96/CD226 network of receptors, each competing for interaction with APC and tumour expressed CD155. Whilst the role of TIGIT and CD226 as inhibitory or stimulatory receptors has been well documented, the function of CD96 within this signalling complex is less well defined. Within murine immunology, CD96 has been demonstrated to inhibit the activation of cytotoxic NK cells, limiting release of IFN-γ [154]. However, targeting of T-cell expressed CD96 utilising agonistic antibodies has highlighted that the receptor can in fact act to augment human T-cell proliferation. Data presented by Chiang et al. effectively demonstrated that the application of anti-CD96 antibodies could induce strong T-cell proliferation and cytokine release, whilst work by Rogel et al. highlighted that this result was in fact reliant on antibody cross-linking with FcγRI [167, 169]. Interestingly, limiting the activity of CD96 either by antibody blockade or genetic ablation impaired pro-inflammatory responses and diminished CD8+ T-cell responses in both

vaccination and *in vivo* tumour models [9]. As such, the work presented here sought to utilise phage-display panning to identify and generate a broader panel of antibodies against both human and mouse CD96, as well as a panel with pan-species specificity which could act to bind both human and mouse CD96 and therefore be utilised in both human and mouse assays. Considering the competition of the CD155 receptors for ligand binding, we also sought to identify non-blocking clones, with the aim of reducing TIGIT binding due to CD155 redirection.

The phage-display strategy utilised for identifying novel CD96 targeting scFv clones involved the panning of phage libraries first against recombinant human CD96v2 or mouse CD96, before further panning against newly generated RBL-CD96 cell lines. To identify scFv clones which would recognise both human and mouse CD96, a further round of panning against the opposite species was carried out. This strategy was successful in identifying a large number of scFv clones specific for human and mouse CD96, as well as a group specific to both. Panning against huCD96v2 generated a total of 37 reactive scFv clones, whilst the panning against mCD96 resulted in 18 reactive scFv clones, each with varied affinity for RBL-huCD96 or RBL-mCD96, respectively. Of the scFv clones found to bind either huCD96v2 or mCD96, we were able to identify only 2 of each which did not impede the binding of recombinant CD155. Further to this was the identification of 22 scFv clones which could bind both huCD96v2 and mCD96, of which all were found to impede both huCD155 and mCD155 binding.

Prior work seeking to better understand how the targeting of specific domains of immunostimulatory receptors may impact T-cell activation has found that antibody binding of the OX40 cysteine-rich domain 4 (CRD4) region induced greater agonistic activity with respect to binding of the CRD1-3 region, with antibody binding outside of the natural ligand binding site enhancing receptor functions, potentially as a combined result of ligand and antibody induced OX40 clustering [139, 221]. Conversely, antibodies targeting the CRD1 region of the co-stimulatory protein CD40 have been found to induce the strongest agonistic action, with T-cell activation decreasing as antibodies bind domains closer to the cell membrane [222]. The interaction of CD96 with CD155 is reported to utilise the most membrane distal domain of CD96, domain 1 [174]. Considering this, as well the reported importance of specific domain interactions by other immunostimulatory antibodies such as OX40 targeting antibodies, we wished to determine the specific domain interactions by these CD96 specific scFv clones.

Domain binding of huCD96 panned scFv clones was overwhelmingly specific to D1 of huCD96v2. This correlates with the observed blocking of huCD155 binding by the majority of scFv clones, whilst both of the two non-blocking scFv clones were in fact found to exhibit preference for D3 of huCD96v2. This result was mirrored by scFv clones panned against mCD96, with antibodies generated from mCD96 scFv clones showing a general preference for D1 of mCD96. Interestingly, the binding of antibodies generated from non-blocking scFv clones exhibited limited binding to recombinant

truncated mCD96. Of those scFv clones panned against both human and mouse CD96, all were found to show strong binding of D1, consistent with their CD155 blocking characteristic.

Of importance when considering the ability of scFv clones to not block CD96 is that both human and mouse CD96 are found to form homodimers in solution. This was shown by Lee et al., who used size exclusion chromatography with multi-angle light scattering (SEC-MALS) to show that the observed molecular weight of both human and mouse CD96 was twice the predicted monomeric value [223]. This result was also found with a truncated D1 of both human and mouse CD96, indicating that this dimerisation occurs through D1. This CD96 homodimer therefore dissociates to bind CD155, forming a CD96:CD155 heterodimer. Certain antibody clones have been shown to mediate the blocking of CD155 despite not binding D1, acting to inhibit the dissociation of CD96 homodimers and thereby blocking the formation of CD96:CD155 complexes [223]. This is thought to be a result of antibodies binding epitopes on two distinct CD96 molecules within a homodimer, effectively bridging the two receptors and limiting CD155 interaction.

Whilst certain scFv clones identified in Chapter 3 may in fact not block the interactions of CD96 with CD155 due to the binding of a single epitope, their conversion to IgG with two binding sites may subsequently result in the engagement of two CD96 molecules, inhibiting the separation of CD96 homodimers and therefore blocking CD155 binding (Figure 6.1). Retrospectively considering this, it would have been of benefit to assess the blocking of scFv clones following their conversion to IgG molecules.

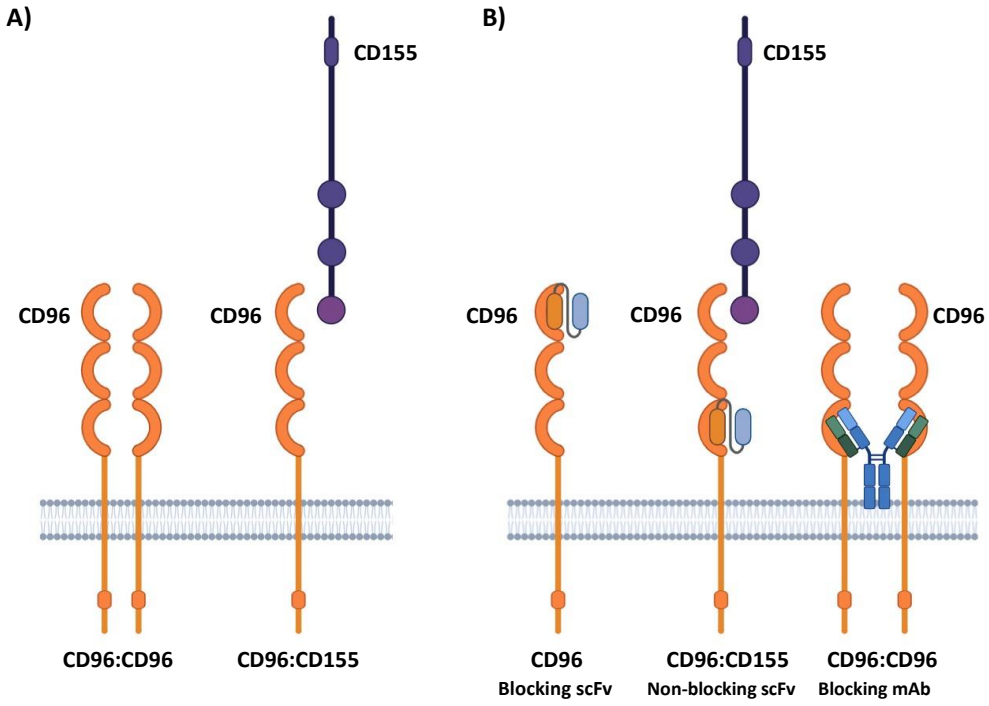

Figure 6.1 Schematic overview of CD96 dimerisation

A) Schematic overview of the homodimers formed between CD96 molecules and heterodimers formed between CD96 and CD155. **B)** Blocking scFv clones interacting with D1 of CD96 directly impedes CD155 binding by competition for domain interactions, whilst non-blocking scFv clones may bind outside of the CD96 D1 therefore allowing CD155 binding. Conversion of the same non-blocking scFv clone to an IgG antibody may allow for the inhibition of CD96 homodimer separation, indirectly blocking CD155 binding. Schematic is not to scale.

In an effort to determine the functional characteristics of CD96 targeting scFv clones, we assessed how those clones identified for their binding of both human and mouse CD96 may induce effective T-cell activation and proliferation when converted to huIgG1 antibodies and presented in a soluble or plate-bound format. Whilst each of these clones were found to impede the binding of CD155, evidenced by a lack of scFv binding to truncated recombinant CD96 lacking D1, assessing their ability to augment T-cell activity was imperative prior to use in future *in vivo* models. Across the panel of antibodies utilised in T-cell proliferation assays, targeting of huCD96 was found to augment T-cell proliferation. Proliferation induced by soluble CD96 with low OKT3 ranged from 25% to 50% of CD4+ and CD8+ T-cells, to 54% to 78% when cultured with high OKT3. Whilst this proliferation was comparable between soluble and plate-bound antibody, scFv affinity had greater impact when antibodies were provided as soluble molecules, with greater affinity inducing greater proliferation. This effect was more prominent in CD8+ T-cells than CD4+ (Figure 3.25).

Antibody isotype has been shown to be crucial in the design of OX40 targeting antibodies. Effective depletion of T_{reg} cells utilising OX40 antibodies has been found to be best suited for the use of a mIgG2a isotype. Interestingly, antibody depletion of OX40-expressing cells preferentially targeted T_{reg} cells due to their increased expression of OX40 over conventional T-cells [224]. Basal expression of CD96 on T_{reg} cells has been found to be also elevated, suggesting that a similar method of T_{reg} depletion using mIgG2a antibodies against CD96 could be implemented [169]. The action of OX40 mIgG1 and mIgG2a antibodies *in vivo* has however suggested that the use of mIgG2a antibodies, whilst efficient at T_{reg} depletion, resulted in poorer induction of T-cell memory responses. However, the use of a mIgG1 antibody against the most membrane proximal OX40 domain provided strong agonistic function whilst inducing similar depleting activity as mIgG2a. Targeting of this domain also ensured that interactions with OX40L were not impeded, potentially aiding agonistic functions. Considering these findings, a similar approach may be applied to CD96 antibodies. Whilst we have failed to identify non-blocking antibodies which bind both human and mouse CD96, two clones were identified as non-blocking for both groups of human or mouse panned scFv. Applying these to determine their capacity to both augment T-cell activation and mediate T_{reg} depletion would be of interest in future studies.

bsAbs represent a relatively new approach to antibody therapy and enable dual-targeting of TAAs and co-stimulatory receptors. B7-H3 is an immune checkpoint receptor, commonly upregulated on

tumours [225]. Extensive work has been carried out targeting the B7-H3 tumour antigen utilising bsAbs, inducing T-cell activation by also targeting activating receptors such as 4-1BB [143]. bsAbs against B7-H3 and PD-1 (B7-H3xPD-1) have also been highlighted to be superior to targeting of PD-1 alone, inducing greater IFN-γ release and ADCC [226]. Incorporating the scFv of CD96 specific antibodies into bsAbs targeting TAAs could represent a method of enhancing T-cell activity against tumours, whilst simultaneously augmenting activation by CD96 co-stimulation. Considering that CD96 has been found to correlate with expression of PD-1, utilising a PD-L1xCD96 bsAb may act to improve infiltrating T-cell potential. NI-3201 is a PD-L1xCD28 bsAb, targeting both PD-L1 and CD28 to block the PD-1/PD-L1 checkpoint whilst providing effective T-cell co-stimulation through CD28 activation [227]. Use of this bsAb enhanced effector functionality and induced effective tumour regression in an MC38 mouse model. Considering the requirement for CD96 cross-linking shown by Rogel et al., bsAbs represent a logical choice of antibody format [169]. In the absence of FcγR expressing cells, bsAbs could still mediate CD96 cross-linking and allow for effective CD96 priming of T-cells.

6.2 Understanding the signalling network utilised by CD96

The IgSF comprises a complex and interconnected network of proteins essential for regulating immune responses. Interactions between IgSF members and their cognate ligands mediate an aspect of the co-stimulatory signalling necessary for effective T-cell priming and activation. As a member of the IgSF, huCD96 has been shown - both in this thesis and in prior literature - to enhance T-cell activation. However, the specific signalling pathways it utilises remain unclear.

In contrast to CD96, the signalling pathways utilised by other IgSF members have been studied in greater detail. CD28, a well characterised co-stimulatory receptor on T-cells, interacts with CD80/86 on opposing APCs. A key motif within the ICD of CD28 is a PRD, and is found to contribute to effector functionality by enhancing TCR-mediated T-cell activation [228]. The presence of this PRD within the CD28 ICD is also found to be beneficial to the release of a number of cytokines in response to CD3/CD28 antibody cross-linking, including IL-2, IFN-γ and TNF-α [228].

Specific PRD consensus sequences have been shown to have preferential interactions with certain groups of kinases and their SH3 domains [157]. These consensus sequences have subsequently been grouped, giving PRDs distinct classes based both on their shared PxxP domains, and the kinase SH3 sites with which they interact. Interestingly, present within the ICD of both human and mouse CD96 are PRD classes I, II and III. Whilst the core PxxP region of PRDs defines the broad binding site for kinase SH3 domains, flanking residues mediate the effective interaction of kinases specific for different PRD classes. The presence of three distinct polyproline domains indicates that CD96 may utilise a number of kinases, each with preference for different PRD classes. Affinity of kinase SH3 sites for PRDs is also not consistent across classes, with kinase SH3 binding of class III PRDs being

much stronger than that of either class I or II, indicating that of the three domains, class III interactions may be the most significant [229]. In their research seeking to understand the preference of kinase SH3 domains for specific PRD classes, Teyra et al. defined a comprehensive list of SH3 containing kinases and their binding of each PRD class [158].

Within data presented in Chapter 4, CD96 T-cell activation is also found to be mediated through a PRD, whereby only a broad proline mutation encompassing each PRD class within CD96 ablated T-cell activation. Within the classification system described by Teyra et al., the kinase ITK was found to have preference for atypical PRD sequences, whilst previous work has indicated that ITK can in fact interact with a class II xPxPxxR/K PRD [190]. Interestingly, this very same consensus sequence is found within the ICD of both human and mouse CD96. Whilst we were unable to directly inhibit ITK utilising the small-molecule inhibitor Ibrutinib as a result of ITKs intrinsic involvement with CD3ζ signalling, further work would be beneficial to understand whether ITK binding of the CD96 PRD is a key trigger for T-cell co-stimulation.

Whilst data in Chapter 4 highlighted the key role of the huCD96 PRD, also present within the huCD96 ICD is a YxxM domain (YHEM), common to both the ICOS receptor (YMFM) and CD28 (YMNM). In CD28, the methionine residue has been shown to allow PI3K binding, suggesting a similar function for huCD96 [63]. Specificity for the binding of the adapter proteins GRB2 and GADS however has been shown to be reliant on the present of asparagine within the CD28 YxxM motif, a residue lacking in huCD96 [64]. Interestingly, whilst huCD96 contains a YxxM domain, mCD96 does not. Considering that antibody cross-linking of both mouse and human CD96 has been found to mediate T-cell activation, the YxxM domain is unlikely to be the primary contributor to CD96 co-stimulation [230]. However, this does not preclude the YxxM motif from contributing to the role of CD96 in human T-cells. As the consensus binding site for PI3K, the YxxM motif in human CD96 may contribute to other downstream functions not made clear by our approach. Interestingly however is that the activity of the kinase AKT was ablated by introducing a P4A mutation with respect to background CD3ζ signalling, indicating that activity of AKT is in fact mediated by the CD96 PRD. Considering that AKT is known to be activated by PI3K, this data may indicate that the YxxM domain of CD96 does not confer any advantage to CD96 in the context of PI3K/AKT signalling [231].

The results detailed in this work seeking to characterise the role of the CD96 ICD suggested that the presence of an inhibitory ITIM motif mediated no inhibitory effect, and that its mutation did not significantly impact T-cell activation. Notable is that the PRD of CD96 in fact overlaps with the ITIM consensus sequence (**I**K**Y**TC**I**). This overlap in binding could result in competition for kinase binding of the CD96 ICD, resulting in limited recruitment of phosphatases know to be recruited by ITIM domains such as SHP-1 or SHP-2. Likewise, it has been previously reported that ITIM consensus sites may in fact serve as sites of activation rather than inhibition. Recruitment of SHP-2 to the ITIM of the TREM-

like Transcript-1 (TLT-1) receptor was found to enhance FcεRI-mediated calcium signalling, indicating a potential role for ITIM sequences as acting to enhance co-stimulatory activity [232]. Considering the reported role of CD96 in mouse NK cells as an inhibitory receptor, where it has been shown to limit release of IFN-γ, this ITIM sequence is unlikely to simply be inactive [154]. Instead, its function may be entirely contextual, relying on intrinsic biological differences between T and NK-cells to instead mediate an inhibitory role. Considering this however, it should be noted that in western blot analysis of AKT activity, the mutation of the PRD in fact reduced AKT phosphorylation to below that of wild-type CD96 (Figure 4.20). This would imply that there is in fact an inhibitory function to CD96 in T-cells which is superseded by the actions of the PRD.

A valid critique of the technique employed to understand CD96 signalling within this thesis is the use of CAR-T to incorporate both the huCD96 and CD3ζ ICD into a single transmembrane protein, reliant on a single ligand interaction to mediate their activation. Physiologically, these two receptors are present as two transmembrane proteins, spatially separated from one another. The spatial organisation of CD96 with respect to CD3ζ in the context of an immune synapse has been briefly shown by Worboys et al., where CD96 was found to be excluded from the synaptic junction [89]. This was in direct contrast to both TIGIT and CD226, which were instead found to coalesce with CD3ζ within the immune synapse. By placing CD96 within such close proximity to CD3ζ, it is likely that the two may act upon one another, mediating signal cross-talk that would in fact not occur were the two spatially distinct. ZAP-70 recruited to the ITAM domains of CD3ζ is known to activate the ITK kinase as part of TCR signalling. Should ITK be recruited to the CD96 PRD as is suggested by kinomics data presented within Chapter 4, by bringing both CD96 and CD3ζ into such close proximity as a single molecule it is likely that active ZAP70 may act upon PRD recruited ITK.

The final results presented within Chapter 4 investigated how the use of a CD96 CAR compared against that of a 4-1BB CAR in primary human T-cells. Interestingly, whilst expansion of 96ζ T-cells was not significantly different than that of either BBζ or ζ T-cells, both the killing of target cells and release of pro-inflammatory cytokines was reduced (Figure 4.24, Figure 4.25). In NK cells, CD96 has been found to limit release of IFN-γ, however whilst IFN-γ release by CAR-96ζ T-cells was reduced with respect to CAR-BBζ, it was not significantly different to that of CAR-ζ. A key aspect of CAR-T design and the incorporation of specific ICDs is the formation of persistent memory CAR-T cells, enabling long-lasting populations of CAR-T to mediate sustained disease remission [233]. Whilst the incorporation of the CD28 ICD into CAR-T designs can be effective, a single mutation within the CD28 YxxM motif from YMNM to YNFM has been found to enhance persistence of CAR-T cells, indicating that even minor changes to CAR design can have beneficial effects [234]. Whilst the YxxM motif of CD96 appeared to have no substantial impact on the function of the CD96 ICD in J-CAR cells (Figure 4.10), its role may in fact extend beyond initial activation of T-cells and therefore be beneficial in the context of sustained CAR-T persistence. The long-term persistence of CAR-T cells utilising the CD96

ICD was not assessed within this work, however how CD96 may impact this would be of interest given current limitations to CAR therapy. Exhaustion of CAR-T cells can be mediated by tonic signalling in the absence of a scFv ligand, often resulting from receptor aggregation. Interestingly, we found that J-CAR expressing a 96ζ CAR had reduced background expression of CD69, a potential indicator that tonic signalling was reduced in CAR-T utilising the CD96 ICD. Going forward with the use of 96ζ CAR, it would be beneficial to understand how 96ζ CAR impacts the long-term health and function of T-cells.

6.3 The role of CD96 within the TIGIT, CD96, and CD226 network

T-cells rely on the expression of both co-stimulatory and inhibitory receptors to regulate their effector functions. These receptors help mediate T-cell activity, ensuring effective immune control over tumours. However, the complex interactions between these receptors make it challenging to fully understand their roles. Work to understand the physiological role of CD96 beyond that of clinical antibody targeting has been limited in literature, therefore we sought to understand how the provision of target cell expressed CD155 would affect the activation of effector cells.

Recent work has shown that cytotoxic CD8+ T-cells can uptake CD155 from target cells through tragocytosis, a process found to be mediated predominantly by CD96 over both TIGIT and CD226 [235]. This process of ligand removal has been suggested to occur in other immunoreceptors such as PD-1 and CTLA-4 [236, 237]. This removal of CD155 from target cells may imply that the role of CD96 is to modulate T-cell responses, limiting ligand availability for other binding partners. The functional role of tragocytosed CD155 in T-cells remains unclear, however CD155 does contain intrinsic signalling motifs which may allow for non-conventional T-cell signalling should it be re-expressed on T-cells [238, 239].

The interaction between CD28 and CD80/86, as well as the competition of CD28 with CTLA-4 for binding, is well documented in the literature and represents signal 2 in the T-cell activation model. Both CD28 and CTLA-4 belong to the same immunoglobulin superfamily (IgSF) as CD96, with their shared ligands, CD80/86, also expressed on APCs. CTLA-4 is upregulated upon T-cell activation, analogous to the late expression of CD96 following TCR activation [153]. CTLA-4 inhibition of TCR signalling is thought to partially involve a YxxM domain (YVKM) and the recruitment of the phosphatase SHP-2, inhibiting the activity of ZAP70 and downstream NFκB activation [240]. Recruitment of SHP-2 to CTLA-4 is in fact reliant on Src family member kinases such as FYN and LCK, which act to phosphorylate the CTLA-4 YxxM domain [241].

As well as a shared YxxM motif, CD28, CTLA-4 and CD96 each contain polyproline regions. The CTLA-4 PRD has been found to recruit the JAK2 kinase, mediating phosphorylation of a neighbouring tyrosine (Y_{165}) residue [242]. Whilst JAK2 activity was augmented by 96ζ signalling, activity was not impacted by either PRD mutation (Chapter 4). Conversely, upregulation of JAK3 activity was ablated by PRD mutations, implicating potential JAK3 recruitment to the CD96 PRD (Chapter 4). The CD28 PRD has been implicated in the CD28 co-stimulatory role, with LCK recruited by SH3 domains. Interestingly however is that LCK activity was reduced by 96ζ signalling, with this reduction ablated following both PRD mutations. Considering that the CD96 PRD has been found to potentially utilise the ITK kinase, this data may indicate that the CD96 PRD also acts to limit CD3ζ mediated LCK activation, implicating a role for CD96 both augmenting and inhibiting distinct aspects of the TCR signalling pathway.

CD96 competes for binding of CD155 with both TIGIT and CD226, with TIGIT having the greatest affinity and CD226 the lowest (TIGIT: K_D = 3.15 nM, CD96: K_D = 37.6 nM, CD226: K_D = 119 nM) [88]. However, the contribution of each receptor to mediating T-cell activation assumes that each would be expressed equally. The data presented here highlights that expression of each receptor is varied amongst donors, but that expression of CD96 across all donors prior to activation is negligible. This may suggest that the initial activation of T-cells interacting with CD155-expressing target cells is defined by their expression of either TIGIT or CD226. Much like CD96, CTLA-4 expression is induced following activation on conventional T-cells, though more rapidly than the 3-4 days associated with CD96 upregulation [153, 243]. Regardless of an intrinsic stimulatory role, increased CD96 expression following T-cell activation would provide increased competition for TIGIT binding of CD155. CD96 is found to be excluded from the immune synapse, potentially removing CD155 available within the synaptic region available for TIGIT engagement and therefore curbing the actions of both the ITT and ITIM domains within the TIGIT ICD [89]. This exclusion of receptors from the immune synapse is not unique to CD96. The tyrosine phosphatase CD45 is also excluded from the immune synapse and has been implicated in both aiding and inhibiting TCR activation. CD45 has been found to inhibit CD3ζ phosphorylation induced by low-affinity antigens, but augment signalling induced by high-affinity antigens by in fact activating LCK [244]. CD96 exclusion from the synapse could indicate a similar role, both removing CD155 available to TIGIT from the synapse whilst mediating the intrinsic signalling indicated within this thesis.

Whilst the aim of using CD155 expressing APCs was to achieve a more physiological model system, this fails to consider the interaction of CD96 with its second ligand, Nectin-1 (CD111). Whilst the affinity of CD96 for CD111 is significantly lower compared to that of CD155, the addition of a second potential ligand for CD96 increases the complexity of the TIGIT/CD96/CD226 network. Work to understand CD111 interactions with CD96 found that expression of huCD111 increased susceptibility of target cells to NK cell cytotoxicity, indicating that despite decreased affinity for CD96, CD111 is still capable of promoting CD96-mediated NK cytotoxicity [245].

Considering the co-expression of TIGIT, CD96 and CD226, more in depth analysis of how their interactions with CD155 may affect one another would have been beneficial to advance our understanding. Concurrent blockade of both TIGIT and CD226 would have provided a stronger argument for the intrinsic role of CD96 in mediating T-cell activity, allowing for the isolation CD96 activity. Blockade of CD96 has indicated a stimulatory role, however this has inevitably resulted in CD155 redirection towards TIGIT, potentially skewing the interpretation of results. Utilising the same model system but blocking other receptors for CD155 would provide valuable evidence for understanding the role of CD96 in the context of other competing receptors.

6.4 Future work and concluding remarks

This project aimed to provide greater understanding to the role of CD96 in the activation and functionality of T-cells. Current approaches to enhancing immunostimulatory antibody therapy have focussed on co-stimulatory receptors such as 4-1BB, OX40 and CD27, however broadening the availability of immunostimulatory antibody therapies available to patients is imperative. A greater understanding of the CD96 mechanisms of action will allow for a stronger argument for utilising CD96 as an immunotherapeutic target.

This work has presented strong evidence, using multiple approaches and methodologies, that CD96 functions as a co-stimulatory receptor in human T-cells. Studies supporting CD96's activating role often involve antibody cross-linking of CD96 and CD3, shown to enhance T-cell proliferation and promote the release of pro-inflammatory cytokines. The identification of a broad panel of novel anti-CD96 antibodies, targeting human, mouse, and pan-species, has enabled the development of antibodies with diverse receptor affinities, blocking capacities, and, in some cases, the ability to avoid ligand interference. Advancing these antibodies into preclinical development will allow for a thorough assessment of their potential as immunostimulatory agents.

Currently, only one CD96-targeting antibody, Nelistotug (huIgG1, GSK6097608), has entered clinical trials. Developed by GSK, it is in Phase 2 trials for patients with recurrent head and neck squamous cell carcinoma. Nelistotug is designed as an antagonistic antibody to block the CD96-CD155 interaction [172, 175]. However, whether blocking CD96 is the optimal strategy remains uncertain, as findings from this thesis suggest that CD96's interaction with CD155 may actually be stimulatory. Antibodies generated against OX40 have indicated that binding of non-blocking domains in fact enhances antibody agonistic activity, likely driven by allowing for OX40-OX40L interactions. Considering the competition of CD155 receptors for binding of ligand, a non-blocking antibody would likely be beneficial. By using a CD96 blocking antibody, CD155 is likely to in fact be redirected to bind TIGIT due to its higher affinity for CD155. Irrespective of the agonistic actions of a CD96 antibody, CD155 interaction with TIGIT would be detrimental to achieving T-cell activation. Further work to characterise the role of this antibody panel may benefit from utilising a CD155 expressing tumour line for *in vivo* models.

Work by Rogel et al. highlighted the requirement of FcγR-mediated antibody crosslinking when targeting CD96 [169]. The dual-targeting of the TAA B7-H3 and co-stimulatory receptors commonly utilise bsAbs, allowing receptor cross-linking independent of FcγRs [143]. Utilising a B7-H3xCD96 bsAb may allow for the required cross-linking of T-cell expressed CD96, enabling the activation of T-cell effector functions against B7-H3 expressing tumour cells. As with the design of mAbs against CD96,

utilising a non-blocking scFv for CD96 targeting bsAbs is likely to be advantageous, limiting CD155 redirection.

By utilising a CAR model in Jurkat T-cells combined with a kinomics platform, we have constructed a predictive signalling map for human CD96 (Figure 4.27). Our findings indicate that the ITK kinase, which has been shown to directly interact with other polyproline consensus sequences also found within the CD96 ICD, is activated by CD96. Additionally, PAK1, a kinase targeted by ITK and essential for cytoskeletal remodelling and cell survival, was also found to be activated by CD96. Further downstream, members of the MAPK family such as MAPK8, MEKK1 and MEK1 and ERK were identified as being activated by CD96 signalling. Whilst this kinase activation cascade was predicted using PamGene UKA, further confirmation of their activity is necessary. Although ITK appears to be recruited to the CD96 PRD, additional work is needed to confirm the hypothesis of its direct physical association with CD96. Similarly, broader analyses using western blotting and targeted small-molecule inhibitors may help validate the roles of downstream kinases.

Whilst we have been able to build a predictive signalling map for CD96 in the Jurkat human T-cell like utilising CARs, how this is applicable to primary T-cells remains to be seen. Caveats in the use of both CAR-T as a model system, as well as the use of Jurkat T-cells, have been examined here. Activation of J-CAR cells using BBζ and 96ζ found similar secretion of cytokines by both CARs, yet their use in primary T-cells highlighted a disparity between the two. This difference indicates that the signalling of CD96 in Jurkat T-cells is likely to be different than that of primary T-cells. Going forward, a similar approach of assessing the kinase activation of CD96 CARs may be beneficial but using primary T-cells in place of immortalised cell lines. CD96 activation of Jurkat T-cells has been shown here to be almost exclusively reliant on the presences of a polyproline domain, concurrent with the role of PRDs within other co-stimulatory receptors such as CD28 and ICOS. However, both these receptors have secondary domains that are involved. Considering this, discounting the role of both the ITIM and YxxM domains from the function of CD96 may be premature.

The formation of specific T-cell subsets such as T_{EM} (CD45RO+CD62L-) following CAR-T activation is crucial to providing longevity protection. This differentiation is dependent on the specific ICDs employed in the design of engineered receptors and is often attributed to specific domains within the utilised ICDs. Initial expansion of primary CAR-T appeared not to be negatively affected by the use of the CD96 ICD, though targeted killing was slightly reduced. Use of the PRD, ITIM, and YxxM mutations utilised for J-CAR analysis with primary T-cells may allow further understanding of how these domains contribute to CD96 signalling. Likewise, more longitudinal studies assessing how the use of a CD96 CAR-T affects the formation of long-lasting memory T-cells may provide evidence for how CD96 CAR differs from that of 4-1BB CAR.

Second generation CAR-T utilise a single co-stimulatory domain with CD3ζ and have been employed here [246, 247]. However, different approaches are being employed to improve both the cytotoxic anti-tumour effects of T-cells as well as increase their release of pro-inflammatory cytokines. Third generation CARs which couple multiple co-stimulatory domains, such as combining both ICOS and 4-1BB with CD3ζ, have been found to enhance T-cell survival as well as improve their *in* vivo expansion [248]. Likewise, combining the OX40 and CD28 ICD with CD3ζ is found to enhance cell survival, with sustained effector functionality [249]. Considering the similarities between ICOS and CD96, both as IgSF members containing key stimulatory motifs, combining CD96 with 4-1BB as a third generation CAR may also be beneficial. Release of IL-12 within the TME by DCs has been shown extensively to recruit members of the innate immune system. Fourth generation CAR designs utilise inducible gene expression of IL-12 upon target recognition, subsequently enhancing the release of IFN-γ and improving T-cell cytotoxicity [59, 106]. Combining these factors with the ICD of CD96 could improve the potential of CAR-T, improving cytotoxicity and enhancing the long-term protection offered by CAR-T therapy.

Understanding the interaction of CD96 with CD155 is complicated by the competition for binding with both TIGIT and CD226. Expression of both these receptors was found to be varied amongst donors and therefore had significant impact on how the blockade of CD96 impacted T-cell activation by CD155. The late upregulation of CD96 and its capacity to outcompete CD226 would suggest that it plays a similar role as CTLA-4 does in mediating inhibition of CD28, yet despite this, both antibody targeting of CD96 as well as the use of CD96 CAR-T imply an activating role. Considering that both of these approaches fail to consider the presence of environmental CD155 and its interaction with both TIGIT and CD226, the physiological role of CD96 is better represented by the SEE model used within Chapter 5. However, in attempting to understand the action of CD96, this model is convoluted by co-expression of the competing receptors and the redirecting of ligand by blocking antibodies.

Using a panel of blocking antibodies against each CD155 receptor would provide a greater understanding of their individual contributions to SEE-mediated T-cell activation and their interdependence. Given that current clinical trials for CD96-targeting therapies primarily use blocking antibodies, these findings suggest that blocking CD96 may not be the most effective approach [172]. Although the antibody used in this study was Fc-engineered to prevent Fc-FcγR interactions, further research using the SEE model with both blocking and non-blocking antibodies in Fc-competent clones could offer greater insight into the clinical suitability of targeting CD96. Additionally, combining a TIGIT-blocking antibody, such as Tiragolumab, with a non-blocking agonistic CD96 antibody could enhance therapeutic efficacy [250]. This strategy may improve T-cell activity by both blocking TIGIT's inhibitory function and redirecting CD155 to CD96 and CD226. Furthermore, activating CD96 while preserving CD155 binding may prove beneficial. A similar approach using non-blocking agonistic

OX40 antibodies has been shown to enhance OX40-mediated T-cell activation, possibly by promoting receptor clustering. Applying this strategy to CD96 could yield comparable benefits.

Taken together, the data presented in this thesis provide a strong foundation for presenting CD96 as a co-stimulatory receptor on human T-cells. Using both CD155-dependent and CD155-independent methods, we have demonstrated that CD96 enhances T-cell activation by amplifying key signalling cascades essential for T-cell function. Additionally, blocking CD96 activity in primary T-cells was shown to inhibit CD155-mediated activity. This work provides evidence that targeting CD96 with immunotherapeutics has the potential to expand the treatment options available to patients.

Bibliography

1. Xu D and Lu W. Defensins: A Double-Edged Sword in Host Immunity. *Front Immunol* 2020; 11: 764. 2020/05/28. DOI: 10.3389/fimmu.2020.00764.

2. Janeway CA Jr TP, Walport M, et al. *Immunobiology: The Immune System in Health and Disease. 5th edition.* New York: Garland Science, 2001.

3. Dunkelberger JR and Song W-C. Complement and its role in innate and adaptive immune responses. *Cell Research* 2010; 20: 34-50. DOI: 10.1038/cr.2009.139.

4. Sarma JV and Ward PA. The complement system. *Cell Tissue Res* 2011; 343: 227-235. 2010/09/15. DOI: 10.1007/s00441-010-1034-0.

5. Duan T, Du Y, Xing C, et al. Toll-Like Receptor Signaling and Its Role in Cell-Mediated Immunity. *Front Immunol* 2022; 13. Review. DOI: 10.3389/fimmu.2022.812774.

6. Akira S, Uematsu S and Takeuchi O. Pathogen recognition and innate immunity. *Cell* 2006; 124: 783-801.

7. Ozato K, Tsujimura H and Tamura T. Toll-like receptor signaling and regulation of cytokine gene expression in the immune system. *Biotechniques* 2002; Suppl: 66-68, 70, 72 passim. 2002/10/25.

8. Geissmann F, Manz MG, Jung S, et al. Development of monocytes, macrophages, and dendritic cells. *Science* 2010; 327: 656-661. 2010/02/06. DOI: 10.1126/science.1178331.

9. Satpathy AT, Kc W, Albring JC, et al. Zbtb46 expression distinguishes classical dendritic cells and their committed progenitors from other immune lineages. *J Exp Med* 2012; 209: 1135-1152. 2012/05/23. DOI: 10.1084/jem.20120030.

10. Sichien D, Scott CL, Martens L, et al. IRF8 Transcription Factor Controls Survival and Function of Terminally Differentiated Conventional and Plasmacytoid Dendritic Cells, Respectively. *Immunity* 2016; 45: 626-640. 2016/09/18. DOI: 10.1016/j.immuni.2016.08.013.

11. van Mierlo GJ, Boonman ZF, Dumortier HM, et al. Activation of dendritic cells that cross-present tumor-derived antigen licenses CD8+ CTL to cause tumor eradication. *The Journal of Immunology* 2004; 173: 6753-6759.

12. Binnewies M, Mujal AM, Pollack JL, et al. Unleashing Type-2 Dendritic Cells to Drive Protective Antitumor CD4+ T Cell Immunity. *Cell* 2019; 177: 556-571.e516. DOI: 10.1016/j.cell.2019.02.005.

13. Cella M, Facchetti F, Lanzavecchia A, et al. Plasmacytoid dendritic cells activated by influenza virus and CD40L drive a potent TH1 polarization. *Nature immunology* 2000; 1: 305-310.

14. Barchet W, Cella M, Odermatt B, et al. Virus-induced interferon α production by a dendritic cell subset in the absence of feedback signaling in vivo. *J Exp Med* 2002; 195: 507-516.

15. Wynn TA, Chawla A and Pollard JW. Macrophage biology in development, homeostasis and disease. *Nature* 2013; 496: 445-455. 2013/04/27. DOI: 10.1038/nature12034.

16. Sehgal A, Irvine KM and Hume DA. Functions of macrophage colony-stimulating factor (CSF1) in development, homeostasis, and tissue repair. *Semin Immunol* 2021; 54: 101509. 2021/11/08. DOI: 10.1016/j.smim.2021.101509.

17. Murray PJ, Allen JE, Biswas SK, et al. Macrophage activation and polarization: nomenclature and experimental guidelines. *Immunity* 2014; 41: 14-20.

18. Qian B-Z and Pollard JW. Macrophage diversity enhances tumor progression and metastasis. *Cell* 2010; 141: 39-51.

19. Williams MR, Azcutia V, Newton G, et al. Emerging mechanisms of neutrophil recruitment across endothelium. *Trends Immunol* 2011; 32: 461-469. 2011/08/16. DOI: 10.1016/j.it.2011.06.009.

20. Mol S, Hafkamp FMJ, Varela L, et al. Efficient Neutrophil Activation Requires Two Simultaneous Activating Stimuli. *Int J Mol Sci* 2021; 22 2021/09/29. DOI: 10.3390/ijms221810106.

21. Hayashi F, Means TK and Luster AD. Toll-like receptors stimulate human neutrophil function. *Blood* 2003; 102: 2660-2669.

22. Monteith AJ, Miller JM, Maxwell CN, et al. Neutrophil extracellular traps enhance macrophage killing of bacterial pathogens. *Sci Adv* 2021; 7: eabj2101. 2021/09/14. DOI: 10.1126/sciadv.abj2101.

23. Ponzetta A, Carriero R, Carnevale S, et al. Neutrophils Driving Unconventional T Cells Mediate Resistance against Murine Sarcomas and Selected Human Tumors. *Cell* 2019; 178: 346-360.e324. DOI: 10.1016/j.cell.2019.05.047.

24. Canli Ö, Nicolas AM, Gupta J, et al. Myeloid cell-derived reactive oxygen species induce epithelial mutagenesis. *Cancer cell* 2017; 32: 869-883. e865.

25. Wolf NK, Kissiov DU and Raulet DH. Roles of natural killer cells in immunity to cancer, and applications to immunotherapy. *Nature Reviews Immunology* 2023; 23: 90-105. DOI: 10.1038/s41577-022-00732-1.

26. Hewitt EW. The MHC class I antigen presentation pathway: strategies for viral immune evasion. *Immunology* 2003; 110: 163-169. 2003/09/27. DOI: 10.1046/j.1365-2567.2003.01738.x.

27. Braud VM, Allan DS, O'Callaghan CA, et al. HLA-E binds to natural killer cell receptors CD94/NKG2A, B and C. *Nature* 1998; 391: 795-799.

28. Bhatnagar N, Ahmad F, Hong HS, et al. FcγRIII (CD16)-mediated ADCC by NK cells is regulated by monocytes and FcγRII (CD32). *European journal of immunology* 2014; 44: 3368-3379.

29. Bauer S, Groh V, Wu J, et al. Activation of NK cells and T cells by NKG2D, a receptor for stress-inducible MICA. *science* 1999; 285: 727-729.

30. Hayes SM, Li L and Love PE. TCR Signal Strength Influences αβ/γδ Lineage Fate. *Immunity* 2005; 22: 583-593. DOI: https://doi.org/10.1016/j.immuni.2005.03.014.

31. Washburn T, Schweighoffer E, Gridley T, et al. Notch activity influences the alphabeta versus gammadelta T cell lineage decision. *Cell* 1997; 88: 833-843. 1997/03/21. DOI: 10.1016/s0092-8674(00)81929-7.

32. García-Peydró M, de Yébenes VG and Toribio ML. Sustained Notch1 signaling instructs the earliest human intrathymic precursors to adopt a gammadelta T-cell fate in fetal thymus organ culture. *Blood* 2003; 102: 2444-2451. 2003/06/28. DOI: 10.1182/blood-2002-10-3261.

33. Constant P, Davodeau F, Peyrat M-A, et al. Stimulation of human γδ T cells by nonpeptidic mycobacterial ligands. *Science* 1994; 264: 267-270.

34. Altvater B, Pscherer S, Landmeier S, et al. Activated human γδ T cells induce peptide-specific CD8+ T-cell responses to tumor-associated self-antigens. *Cancer Immunology, Immunotherapy* 2012; 61: 385-396.

35. Himoudi N, Morgenstern DA, Yan M, et al. Human γδ T lymphocytes are licensed for professional antigen presentation by interaction with opsonized target cells. *The Journal of Immunology* 2012; 188: 1708-1716.

36. Viey E, Fromont Gl, Escudier B, et al. Phosphostim-activated γδ T cells kill autologous metastatic renal cell carcinoma. *The Journal of Immunology* 2005; 174: 1338-1347.

37. Tokuyama H, Hagi T, Mattarollo SR, et al. Vγ9Vδ2 T cell cytotoxicity against tumor cells is enhanced by monoclonal antibody drugs—rituximab and trastuzumab. *International journal of cancer* 2008; 122: 2526-2534.

38. Zhou F. Molecular mechanisms of IFN-gamma to up-regulate MHC class I antigen processing and presentation. *Int Rev Immunol* 2009; 28: 239-260. 2009/10/09. DOI: 10.1080/08830180902978120.

39. Gardell JL and Parker DC. CD40L is transferred to antigen-presenting B cells during delivery of T-cell help. *Eur J Immunol* 2017; 47: 41-50. 2016/10/19. DOI: 10.1002/eji.201646504.

40. Crotty S. A brief history of T cell help to B cells. *Nat Rev Immunol* 2015; 15: 185-189. 2015/02/14. DOI: 10.1038/nri3803.

41. Sun L, Su Y, Jiao A, et al. T cells in health and disease. *Signal Transduction and Targeted Therapy* 2023; 8: 235. DOI: 10.1038/s41392-023-01471-y.

42. Klein L, Kyewski B, Allen PM, et al. Positive and negative selection of the T cell repertoire: what thymocytes see (and don't see). *Nature Reviews Immunology* 2014; 14: 377-391. DOI: 10.1038/nri3667.

43. Anderson MS, Venanzi ES, Klein L, et al. Projection of an immunological self shadow within the thymus by the aire protein. *Science* 2002; 298: 1395-1401. 2002/10/12. DOI: 10.1126/science.1075958.

44. Kroger CJ, Spidale NA, Wang B, et al. Thymic Dendritic Cell Subsets Display Distinct Efficiencies and Mechanisms of Intercellular MHC Transfer. *J Immunol* 2017; 198: 249-256. 2016/11/30. DOI: 10.4049/jimmunol.1601516.

45. Xing Y, Wang X, Jameson SC, et al. Late stages of T cell maturation in the thymus involve NF-κB and tonic type I interferon signaling. *Nat Immunol* 2016; 17: 565-573. 2016/04/05. DOI: 10.1038/ni.3419.

46. Straus DB and Weiss A. The CD3 chains of the T cell antigen receptor associate with the ZAP-70 tyrosine kinase and are tyrosine phosphorylated after receptor stimulation. *J Exp Med* 1993; 178: 1523-1530. DOI: 10.1084/jem.178.5.1523.

47. Lovatt M, Filby A, Parravicini V, et al. Lck regulates the threshold of activation in primary T cells, while both Lck and Fyn contribute to the magnitude of the extracellular signal-related kinase response. *Mol Cell Biol* 2006; 26: 8655-8665. 2006/09/13. DOI: 10.1128/mcb.00168-06.

48. Kallies A and Good-Jacobson KL. Transcription Factor T-bet Orchestrates Lineage Development and Function in the Immune System. *Trends Immunol* 2017; 38: 287-297. 2017/03/11. DOI: 10.1016/j.it.2017.02.003.

49. Szabo SJ, Kim ST, Costa GL, et al. A Novel Transcription Factor, T-bet, Directs Th1 Lineage Commitment. *Cell* 2000; 100: 655-669. DOI: https://doi.org/10.1016/S0092-8674(00)80702-3.

50. Smeltz RB, Chen J, Ehrhardt R, et al. Role of IFN-γ in Th1 Differentiation: IFN-γ Regulates IL-18Rα Expression by Preventing the Negative Effects of IL-4 and by Inducing/Maintaining IL-12 Receptor β2 Expression. *The Journal of Immunology* 2002; 168: 6165-6172. DOI: 10.4049/jimmunol.168.12.6165.

51. Mosmann TR, Cherwinski H, Bond MW, et al. Two types of murine helper T cell clone. I. Definition according to profiles of lymphokine activities and secreted proteins. *J Immunol* 1986; 136: 2348-2357. 1986/04/01.

52. Chen W, Jin W, Hardegen N, et al. Conversion of peripheral CD4+CD25- naive T cells to CD4+CD25+ regulatory T cells by TGF-beta induction of transcription factor Foxp3. *J Exp Med* 2003; 198: 1875-1886. 2003/12/17. DOI: 10.1084/jem.20030152.

53. Plumlee CR, Obar JJ, Colpitts SL, et al. Early Effector CD8 T Cells Display Plasticity in Populating the Short-Lived Effector and Memory-Precursor Pools Following Bacterial or Viral Infection. *Scientific Reports* 2015; 5: 12264. DOI: 10.1038/srep12264.

54. Joshi NS, Cui W, Chandele A, et al. Inflammation directs memory precursor and short-lived effector CD8(+) T cell fates via the graded expression of T-bet transcription factor. *Immunity* 2007; 27: 281-295. 2007/08/29. DOI: 10.1016/j.immuni.2007.07.010.

55. Lefrançois L and Obar JJ. Once a killer, always a killer: from cytotoxic T cell to memory cell. *Immunol Rev* 2010; 235: 206-218. 2010/06/12. DOI: 10.1111/j.0105-2896.2010.00895.x.

56. Curtsinger JM, Johnson CM and Mescher MF. CD8 T Cell Clonal Expansion and Development of Effector Function Require Prolonged Exposure to Antigen, Costimulation, and Signal 3 Cytokine. *The Journal of Immunology* 2003; 171: 5165-5171. DOI: 10.4049/jimmunol.171.10.5165.

57. Sanjabi S, Mosaheb MM and Flavell RA. Opposing Effects of TGF-β and IL-15 Cytokines Control the Number of Short-Lived Effector CD8+ T Cells. *Immunity* 2009; 31: 131-144. DOI: https://doi.org/10.1016/j.immuni.2009.04.020.

58. Joffre OP, Segura E, Savina A, et al. Cross-presentation by dendritic cells. *Nature Reviews Immunology* 2012; 12: 557-569. DOI: 10.1038/nri3254.

59. Curtsinger JM, Lins DC and Mescher MF. Signal 3 determines tolerance versus full activation of naive CD8 T cells: dissociating proliferation and development of effector function. *J Exp Med* 2003; 197: 1141-1151. 2003/05/07. DOI: 10.1084/jem.20021910.

60. Schietinger A and Greenberg PD. Tolerance and exhaustion: defining mechanisms of T cell dysfunction. *Trends Immunol* 2014; 35: 51-60. 2013/11/12. DOI: 10.1016/j.it.2013.10.001.

61. Riha P and Rudd CE. CD28 co-signaling in the adaptive immune response. *Self Nonself* 2010; 1: 231-240. 2011/04/14. DOI: 10.4161/self.1.3.12968.

62. Shahinian A, Pfeffer K, Lee KP, et al. Differential T cell costimulatory requirements in CD28-deficient mice. *Science* 1993; 261: 609-612. 1993/07/30. DOI: 10.1126/science.7688139.

63. Prasad KV, Cai YC, Raab M, et al. T-cell antigen CD28 interacts with the lipid kinase phosphatidylinositol 3-kinase by a cytoplasmic Tyr(P)-Met-Xaa-Met motif. *Proceedings of the National Academy of Sciences* 1994; 91: 2834-2838. DOI: doi:10.1073/pnas.91.7.2834.

64. Raab M, Cai YC, Bunnell SC, et al. p56Lck and p59Fyn regulate CD28 binding to phosphatidylinositol 3-kinase, growth factor receptor-bound protein GRB-2, and T cell-specific protein-tyrosine kinase ITK: implications for T-cell costimulation. *Proc Natl Acad Sci U S A* 1995; 92: 8891-8895. 1995/09/12. DOI: 10.1073/pnas.92.19.8891.

65. Boise LH, Minn AJ, Noel PJ, et al. CD28 costimulation can promote T cell survival by enhancing the expression of Bcl-XL. *Immunity* 1995; 3: 87-98. 1995/07/01. DOI: 10.1016/1074-7613(95)90161-2.

66. Kane LP, Andres PG, Howland KC, et al. Akt provides the CD28 costimulatory signal for up-regulation of IL-2 and IFN-γ but not TH2 cytokines. *Nature Immunology* 2001; 2: 37-44. DOI: 10.1038/83144.

67. Holdorf AD, Green JM, Levin SD, et al. Proline residues in CD28 and the Src homology (SH)3 domain of Lck are required for T cell costimulation. *J Exp Med* 1999; 190: 375-384. DOI: 10.1084/jem.190.3.375.

68. Okkenhaug K and Rottapel R. Grb2 Forms an Inducible Protein Complex with CD28 through a Src Homology 3 Domain-Proline Interaction*. *Journal of Biological Chemistry* 1998; 273: 21194-21202. DOI: https://doi.org/10.1074/jbc.273.33.21194.

69. Bhoj VG and Chen ZJ. Ubiquitylation in innate and adaptive immunity. *Nature* 2009; 458: 430-437. 2009/03/28. DOI: 10.1038/nature07959.

70. Xu Y-R and Lei C-Q. TAK1-TABs Complex: A Central Signalosome in Inflammatory Responses. *Front Immunol* 2021; 11. Review. DOI: 10.3389/fimmu.2020.608976.

71. Schwenzer R, Siemienski K, Liptay S, et al. The human tumor necrosis factor (TNF) receptor-associated factor 1 gene (TRAF1) is up-regulated by cytokines of the TNF ligand family and modulates TNF-induced activation of NF-kappaB and c-Jun N-terminal kinase. *J Biol Chem* 1999; 274: 19368-19374. 1999/06/26. DOI: 10.1074/jbc.274.27.19368.

72. Dardalhon V, Schubart AS, Reddy J, et al. CD226 is specifically expressed on the surface of Th1 cells and regulates their expansion and effector functions. *J Immunol* 2005; 175: 1558-1565. 2005/07/22. DOI: 10.4049/jimmunol.175.3.1558.

73. Tahara-Hanaoka S, Shibuya K, Onoda Y, et al. Functional characterization of DNAM-1 (CD226) interaction with its ligands PVR (CD155) and nectin-2 (PRR-2/CD112). *Int Immunol* 2004; 16: 533-538. 2004/03/25. DOI: 10.1093/intimm/dxh059.

74. Wang H, Qi J, Zhang S, et al. Binding mode of the side-by-side two-IgV molecule CD226/DNAM-1 to its ligand CD155/Necl-5. *Proc Natl Acad Sci U S A* 2019; 116: 988-996. 2018/12/29. DOI: 10.1073/pnas.1815716116.

75. Shibuya K, Lanier LL, Phillips JH, et al. Physical and functional association of LFA-1 with DNAM-1 adhesion molecule. *Immunity* 1999; 11: 615-623. 1999/12/11. DOI: 10.1016/s1074-7613(00)80136-3.

76. Zhang Z, Wu N, Lu Y, et al. DNAM-1 controls NK cell activation via an ITT-like motif. *J Exp Med* 2015; 212: 2165-2182. 2015/11/11. DOI: 10.1084/jem.20150792.

77. Wang X, Teng F, Kong L, et al. PD-L1 expression in human cancers and its association with clinical outcomes. *Onco Targets Ther* 2016; 9: 5023-5039. 2016/08/31. DOI: 10.2147/ott.S105862.

78. Chikuma S, Terawaki S, Hayashi T, et al. PD-1-mediated suppression of IL-2 production induces CD8+ T cell anergy in vivo. *J Immunol* 2009; 182: 6682-6689. 2009/05/21. DOI: 10.4049/jimmunol.0900080.

79. Oestreich KJ, Yoon H, Ahmed R, et al. NFATc1 regulates PD-1 expression upon T cell activation. *J Immunol* 2008; 181: 4832-4839. 2008/09/20. DOI: 10.4049/jimmunol.181.7.4832.

80. Shi L, Chen S, Yang L, et al. The role of PD-1 and PD-L1 in T-cell immune suppression in patients with hematological malignancies. *Journal of Hematology & Oncology* 2013; 6: 74. DOI: 10.1186/1756-8722-6-74.

81. Sheppard K-A, Fitz LJ, Lee JM, et al. PD-1 inhibits T-cell receptor induced phosphorylation of the ZAP70/CD3ζ signalosome and downstream signaling to PKCθ. *FEBS letters* 2004; 574: 37-41.

82. Hui E, Cheung J, Zhu J, et al. T cell costimulatory receptor CD28 is a primary target for PD-1-mediated inhibition. *Science* 2017; 355: 1428-1433. 2017/03/11. DOI: 10.1126/science.aaf1292.

83. Buchbinder EI and Desai A. CTLA-4 and PD-1 Pathways: Similarities, Differences, and Implications of Their Inhibition. *Am J Clin Oncol* 2016; 39: 98-106. 2015/11/13. DOI: 10.1097/coc.0000000000000239.

84. Linsley PS, Bradshaw J, Greene J, et al. Intracellular trafficking of CTLA-4 and focal localization towards sites of TCR engagement. *Immunity* 1996; 4: 535-543. 1996/06/01. DOI: 10.1016/s1074-7613(00)80480-x.

85. van der Merwe PA, Bodian DL, Daenke S, et al. CD80 (B7-1) binds both CD28 and CTLA-4 with a low affinity and very fast kinetics. *J Exp Med* 1997; 185: 393-403. 1997/02/03. DOI: 10.1084/jem.185.3.393.

86. Schneider H, Dias SdR, Hu H, et al. A regulatory role for cytoplasmic YVKM motif in CTLA-4 inhibition of TCR signaling. *European Journal of Immunology* 2001; 31: 2042-2050. DOI: https://doi.org/10.1002/1521-4141(200107)31:7<2042::AID-IMMU2042>3.0.CO;2-D.

87. Dougall WC, Kurtulus S, Smyth MJ, et al. TIGIT and CD96: new checkpoint receptor targets for cancer immunotherapy. *Immunol Rev* 2017; 276: 112-120. 2017/03/05. DOI: 10.1111/imr.12518.

88. Yu X, Harden K, C Gonzalez L, et al. The surface protein TIGIT suppresses T cell activation by promoting the generation of mature immunoregulatory dendritic cells. *Nature Immunology* 2009; 10: 48-57. DOI: 10.1038/ni.1674.

89. Worboys JD, Vowell KN, Hare RK, et al. TIGIT can inhibit T cell activation via ligation-induced nanoclusters, independent of CD226 co-stimulation. *Nature Communications* 2023; 14: 5016. DOI: 10.1038/s41467-023-40755-3.

90. Inozume T, Yaguchi T, Furuta J, et al. Melanoma Cells Control Antimelanoma CTL Responses via Interaction between TIGIT and CD155 in the Effector Phase. *Journal of Investigative Dermatology* 2016; 136: 255-263. DOI: https://doi.org/10.1038/JID.2015.404.

91. Rishiq A, Bsoul R, Pick O, et al. Studying TIGIT activity against tumors through the generation of knockout mice. *Oncoimmunology* 2023; 12: 2217735. 2023/06/01. DOI: 10.1080/2162402x.2023.2217735.

92. Stanietsky N, Simic H, Arapovic J, et al. The interaction of TIGIT with PVR and PVRL2 inhibits human NK cell cytotoxicity. *Proceedings of the National Academy of Sciences* 2009; 106: 17858-17863. DOI: 10.1073/pnas.0903474106.

93. Li M, Xia P, Du Y, et al. T-cell immunoglobulin and ITIM domain (TIGIT) receptor/poliovirus receptor (PVR) ligand engagement suppresses interferon-γ production of natural killer cells via β-arrestin 2-mediated negative signaling. *J Biol Chem* 2014; 289: 17647-17657. 2014/05/13. DOI: 10.1074/jbc.M114.572420.

94. Liu S, Zhang H, Li M, et al. Recruitment of Grb2 and SHIP1 by the ITT-like motif of TIGIT suppresses granule polarization and cytotoxicity of NK cells. *Cell Death & Differentiation* 2013; 20: 456-464. DOI: 10.1038/cdd.2012.141.

95. UK CR. Cancer risk statistics, https://www.cancerresearchuk.org/health-professional/cancer-statistics/risk (2025, accessed January 2025).

96. Dunn GP, Koebel CM and Schreiber RD. Interferons, immunity and cancer immunoediting. *Nat Rev Immunol* 2006; 6: 836-848. 2006/10/26. DOI: 10.1038/nri1961.

97. Burnet M. Cancer; a biological approach. I. The processes of control. *Br Med J* 1957; 1: 779-786. 1957/04/06. DOI: 10.1136/bmj.1.5022.779.

98. Dunn GP, Old LJ and Schreiber RD. The three Es of cancer immunoediting. *Annu Rev Immunol* 2004; 22: 329-360. 2004/03/23. DOI: 10.1146/annurev.immunol.22.012703.104803.

99. Hayakawa Y, Kelly JM, Westwood JA, et al. Cutting Edge: Tumor Rejection Mediated by NKG2D Receptor-Ligand Interaction Is Dependent upon Perforin. *The Journal of Immunology* 2002; 169: 5377-5381. DOI: 10.4049/jimmunol.169.10.5377.

100. López-Soto A, Huergo-Zapico L, Acebes-Huerta A, et al. NKG2D signaling in cancer immunosurveillance. *Int J Cancer* 2015; 136: 1741-1750. 2014/03/13. DOI: 10.1002/ijc.28775.

101. Laad AD, Thomas ML, Fakih AR, et al. Human gamma delta T cells recognize heat shock protein-60 on oral tumor cells. *Int J Cancer* 1999; 80: 709-714. 1999/02/27. DOI: 10.1002/(sici)1097-0215(19990301)80:5<709::aid-ijc14>3.0.co;2-r.

102. Payne KK, Mine JA, Biswas S, et al. BTN3A1 governs antitumor responses by coordinating αβ and γδ T cells. *Science* 2020; 369: 942-949. 2020/08/21. DOI: 10.1126/science.aay2767.

103. Rigau M, Uldrich AP and Behren A. Targeting butyrophilins for cancer immunotherapy. *Trends in Immunology* 2021; 42: 670-680. DOI: https://doi.org/10.1016/j.it.2021.06.002.

104. Liang F, Zhang C, Guo H, et al. Comprehensive analysis of BTN3A1 in cancers: mining of omics data and validation in patient samples and cellular models. *FEBS Open Bio* 2021; 11: 2586-2599. 2021/07/23. DOI: 10.1002/2211-5463.13256.

105. Roberts EW, Broz ML, Binnewies M, et al. Critical Role for CD103(+)/CD141(+) Dendritic Cells Bearing CCR7 for Tumor Antigen Trafficking and Priming of T Cell Immunity in Melanoma. *Cancer Cell* 2016; 30: 324-336. 2016/07/19. DOI: 10.1016/j.ccell.2016.06.003.

106. Valenzuela J, Schmidt C and Mescher M. The roles of IL-12 in providing a third signal for clonal expansion of naive CD8 T cells. *J Immunol* 2002; 169: 6842-6849. 2002/12/10. DOI: 10.4049/jimmunol.169.12.6842.

107. Xia P, Shao Y-Q, Yu C-C, et al. NLRP3 inflammasome up-regulates major histocompatibility complex class I expression and promotes inflammatory infiltration in polymyositis. *BMC Immunology* 2022; 23: 39. DOI: 10.1186/s12865-022-00515-2.

108. Voskoboinik I, Whisstock JC and Trapani JA. Perforin and granzymes: function, dysfunction and human pathology. *Nature Reviews Immunology* 2015; 15: 388-400. DOI: 10.1038/nri3839.

109. Chowdhury D and Lieberman J. Death by a thousand cuts: granzyme pathways of programmed cell death. *Annu Rev Immunol* 2008; 26: 389-420. 2008/02/29. DOI: 10.1146/annurev.immunol.26.021607.090404.

110. Lieberman J. Granzyme A activates another way to die. *Immunol Rev* 2010; 235: 93-104. 2010/06/12. DOI: 10.1111/j.0105-2896.2010.00902.x.

111. Afonina IS, Cullen SP and Martin SJ. Cytotoxic and non-cytotoxic roles of the CTL/NK protease granzyme B. *Immunological Reviews* 2010; 235: 105-116. DOI: https://doi.org/10.1111/j.0105-2896.2010.00908.x.

112. Koebel CM, Vermi W, Swann JB, et al. Adaptive immunity maintains occult cancer in an equilibrium state. *Nature* 2007; 450: 903-907. 2007/11/21. DOI: 10.1038/nature06309.

113. Martini M, Testi MG, Pasetto M, et al. IFN-gamma-mediated upmodulation of MHC class I expression activates tumor-specific immune response in a mouse model of prostate cancer. *Vaccine* 2010; 28: 3548-3557. 2010/03/23. DOI: 10.1016/j.vaccine.2010.03.007.

114. Zaidi MR. The Interferon-Gamma Paradox in Cancer. *J Interferon Cytokine Res* 2019; 39: 30-38. 2018/11/06. DOI: 10.1089/jir.2018.0087.

115. Seliger B, Maeurer MJ and Ferrone S. Antigen-processing machinery breakdown and tumor growth. *Immunology Today* 2000; 21: 455-464. DOI: https://doi.org/10.1016/S0167-5699(00)01692-3.

116. Duan L and Mukherjee E. *Janeway's Immunobiology, Ninth Edition*. Yale J Biol Med. 2016 Sep 30;89(3):424-5. eCollection 2016 Sep.

117. REDPATH†, MICHAELSEN, SANDLIE, et al. Activation of complement by human IgG1 and human IgG3 antibodies against the human leucocyte antigen CD52. *Immunology* 1998; 93: 595-600. DOI: https://doi.org/10.1046/j.1365-2567.1998.00472.x.

118. Isaacs JD, Wing MG, Greenwood JD, et al. A therapeutic human IgG4 monoclonal antibody that depletes target cells in humans. *Clinical and Experimental Immunology* 2003; 106: 427-433. DOI: 10.1046/j.1365-2249.1996.d01-876.x.

119. Yu J, Song Y and Tian W. How to select IgG subclasses in developing anti-tumor therapeutic antibodies. *Journal of Hematology & Oncology* 2020; 13: 45. DOI: 10.1186/s13045-020-00876-4.

120. Kretschmer A, Schwanbeck R, Valerius T, et al. Antibody Isotypes for Tumor Immunotherapy. *Transfus Med Hemother* 2017; 44: 320-326. 2017/10/27. DOI: 10.1159/000479240.

121. Shields RL, Lai J, Keck R, et al. Lack of fucose on human IgG1 N-linked oligosaccharide improves binding to human Fcgamma RIII and antibody-dependent cellular toxicity. *J Biol Chem* 2002; 277: 26733-26740. 20020501. DOI: 10.1074/jbc.M202069200.

122. Lazar GA, Dang W, Karki S, et al. Engineered antibody Fc variants with enhanced effector function. *Proceedings of the National Academy of Sciences* 2006; 103: 4005-4010. DOI: doi:10.1073/pnas.0508123103.

123. Qi X, Li F, Wu Y, et al. Optimization of 4-1BB antibody for cancer immunotherapy by balancing agonistic strength with FcγR affinity. *Nature Communications* 2019; 10: 2141. DOI: 10.1038/s41467-019-10088-1.

124. Daud A, Albany C, Velcheti V, et al. First-in-human, phase 1a dose finding of LVGN6051 CD137/4-1BB agonistic antibody with or without pembrolizumab in patients with advanced solid tumors. *Journal of Clinical Oncology* 2023; 41: 2525-2525. DOI: 10.1200/JCO.2023.41.16_suppl.2525.

125. Salles G, Barrett M, Foà R, et al. Rituximab in B-Cell Hematologic Malignancies: A Review of 20 Years of Clinical Experience. *Adv Ther* 2017; 34: 2232-2273. 2017/10/07. DOI: 10.1007/s12325-017-0612-x.

126. Merkt W, Lorenz HM and Watzl C. Rituximab induces phenotypical and functional changes of NK cells in a non-malignant experimental setting. *Arthritis Res Ther* 2016; 18: 206. 20160915. DOI: 10.1186/s13075-016-1101-3.

127. Weiner GJ. Rituximab: mechanism of action. *Semin Hematol* 2010; 47: 115-123. 2010/03/31. DOI: 10.1053/j.seminhematol.2010.01.011.

128. Xu ZZ, Xia ZG, Wang AH, et al. Activation of the PI3K/AKT/mTOR pathway in diffuse large B cell lymphoma: clinical significance and inhibitory effect of rituximab. *Ann Hematol* 2013; 92: 1351-1358. 2013/05/03. DOI: 10.1007/s00277-013-1770-9.

129. Jazirehi AR, Huerta-Yepez S, Cheng G, et al. Rituximab (chimeric anti-CD20 monoclonal antibody) inhibits the constitutive nuclear factor-{kappa}B signaling pathway in non-Hodgkin's lymphoma B-cell lines: role in sensitization to chemotherapeutic drug-induced apoptosis. *Cancer Res* 2005; 65: 264-276. 2005/01/25.

130. Shih T and Lindley C. Bevacizumab: an angiogenesis inhibitor for the treatment of solid malignancies. *Clinical therapeutics* 2006; 28: 1779-1802.

131. Kazazi-Hyseni F, Beijnen JH and Schellens JH. Bevacizumab. *Oncologist* 2010; 15: 819-825. 20100805. DOI: 10.1634/theoncologist.2009-0317.

132. Tarhini A, Lo E and Minor DR. Releasing the brake on the immune system: ipilimumab in melanoma and other tumors. *Cancer Biother Radiopharm* 2010; 25: 601-613. 2011/01/06. DOI: 10.1089/cbr.2010.0865.

133. Andre T, Elez E, Cutsem EV, et al. Nivolumab plus Ipilimumab in Microsatellite-Instability–High Metastatic Colorectal Cancer. *New England Journal of Medicine* 2024; 391: 2014-2026. DOI: doi:10.1056/NEJMoa2402141.

134. Jiang H, Xu A, Xia W, et al. Nivolumab monotherapy or combination therapy with ipilimumab for lung cancer: a systemic review and meta-analysis. *Cancer Cell Int* 2021; 21: 426. 2021/08/16. DOI: 10.1186/s12935-021-02100-w.

135. Larkin J, Chiarion-Sileni V, Gonzalez R, et al. Five-Year Survival with Combined Nivolumab and Ipilimumab in Advanced Melanoma. *New England Journal of Medicine* 2019; 381: 1535-1546. DOI: doi:10.1056/NEJMoa1910836.

136. Wilcox RA, Flies DB, Zhu G, et al. Provision of antigen and CD137 signaling breaks immunological ignorance, promoting regression of poorly immunogenic tumors. *J Clin Invest* 2002; 109: 651-659. 2002/03/06. DOI: 10.1172/jci14184.

137. Khushalani NI, Ott PA, Ferris RL, et al. Final results of urelumab, an anti-CD137 agonist monoclonal antibody, in combination with cetuximab or nivolumab in patients with advanced solid tumors. *Journal for ImmunoTherapy of Cancer* 2024; 12: e007364. DOI: 10.1136/jitc-2023-007364.

138. Timmerman J, Herbaux C, Ribrag V, et al. Urelumab alone or in combination with rituximab in patients with relapsed or refractory B-cell lymphoma. *Am J Hematol* 2020; 95: 510-520. 20200229. DOI: 10.1002/ajh.25757.

139. Griffiths J, Hussain K, Smith HL, et al. Domain binding and isotype dictate the activity of anti-human OX40 antibodies. *J Immunother Cancer* 2020; 8 2021/01/12. DOI: 10.1136/jitc-2020-001557.

140. Willoughby JE, Dou L, Bhattacharya S, et al. Impact of isotype on the mechanism of action of agonist anti-OX40 antibodies in cancer: implications for therapeutic combinations. *Journal for ImmunoTherapy of Cancer* 2024; 12: e008677. DOI: 10.1136/jitc-2023-008677.

141. Attarwala H. TGN1412: From Discovery to Disaster. *J Young Pharm* 2010; 2: 332-336. DOI: 10.4103/0975-1483.66810.

142. Eastwood D, Findlay L, Poole S, et al. Monoclonal antibody TGN1412 trial failure explained by species differences in CD28 expression on CD4+ effector memory T-cells. *Br J Pharmacol* 2010; 161: 512-526. DOI: 10.1111/j.1476-5381.2010.00922.x.

143. You G, Lee Y, Kang Y-W, et al. B7-H3x4-1BB bispecific antibody augments antitumor immunity by enhancing terminally differentiated CD8+ tumor-infiltrating lymphocytes. *Science Advances* 2021; 7: eaax3160. DOI: doi:10.1126/sciadv.aax3160.

144. Subklewe M, von Bergwelt-Baildon M and Humpe A. Chimeric Antigen Receptor T Cells: A Race to Revolutionize Cancer Therapy. *Transfus Med Hemother* 2019; 46: 15-24. 2019/06/28. DOI: 10.1159/000496870.

145. Martinez M and Moon EK. CAR T Cells for Solid Tumors: New Strategies for Finding, Infiltrating, and Surviving in the Tumor Microenvironment. *Front Immunol* 2019; 10. Review. DOI: 10.3389/fimmu.2019.00128.

146. Ahmed N, Ratnayake M, Savoldo B, et al. Regression of experimental medulloblastoma following transfer of HER2-specific T cells. *Cancer Res* 2007; 67: 5957-5964. DOI: 10.1158/0008-5472.Can-06-4309.

147. Nellan A, Rota C, Majzner R, et al. Durable regression of Medulloblastoma after regional and intravenous delivery of anti-HER2 chimeric antigen receptor T cells. *J Immunother Cancer* 2018; 6: 30. 2018/05/02. DOI: 10.1186/s40425-018-0340-z.

148. Chmielewski M, Hombach A, Heuser C, et al. T cell activation by antibody-like immunoreceptors: increase in affinity of the single-chain fragment domain above threshold does not increase T cell activation against antigen-positive target cells but decreases selectivity. *The Journal of Immunology* 2004; 173: 7647-7653.

149. Ali S, Kjeken R, Niederlaender C, et al. The European Medicines Agency Review of Kymriah (Tisagenlecleucel) for the Treatment of Acute Lymphoblastic Leukemia and Diffuse Large B-Cell Lymphoma. *The Oncologist* 2019; 25: e321-e327. DOI: 10.1634/theoncologist.2019-0233.

150. Papadouli I, Mueller-Berghaus J, Beuneu C, et al. EMA Review of Axicabtagene Ciloleucel (Yescarta) for the Treatment of Diffuse Large B-Cell Lymphoma. *Oncologist* 2020; 25: 894-902. 2020/04/28. DOI: 10.1634/theoncologist.2019-0646.

151. Seimetz D, Heller K and Richter J. Approval of First CAR-Ts: Have we Solved all Hurdles for ATMPs? *Cell Med* 2019; 11: 2155179018822781. 2019/01/22. DOI: 10.1177/2155179018822781.

152. Georgiev H, Ravens I, Papadogianni G, et al. Coming of Age: CD96 Emerges as Modulator of Immune Responses. *Front Immunol* 2018; 9: 1072. 2018/06/06. DOI: 10.3389/fimmu.2018.01072.

153. Wang PL, O'Farrell S, Clayberger C, et al. Identification and molecular cloning of tactile. A novel human T cell activation antigen that is a member of the Ig gene superfamily. *The Journal of Immunology* 1992; 148: 2600-2608.

154. Chan CJ, Martinet L, Gilfillan S, et al. The receptors CD96 and CD226 oppose each other in the regulation of natural killer cell functions. *Nat Immunol* 2014; 15: 431-438. 2014/03/25. DOI: 10.1038/ni.2850.

155. Miller J, Baker C, Cook K, et al. Two pathways of costimulation through CD28. *Immunologic Research* 2009; 45: 159. DOI: 10.1007/s12026-009-8097-6.

156. Meyer D, Seth S, Albrecht J, et al. CD96 Interaction with CD155 via Its First Ig-like Domain Is Modulated by Alternative Splicing or Mutations in Distal Ig-like Domains *. *Journal of Biological Chemistry* 2009; 284: 2235-2244. DOI: 10.1074/jbc.M807698200.

157. Carducci M, Perfetto L, Briganti L, et al. The protein interaction network mediated by human SH3 domains. *Biotechnology Advances* 2012; 30: 4-15. DOI: https://doi.org/10.1016/j.biotechadv.2011.06.012.

158. Teyra J, Huang H, Jain S, et al. Comprehensive Analysis of the Human SH3 Domain Family Reveals a Wide Variety of Non-canonical Specificities. *Structure* 2017; 25: 1598-1610.e1593. 2017/09/12. DOI: 10.1016/j.str.2017.07.017.

159. Yang WC, Ghiotto M, Barbarat B, et al. The role of Tec protein-tyrosine kinase in T cell signaling. *J Biol Chem* 1999; 274: 607-617. 1999/01/05. DOI: 10.1074/jbc.274.2.607.

160. Chauvin J-M and Zarour HM. TIGIT in cancer immunotherapy. *Journal for ImmunoTherapy of Cancer* 2020; 8: e000957. DOI: 10.1136/jitc-2020-000957.

161. Liu L, Wang A, Liu X, et al. Blocking TIGIT/CD155 signalling reverses CD8+ T cell exhaustion and enhances the antitumor activity in cervical cancer. *Journal of Translational Medicine* 2022; 20: 280. DOI: 10.1186/s12967-022-03480-x.

162. Fuchs A, Cella M, Giurisato E, et al. Cutting edge: CD96 (tactile) promotes NK cell-target cell adhesion by interacting with the poliovirus receptor (CD155). *J Immunol* 2004; 172: 3994-3998. 2004/03/23. DOI: 10.4049/jimmunol.172.7.3994.

163. Nakamura K and Smyth MJ. Immunoediting of cancer metastasis by NK cells. *Nature Cancer* 2020; 1: 670-671. DOI: 10.1038/s43018-020-0081-z.

164. Roman Aguilera A, Lutzky VP, Mittal D, et al. CD96 targeted antibodies need not block CD96-CD155 interactions to promote NK cell anti-metastatic activity. *Oncoimmunology* 2018; 7: e1424677. 2018/05/04. DOI: 10.1080/2162402x.2018.1424677.

165. Blake SJ, Stannard K, Liu J, et al. Suppression of Metastases Using a New Lymphocyte Checkpoint Target for Cancer Immunotherapy. *Cancer Discov* 2016; 6: 446-459. 2016/01/21. DOI: 10.1158/2159-8290.CD-15-0944.

166. Matsuo S, Nabekura T, Shibuya K, et al. CD96 enhances the anti-viral activity of natural killer cells by promoting Ly49H-mediated activation during mouse cytomegalovirus infection. *Molecular Immunology* 2025; 179: 65-70.

167. Chiang EY, de Almeida PE, de Almeida Nagata DE, et al. CD96 functions as a co-stimulatory receptor to enhance CD8(+) T cell activation and effector responses. *Eur J Immunol* 2020; 50: 891-902. 2020/02/12. DOI: 10.1002/eji.201948405.

168. Chen L and Flies DB. Molecular mechanisms of T cell co-stimulation and co-inhibition. *Nat Rev Immunol* 2013; 13: 227-242. 2013/03/09. DOI: 10.1038/nri3405.

169. Rogel A, Ibrahim FM, Thirdborough SM, et al. Fcγ receptor–mediated cross-linking codefines the immunostimulatory activity of anti-human CD96 antibodies. *JCI Insight* 2022; 7. DOI: 10.1172/jci.insight.158444.

170. Bruhns P. Properties of mouse and human IgG receptors and their contribution to disease models. *Blood* 2012; 119: 5640-5649. DOI: 10.1182/blood-2012-01-380121.

171. Bruhns P, Iannascoli B, England P, et al. Specificity and affinity of human Fcγ receptors and their polymorphic variants for human IgG subclasses. *Blood* 2009; 113: 3716-3725. DOI: 10.1182/blood-2008-09-179754.

172. Hamid O, Baxter D, Easton R, et al. 488 Phase 1 trial of first-in-class anti-CD96 monoclonal antibody inhibitor, GSK6097608, monotherapy and combination with anti–PD-1 monoclonal antibody, dostarlimab, in advanced solid tumors. *Journal for ImmunoTherapy of Cancer* 2021; 9: A518-A518. DOI: 10.1136/jitc-2021-SITC2021.488.

173. Liu F, Huang J, He F, et al. CD96, a new immune checkpoint, correlates with immune profile and clinical outcome of glioma. *Sci Rep* 2020; 10: 10768. 2020/07/03. DOI: 10.1038/s41598-020-66806-z.

174. Meyer D, Seth S, Albrecht J, et al. CD96 interaction with CD155 via its first Ig-like domain is modulated by alternative splicing or mutations in distal Ig-like domains. *J Biol Chem* 2009; 284: 2235-2244. 2008/12/06. DOI: 10.1074/jbc.M807698200.

175. Degenhardt Y, Guan J, Morley P, et al. Abstract 6268: Discovery and characterization of the CD96 antibody GSK6097608, a high-affinity, antagonistic anti-CD96 antibody for cancer immunotherapy. *Cancer Research* 2022; 82: 6268-6268. DOI: 10.1158/1538-7445.Am2022-6268.

176. Consortium TU. UniProt: the Universal Protein Knowledgebase in 2023. *Nucleic Acids Research* 2022; 51: D523-D531. DOI: 10.1093/nar/gkac1052.

177. Szymczak AL, Workman CJ, Wang Y, et al. Correction of multi-gene deficiency in vivo using a single 'self-cleaving' 2A peptide–based retroviral vector. *Nature Biotechnology* 2004; 22: 589-594. DOI: 10.1038/nbt957.

178. Philip B, Kokalaki E, Mekkaoui L, et al. A highly compact epitope-based marker/suicide gene for easier and safer T-cell therapy. *Blood* 2014; 124: 1277-1287. DOI: 10.1182/blood-2014-01-545020.

179. Reichenbach P, Giordano Attianese GMP, Ouchen K, et al. A lentiviral vector for the production of T cells with an inducible transgene and a constitutively expressed tumour-targeting receptor. *Nature Biomedical Engineering* 2023; 7: 1063-1080. DOI: 10.1038/s41551-023-01013-5.

180. Rajabzadeh A, Hamidieh AA and Rahbarizadeh F. Spinoculation and retronectin highly enhance the gene transduction efficiency of Mucin-1-specific chimeric antigen receptor (CAR) in human primary T cells. *BMC Molecular and Cell Biology* 2021; 22: 57. DOI: 10.1186/s12860-021-00397-z.

181. Bloemberg D, Nguyen T, MacLean S, et al. A High-Throughput Method for Characterizing Novel Chimeric Antigen Receptors in Jurkat Cells. *Molecular Therapy - Methods & Clinical Development* 2020; 16: 238-254. DOI: 10.1016/j.omtm.2020.01.012.

182. Montagna E, de Campos NSP, Porto VA, et al. CD19 CAR T cells for B cell malignancies: a systematic review and meta-analysis focused on clinical impacts of CAR structural domains, manufacturing conditions, cellular product, doses, patient's age, and tumor types. *BMC Cancer* 2024; 24: 1037. DOI: 10.1186/s12885-024-12651-6.

183. Gomes-Silva D, Mukherjee M, Srinivasan M, et al. Tonic 4-1BB Costimulation in Chimeric Antigen Receptors Impedes T Cell Survival and Is Vector-Dependent. *Cell Rep* 2017; 21: 17-26. 2017/10/06. DOI: 10.1016/j.celrep.2017.09.015.

184. Lepletier A, Lutzky VP, Mittal D, et al. The immune checkpoint CD96 defines a distinct lymphocyte phenotype and is highly expressed on tumor-infiltrating T cells. *Immunol Cell Biol* 2019; 97: 152-164. 2018/09/18. DOI: 10.1111/imcb.12205.

185. Kim HH, Tharayil M and Rudd CE. Growth factor receptor-bound protein 2 SH2/SH3 domain binding to CD28 and its role in co-signaling. *J Biol Chem* 1998; 273: 296-301. 1998/02/07. DOI: 10.1074/jbc.273.1.296.

186. Shan X, Czar MJ, Bunnell SC, et al. Deficiency of PTEN in Jurkat T cells causes constitutive localization of Itk to the plasma membrane and hyperresponsiveness to CD3 stimulation. *Mol Cell Biol* 2000; 20: 6945-6957. 2000/08/25. DOI: 10.1128/mcb.20.18.6945-6957.2000.

187. Shim J, Lim H, R.Yates J, et al. Nuclear Export of NF90 Is Required for Interleukin-2 mRNA Stabilization. *Molecular Cell* 2002; 10: 1331-1344. DOI: https://doi.org/10.1016/S1097-2765(02)00730-X.

188. Pei Y, Zhu P, Dang Y, et al. Nuclear export of NF90 to stabilize IL-2 mRNA is mediated by AKT-dependent phosphorylation at Ser647 in response to CD28 costimulation. *J Immunol* 2008; 180: 222-229. 2007/12/22. DOI: 10.4049/jimmunol.180.1.222.

189. Cai YC, Cefai D, Schneider H, et al. Selective CD28pYMNM mutations implicate phosphatidylinositol 3-kinase in CD86-CD28-mediated costimulation. *Immunity* 1995; 3: 417-426. 1995/10/01. DOI: 10.1016/1074-7613(95)90171-x.

190. Andersen TCB, Kristiansen PE, Huszenicza Z, et al. The SH3 domains of the protein kinases ITK and LCK compete for adjacent sites on T cell-specific adapter protein. *J Biol Chem* 2019; 294: 15480-15494. 2019/09/06. DOI: 10.1074/jbc.RA119.008318.

191. Marengère LE, Okkenhaug K, Clavreul A, et al. The SH3 domain of Itk/Emt binds to proline-rich sequences in the cytoplasmic domain of the T cell costimulatory receptor CD28. *J Immunol* 1997; 159: 3220-3229. 1997/10/08.

192. Dubovsky JA, Beckwith KA, Natarajan G, et al. Ibrutinib is an irreversible molecular inhibitor of ITK driving a Th1-selective pressure in T lymphocytes. *Blood* 2013; 122: 2539-2549. 2013/07/28. DOI: 10.1182/blood-2013-06-507947.

193. Kim EH, Sullivan JA, Plisch EH, et al. Signal Integration by Akt Regulates CD8 T Cell Effector and Memory Differentiation. *The Journal of Immunology* 2012; 188: 4305-4314. DOI: 10.4049/jimmunol.1103568.

194. He Y, Sun MM, Zhang GG, et al. Targeting PI3K/Akt signal transduction for cancer therapy. *Signal Transduction and Targeted Therapy* 2021; 6: 425. DOI: 10.1038/s41392-021-00828-5.

195. Ku GM, Yablonski D, Manser E, et al. A PAK1-PIX-PKL complex is activated by the T-cell receptor independent of Nck, Slp-76 and LAT. *Embo j* 2001; 20: 457-465. 2001/02/07. DOI: 10.1093/emboj/20.3.457.

196. Das S, Cho J, Lambertz I, et al. Tpl2/cot signals activate ERK, JNK, and NF-kappaB in a cell-type and stimulus-specific manner. *J Biol Chem* 2005; 280: 23748-23757. 2005/04/19. DOI: 10.1074/jbc.M412837200.

197. Belich MP, Salmerón A, Johnston LH, et al. TPL-2 kinase regulates the proteolysis of the NF-κB-inhibitory protein NF-κB1 p105. *Nature* 1999; 397: 363-368. DOI: 10.1038/16946.

198. Melenhorst JJ, Chen GM, Wang M, et al. Decade-long leukaemia remissions with persistence of CD4+ CAR T cells. *Nature* 2022; 602: 503-509. DOI: 10.1038/s41586-021-04390-6.

199. Fulton RB, Hamilton SE, Xing Y, et al. The TCR's sensitivity to self peptide-MHC dictates the ability of naive CD8(+) T cells to respond to foreign antigens. *Nat Immunol* 2015; 16: 107-117. 2014/11/25. DOI: 10.1038/ni.3043.

200. Kouro T, Himuro H and Sasada T. Exhaustion of CAR T cells: potential causes and solutions. *Journal of Translational Medicine* 2022; 20: 239. DOI: 10.1186/s12967-022-03442-3.

201. Chen J, Qiu S, Li W, et al. Tuning charge density of chimeric antigen receptor optimizes tonic signaling and CAR-T cell fitness. *Cell Research* 2023; 33: 341-354. DOI: 10.1038/s41422-023-00789-0.

202. Salter AI, Ivey RG, Kennedy JJ, et al. Phosphoproteomic analysis of chimeric antigen receptor signaling reveals kinetic and quantitative differences that affect cell function. *Science Signaling* 2018; 11: eaat6753. DOI: doi:10.1126/scisignal.aat6753.

203. Yasukawa M, Ohminami H, Arai J, et al. Granule exocytosis, and not the fas/fas ligand system, is the main pathway of cytotoxicity mediated by alloantigen-specific CD4(+) as well as CD8(+) cytotoxic T lymphocytes in humans. *Blood* 2000; 95: 2352-2355. 2000/03/25.

204. Dobrin A, Lindenbergh PL, Shi Y, et al. Synthetic dual co-stimulation increases the potency of HIT and TCR-targeted cell therapies. *Nature Cancer* 2024; 5: 760-773. DOI: 10.1038/s43018-024-00744-x.

205. Aktas E, Kucuksezer UC, Bilgic S, et al. Relationship between CD107a expression and cytotoxic activity. *Cell Immunol* 2009; 254: 149-154. 2008/10/07. DOI: 10.1016/j.cellimm.2008.08.007.

206. Banta KL, Xu X, Chitre AS, et al. Mechanistic convergence of the TIGIT and PD-1 inhibitory pathways necessitates co-blockade to optimize anti-tumor CD8(+) T cell responses. *Immunity* 2022; 55: 512-526.e519. 2022/03/10. DOI: 10.1016/j.immuni.2022.02.005.

207. Karp DR and Long EO. Identification of HLA-DR1 beta chain residues critical for binding staphylococcal enterotoxins A and E. *J Exp Med* 1992; 175: 415-424. 1992/02/01. DOI: 10.1084/jem.175.2.415.

208. Hargreaves RE, Brehm RD, Tranter H, et al. Definition of sites on HLA-DR1 involved in the T cell response to staphylococcal enterotoxins E and C2. *Eur J Immunol* 1995; 25: 3437-3444. 1995/12/01. DOI: 10.1002/eji.1830251235.

209. Andersen PS, Lavoie PM, Sékaly R-P, et al. Role of the T Cell Receptor α Chain in Stabilizing TCR-Superantigen-MHC Class II Complexes. *Immunity* 1999; 10: 473-483. DOI: https://doi.org/10.1016/S1074-7613(00)80047-3.

210. Makida R, Hofer MF, Takase K, et al. Bacterial superantigens induce V beta-specific T cell receptor internalization. *Mol Immunol* 1996; 33: 891-900. 1996/07/01. DOI: 10.1016/0161-5890(96)84615-3.

211. Türk L, Filippov I, Arnold C, et al. Cytotoxic CD8(+) Temra cells show loss of chromatin accessibility at genes associated with T cell activation. *Front Immunol* 2024; 15: 1285798. 2024/02/19. DOI: 10.3389/fimmu.2024.1285798.

212. Tian Y, Babor M, Lane J, et al. Unique phenotypes and clonal expansions of human CD4 effector memory T cells re-expressing CD45RA. *Nature Communications* 2017; 8: 1473. DOI: 10.1038/s41467-017-01728-5.

213. Simon S, Voillet V, Vignard V, et al. PD-1 and TIGIT coexpression identifies a circulating CD8 T cell subset predictive of response to anti-PD-1 therapy. *Journal for ImmunoTherapy of Cancer* 2020; 8: e001631. DOI: 10.1136/jitc-2020-001631.

214. Yang ZZ, Kim HJ, Wu H, et al. TIGIT Expression Is Associated with T-cell Suppression and Exhaustion and Predicts Clinical Outcome and Anti-PD-1 Response in Follicular Lymphoma. *Clin Cancer Res* 2020; 26: 5217-5231. 2020/07/08. DOI: 10.1158/1078-0432.Ccr-20-0558.

215. Josefsson SE, Huse K, Kolstad A, et al. T Cells Expressing Checkpoint Receptor TIGIT Are Enriched in Follicular Lymphoma Tumors and Characterized by Reversible Suppression of T-cell Receptor Signaling. *Clin Cancer Res* 2018; 24: 870-881. 2017/12/09. DOI: 10.1158/1078-0432.Ccr-17-2337.

216. Johnston RJ, Comps-Agrar L, Hackney J, et al. The immunoreceptor TIGIT regulates antitumor and antiviral CD8+ T cell effector function. *Cancer cell* 2014; 26: 923-937.

217. Wherry EJ and Kurachi M. Molecular and cellular insights into T cell exhaustion. *Nat Rev Immunol* 2015; 15: 486-499. 2015/07/25. DOI: 10.1038/nri3862.

218. Watts TH. TNF/TNFR family members in costimulation of T cell responses. *Annu Rev Immunol* 2005; 23: 23-68.

219. Weinberg AD, Rivera M-M, Prell R, et al. Engagement of the OX-40 receptor in vivo enhances antitumor immunity. *The Journal of Immunology* 2000; 164: 2160-2169.

220. Andarini S, Kikuchi T, Nukiwa M, et al. Adenovirus vector-mediated in vivo gene transfer of OX40 ligand to tumor cells enhances antitumor immunity of tumor-bearing hosts. *Cancer research* 2004; 64: 3281-3287.

221. Zhang P, Tu GH, Wei J, et al. Ligand-Blocking and Membrane-Proximal Domain Targeting Anti-OX40 Antibodies Mediate Potent T Cell-Stimulatory and Anti-Tumor Activity. *Cell Reports* 2019; 27: 3117-3123.e3115. DOI: https://doi.org/10.1016/j.celrep.2019.05.027.

222. Yu X, Chan HTC, Orr CM, et al. Complex Interplay between Epitope Specificity and Isotype Dictates the Biological Activity of Anti-human CD40 Antibodies. *Cancer Cell* 2018; 33: 664-675.e664. 2018/03/27. DOI: 10.1016/j.ccell.2018.02.009.

223. Lee PS, Chau B, Barman I, et al. Antibody blockade of CD96 by distinct molecular mechanisms. *MAbs* 2021; 13: 1979800. 2021/10/02. DOI: 10.1080/19420862.2021.1979800.

224. Bulliard Y, Jolicoeur R, Zhang J, et al. OX40 engagement depletes intratumoral Tregs via activating FcγRs, leading to antitumor efficacy. *Immunology & Cell Biology* 2014; 92: 475-480. DOI: https://doi.org/10.1038/icb.2014.26.

225. Flem-Karlsen K, Fodstad Ø, Tan M, et al. B7-H3 in cancer–beyond immune regulation. *Trends in cancer* 2018; 4: 401-404.

226. Li H-y, Chen Y-l, Deng X-n, et al. Bispecific antibody targeting both B7-H3 and PD-L1 exhibits superior antitumor activities. *Acta Pharmacologica Sinica* 2023; 44: 2322-2330. DOI: 10.1038/s41401-023-01118-2.

227. Majocchi S, Lloveras P, Nouveau L, et al. NI-3201 Is a Bispecific Antibody Mediating PD-L1-Dependent CD28 Co-stimulation on T Cells for Enhanced Tumor Control. *Cancer Immunol Res* 2025: Of1-of19. 2025/01/06. DOI: 10.1158/2326-6066.Cir-24-0298.

228. Friend LD, Shah DD, Deppong C, et al. A dose-dependent requirement for the proline motif of CD28 in cellular and humoral immunity revealed by a targeted knockin mutant. *Journal of Experimental Medicine* 2006; 203: 2121-2133. DOI: 10.1084/jem.20052230.

229. Li SS. Specificity and versatility of SH3 and other proline-recognition domains: structural basis and implications for cellular signal transduction. *Biochem J* 2005; 390: 641-653. 2005/09/02. DOI: 10.1042/bj20050411.

230. Chiang EY, de Almeida PE, de Almeida Nagata DE, et al. CD96 functions as a co-stimulatory receptor to enhance CD8(+) T cell activation and effector responses. *Eur J Immunol* 2020; 50: 891-902. 2020/02/12. DOI: 10.1002/eji.201948405.

231. Okkenhaug K. Signaling by the phosphoinositide 3-kinase family in immune cells. *Annu Rev Immunol* 2013; 31: 675-704. 2013/01/22. DOI: 10.1146/annurev-immunol-032712-095946.

232. Barrow AD, Astoul E, Floto A, et al. Cutting edge: TREM-like transcript-1, a platelet immunoreceptor tyrosine-based inhibition motif encoding costimulatory immunoreceptor that enhances, rather than inhibits, calcium signaling via SHP-2. *The Journal of Immunology* 2004; 172: 5838-5842.

233. Porter DL, Hwang W-T, Frey NV, et al. Chimeric antigen receptor T cells persist and induce sustained remissions in relapsed refractory chronic lymphocytic leukemia. *Science translational medicine* 2015; 7: 303ra139-303ra139.

234. Guedan S, Madar A, Casado-Medrano V, et al. Single residue in CD28-costimulated CAR-T cells limits long-term persistence and antitumor durability. *The Journal of clinical investigation* 2020; 130: 3087-3097.

235. Huang X, Pawge G, Snicer CE, et al. PVR exposure influences the activation, adhesion, and protein expression of human CD8+ T cells, including the CD96-mediated transfer of PVR. *The Journal of Immunology* 2025; 214: 55-71. DOI: 10.1093/jimmun/vkae002.

236. Tekguc M, Wing JB, Osaki M, et al. Treg-expressed CTLA-4 depletes CD80/CD86 by trogocytosis, releasing free PD-L1 on antigen-presenting cells. *Proceedings of the National Academy of Sciences* 2021; 118: e2023739118.

237. Hasim MS, Marotel M, Hodgins JJ, et al. When killers become thieves: Trogocytosed PD-1 inhibits NK cells in cancer. *Sci Adv* 2022; 8: eabj3286. 2022/04/14. DOI: 10.1126/sciadv.abj3286.

238. Mueller S, Cao X, Welker R, et al. Interaction of the poliovirus receptor CD155 with the dynein light chain Tctex-1 and its implication for poliovirus pathogenesis. *Journal of Biological Chemistry* 2002; 277: 7897-7904.

239. Oda T, Ohka S and Nomoto A. Ligand stimulation of CD155α inhibits cell adhesion and enhances cell migration in fibroblasts. *Biochemical and biophysical research communications* 2004; 319: 1253-1264.

240. Schneider H, Smith X, Liu H, et al. CTLA-4 disrupts ZAP70 microcluster formation with reduced T cell/APC dwell times and calcium mobilization. *European journal of immunology* 2008; 38: 40-47.

241. Chuang E, Lee K-M, Robbins MD, et al. Regulation of cytotoxic T lymphocyte-associated molecule-4 by Src kinases. *The Journal of Immunology* 1999; 162: 1270-1277.

242. Chikuma S, Murakami M, Tanaka K, et al. Janus kinase 2 is associated with a box 1-like motif and phosphorylates a critical tyrosine residue in the cytoplasmic region of cytotoxic T lymphocyte associated molecule-4. *Journal of Cellular Biochemistry* 2000; 78: 241-250.

243. Krummel MF and Allison JP. CTLA-4 engagement inhibits IL-2 accumulation and cell cycle progression upon activation of resting T cells. *J Exp Med* 1996; 183: 2533-2540.

244. Courtney AH, Shvets AA, Lu W, et al. CD45 functions as a signaling gatekeeper in T cells. *Sci Signal* 2019; 12 2019/10/24. DOI: 10.1126/scisignal.aaw8151.

245. Holmes VM, Maluquer de Motes C, Richards PT, et al. Interaction between nectin-1 and the human natural killer cell receptor CD96. *PloS one* 2019; 14: e0212443-e0212443. DOI: 10.1371/journal.pone.0212443.

246. Kalos M, Levine BL, Porter DL, et al. T cells with chimeric antigen receptors have potent antitumor effects and can establish memory in patients with advanced leukemia. *Sci Transl Med* 2011; 3: 95ra73. 2011/08/13. DOI: 10.1126/scitranslmed.3002842.

247. Song DG, Ye Q, Carpenito C, et al. In vivo persistence, tumor localization, and antitumor activity of CAR-engineered T cells is enhanced by costimulatory signaling through CD137 (4-1BB). *Cancer Res* 2011; 71: 4617-4627. 2011/05/07. DOI: 10.1158/0008-5472.CAN-11-0422.

248. Guedan S, Posey AD, Jr., Shaw C, et al. Enhancing CAR T cell persistence through ICOS and 4-1BB costimulation. *JCI Insight* 2018; 3 2018/01/13. DOI: 10.1172/jci.insight.96976.

249. Guercio M, Orlando D, Di Cecca S, et al. CD28.OX40 co-stimulatory combination is associated with long in vivo persistence and high activity of CAR.CD30 T-cells. *Haematologica* 2021; 106: 987-999. 2020/05/10. DOI: 10.3324/haematol.2019.231183.

250. Rudin CM, Liu SV, Soo RA, et al. SKYSCRAPER-02: Tiragolumab in Combination With Atezolizumab Plus Chemotherapy in Untreated Extensive-Stage Small-Cell Lung Cancer. *Journal of Clinical Oncology* 2024; 42: 324-335. DOI: 10.1200/jco.23.01363.

Appendix A γ-retrovirus maps

A.1 pMP71-huCD96v2 plasmid map

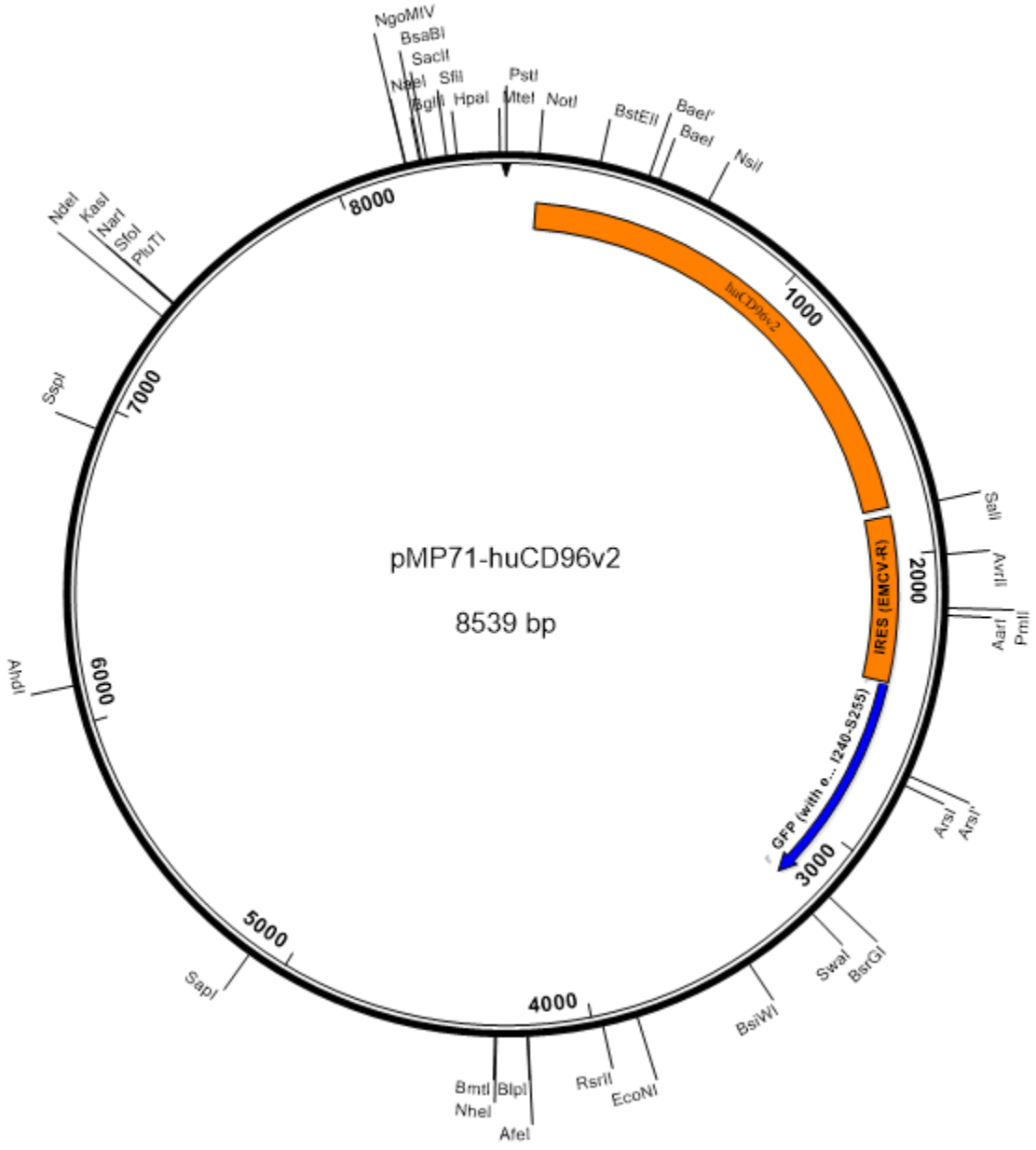

Appendix 1 Plasmid map of pMP71-huCD96v2

A.2 pMP71-mCD96 plasmid map

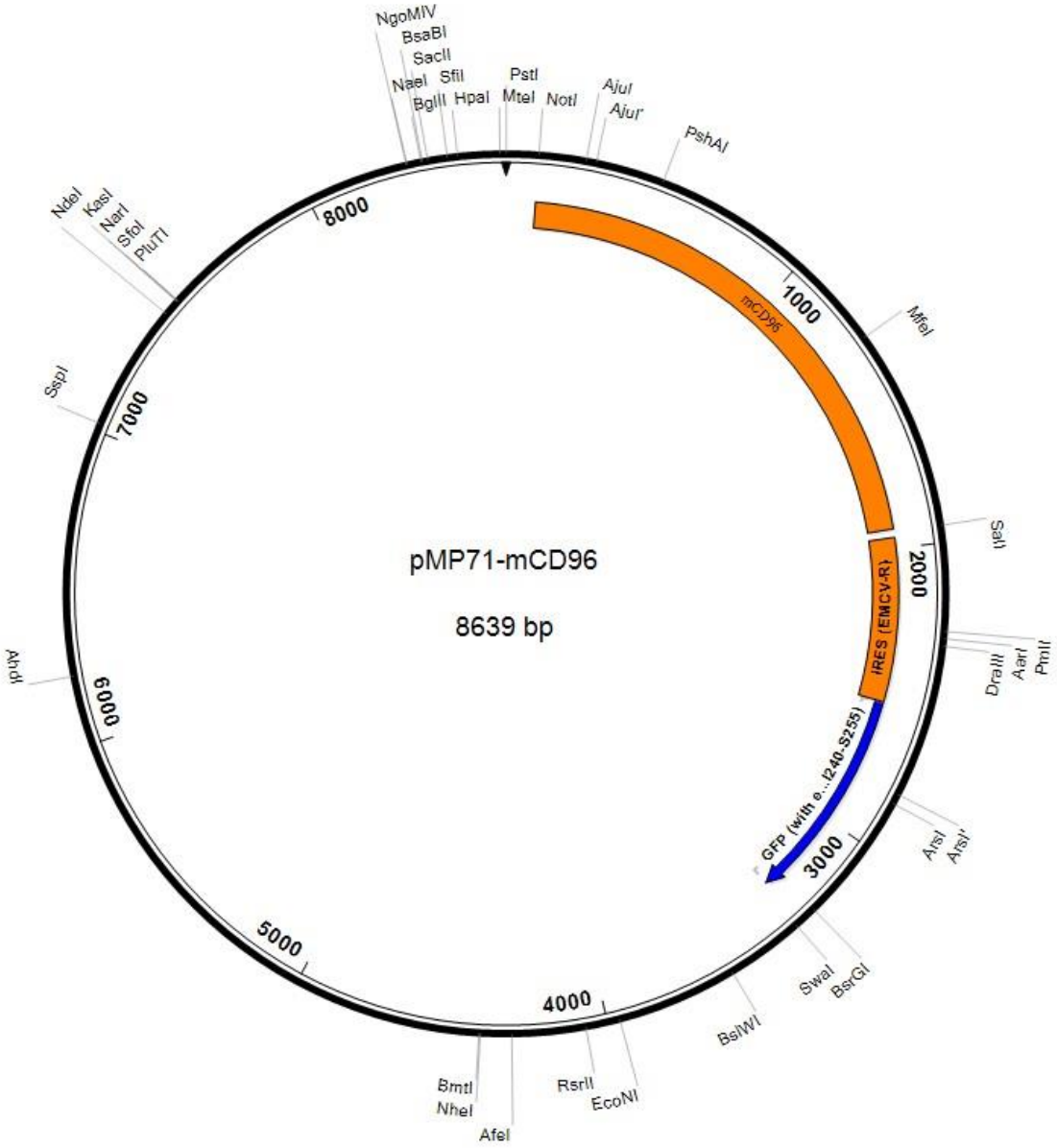

Appendix 2 Plasmid map of pMP71-mCD96

A.3 pMP71-huCD226 plasmid map

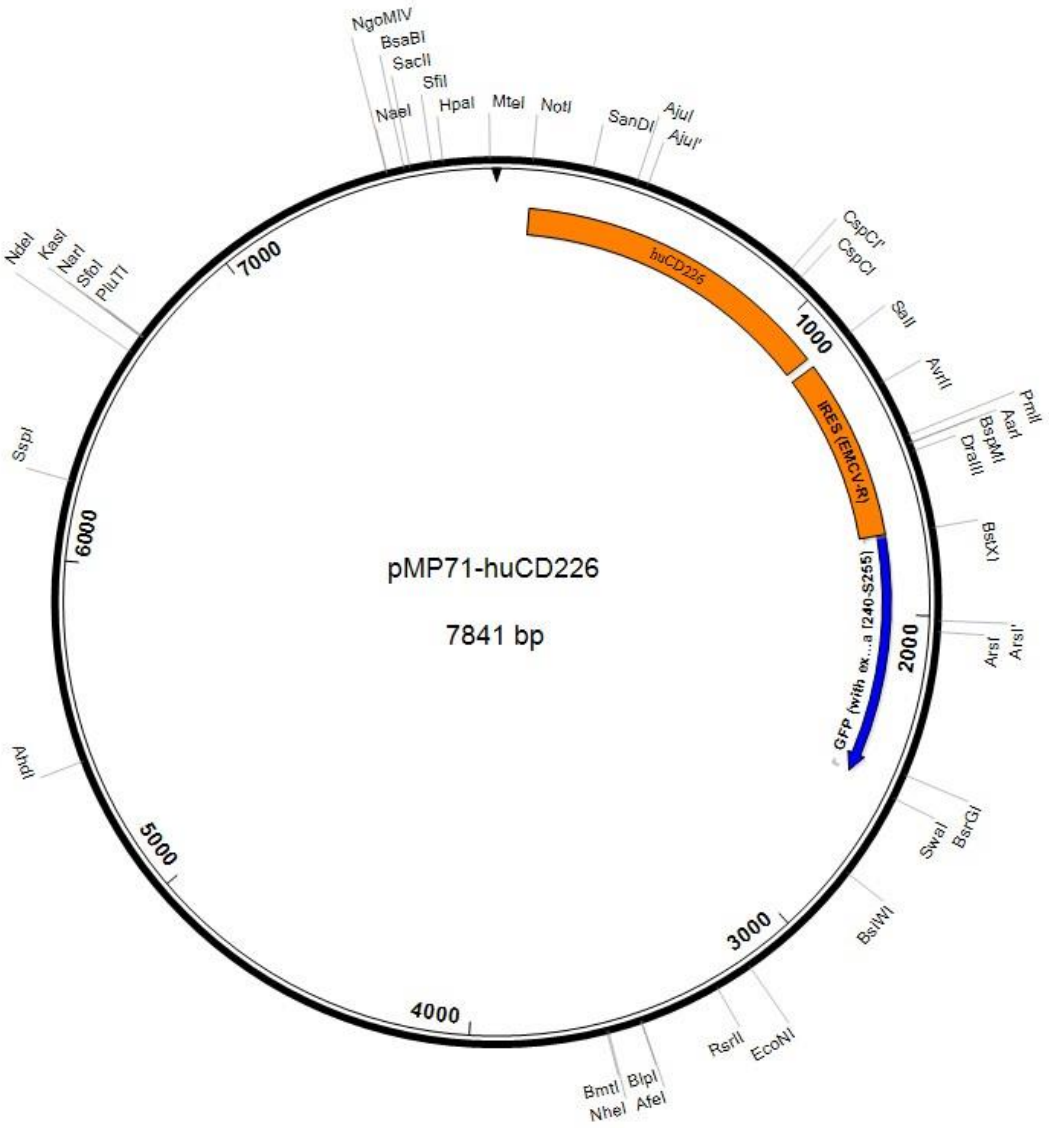

Appendix 3 Plasmid map of pMP71-huCD226

A.4 pMP71-mCD226 plasmid map

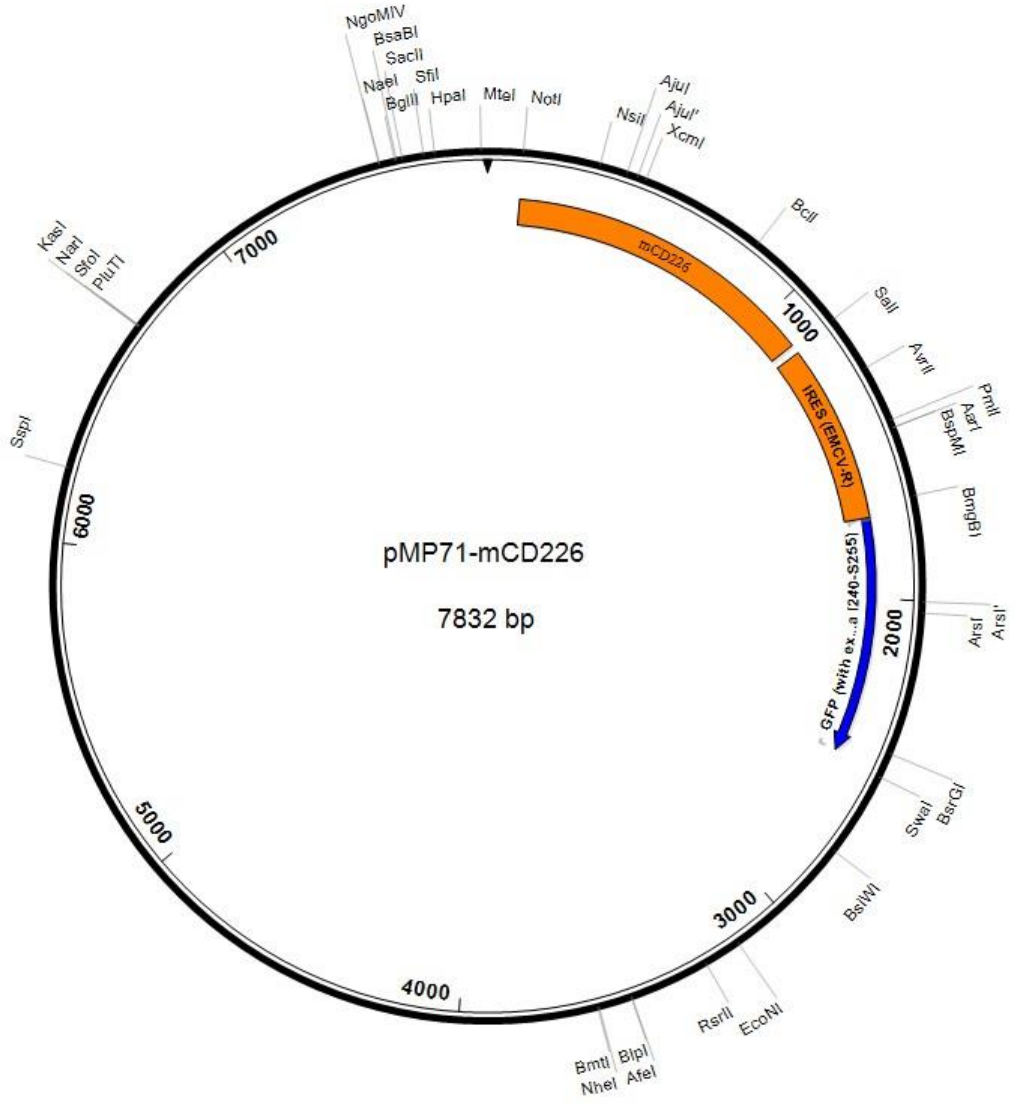

Appendix 4 Plasmid map of pMP71-mCD226

A.5 pCL-Eco plasmid map

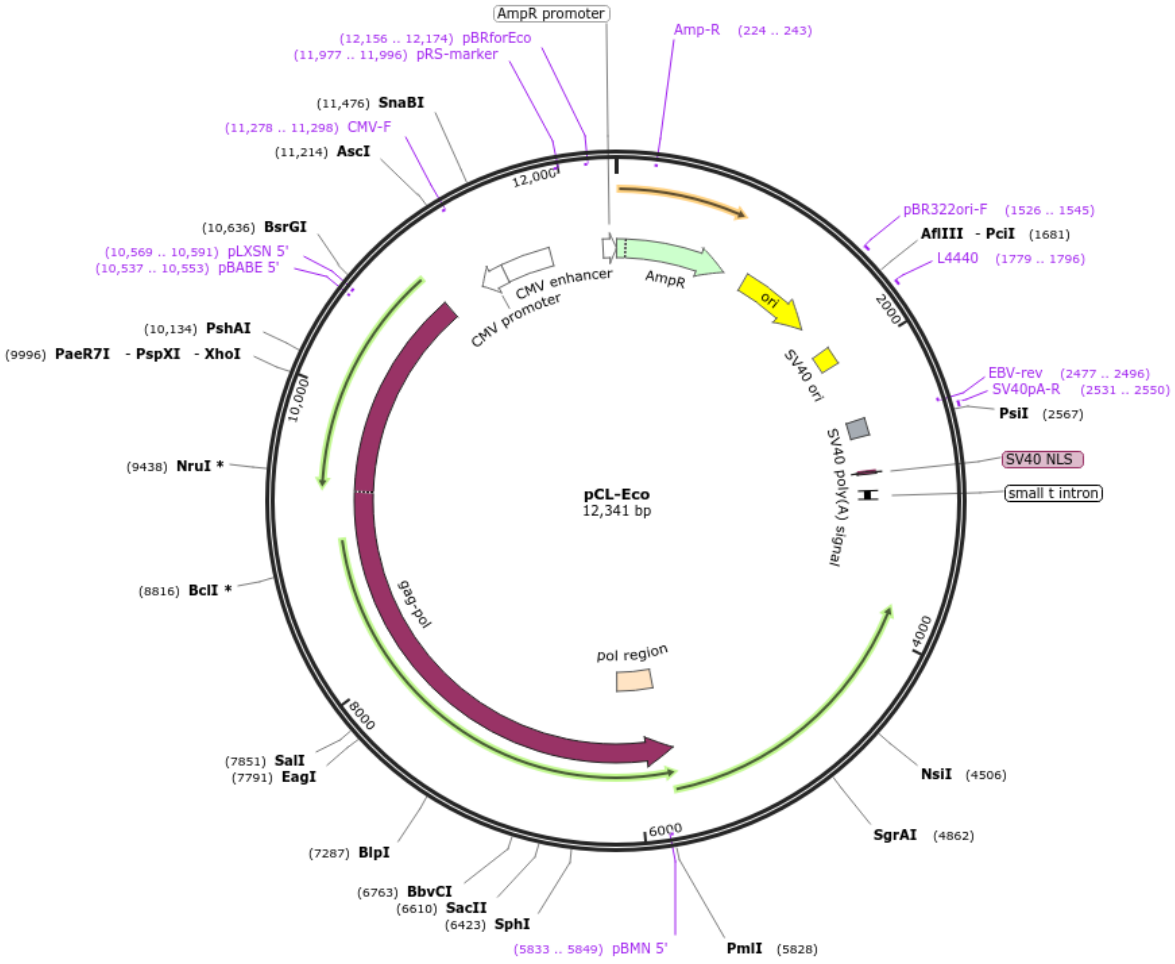

Appendix 5 Plasmid map of pCL-Eco

Appendix B Lentivirus plasmid maps

B.1 pM13328 Plasmid Map

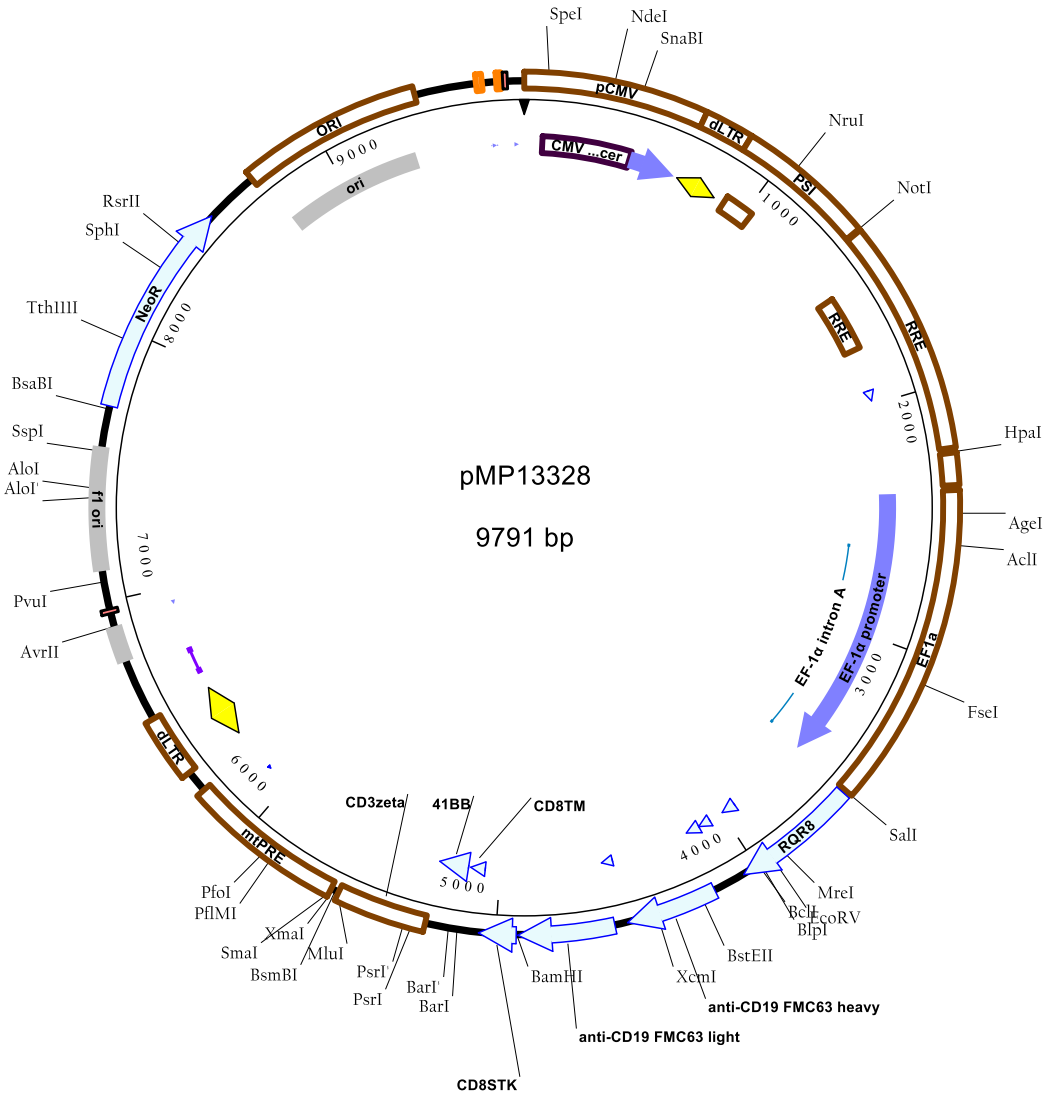

Appendix 6 Plasmid map of pMP13328

B.2 pMDG.1 Plasmid Map

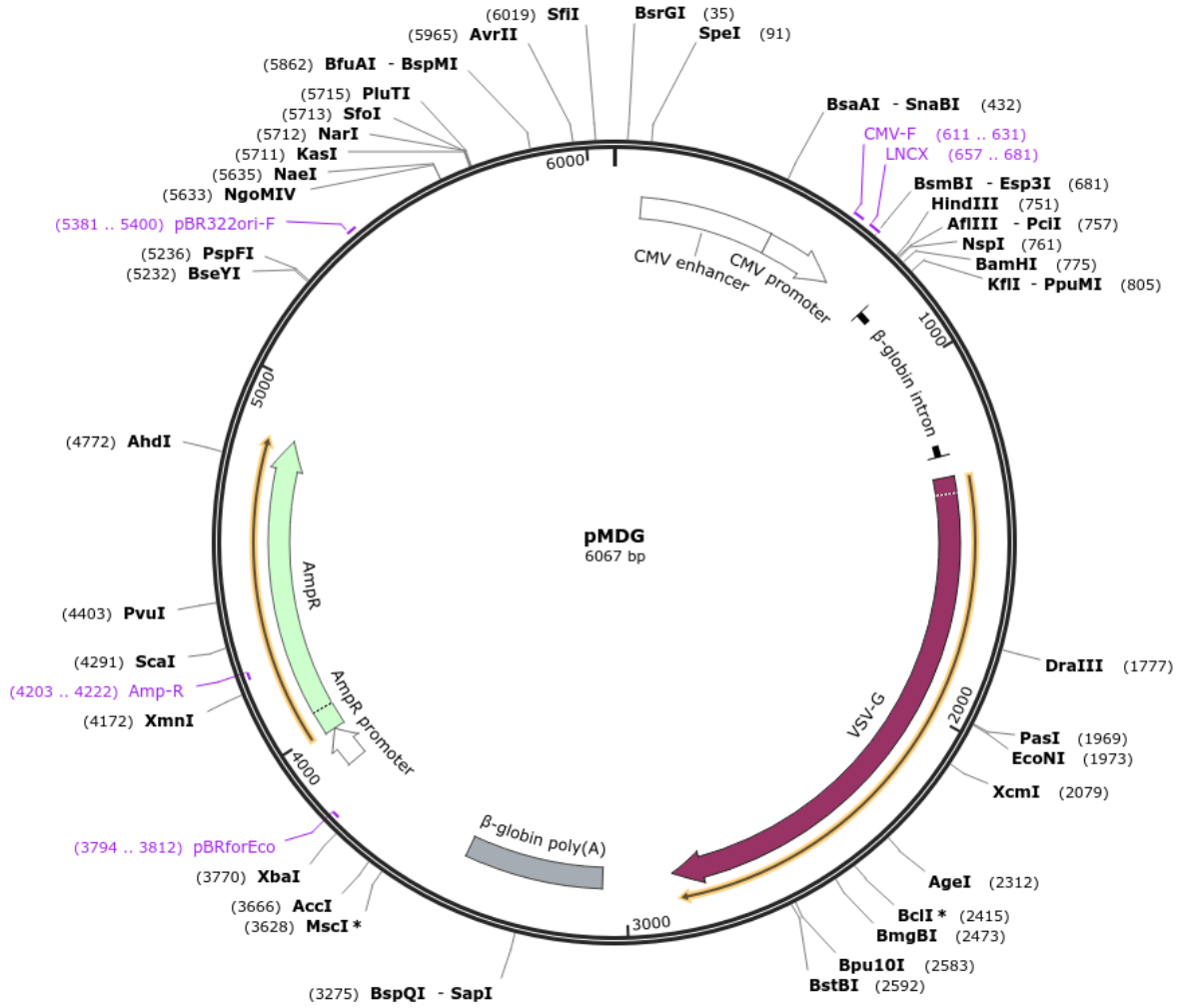

Appendix 7 Plasmid map of pMDG.1

B.1 pMDLgp.RRE Plasmid Map

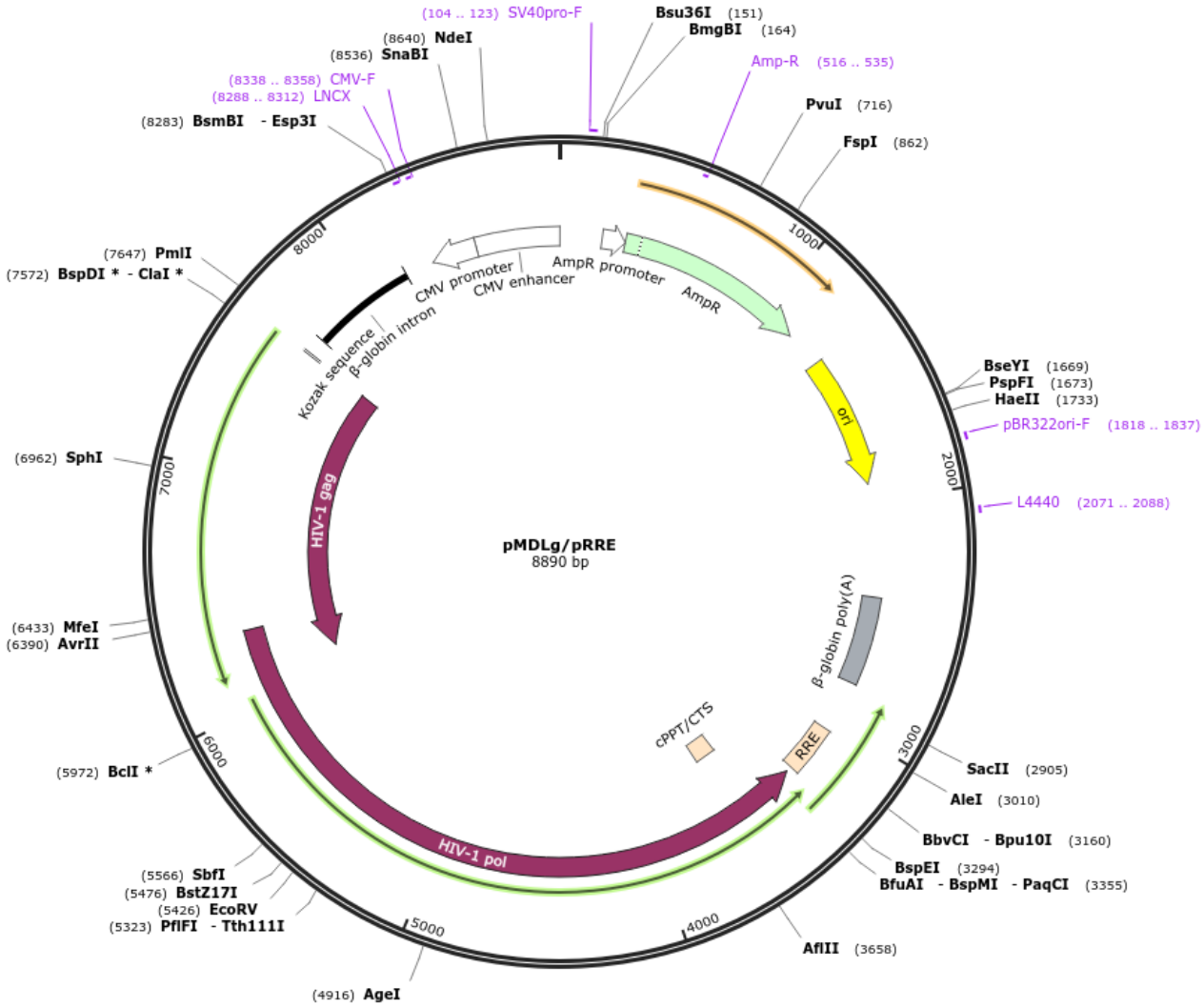

Appendix 8 Plasmid map of pMDL/pRRE

B.1 pRSV.Rev Plasmid Map

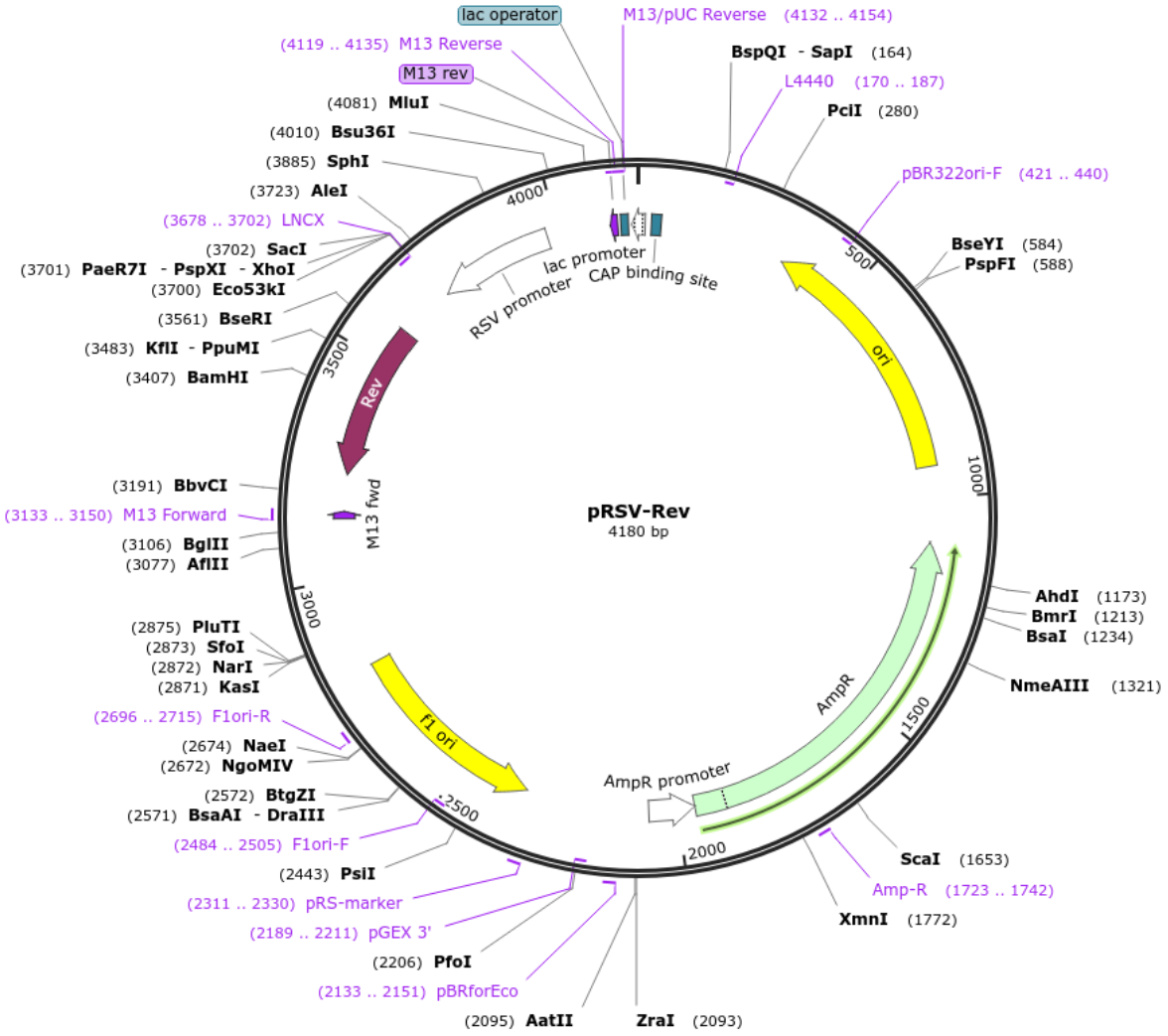

Appendix 9 Plasmid map of pRSV-Rev

Appendix C CD96 CAR Sequences

RQR8-CD8TM-T2A-FMC63-CD8TM-4-1BB-CD3Z

MLTSLLCWMALCLLGADHADACPYSNPSLCSGGGGSELPTQGTFSNVSTNVSPAKPTTTACPYSNPSLCSGGGGSP
APRPPTPAPTIASQPLSLRPEACRPAAGGAVHTRGLDFACDIYIWAPLAGTCGVLLLSLVITLYCNHRNRRRVCKCPR
PVVRAEGRGSLLTCGDVEENPGPMETDTLLLWVLLLWVPGSTGDIQMTQTTSSLSASLGDRVTISCRASQDISKYLN
WYQQKPDGTVKLLIYHTSRLHSGVPSRFSGSGSGTDYSLTISNLEQEDIATYFCQQGNTLPYTFGGGTKLEITKAGGG
GSGGGGSGGGGSGGGGSEVKLQESGPGLVAPSQSLSVTCTVSGVSLPDYGVSWIRQPPRKGLEWLGVIWGSETTY
YNSALKSRLTIIKDNSKSQVFLKMNSLQTDDTAIYYCAKHYYYGGSYAMDYWGQGTSVTVSSDPTTTPAPRPPTPAP
TIASQPLSLRPEACRPAAGGAVHTRGLDFACDIYIWAPLAGTCGVLLLSLVITLYCKRGRKKLLYIFKQPFMRPVQTTQ
EEDGCSCRFPEEEEGGCELRVKFSRSADAPAYQQGQNQLYNELNLGRREEYDVLDKRRGRDPEMGGKPRRKNPQE
GLYNELQKDKMAEAYSEIGMKGERRRGKGHDGLYQGLSTATKDTYDALHMQALPPR

RQR8-CD8TM-T2A-FMC63-CD8TM-CD3Z

MLTSLLCWMALCLLGADHADACPYSNPSLCSGGGGSELPTQGTFSNVSTNVSPAKPTTTACPYSNPSLCSGGGGSP
APRPPTPAPTIASQPLSLRPEACRPAAGGAVHTRGLDFACDIYIWAPLAGTCGVLLLSLVITLYCNHRNRRRVCKCPR
PVVRAEGRGSLLTCGDVEENPGPMETDTLLLWVLLLWVPGSTGDIQMTQTTSSLSASLGDRVTISCRASQDISKYLN
WYQQKPDGTVKLLIYHTSRLHSGVPSRFSGSGSGTDYSLTISNLEQEDIATYFCQQGNTLPYTFGGGTKLEITKAGGG
GSGGGGSGGGGSGGGGSEVKLQESGPGLVAPSQSLSVTCTVSGVSLPDYGVSWIRQPPRKGLEWLGVIWGSETTY
YNSALKSRLTIIKDNSKSQVFLKMNSLQTDDTAIYYCAKHYYYGGSYAMDYWGQGTSVTVSSDPTTTPAPRPPTPAP
TIASQPLSLRPEACRPAAGGAVHTRGLDFACDIYIWAPLAGTCGVLLLSLVITLYCRVKFSRSADAPAYQQGQNQLYN
ELNLGRREEYDVLDKRRGRDPEMGGKPRRKNPQEGLYNELQKDKMAEAYSEIGMKGERRRGKGHDGLYQGLSTA
TKDTYDALHMQALPPR

RQR8-CD8TM-T2A-FMC63-CD8TM-4-1BBnull-CD3Z

MLTSLLCWMALCLLGADHADACPYSNPSLCSGGGGSELPTQGTFSNVSTNVSPAKPTTTACPYSNPSLCSGGGGSP
APRPPTPAPTIASQPLSLRPEACRPAAGGAVHTRGLDFACDIYIWAPLAGTCGVLLLSLVITLYCNHRNRRRVCKCPR
PVVRAEGRGSLLTCGDVEENPGPMETDTLLLWVLLLWVPGSTGDIQMTQTTSSLSASLGDRVTISCRASQDISKYLN
WYQQKPDGTVKLLIYHTSRLHSGVPSRFSGSGSGTDYSLTISNLEQEDIATYFCQQGNTLPYTFGGGTKLEITKAGGG
GSGGGGSGGGGSGGGGSEVKLQESGPGLVAPSQSLSVTCTVSGVSLPDYGVSWIRQPPRKGLEWLGVIWGSETTY
YNSALKSRLTIIKDNSKSQVFLKMNSLQTDDTAIYYCAKHYYYGGSYAMDYWGQGTSVTVSSDPTTTPAPRPPTPAP
TIASQPLSLRPEACRPAAGGAVHTRGLDFACDIYIWAPLAGTCGVLLLSLVITLYCK

RQR8-CD8TM-T2A-FMC63-CD8TM-CD96-CD3Z

MLTSLLCWMALCLLGADHADACPYSNPSLCSGGGGSELPTQGTFSNVSTNVSPAKPTTTACPYSNPSLCSGGGGSP
APRPPTPAPTIASQPLSLRPEACRPAAGGAVHTRGLDFACDIYIWAPLAGTCGVLLLSLVITLYCNHRNRRRVCKCPR
PVVRAEGRGSLLTCGDVEENPGPMETDTLLLWVLLLWVPGSTGDIQMTQTTSSLSASLGDRVTISCRASQDISKYLN
WYQQKPDGTVKLLIYHTSRLHSGVPSRFSGSGSGTDYSLTISNLEQEDIATYFCQQGNTLPYTFGGGTKLEITKAGGG
GSGGGGSGGGGSGGGGSEVKLQESGPGLVAPSQSLSVTCTVSGVSLPDYGVSWIRQPPRKGLEWLGVIWGSETTY
YNSALKSRLTIIKDNSKSQVFLKMNSLQTDDTAIYYCAKHYYYGGSYAMDYWGQGTSVTVSSDPTTTPAPRPPTPAP
TIASQPLSLRPEACRPAAGGAVHTRGLDFACDIYIWAPLAGTCGVLLLSLVITLYCRKWCQYQKEIMERPPPFKPPPP
PIKYTCIQEPNESDLPYHEMETLRVKFSRSADAPAYQQGQNQLYNELNLGRREEYDVLDKRRGRDPEMGGKPRRK
NPQEGLYNELQKDKMAEAYSEIGMKGERRRGKGHDGLYQGLSTATKDTYDALHMQALPPR

RQR8-CD8TM-T2A-FMC63-CD8TM-CD96.Y566A-CD3Z

MLTSLLCWMALCLLGADHADACPYSNPSLCSGGGGSELPTQGTFSNVSTNVSPAKPTTTACPYSNPSLCSGGGGSP
APRPPTPAPTIASQPLSLRPEACRPAAGGAVHTRGLDFACDIYIWAPLAGTCGVLLLSLVITLYCNHRNRRRVCKCPR
PVVRAEGRGSLLTCGDVEENPGPMETDTLLLWVLLLWVPGSTGDIQMTQTTSSLSASLGDRVTISCRASQDISKYLN
WYQQKPDGTVKLLIYHTSRLHSGVPSRFSGSGSGTDYSLTISNLEQEDIATYFCQQGNTLPYTFGGGTKLEITKAGGG
GSGGGGSGGGGSGGGGSEVKLQESGPGLVAPSQSLSVTCTVSGVSLPDYGVSWIRQPPRKGLEWLGVIWGSETTY
YNSALKSRLTIIKDNSKSQVFLKMNSLQTDDTAIYYCAKHYYYGGSYAMDYWGQGTSVTVSSDPTTTPAPRPPTPAP
TIASQPLSLRPEACRPAAGGAVHTRGLDFACDIYIWAPLAGTCGVLLLSLVITLYCRKWCQYQKEIMERPPPFKPPPP
PIKATCIQEPNESDLPYHEMETLRVKFSRSADAPAYQQGQNQLYNELNLGRREEYDVLDKRRGRDPEMGGKPRRK
NPQEGLYNELQKDKMAEAYSEIGMKGERRRGKGHDGLYQGLSTATKDTYDALHMQALPPR

RQR8-CD8TM-T2A-FMC63-CD8TM-CD96.YAMA-CD3Z

MLTSLLCWMALCLLGADHADACPYSNPSLCSGGGGSELPTQGTFSNVSTNVSPAKPTTTACPYSNPSLCSGGGGSP
APRPPTPAPTIASQPLSLRPEACRPAAGGAVHTRGLDFACDIYIWAPLAGTCGVLLLSLVITLYCNHRNRRRVCKCPR
PVVRAEGRGSLLTCGDVEENPGPMETDTLLLWVLLLWVPGSTGDIQMTQTTSSLSASLGDRVTISCRASQDISKYLN
WYQQKPDGTVKLLIYHTSRLHSGVPSRFSGSGSGTDYSLTISNLEQEDIATYFCQQGNTLPYTFGGGTKLEITKAGGG
GSGGGGSGGGGSGGGGSEVKLQESGPGLVAPSQSLSVTCTVSGVSLPDYGVSWIRQPPRKGLEWLGVIWGSETTY
YNSALKSRLTIIKDNSKSQVFLKMNSLQTDDTAIYYCAKHYYYGGSYAMDYWGQGTSVTVSSDPTTTPAPRPPTPAP
TIASQPLSLRPEACRPAAGGAVHTRGLDFACDIYIWAPLAGTCGVLLLSLVITLYCRKWCQYQKEIMERPPPFKPPPP
PIKYTCIQEPNESDLPAHEAETLRVKFSRSADAPAYQQGQNQLYNELNLGRREEYDVLDKRRGRDPEMGGKPRRKN
PQEGLYNELQKDKMAEAYSEIGMKGERRRGKGHDGLYQGLSTATKDTYDALHMQALPPR

RQR8-CD8TM-T2A-FMC63-CD8TM-CD96.P3A-CD3Z

MLTSLLCWMALCLLGADHADACPYSNPSLCSGGGGSELPTQGTFSNVSTNVSPAKPTTTACPYSNPSLCSGGGGSP
APRPPTPAPTIASQPLSLRPEACRPAAGGAVHTRGLDFACDIYIWAPLAGTCGVLLLSLVITLYCNHRNRRRVCKCPR
PVVRAEGRGSLLTCGDVEENPGPMETDTLLLWVLLLWVPGSTGDIQMTQTTSSLSASLGDRVTISCRASQDISKYLN
WYQQKPDGTVKLLIYHTSRLHSGVPSRFSGSGSGTDYSLTISNLEQEDIATYFCQQGNTLPYTFGGGTKLEITKAGGG
GSGGGGSGGGGSGGGGSEVKLQESGPGLVAPSQSLSVTCTVSGVSLPDYGVSWIRQPPRKGLEWLGVIWGSETTY
YNSALKSRLTIIKDNSKSQVFLKMNSLQTDDTAIYYCAKHYYYGGSYAMDYWGQGTSVTVSSDPTTTPAPRPPTPAP
TIASQPLSLRPEACRPAAGGAVHTRGLDFACDIYIWAPLAGTCGVLLLSLVITLYCRKWCQYQKEIMERAAAFKPPPP
PIKYTCIQEPNESDLPYHEMETLRVKFSRSADAPAYQQGQNQLYNELNLGRREEYDVLDKRRGRDPEMGGKPRRK
NPQEGLYNELQKDKMAEAYSEIGMKGERRRGKGHDGLYQGLSTATKDTYDALHMQALPPR

RQR8-CD8TM-T2A-FMC63-CD8TM-CD96.P4A-CD3Z

MLTSLLCWMALCLLGADHADACPYSNPSLCSGGGGSELPTQGTFSNVSTNVSPAKPTTTACPYSNPSLCSGGGGSP
APRPPTPAPTIASQPLSLRPEACRPAAGGAVHTRGLDFACDIYIWAPLAGTCGVLLLSLVITLYCNHRNRRRVCKCPR
PVVRAEGRGSLLTCGDVEENPGPMETDTLLLWVLLLWVPGSTGDIQMTQTTSSLSASLGDRVTISCRASQDISKYLN
WYQQKPDGTVKLLIYHTSRLHSGVPSRFSGSGSGTDYSLTISNLEQEDIATYFCQQGNTLPYTFGGGTKLEITKAGGG
GSGGGGSGGGGSGGGGSEVKLQESGPGLVAPSQSLSVTCTVSGVSLPDYGVSWIRQPPRKGLEWLGVIWGSETTY
YNSALKSRLTIIKDNSKSQVFLKMNSLQTDDTAIYYCAKHYYYGGSYAMDYWGQGTSVTVSSDPTTTPAPRPPTPAP
TIASQPLSLRPEACRPAAGGAVHTRGLDFACDIYIWAPLAGTCGVLLLSLVITLYCRKWCQYQKEIMERPPAFKAAPP
AIKYTCIQEPNESDLPYHEMETLRVKFSRSADAPAYQQGQNQLYNELNLGRREEYDVLDKRRGRDPEMGGKPRRK
NPQEGLYNELQKDKMAEAYSEIGMKGERRRGKGHDGLYQGLSTATKDTYDALHMQALPPR

Appendix D T-cell co-culture with unloaded Raji

D.1 TIGIT^{LO}CD226^{HI} T-cell proliferation induced by unloaded Raji

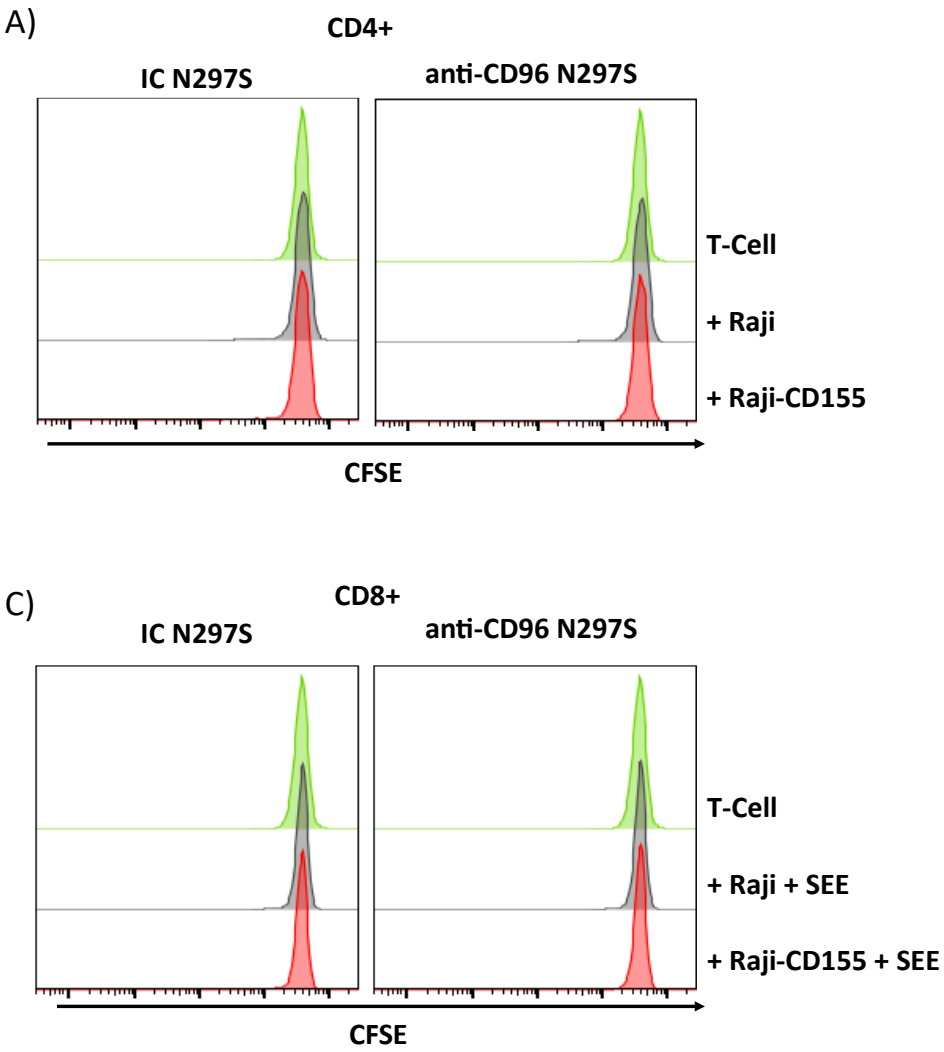

Appendix 10 Co-culture of TIGIT ^{LO}CD226^{HI} T-cells with unloaded Raji fails to induce T-cell proliferation

A) Representative histograms of CD4+ TIGIT ^{LO}CD226^{HI} T-cell CFSE dilution when cultured with non-blocking antibody (Left) or CD96 blocking antibody (Right). Conditions shown are T-cells alone (Green), with unloaded Raji (Grey) or with unloaded Raji-CD155 (Red). **B)** Representative histograms of CD8+ TIGIT ^{LO}CD226^{HI} T-cell CFSE dilution when cultured with non-blocking antibody (Left) or CD96 blocking antibody (Right). Conditions shown are T-cells alone (Green), with unloaded Raji (Grey) or with unloaded Raji-CD155 (Red).

D.2 TIGIT^{INT}CD226^{LO} T-cell proliferation induced by unloaded Raji cell

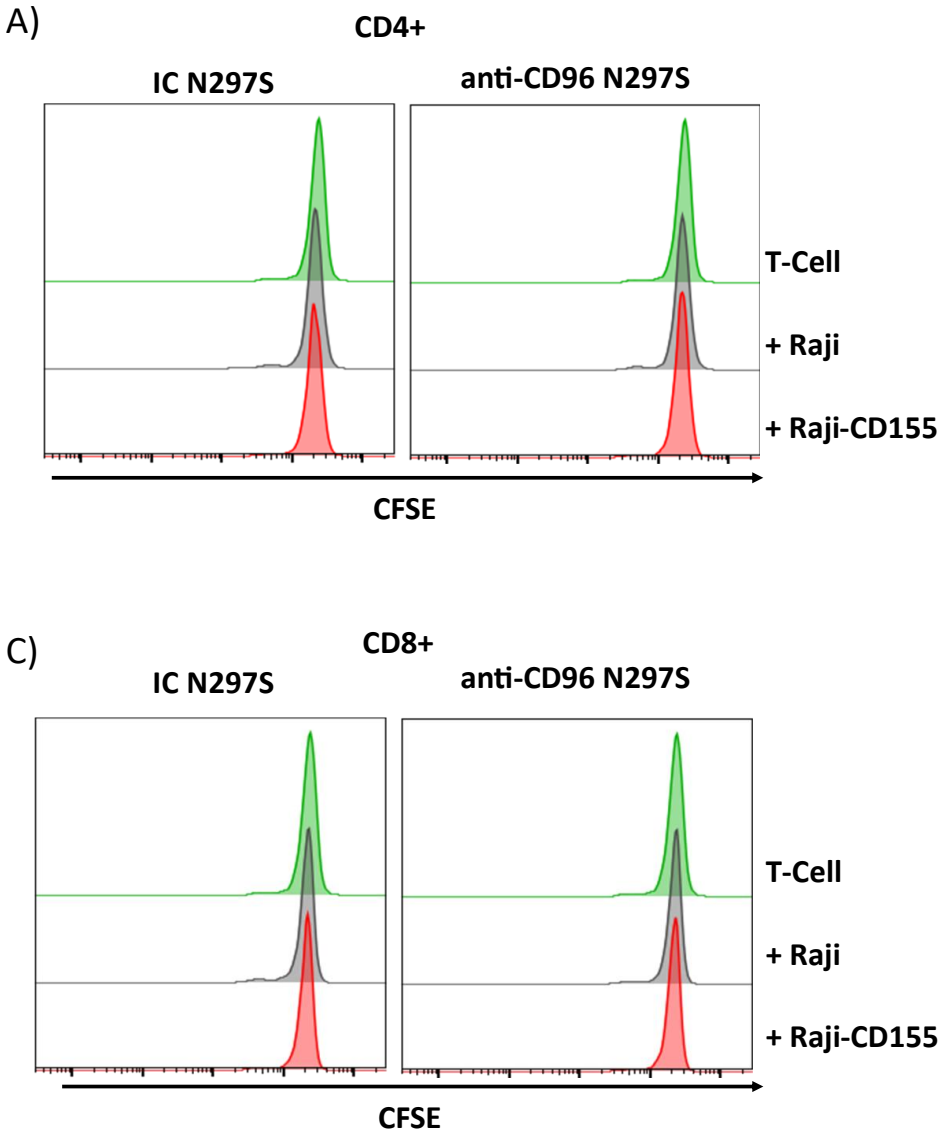

Appendix 11 Co-culture of TIGIT^{INT}CD226^{LO} T-cells with unloaded target cells fails to induce T-cell proliferation

A) Representative histograms of CD4+ TIGIT^{INT}CD226^{LO} T-cell CFSE dilution when cultured with non-blocking antibody (Left) or CD96 blocking antibody (Right). Conditions shown are T-cells alone (Green), with unloaded Raji (Grey) or with unloaded Raji-CD155 (Red). **B)** Representative histograms of CD8+ TIGIT^{INT}CD226^{LO} T-cell CFSE dilution when cultured with non-blocking antibody (Left) or CD96 blocking antibody (Right). Conditions shown are T-cells alone (Green), with unloaded Raji (Grey) or with unloaded Raji-CD155 (Red).

D.3 TIGIT^{HI}CD226^{HI} T-cell proliferation induced by unloaded Raji cell

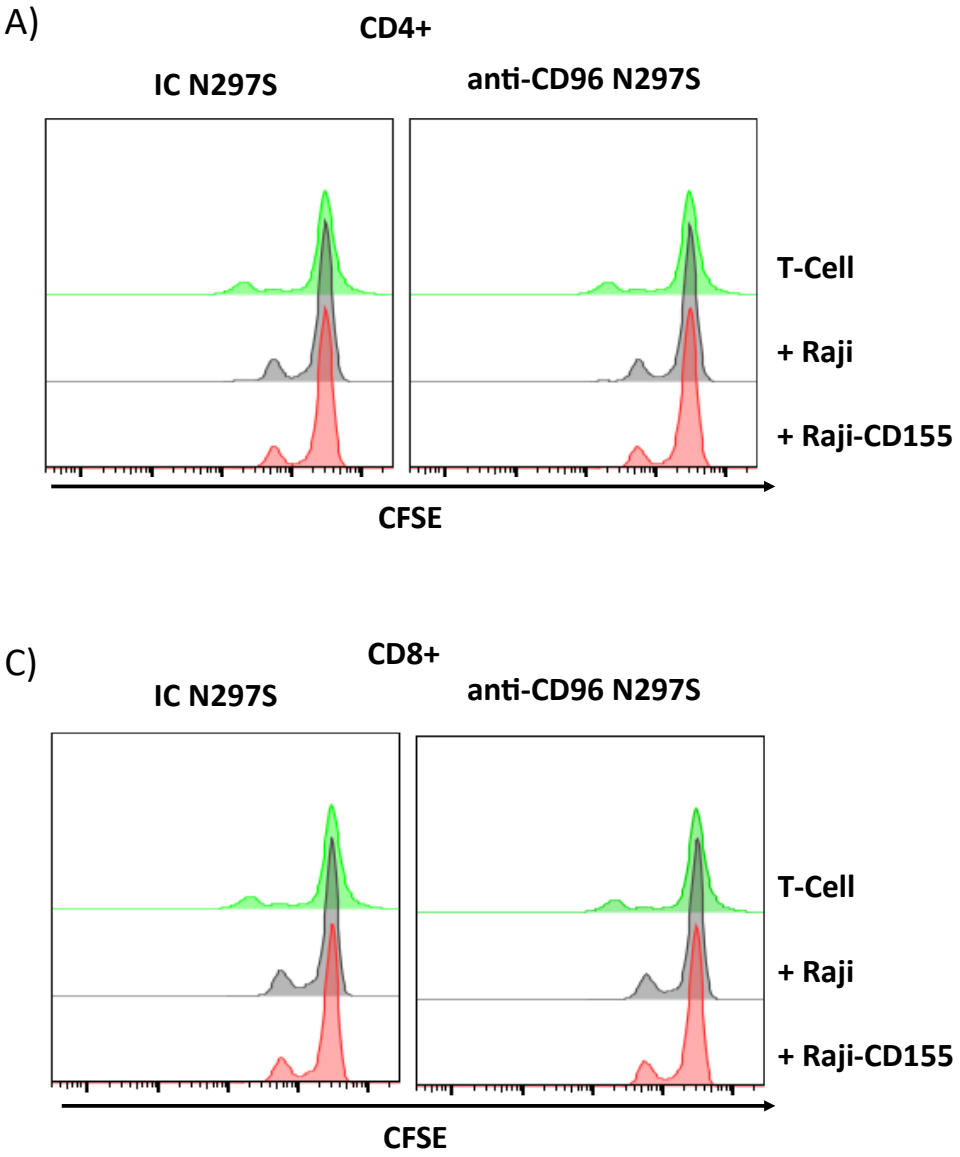

Appendix 12 Co-culture of TIGIT^{HI}CD226^{HI} T-cells with unloaded target cells fails to induce T-cell proliferation

A) Representative histograms of CD4+ TIGIT^{HI}CD226^{HI} T-cell CFSE dilution when cultured with non-blocking antibody (Left) or CD96 blocking antibody (Right). Conditions shown are T-cells alone (Green), with unloaded Raji (Grey) or with unloaded Raji-CD155 (Red). **B)** Representative histograms of CD8+ TIGIT^{HI}CD226^{HI} T-cell CFSE dilution when cultured with non-blocking antibody (Left) or CD96 blocking antibody (Right). Conditions shown are T-cells alone (Green), with unloaded Raji (Grey) or with unloaded Raji-CD155 (Red).